Czech University of Life Sciences Prague

Faculty of Forestry and Wood Sciences

Forest Risk Research Centre

Forest disturbance mapping by integrating heterogeneous remote sensing and ground data

Author: Prosper Washaya

Supervisor: prof. RNDr. Tomáš Hlásny, Ph.D.

Prague

2026

Author's Declaration

I hereby declare that this Doctoral Thesis **(Forest disturbance mapping by integrating heterogeneous remote sensing and ground data)** is my own work and quoted only according to the references listed within. Neither part of this thesis has been submitted as fulfilment to award a degree to any other institution. This thesis was written under the guidance of prof. RNDr. Tomáš Hlásny, Ph.D.

I agree to the publication of the thesis according to Act No. 111/1998 Coll. on universities as amended, regardless of the outcome of its defense.

Prague, 2026 Signature……

Abstract

Central European forests have experienced unprecedented drought-driven disturbance after 2018, reshaping landscape structures and raising concerns about long-term ecosystem resilience. This thesis develops an integrated multisensor remote sensing and machine-learning framework to map, quantify, and interpret disturbance and early recovery dynamics across Czechia between 2016 and 2024. Using fused Sentinel-1 SAR, Sentinel-2 optical imagery, airborne normalized digital surface models, and UAV-derived canopy height models, the study establishes a scalable approach for detecting annual disturbance, mapping vertical forest structure, and characterizing regeneration trajectories from national to landscape scales.

A convolutional neural network was adapted into an image-to-image framework for annual disturbance mapping, enabling identification of seven outbreak hotspots across the Czech Republic and quantification of tree mortality. These disturbance maps informed landscape-level simulations of bark beetle spread, outbreak progression, and resource depletion dynamics. Landscape-level analysis revealed extensive forest loss and pronounced landscape fragmentation within the main outbreak zone. Recovery dynamics were assessed using multisensor predictors and survival-analysis-based recovery functions, showing strong but spatially heterogeneous regeneration patterns, characterized by the predominance of bare soils class after the disturbance and the occurrence of temporary regeneration failures.

Vertical structure mapping employed machine-learning and deep-learning models, demonstrating that canopy height in a highly heterogeneous post-disturbance environment can be predicted with a relatively high accuracy using multisensor satellite features. A newly released Google's Alpha-Earth foundation-model embeddings substantially outperformed traditional Sentinel-1/2 predictors, highlighting the potential of foundation models for structural forest mapping.

Together, the results show that a multisensor and machine-learning approach can capture both the pulse of disturbance and the early structural response at ecologically meaningful scales. The framework provides new insight into the drivers, spatial patterns, and early outcomes of one of Europe's largest documented forest mortality events and offers a transferable methodology for monitoring disturbance–recovery interactions in climate-sensitive forest regions.

Keywords: bark beetle outbreak, remote sensing, multisensor data fusion, synthetic aperture radar, optical imagery, unmanned aerial vehicle, post-disturbance recovery, machine learning

Abstrakt (Czech)

Lesy střední Evropy zažily po roce 2018 bezprecedentní poruchy vyvolané suchem, které zásadně přetvořily strukturu krajiny a vyvolaly obavy o dlouhodobou odolnost ekosystémů. Tato disertační práce vyvinula integrovaný multisenzorový rámec dálkového průzkumu Země a strojového učení pro mapování, kvantifikaci a interpretaci dynamiky disturbancí a časné obnovy na území České republiky v období 2016–2024. Pomocí fúze dat Sentinel-1 SAR, optických snímků Sentinel-2, leteckých normalizovaných digitálních modelů povrchu a výškových modelů porostu odvozených z bezpilotních letadel byl vytvořen škálovatelný rámec pro detekci ročních disturbancí, mapování vertikální struktury lesa a charakterizaci regeneračních trajektorií od národní po krajinnou úroveň.

Konvoluční neuronová síť byla adaptována do schématu image-to-image pro roční mapování disturbancí, což umožnilo identifikaci sedmi hlavních ohnisek kalamity v České republice a kvantifikaci mortality stromů. Tyto mapy disturbancí sloužily jako vstup pro krajinné simulace šíření lýkožrouta, průběhu gradace a dynamiky vyčerpávání zdrojů. Analýza na úrovni krajiny odhalila rozsáhlé ztráty lesních porostů a výraznou fragmentaci krajiny v hlavní zóně kalamity.

Dynamika obnovy byla hodnocena pomocí multisenzorových prediktorů a obnovných modelů založených na analýze přežití, které prokázaly silné, avšak prostorově heterogenní regenerační vzorce, charakterizované převahou třídy holých půd po disturbanci a výskytem dočasných selhání obnovy.

Mapování vertikální struktury využívalo modely strojového učení a hlubokého učení a ukázalo, že výšku korunového patra v silně heterogenním prostředí po disturbanci lze s relativně vysokou přesností predikovat pomocí multisenzorových satelitních proměnných.

Nově publikované embeddingy základního modelu Google Alpha-Earth výrazně překonaly tradiční prediktory ze Sentinel-1/2, což zdůrazňuje potenciál foundation modelů pro mapování strukturních charakteristik lesa. Souhrnně výsledky ukazují, že multisenzorový přístup založený na strojovém učení dokáže zachytit jak pulz disturbancí, tak časnou strukturální odezvu v ekologicky relevantních měřítkách. Navržený rámec přináší nové poznatky o hybných silách, prostorových vzorcích a raných důsledcích jedné z největších zdokumentovaných epizod lesní mortality v Evropě a nabízí přenositelnou metodiku pro monitorování interakcí mezi disturbancí a obnovou v klimaticky citlivých lesních regionech.

Klíčová slova: kalamita lýkožrouta, dálkový průzkum Země, fúze multisenzorových dat, syntetická apertura radar, optická data, bezpilotní letadla, obnova po disturbanci, strojové učení

Pfupiso (Shona)

Masango eCentral Europe akasangana nekukanganiswa kukuru kwakakonzerwa nekusanaya kwemvura mushure megore ra2018, zvichichinja chimiro chenzvimbo dzemasango uye zvichimutsa kunetseka pamusoro pekusimba kwemasisitimu ezvakatipoteredza kwenguva refu. Tsvakiridzo yebeba rino inogadzira nzira dzeku ongorora pasi rose nemasaisai ari kure pamwe chete nemichina inodzidza (machine learning), kuitira kuratidza pamepu, kukanganisika pamwe nekutanga kumera kwemiti yemasango emuCzechia pakati pa2016 na2024. Kuburikidza nekubatanidza mifananidzo yemuchadenga ine masaisai (Sentinel-1), mifananidzo inoonekwa nemaziso (Sentinel-2), mamodheru anoratidza kureba kwemiti akatorwa nendege, pamwe nemamodheru ehurefu hwesango akatorwa ndege inobhururuka isina mutyairi (UAV), chidzidzo ichi buditsa nzira inokwanisa kuwedzerwa pakuyera kukanganisika kwegore negore, kuyera chimiro chekurikuenda kumera kwemasango kwenguva yakareba, uye kutsanangura nzira dzekudzokera kwesango kubva padanho renyika kusvika padanho renharaunda.

Muchina unodzidza zvakadzama (convolutional neural network) wakashandiswa pamifananidzo wegore ne gore, izvo zvakabatsira kuwana nzimbo nomwe dzakanyanya kunganiswa ne denda rezvipukanana zvinouraya miti munyika yose. Kuongorora kwenharaunda kwakaratidza kurasika kukuru kwemasango uye kupatsanuka kwakanyanya kwenzvimbo dzemasango munzvimbo huru yakarohwa nedenda. Maitiro ekupora kwemasango akaongororwa achishandisa mifananidzo yakasiyanasiyana.

Kuyerwa kwechimiro chekureba kwemiti yemumasango kwakaitwa kubudikidza nemichina inodza zvakadzama, zvichiratidza kuti kureba kwemiti kunogona kuitwa nemifananidzo yakasiyanasiyana nemazvo. Maembeddings matsva eGoogle Alpha-Earth foundation model akakunda zvakanyanya predictors dzinosomboshandiswa dzeSentinel-1/2, zvichiratidza mukana mukuru wemafoundation models pakumepa chimiro chemasango.

Pakazara, mhedziso inoratidza kuti nzira yakabatanidzwa yemasisitimu akawanda emasaisai pamwe nemichina inodzidza inokwanisa kubata zvese zvinoitika mumasango nguva yedenda. Hurongwa uhwu hunopa ruzivo rutsva pamusoro pezvikonzero, mapatani enzvimbo, uye mhedzisiro dzekutanga dzechimwe chezviitiko zvikuru zvekufa kwemasango zvakambonyorwa muEurope, uye hunopa nzira inokwanisa kutamiswa nekushandiswa mune dzimwe nzvimbo dzemasango dzinonyanya kunzwa kushanduka kwemamiriro ekunze pakutevera kudyidzana pakati pekukanganisika nekupora.

Mazwi akakosha: denda rezvipukanana zvinouraya miti, kuongorora kwepasi nemasaisai ari kure, kubatanidza ruzivo rwakawanda, masaisai emuchadenga anopinda nepamusoro pevhu, mifananidzo inoonekwa, midziyo inobhururuka isina mutyairi, kupora mushure mekukanganisika, kudzidza kwemichina

Acknowledgements

First and foremost, I express my deepest gratitude to prof. Tomáš Hlásny for his supervision, guidance, and support throughout my PhD journey. I am also sincerely thankful to my team members Roman, Maja, Marco, Agnish, Gokul, Arunima, Karim, and the rest of the group for creating an encouraging, collaborative, and inspiring research environment.

To my FLD friends: Astrid, Audrey, Arka, Aditya, Carol, Sandra, Astrid, Molly, Mayuri and the Forest People Group, thank you for the coffee breaks, conversations, and company provided motivation, balance, and much-needed laughter.

To my family: Yvonne, Ronny, Eli, Tafadzwa, Tatenda, thank you for your unwavering support, patience, and belief in me. Your encouragement has carried me through every stage of this work. Finally, my deepest thanks go to 刘丹, whose constant support, understanding, and love have been a source of strength throughout this entire journey.

CZECH UNIVERSITY OF LIFE SCIENCES PRAGUE

Faculty of Forestry and Wood Sciences

Ph.D. THESIS ASSIGNMENT

Prosper Tatenda Washaya, MSc

Applied geoinformatics and remote sensing in forestry

Thesis title

Forest disturbance mapping by integrating heterogeneous remote sensing and ground data

---

Objectives of thesis

This dissertation aims to (i) develop and test disturbance detection procedures and semi-automatized workflows, and (ii) deliver new knowledge about mechanisms and patterns of natural disturbances amplified by climate change, particularly bark beetle outbreaks triggered by drought. We will test various change detection and data fusion algorithms for forest disturbance mapping to create a workflow for a semi-automatized assessment on the annual basis. The following objectives will be addressed:

1. To review various change detection algorithms and select those most promising for bark beetle disturbance mapping, including different manifestations of tree mortality, such as standing, downed, and salvaged trees.
2. To test the selected algorithms and techniques for their ability to integrate data from different sensors (particularly different optical and SAR data) and auxiliary ground data, such as topography. We use extensive reference (ground-truth) data to train the algorithms and test the accuracy of disturbance mapping
3. To use the annual disturbance maps to evaluate the specific mortality patterns, their drivers, and changes in time in order to better understand the recent outbreak dynamics

Methodology

This dissertation will use various remote sensing, ancillary, and ground data to map natural forest disturbances, particularly from wind and bark beetles. We will test various change detection and data fusion algorithms for forest disturbance mapping to create a workflow for a semi-automatized assessment on annual basis, focusing primarily on the recent bark beetle outbreak in Czechia, with the potential to expand it to other agents and areas. Further, we will use annual forest change maps to understand outbreak dynamics by evaluating specific infestation patterns and their changes in time. Finally, we aim to attribute these effects, i.e., to identify the underlying mechanisms of drought-driven outbreaks, which is a rather new phenomenon in Europe. As the main output, we develop a versatile machine learning-based workflow for disturbance mapping, integrating diverse remote sensing and ground data, provide an extensive model validation, and conduct several studies aimed at both methodological advances and understanding the emerging disturbance dynamics in Central Europe.

Main elements of the proposed solution

Literature review and pilot tests: A thorough literature review will be conducted to review available change detection algorithms, their performance, and suitability for large-scale disturbance mapping, particularly from bark-beetle infestations.

Data Collection: Remote Sensing data will be obtained from multiple sources including different optical and SAR imagery. In the frame of the machine learning-based data fusion, also the effect of other data types on detection performance will be tested, such as topography, forest ownership, etc. The reference data used for model testing and training will be obtained from the Forest Management Institute, Czech Republic.

Software and algorithms for data analysis We will use the Google Earth Engine platform for data pre- processing, analysis and implementing various machine learning and deep learning algorithms, using TensorFlow in both JavaScript and the Python APIs. We will also use the SNAP toolbox for SAR data processing. Machine learning algorithms and statistical analysis will be implemented in Python and R, while post processing will be done in ArcGIS and QGIS.

Area of Interest: We will focus on the Czech Republic, which became one of the major hotspots of disturbance intensification in Europe. Forests in the country cover 37.5% of the total area, 50% of which is dominated by Norway Spruce. Salvaged tree volumes killed by bark beetles increased from approximately 1.5 million to 26 million cubic meters between 2014 and 2019. Further, spruce growing stock decreased by 16% during the same period. We also intend to extend our research to other regions of Europe, to test the performance of the proposed algorithms.

Pre-Processing and Analysis: Annual optical and SAR remote sensing data acquired during the period between June and September for the period 2014-2022 will be used. The images will be obtained for the whole Czech Republic and merged into one single mosaic for each year. Images with the lowest percentage of cloud cover will be acquired. Top of the atmosphere (TOA) correction will be done for each image to produce surface reflectance (SR) images to reduce the effect of aerosols and atmospheric gases. Mosaics will be then produced for each of the years between 2014 and 2022. For SAR, the pre-processing steps require radiometric normalization from Ground Range Detected (GRD) data obtained from ESA Copernicus website or directly from the Google Earth Engine platform. For SAR images collected in the interferometric broad swath mode, the default acquisition mode of Sentinel-1 will be used. The calibrated images will be orthorectified to ground geometry using SRTM DEM. Finally, the orthorectified images will be clipped and mosaicked into a single annual image for the period between 2014 and 2022. A mask based on the Corine dataset (CLC 2012) will be applied to both SAR and optical to classify the study area into forest and non-forest areas to represent forest conditions before the outbreak period. An accurate cloud mask is also applied on the optical data to remove clouds and shadows from the imagery. As inputs to the disturbance mapping, we will use the change maps derived from NDVI differences based on optical images during the outbreak periods and image-based ratio thresholding. In addition, we will include ancillary data to combine with the SAR and optical data, including elevation information, slope and aspect derived from a Digital Elevation Model (DEM), Enhanced Wetness Difference Index (EWDI), and solar radiation.

Creating disturbance Maps: The NDVI change maps, SAR change maps and ancillary data will be used as inputs to different classification algorithms (for example, a neural network-approximated logistic regression model). Reference data in forest changes derived by differencing the airborne Normalized Digital Surface Model (Source: Forest Management Institute) will be used for model training. Other training dataset will be considered, depending on their availability. The logistic regression model is well suited for disturbance detection as it can predict the probability of a dichotomous variable taking on either state (i.e., change or no-change). All these analyses will be conducted in the TensorFlow framwork.

Patterns and drivers of disturbance dynamics: We will use the annual disturbance maps produced by the procedure above to conduct several case studies (each of them resulting in a research paper). We will use different GIS and spatial statistics tools to identify outbreak development, including identification of new mortality spots, their expansion, and the collapse. By correlating these patterns with climate, ownership, management and other data, we identify main drivers of these dynamics. More detailed design of case studies will be formulated during the study period.

The proposed extent of the thesis

dsds

Keywords

Remote Sensing, Natural Disturbances, Machine Learning, Data Fusion, Synthetic Aperture Radar, Google Earth Engine

---

Recommended information sources

Baier, P., Pennerstorfer, J., & Schopf, A. (2007). PHENIPS-A comprehensive phenology model of Ips typographus (L.) (Col., Scolytinae) as a tool for hazard rating of bark beetle infestation. Forest Ecology and Management, 249(3), 171–186. https://doi.org/10.1016/j.foreco.2007.05.020

Biedermann, P. H. W., Müller, J., Grégoire, J. C., Gruppe, A., Hagge, J., Hammerbacher, A., Hofstetter, R. W., Kandasamy, D., Kolarik, M., Kostovcik, M., Krokene, P., Sallé, A., Six, D. L., Turrini, T., Vanderpool, D., Wingfield, M. J., & Bässler, C. (2019). Bark Beetle Population Dynamics in the Anthropocene: Challenges and Solutions. In Trends in Ecology and Evolution (Vol. 34, Issue 10, pp. 914–924). Elsevier Ltd. https://doi.org/10.1016/j.tree.2019.06.002

Buma, B. (2015). Disturbance interactions: Characterization, prediction, and the potential for cascading effects. Ecosphere, 6(4), 1–15. https://doi.org/10.1890/ES15-00058.1

DeVries, B., Verbesselt, J., Kooistra, L., & Herold, M. (2015). Robust monitoring of small-scale forest disturbances in a tropical montane forest using Landsat time series. Remote Sensing of Environment, 161, 107-121.

Hlásny, T., König, L., Krokene, P., Lindner, M., Montagné-Huck, C., Müller, J., Qin, H., Raffa, K. F., Schelhaas, M.-J., Svoboda, M., Viiri, H., & Seidl, R. (n.d.). Bark Beetle Outbreaks in Europe: State of Knowledge and Ways Forward for Management. https://doi.org/10.1007/s40725-021-00142-x/Published

Hlásny, T., Zimová, S., & Bentz, B. (2021). Scientific response to intensifying bark beetle outbreaks in Europe and North America. Forest Ecology and Management, 499. https://doi.org/10.1016/j.foreco.2021.119599

Kautz, M., Meddens, A. J. H., Hall, R. J., & Arneth, A. (2017). Biotic disturbances in Northern Hemisphere forests – a synthesis of recent data, uncertainties and implications for forest monitoring and modelling. In Global Ecology and Biogeography (Vol. 26, Issue 5, pp. 533–552). Blackwell Publishing Ltd. https://doi.org/10.1111/geb.12558

McDowell, N. G., & Allen, C. D. (2015). Darcy's law predicts widespread forest mortality under climate warming. Nature Climate Change, 5(7), 669–672. https://doi.org/10.1038/nclimate2641

Trigg, S. N., Curran, L. M., & McDonald, A. K. (2006). Utility of Landsat 7 satellite data for continued monitoring of forest cover change in protected areas in Southeast Asia. Singapore Journal of Tropical Geography, 27(1), 49-66.

Woodcock, C. E., Macomber, S. A., Pax-Lenney, M., & Cohen, W. B. (2001). Monitoring large areas for forest change using Landsat: Generalization across space, time and Landsat sensors. Remote sensing of environment, 78(1-2), 194-203.

Expected date
2023/24 WS – FFWS – State Doctoral Examinations

Thesis supervisor
prof. RNDr. Tomáš Hlásny, PhD.

Supervising department
The Forest Risk Research Centre

Advisor of thesis
Ing. Martin Mokroš, PhD
Ing. Martin Mokroš, PhD

Electronic approval: 14. 01. 2026
prof. RNDr. Tomáš Hlásny, PhD.
Head of Institute

Electronic approval: 14. 01. 2026
doc. Ing. Peter Surový, PhD.
Chairperson of Field of Study Board

Electronic approval: 14. 01. 2026
prof. Ing. Róbert Marušák, PhD.
Dean

Prague on 15. 01. 2026

Table of Contents

List of Figures

List of Tables

List of abbreviations

AEF – AlphaEarth Foundation (Google Earth observation foundation model embeddings)

CNN – Convolutional Neural Network

CHM – Canopy Height Model

DSM – Digital Surface Model

FMs – Foundation Models

GEE – Google Earth Engine

HR – High Resolution

InSAR – Interferometric Synthetic Aperture Radar

LiDAR – Light Detection and Ranging

MR – Medium Resolution

NDVI – Normalized Difference Vegetation Index

NDWI – Normalized Difference Water Index

NBR – Normalized Burn Ratio

RF – Random Forest

RGB – Red–Green–Blue (true color composite)

SAR – Synthetic Aperture Radar

SR – Spectral Reflectance

UAV – Unmanned Aerial Vehicle

VH – Vertical–Horizontal polarization (cross-polarized SAR)

VV – Vertical–Vertical polarization (co-polarized SAR)

HH – Horizontal–Horizontal polarization (co-polarized SAR)

VHR – Very High Resolution

List of publications included in this thesis:

This thesis is based on data presented in the following articles, referred to by the Roman Numerals I-III:

I. **Washaya, P.,** Modlinger, R., Tyšer, D., & Hlásny, T. (2024). Patterns and impacts of an unprecedented outbreak of bark beetles in Central Europe: A glimpse into the future? Forest Ecosystems, 11, 100243. https://doi.org/10.1016/j.fecs.2024.100243

   This study provides the national-scale foundation for the entire thesis by mapping and analyzing the 2016–2022 spruce bark beetle outbreak outbreak using multi-source remote sensing (Landsat 8, Sentinel-1, airborne imagery) integrated through a Convolutional Neural Network model. It identifies seven major outbreak hotspots across >15,000 km², including the largest core region (~9,000 km²) that becomes the focal area for subsequent papers. Disturbances followed a consistent temporal pattern of multi-year build-up, a sharp peak (2018–2021), and rapid collapse driven not by host depletion but by fragmentation and climatic moderation. Nationally, 11% of forests and 17% of spruce stands were affected (~100 million m³ of timber loss), with extreme landscape fragmentation in the focal zone.

   This paper establishes the spatial context for the thesis: it determines where disturbances occurred, how severely they transformed the landscape, and which areas should be selected for deeper structural and recovery analyses. It also produces the disturbance maps used later to evaluate regeneration dynamics (Paper II) and to calibrate and validate mechanistic bark beetle simulations (Paper IV).

II. **Washaya, P.,** Potterf, M., Modlinger, R., Hüttnerová, T., Melichová, Z., & Hlásny, T. (2025). Severely disturbed forests in Central Europe retain robust recovery capacity but face resilience loss due to spatial homogenization. Landscape Ecology. https://doi.org/10.1007/s10980-025-02264-0

   Anchored in the major disturbance hotspot area delineated in Paper I, this study uses multi-source remote sensing (Sentinel-1, Sentinel-2, Unmanned Areal Vehicles-based Canopy Height Model data) integrated through U-Net and Random Forest models to track forest recovery from 2018 to 2024. Disturbance-to-recovery transitions were mapped at high spatial resolution, revealing both the regenerative potential and the structural vulnerabilities of post-outbreak forests.

Recovery was vigorous but uneven: bare soil declined from 92% (2018) to 46% (2024), while regrowth expanded, yet one-third of pixels reverted to bare soil annually. Large bare-soil patches (up to 600 ha) remained structurally homogenized, while vegetated patches were small and fragmented. Mean time to initial revegetation was 3.8 years, and ~7 years to reach established regrowth.

This paper extends the disturbance and structure analyses by linking disturbance severity (Paper I) and height structure (Paper III) to ecological trajectories. It shows that while forests recover, spatial homogenization and recurrent setbacks threaten long-term resilience—insights essential for interpreting future disturbance modelling outcomes in Paper 4.

III. Karim, M. F., **Washaya, P.,** Potterf, M., Modlinger, R., & Hlásny, T. (submitted). AlphaEarth Foundations provides superior accuracy in forest height mapping across severely disturbed areas. Remote Sensing of Environment.

Building directly on the disturbance patterns identified in Paper I, this study focuses on the structural consequences of the bark beetle outbreak within the main disturbance hotspot (C4). It evaluates the ability of the new AlphaEarth Foundations (AEF) dataset to map forest height in complex, severely disturbed environments. A systematic review of existing predictors (optical and SAR) was combined with model comparisons (Random Forest, U-Net) to benchmark traditional height-mapping approaches against AEF.

AEF consistently outperformed conventional methods, increasing R^2 from 0.70–0.77 to 0.81 and reducing mean absolute error by ~35%. Its robustness in highly heterogeneous, post-disturbance conditions makes it particularly valuable for the C4 region, where salvage logging, canopy collapse, and patch fragmentation challenge traditional remote sensing products.

This paper extends the disturbance narrative by quantifying post-disturbance height structure, providing the vertical information necessary to understand ecosystem reorganization and forming a methodological bridge to the recovery analysis conducted in Paper II.

IV. Das, A. K., Baldo, M., Dobor, L., Seidl, R., Rammer, W., Modlinger, R., **Washaya, P.,** Merganičová, K., & Hlásny, T. (2025). The increasing role of drought as an inciting

factor of bark beetle outbreaks can cause large-scale transformation of Central European forests. Landscape Ecology, 40, 108. https://doi.org/10.1007/s10980-025-02125-w

This study uses the methodology used in Paper 1 to produced disturbance maps as empirical data to improve and validate mechanistic simulations of bark beetle dynamics in the iLand model.In this paper, a drought-trigger mechanism is introduced based on summer Vapour Pressure Deficient, enabling the model to reproduce the unprecedented post-2018 outbreak without relying on windthrow events. The disturbance map generation methodology was central for producing maps to calibrate the drought threshold (0.84 kPa), constraining outbreak trajectories, and evaluating simulated disturbance intensity and timing.

Simulations show that severe drought now independently initiates outbreaks, leading to larger and more frequent disturbances, 36% higher under RCP8.5 than wind-only scenarios, and driving a long-term collapse of Norway spruce (up to 92% loss by 2100), with a shift toward beech–pine forests.

This paper closes the thesis narrative by demonstrating how empirically mapped disturbances (Paper I) enable more realistic, climate-sensitive simulation models. Together with insights on structural change (Paper III) and recovery capacity (Paper II), it provides a comprehensive framework for understanding and anticipating future forest trajectories under climate stress.

On the top of the previous papers, which constitute the core of this thesis, I have coauthored the following paper:

V. Yao, S., Balz, T., **Washaya, P.,** Sultanbekova, A., & Sönmez Boyoğlu, C. (2025). Coherence in SAR images: A review of estimation methodologies and applications. IEEE Geoscience and Remote Sensing Magazine, in review.

I served as the principal author for papers I and II and as a contributing author for papers III, IV and V. Responsibilities included writing the original drafts, conducting review and editing, processing all remote sensing datasets, developing the disturbance and recovery classification algorithms, performing data analyses to characterize disturbance dynamics and post-disturbance recovery, and producing visualizations.

1. Introduction

1.1. Research background

Remote sensing has become a primary tool for monitoring forest ecosystem change, offering spatially comprehensive, repeated observations that far exceed the capacity of field-based surveys (Kennedy et al., 2010; Wulder et al., 2012). Advances in high-resolution optical, SAR, and LiDAR systems, combined with multi-sensor data fusion and modern machine learning, now enable detailed detection of forest disturbance, quantification of structural loss, and assessment of early post-disturbance recovery at landscape to national scales (Fassnacht et al., 2016; X. Huang et al., 2022). These developments are especially important for managed forests, where mixed disturbance agents, salvage logging, and heterogeneous regeneration pathways complicate the interpretation of forest change.

The need for robust remote sensing approaches has grown as forest disturbance regimes intensify globally. Rising temperatures, prolonged droughts, and more frequent climatic extremes have increased disturbance extent and severity across temperate and boreal forests (Turner & Seidl, 2023). In Europe, drought-driven disturbance pulses have become a dominant force, synchronizing mortality across large regions and amplifying the effects of insects and pathogens (Netherer & Hammerbacher, 2022). Among these, outbreaks of the spruce bark beetle (Ips typographus) have reached unprecedented scales, driven by drought-weakened defenses, accelerated beetle development, and favorable climatic conditions (Hlásny, König, et al., 2021; Raffa et al., 2008).

The Czech Republic represents one of the most extreme examples of this transformation. Between 2018 and 2022, a combination of severe drought and heat triggered record Norway spruce (*Picea abies*) mortality and extensive salvage logging, creating a highly fragmented post-disturbance landscape dominated by low vegetation and depleted canopy structure (Pirtskhalava-Karpova et al., 2024; Washaya et al 2024; Washaya et al 2025; Hlasny etal 2021). Given the increasing complexity of disturbance impacts, along with a growing recognition of disturbance legacies, there is a critical need to integrate multisource and multisensory RS data. Such integration offers a more comprehensive view of disturbance and recovery dynamics than would be possible with single datasets alone.

1.2. Research Aims and Objectives

This thesis applies an integrated, multi-scale remote sensing framework to quantify forest disturbance and post-disturbance dynamics in Central Europe between 2016 and 2024 See figure 1). The work is structured around four primary research objectives, which collectively aim to map disturbance patterns, identify major outbreak hotspots, assess forest recovery trajectories, and characterize post-disturbance vertical structure. By integrating multisource satellite and UAV data and evaluating both machine learning and deep learning approaches, the thesis offers new insights into the drivers, patterns, and regeneration pathways of disturbance-affected forests.

Research objectives:

1. Develop a scalable remote sensing approach for annual, country-wide forest disturbance mapping by integrating multisource data (optical satellite imagery, SAR backscatter, and airborne nDSMs), and use these maps to quantify the extent, timing, and spatial progression of regional drought-driven bark beetle outbreaks and their impacts on forest composition and landscape structure.

2. Map post-disturbance vertical structure across the heavily affected landscape by building a remote sensing workflow that combines satellite predictors with UAV-derived canopy height models to characterize the emerging structural heterogeneity following large-scale mortality.

3. Establish a multi-sensor fusion framework to detect early recovery phases by integrating optical, SAR, and UAV data to distinguish transitions from recent disturbance to initial stages of vegetation regeneration.

4. Quantify post-disturbance recovery trajectories by analysing transitions among regeneration stages and evaluating their spatial and temporal variability, identifying the pace, pathways, and potential bottlenecks of ecosystem recovery.

The thesis is based on the following hypotheses:

1. Integrating multisource satellite and airborne data produces higher accuracy in mapping drought-driven bark beetle mortality than single-sensor approaches.

2. Areas affected by severe bark beetle outbreaks and post-disturbance salvage logging exhibit greater spatial homogenization and fragmentation than unaffected or lightly disturbed areas.

3. Fused optical–SAR satellite data can classify post-disturbance vegetation into distinct structural stages with accuracy above random chance, and these stages follow predictable temporal trajectories.

4. Multi-source satellite predictors, including learned feature embeddings, predict vertical forest structure in disturbed areas more accurately than single-sensor models across heterogeneous post-disturbance conditions.

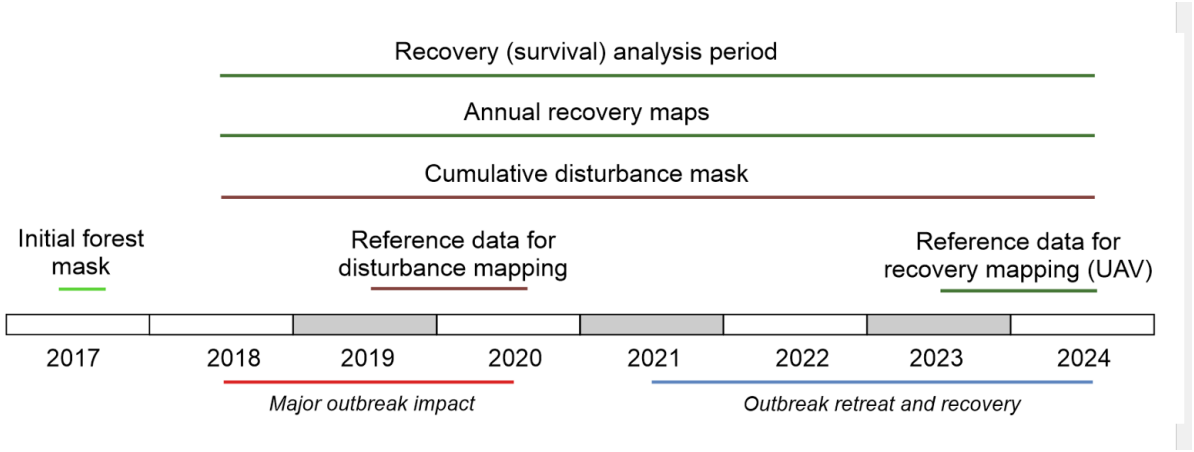

Figure 1: Overview of the experimental design. The study spans the full disturbance cycle, from outbreak onset (2017) through the peak (2018–2020) and into the recovery phase. (Source: Washaya et al., 2025).

1.3. Thesis Structure

Chapter 1 Introduction: frames the thesis by outlining the motivation, research gaps, hypotheses and objectives related to climate-driven forest disturbances and post-disturbance recovery. It defines the central hypotheses and objectives, clarifies the role of remote sensing as the core analytical tool, and positions the study within current challenges in monitoring large-scale forest change under accelerating climate stress.

Chapter 2 Literature Review: provides the scientific foundation of this thesis through a literature review on the changing dynamics of forest disturbances under climate change. It begins by introducing remote sensing principles relevant to forest ecosystem monitoring, including sensor types, platforms, and commonly used datasets. It then reviews techniques for integrating multisource data optical, SAR, and LiDAR for mapping and quantifying forest changes. The second part of the chapter focuses on climate-driven forest disturbances, emphasizing the shift from wind- to drought-driven bark beetle outbreaks and the resulting large-scale spatiotemporal synchrony across Europe. Finally, the chapter discusses post-disturbance forest recovery, highlighting patterns of regeneration, resilience, and structural transformation following bark beetle outbreaks.

Chapter 3 Study Area and Workflow of Methodology: outlines the methodological framework used across the thesis. It introduces the Czech Republic study area and the main disturbance hotspot that serves as the focal region for later vegetation height structure and recovery analyses. The chapter describes the multi-source remote sensing datasets, Landsat 8, Sentinel-1, Sentinel-2, airborne imagery, and UAV canopy-height models, and the preprocessing steps required to integrate them. It then summarizes the deep learning approach used for large-scale disturbance mapping, the generation of annual disturbance layers, and the methods applied to analyze outbreak dynamics and landscape fragmentation. Procedures for mapping post-disturbance recovery using Random Forest classification are also presented, along with the landscape-ecological and statistical techniques used to quantify recovery rates, patch transitions, and structural changes. Together, these methods provide a unified framework that supports the thesis's progression from disturbance detection to structural assessment, recovery analysis, and later integration of disturbance information into modelling.

Chapter 4 Results: presents the peer-reviewed articles that form the core of this thesis. Each paper addresses a specific objectives of the overall research framework, including disturbance detection, spatial outbreak dynamics, recovery processes, vegetation height mapping, and

integration with simulation models. Together, the papers provide the empirical and methodological foundation supporting the thesis objectives.

Chapter 5 Discussion: synthesizes the thesis findings and highlights the central role of remote sensing in understanding disturbance regimes, structural change, ecosystem recovery, and future outbreak dynamics. It discusses how multi-sensor satellite and airborne datasets enabled large-scale disturbance mapping, revealing the drought-driven outbreak and associated landscape fragmentation. The chapter then considers how advanced remote sensing approaches, including AlphaEarth Foundations embeddings and UAV canopy-height models, improved characterization of post-disturbance height structure in the main hotspot. The discussion also evaluates how combined Sentinel-1, Sentinel-2, and UAV data captured fine-scale recovery trajectories, regeneration failures, and emerging spatial homogenization. Finally, it emphasizes how remote-sensing-derived disturbance maps strengthened simulation modelling by providing empirical calibration and validation data for drought-triggered outbreak dynamics.

Chapter 6 concludes the thesis by summarizing the key findings, confirming the unprecedented scale and drought-driven nature of the bark beetle outbreak, its severe landscape impacts, and the forests' strong but uneven recovery capacity. It outlines the study's scientific and management contributions, particularly in advancing understanding of climate-amplified disturbance dynamics and recovery processes. Finally, it identifies research priorities, including long-term monitoring, species composition studies, regeneration drivers, innovative management strategies, socio-economic considerations, and further development of remote sensing approaches.

2. Literature Review

2.1. Remote Sensing in Disturbance Mapping

Remote sensing provides an essential means for detecting and monitoring forest disturbances across large spatial and temporal scales. It enables the observation of both abrupt, high-intensity events, such as fires, windthrows, and clearcuts and more subtle, progressive processes including insect infestations, degradation, and selective logging (Cohen et al., 2017; Senf & Seidl, 2021b). By capturing consistent, repetitive measurements of the Earth's surface, remote sensing supports long-term assessments of forest condition, disturbance dynamics, and recovery trajectories (Wulder et al., 2012). Advances in forest disturbance monitoring increasingly rely on the integration of multi-sensor and multi-temporal datasets, combining optical and radar information across multiple spectral dimensions to enhance detection accuracy (DeVries et al., 2015; Hirschmugl et al., 2017; Lehmann et al., 2015). While methodological choices, such as disturbance thresholds or algorithmic design, may lead to differences among disturbance maps, ensemble and data fusion approaches can effectively reduce uncertainties and improve classification reliability (Xu et al., 2018; Ye et al., 2019). These integrated frameworks underpin the subsequent developments in change detection, sensor selection, data fusion, and machine learning–based classification techniques discussed in the following sections.

2.1.2 Change Detection Approaches

Two main methods used in forest change detection with high resolution (HR) data are image-to-image detection and time-series analysis. In contrast to image-to-image approaches that rely on only two temporal images, time-series analysis utilizes multiple observations to derive more robust information about change dynamics (Hussain et al., 2013; Kennedy et al., 2010; Masiliūnas et al., 2021). For instance, the Landsat-based Detection of Trends in Disturbance and Recovery (LandTrendr) algorithm represents a time-series approach based on trajectory segmentation, allowing for the identification of both short-term events (e.g., disturbances) and long-term processes (e.g., regrowth) (Kennedy et al., 2010). Pflugmacher et al., (2012) used LandTrendr to characterize vegetation changes between 1972 and 2010 by extracting spectral trajectories and change metrics associated with disturbance and recovery. Similarly, Senf & Seidl (2021) applied LandTrendr to map three decades of forest disturbances across Europe, analysing changes in disturbance size, frequency, and severity.

Time-series analysis methods can be grouped into four main categories (Hirschmugl et al., 2017): threshold-based detection, curve fitting, trajectory fitting, and trajectory segmentation (Figure 2). Threshold-based methods, such as those used in the ForWarn system (Norman et al., 2013), apply statistical thresholds (e.g., Z-scores) to detect anomalies but are limited by their empirical and region-specific nature. Curve fitting applies regression models to describe temporal trends in spectral indices, whereas trajectory fitting uses predefined degradation curves to represent characteristic disturbance types (Banskota et al., 2014; Verbesselt et al., 2010). Trajectory segmentation, implemented in tools like LandTrendr (Kennedy et al., 2010), partitions time-series into linear segments representing disturbance and recovery phases and has been successfully used to map continental disturbance dynamics (Senf & Seidl, 2021b). However, it requires correction for phenological variability.

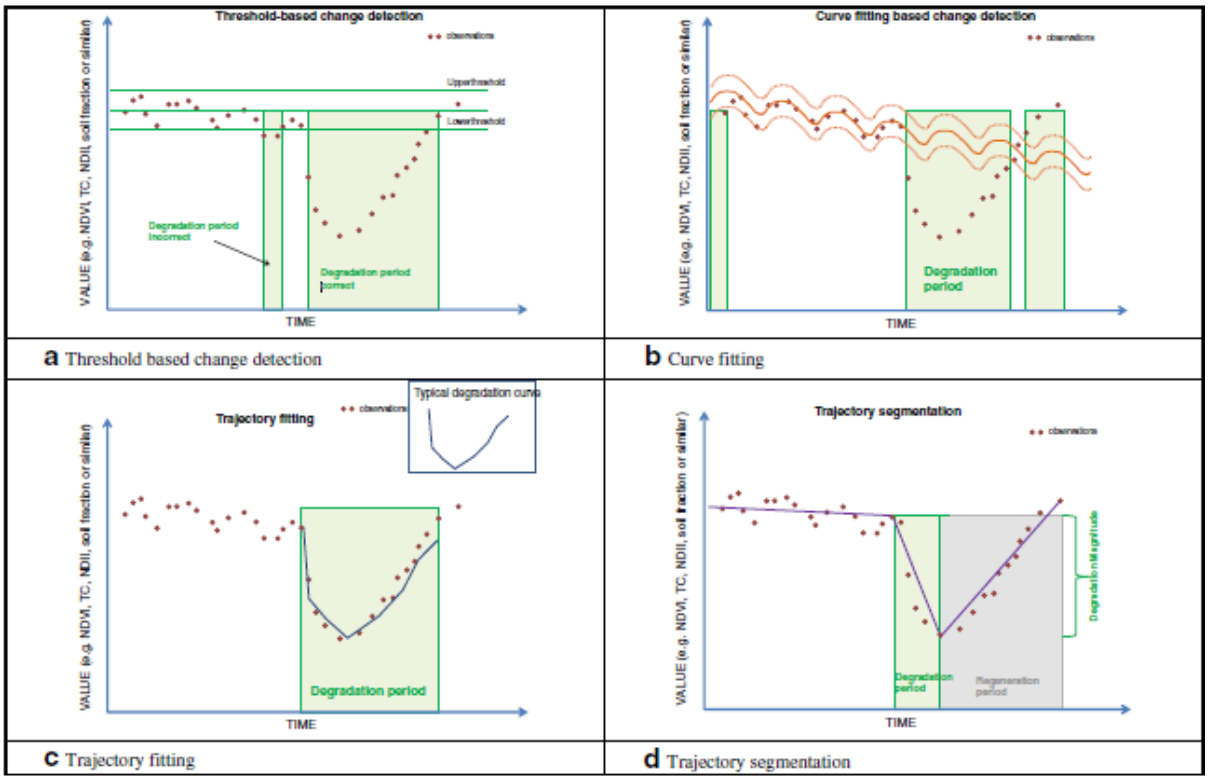

Figure 2: Schematic illustration of different time series analysis (Source: Hirschmugl et al., 2017)

Image-to-image methods, illustrated in figure 3, remain widely applied in forest disturbance mapping (Washaya et al., 2024, Havašová et al., 2015; Margono et al., 2012; Matricardi et al., 2010). These approaches detect change directly from reflectance values, vegetation indices (e.g., NDVI, NBR), or backscatter differences between dates (Huete et al., 2002; Zeng et al., 2022). Although simpler to implement, they are more sensitive to illumination, atmospheric, and seasonal differences than time-series approaches.

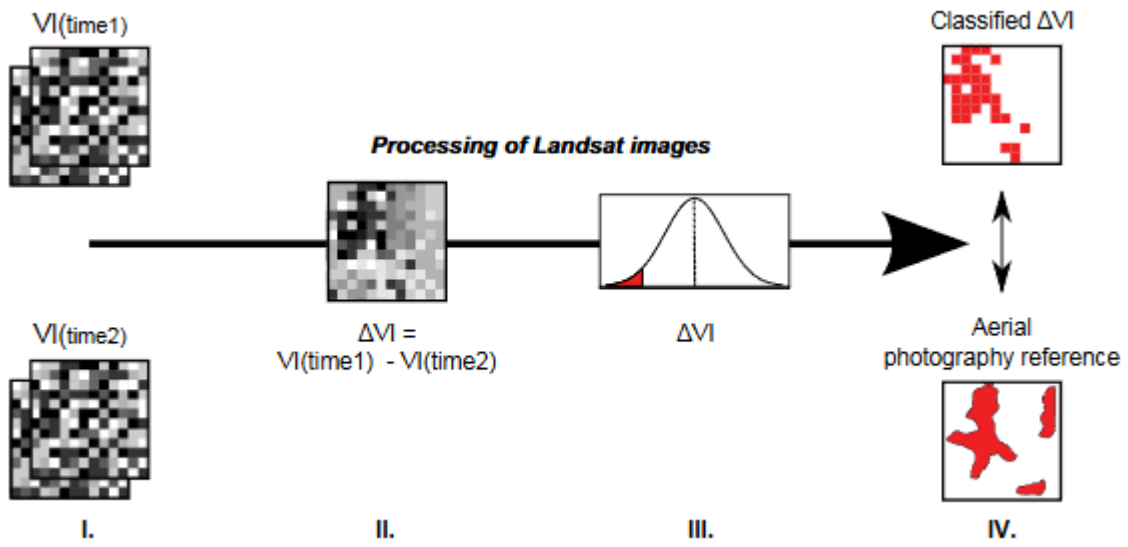

Figure 3: Schematic overview of the image-to-image change-detection workflow: (I) calculation of vegetation indices (VI) for individual years; (II) VI differencing to obtain ΔVI; (III) classification of ΔVI using threshold values; and (IV) validation against reference aerial imagery to derive accuracy metrics (kappa, ROC). (Soruce:Havašová et al., 2015).

2.1.3. Sensor Characteristics and Data Selection

Selecting remote sensing data for forest disturbance mapping requires balancing spatial, temporal, and spectral resolution with spatial coverage and cost (Wulder et al., 2008). The optimal data source depends on the disturbance type, study scale, and monitoring objectives. Very High Resolution (VHR) sensors (<4 m) capture fine-scale changes but are costly and limited in coverage (Akca et al., 2016). Medium to Coarse Resolution (MR) sensors (≥60 m), such as MODIS, offer frequent, wide-area observations but lack the spatial detail needed to detect localized impacts (Chen et al., 2017; Hansen et al., 2013a). High Resolution (HR) sensors (5–30 m), including Landsat and Sentinel-2, provide an effective balance between spatial detail and regional coverage (Chen et al., 2021; DeVries et al., 2015). The open-access Landsat policy since 2008 has been particularly transformative, enabling consistent, long-term monitoring of forest disturbances worldwide (Wulder et al., 2012).

2.1.3.1. Optical Remote Sensing

Optical sensors, such as Landsat, Sentinel-2, and MODIS, operate in the visible to infrared spectrum, capturing reflected light that provides detailed spectral information on vegetation structure and condition (Huete et al., 2002; Zeng et al., 2022). These data are fundamental for assessing forest health and monitoring disturbances (Cohen et al., 2017).

A key application of optical remote sensing is the use of vegetation indices (VIs)—mathematical combinations of spectral bands that represent canopy vigour, chlorophyll content, and moisture status (Zeng et al., 2022). Common indices include the Simple Ratio (SR) (Rouse, 1973), Normalized Difference Vegetation Index (NDVI) (Tucker, 1979), Enhanced Vegetation Index (EVI) (Huete et al., 2002), Normalized Difference Water Index (NDWI) (X. Gao, 2000; Mcfeeters, 1996), and Normalized Burn Ratio (NBR) (Chuvieco et al., 2002).

Numerous studies have demonstrated the value of optical data for forest disturbance monitoring. Havašová et al., (2015); König et al., (2023) identified sensitive VIs for detecting bark beetle outbreaks, while (Bryk et al., 2020) confirmed NDVI's ability to assess post-attack forest health. Sentinel-2 indices have been shown to outperform MODIS in capturing bark beetle-induced spectral changes due to their higher spatial and spectral resolution (Gomez et al., 2020). Multi-temporal Sentinel-2 frameworks further improved disturbance mapping accuracy and robustness (Fernandez-Carrillo et al., 2020; König et al., 2023), with classification accuracies exceeding 0.80 when combining multiple indices. These findings are consistent with broader reviews emphasizing the effectiveness of optical time-series approaches for forest disturbance detection (Hirschmugl et al., 2017).

However, optical imagery is constrained by cloud cover, haze, and illumination variability, which limit data availability, especially in cloudy regions (Hirschmugl et al., 2017; Trisasongko, 2010). Synthetic Aperture Radar (SAR) sensors mitigate these limitations by acquiring data independent of daylight and weather (Einzmann et al., 2012; Nakamura et al., 2004). Integrating optical and SAR datasets enables dense, all-weather time series essential for continuous forest disturbance monitoring (Hirschmugl et al., 2020; Lehmann et al., 2015).

2.1.3.2. Synthetic Aperture Radar

Synthetic Aperture Radar (SAR) provides complementary information to optical data, particularly under cloudy or low-light conditions. Operating in the microwave spectrum, SAR actively transmits and receives electromagnetic pulses, measuring the backscattered signal from the surface. By coherently combining successive echoes from a moving platform, SAR synthesizes a large antenna aperture, achieving high spatial resolution independent of illumination or weather (Moreira et al., 2013).

SAR's sensitivity to dielectric properties, surface roughness, and polarization (HH, HV, VV, VH) enables the detection of forest structure and disturbance dynamics not captured by optical

sensors (Kobayashi et al., 2000; Ouchi, 2013). Longer wavelengths (L- and P-bands) penetrate vegetation canopies and provide information on sub-canopy and soil conditions. Recent studies have demonstrated SAR's effectiveness in disturbance monitoring: Tariq et al., (2021) used Sentinel-1 data to detect 95% of fire events identified by optical indices, while Bouvet et al. (2018) achieved >95% deforestation detection accuracy using geometric shadow analysis.

Beyond backscatter intensity, Interferometric SAR (InSAR) exploits phase differences between multiple acquisitions to derive coherence, which reflects structural and temporal forest properties (Bouvet et al., 2018; Fransson et al., 2001). High coherence indicates stable surfaces; low coherence results from canopy motion and volumetric scattering. Missions such as TanDEM-X (X-band), ALOS-2 (L-band), and Sentinel-1 (C-band) have enhanced InSAR's capacity to map forest structure, height, and biomass (Praks et al., 2007). Single-pass systems like TanDEM-X minimize temporal decorrelation, enabling accurate structural retrievals. Emerging missions ESA BIOMASS and NASA–ISRO NISA will further advance global, coherence-based forest monitoring.

2.1.4 Data fusion

Data fusion in remote sensing integrates information from multiple sensors such as optical, SAR, and LiDAR operating at different spatial, spectral, and temporal resolutions to produce more comprehensive datasets (Pohl & Van Genderen, 1998). Fusion techniques are commonly categorized into three levels: pixel-level, which combines raw data to enhance resolution; feature-level, which merges extracted features such as texture or edges; and decision-level, which integrates results from independent analyses (Zhang, 2010).

Pixel-level fusion provides the most detailed integration but remains challenging for heterogeneous data such as optical and SAR due to their differing physical properties. Improper fusion can degrade spectral or backscatter information. Thus, developing robust methods that preserve each sensor's distinct characteristics is a continuing research priority (Zhang, 2010).

Recent advances in machine learning and deep learning have transformed multi-sensor fusion, enabling models to learn nonlinear relationships between data sources automatically. Ensemble and neural network-based approaches now outperform traditional statistical and rule-based methods, improving land cover and disturbance classification accuracy (Xu et al., 2018; Ye et al., 2019). Integrating data fusion with learning-based techniques has become central to modern remote sensing, particularly for forest disturbance mapping that requires harmonizing multi-sensor data across scales.

2.1.5 Advances in Classification Techniques

2.1.5.1. Classical Machine Learning Approaches in forest Disturbance Mapping

Machine learning algorithms have long been applied in the remote sensing community, ranging from simple to more sophisticated frameworks. Early approaches included techniques such as Principal Component Analysis (PCA) and K-Means clustering, while later developments introduced more advanced supervised classifiers such as Support Vector Machines (SVMs) (Jiang et al., 2011) and Random Forests (RFs) (Pal, et al., 2003).

With the rapid expansion of Earth observation data and advancements in computing power, machine learning approaches have evolved to handle increasingly large and complex datasets. Improved algorithmic design and the availability of specialized hardware have made it possible to apply computationally intensive methods such as deep learning and convolutional neural networks that were previously avoided due to high processing demands (Hänsch et al., 2018).

The continued growth of remote sensing "big data," supported by advances in cloud computing and parallel processing, has thus driven a shift from traditional machine learning methods to more advanced deep learning frameworks (Zhang et al., 2022).

2.1.5.2. Deep learning approaches to disturbance mapping

Deep learning techniques gained prominence in remote sensing due to their ability to learn hierarchical and non-linear representations directly from data, enabling the joint modeling of spatial, spectral, and contextual information from multisource inputs. Deep neural networks (DNNs) overcome key limitations of traditional machine learning by replacing hand-crafted features with data-driven feature learning, allowing complex interactions between sensors and scales to be captured implicitly (LeCun et al., 2015; Zhu et al., 2017). In particular, convolutional neural networks (CNNs) exploit local spatial connectivity and weight sharing to efficiently model spatial patterns, while deeper layers progressively encode higher-level semantic information (Gao et al., 2023). Early work by demonstrated the potential of neural networks to integrate multisource data, such as Landsat and topographic variables, outperforming conventional statistical classifiers. More recent CNN-based fusion frameworks explicitly leverage these architectural properties for multisensor integration, resulting in improved robustness and generalization compared to conventional machine learning approaches (Xu et al., 2018; Ye et al., 2019). Such architectures are particularly well suited for complex remote sensing classification tasks where sensor characteristics, spatial context, and non-linear feature interactions play a critical role.

Deep learning methods are increasingly applied in ecological research. For example, Rammer & Seidl, (2019) used bark beetle outbreaks in conifer-dominated forests to demonstrate the potential of DNNs for predicting both short-term infestation risk and long-term outbreak dynamics at landscape scale. This study highlighted the potential of deep neural networks as a core component of future forest disturbance forecasting systems.

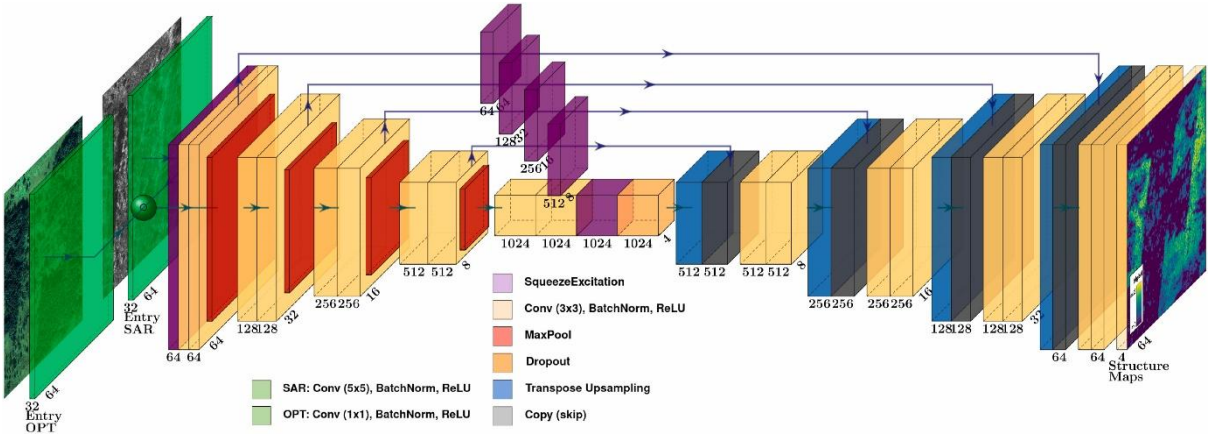

Figure 4: Modified Unet model support pixel-wise mapping of forest height, mean height, fractional cover, and stem density using high-resolution X-band SAR and optical images. (Source: Gazzea et al., 2023).

2.1.5.3. Foundation Models for Earth Observation

Traditional forest monitoring has relied on task-specific models focused on species classification, disturbance detection, or forest height estimation (Fassnacht et al., 2016; Potapov et al., 2021; Senf & Seidl, 2020). While these approaches simplify label collection and enable large datasets, they often yield localized results with limited transferability. Common remote sensing features such as vegetation indices, backscatter polarizations, and InSAR coherence capture structural information but remain noisy and sensor-dependent.

Recent advances in foundation models (FMs) offer a scalable alternative. These models learn generalizable representations from massive, multi-sensor Earth observation datasets through self-supervised pretraining, followed by fine-tuning for specific downstream tasks (Klemmer et al., 2025). FMs such as Prithvi-EO-2.0 (IBM–NASA) and TESSERA (Hong et al., 2024) have demonstrated state-of-the-art performance in scene classification and semantic segmentation (Szwarcman et al., 2025).

A key milestone is Google's AlphaEarth Foundation (AEF) model (Brown et al., 2025), which integrates multimodal and temporal information across global scales. AEF combines Sentinel-

1 SAR, Sentinel-2 optical, GEDI, ERA5, and auxiliary data (e.g., GBIF, geotagged Wikipedia entries) into a unified spatial grid, learning robust 64-dimensional embeddings at 10 m resolution (see figure 5). Annual embedding summaries, available from 2017 onward via Google Earth Engine, encapsulate cross-sensor information without requiring preprocessing such as cloud masking or feature engineering. In this study, these AEF embeddings are used to integrate multi-source environmental information into downstream learning tasks.

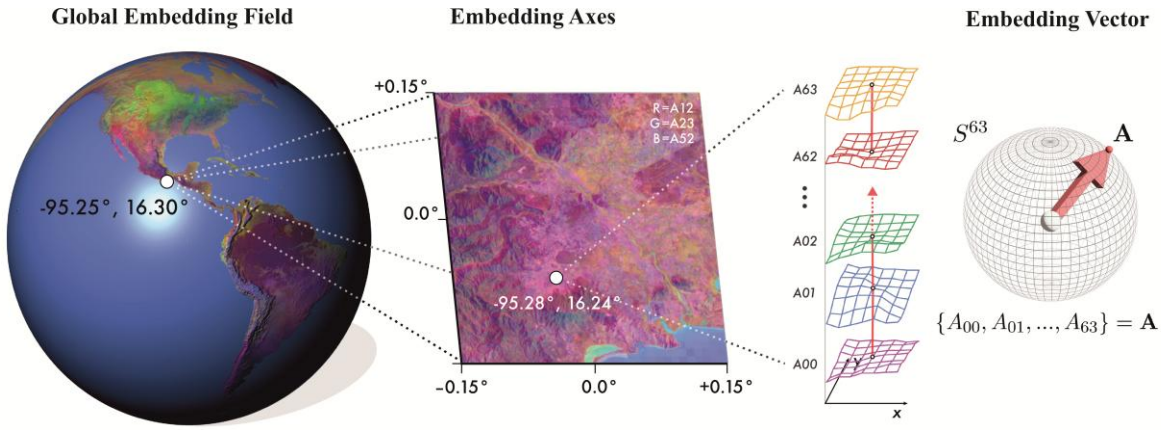

Figure 5: Conceptual diagram of the AlphaEarth Foundation embedding field. (Source: Brown et al., 2025)

2.1.5. Remote sensing products and techniques for forest disturbance mapping

Large-scale forest disturbance monitoring has advanced rapidly through both global and regional mapping products. Global Forest Change (Hansen et al., 2013a), Global Forest Watch, and the GEDI-based Global Ecosystem Dynamics datasets provide annual information on canopy loss and structure, while the European Forest Disturbance Atlas (Senf et al., 2017; Senf & Seidl, 2020) offers harmonized disturbance maps across Europe based on Landsat time-series segmentation. Several countries maintain national operational systems including the Czech Kůrovcová mapa for bark-beetle damage (Lukeš, 2021), Germany's Waldzustandsmonitoring, and Austria's bark beetle monitoring portals (Löw & Koukal, 2020), each using distinct algorithms, typically threshold-based or spectral-trajectory methods. In addition, numerous regional studies employ established time-series algorithms such as Landsat-based Detection of Trends in Disturbance and Recovery (LandTrendr), Breaks For Additive Season and Trend (BFAST), and Continuous Change Detection and Classification (CCDC) to identify disturbance hotspots and characterize long-term forest dynamics.

Advanced time-series and multisensor remote sensing methods now underpin most large-scale forest disturbance analyses. Contemporary frameworks increasingly rely on temporal segmentation algorithms, particularly LandTrendr, which extracts disturbance and recovery

trajectories from dense Landsat time series while reducing phenological and atmospheric noise (Kennedy et al., 2010; Senf & Seidl, 2020). These approaches flexibly capture both abrupt mortality events and gradual regrowth by modelling changes in spectral indices, especially those derived from the SWIR domain, such as NBR and Tasseled Cap Wetness, which consistently emerge as the most sensitive predictors of disturbance magnitude and timing (Paulino et al., 2024).

In parallel, the field has shifted toward multisensor Earth observation, integrating optical, SAR, lidar, and UAV data to overcome the spatial, spectral, and temporal constraints of single-sensor time series (Paulino et al., 2024). Multi-level data fusion (pixel, feature, and decision level) has improved disturbance detection robustness, while machine learning models, especially Random Forest and deep CNN architectures, increasingly dominate large-area mapping. Sentinel-1 and 2 based bark beetle monitoring pipelines further demonstrate the value of high-resolution, multisensor annual composites for operational early warning (Dalponte et al., 2022).

2.1.5. Forest height mapping in remote sensing

While forest disturbance mapping is increasingly based on multisensor techniques, parallel advances have transformed how forest structure, particularly vegetation height, is estimated using remote sensing. Multi-sensor vegetation height mapping has grown rapidly in response to the limitations of individual sensors in capturing forest structural complexity. Early integration attempts combined optical and single-polarization SAR predictors through simple feature concatenation (Liu et al., 2019), yielding only modest improvements. Recent work, however, shows that advanced fusion strategies incorporating optical, multi-frequency SAR, and temporal observations substantially increase prediction accuracy.

Furthermore, incorporating spaceborne LiDAR, especially GEDI and ICESat-2, have been essential in providing direct 3D structural measurements and greatly strengthen satellite-based height models (Lei et al., 2024; Sothe et al., 2022). Studies repeatedly demonstrate that combining LiDAR metrics with optical and SAR predictors outperforms any individual sensor, with correlation coefficients rising from <0.50 for single-sensor approaches to 0.60–0.70 for fused systems (Wang et al., 2019).

Sensor complementarity is a central driver of improved performance. Optical Sentinel-2 bands capture canopy vigor and spectral variation, typically achieving correlations around 0.60 on their own (Torres de Almeida et al., 2022), while SAR backscatter contributes structure- and moisture-sensitive information independent of cloud cover (Xi et al., 2022). Multi-frequency

SAR fusion, e.g., C-band Sentinel-1 with L-band ALOS-2, further enhances sensitivity to canopy and subcanopy elements, yielding R^2 values up to 0.72 in conifer forests (Xi et al., 2022). Machine learning approaches, especially Random Forest, Gradient Boosting, and deep neural networks, consistently outperform linear models in multi-sensor settings (Li et al., 2020).

Across studies, multi-sensor integration has been seen to reliably reduce RMSE, mitigates saturation effects in tall canopies, and improves robustness across forest types and terrain (Zhu et al., 2023). Emerging research now emphasizes uncertainty quantification, showing that fused models not only achieve higher accuracy but also produce more stable and reliable predictions than single-sensor counterparts (Liu et al., 2024; Sothe et al., 2022). Deep learning models, particularly CNNs, effectively capture hierarchical spatial structure and outperform classical approaches on multisensor datasets, (Liu et al., 2024). U-Net architectures further improve pixel-level height mapping, with correlations above 0.85 in optimized implementations. (Gazzea et al., 2023) demonstrates that single high-resolution X-band SAR and optical images can support pixel-wise mapping of forest height, mean height, fractional cover, and stem density at 0.5 m spatial resolution. Working in Western Norway across lowland to montane forests, the study introduces a modified U-Net integrating recent advances in forest-structure mapping (figure 4), and reports competitive performance compared with current state-of-the-art models.

2.2. Forest Disturbances in a Changing Climate

2.2.1. Escalation of forest disturbances

Forests cover approximately 41 million km^2 of the Earth's land surface and play a fundamental role in the global carbon cycle, regulating climate and supporting biodiversity (Forzieri et al., 2021). However, the global rise in temperature has been accompanied by an increasing frequency of droughts and heatwaves. Such climatic shifts profoundly alter forest ecosystems through complex interactions among temperature, precipitation, and radiation regimes (Hartmann et al., 2022). While natural disturbances have always been integral to forest dynamics (Turner et al., 2020), recent climatic changes have amplified both their frequency and severity. As a result, large-scale bark beetle outbreaks, drought-induced mortality, and megafires have become increasingly common across multiple regions (Sommerfeld et al., 2018). Mounting evidence thus indicates that disturbance regimes are undergoing fundamental

transformations in response to global climate change, with far-reaching implications for ecosystem stability and function.

Even regions previously considered resilient to climatic extremes now exhibit marked shifts in forest dynamics. For instance, the severe drought of 2018 in Europe intensified by consecutive heatwaves triggered unprecedented levels of forest disturbance, particularly across Central and Eastern Europe (Senf & Seidl, 2021b). These events corresponded closely with anomalies in soil moisture and vapor pressure deficit, highlighting drought as a principal driver of widespread forest mortality (Rakovec et al., 2022). Unlike anthropogenic disturbances, such as logging, natural events including windstorms, droughts, and insect outbreaks are inherently linked to climatic variability (Seidl, Thom, et al., 2017). Consequently, the recent escalation in climate-driven disturbances raises increasing concern about the long-term resilience and adaptive capacity of global forests.

2.2.2. Natural Disturbance Agents and Changing Regimes

Natural forest disturbances arise from biotic agents, such as insects and pathogens, and abiotic forces, including storms, droughts, and fires (Malmström & Raffa, 2000; Senf & Seidl, 2021b). In Europe, storms, fires, and bark beetles dominate, with their dynamics increasingly shaped by climate change (Seidl, Vigl, et al., 2017). Warmer, drier conditions intensify fire, drought stress, and bark beetle outbreaks, while warmer, wetter conditions favor wind and pathogen disturbances.

Evidence shows that these shifts are already altering disturbance regimes. (Pechony & Shindell, 2010) demonstrated that anthropogenic factors have replaced precipitation as the main driver of global fire activity, with temperature projected to dominate in the 21st century. Similarly, insect outbreaks have risen in frequency and severity, contributing to large-scale tree mortality comparable to fire (Kautz et al., 2017). Drought-induced mortality, particularly among tall trees, threatens carbon storage and ecosystem functioning (McDowell & Allen, 2015). Long-term empirical records from Europe confirm this intensification, with total forest disturbance impacts increasing markedly since 1950 and bark beetle damage doubling its share of total disturbance in the last two decades (Patacca et al., 2023) Comparative analyses further reveal that fire, wind, and bark beetle disturbances differ in their effects on ecosystem services and biodiversity (Thom & Seidl, 2016), and that increasing disturbance interactions can offset management gains in carbon sequestration (Seidl, 2014).

Overall, climate change is expected to intensify fire, insect, and pathogen disturbances, reshaping forest structure, composition, and function worldwide (Seidl, Vigl, et al., 2017). Among these, bark beetles are a major driver of tree mortality in temperate forests, with dynamics closely linked to climate and forest structure, underscoring their importance for anticipating future disturbance patterns.

2.3. Bark Beetle Outbreak dynamics in Central Europe and Czech Republic

Tree-killing bark beetles are important biotic disturbance agents in temperate biomes, influencing forest structure, composition, and functioning (figure 6). In particular, the spruce bark beetle (*Ips typographus*) primarily attacks Norway spruce (*Picea abies*), a key species for timber production across Europe (Hlásny, König, et al., 2021). Recent decades have seen a marked increase in disturbances caused by *I. typographus* (Bentz et al., 2010), and current projections indicate that this trend is likely to continue due to rising temperatures and recurrent droughts. This has raised concerns about timber market stability, environmental impacts, and associated socio-economic consequences (Hlásny, König, et al., 2021).

2.3.1. Climatic Drivers of Bark Beetle Outbreaks

Climate change influences bark beetle outbreaks through two main pathways. First, it directly affects beetle biology, including the timing of phenology, the number of generations per year, and off-season mortality (Baier et al., 2007). Second, it alters host tree vulnerability, as drought and heat stress weaken tree defenses, increasing the likelihood of successful beetle attacks(Huang et al., 2020). These mechanisms together increase the probability that beetle populations will exceed epidemic thresholds, resulting in larger and more frequent outbreaks. Studies project a 60–220% increase in bark beetle outbreaks during the 21st century, depending on climate and forest conditions (Dobor et al., 2018).

2.3.2. Forest Structure and Bark Beetle Outbreaks

In Central Europe, *Picea abies* has been extensively planted outside its natural range to meet industrial timber demands (Spiecker, 2000). Combined with widespread clear-cutting and long-term management practices favoring monocultures, these interventions have created homogeneous forests with limited resilience to disturbances (Hanewinkel et al., 2008). Recent syntheses show that these structurally simplified spruce forests have experienced unprecedented bark beetle outbreaks, strongly amplified by warming temperatures and

recurrent drought, pushing disturbance regimes beyond historical variability (Hlásny et al., 2025). Consequently, the interaction between recent climate trends and historical management practices has amplified bark beetle outbreaks in Europe.

Despite the negative consequences for timber production and forest ecosystems, bark beetle disturbances can also have positive ecological effects. They contribute to heterogeneity in forest structure, support biodiversity, and may create complex forest mosaics that enhance ecosystem functioning (Beudert et al., 2015; Donato et al., 2012). In unmanaged and conservation-oriented forests, such disturbances are increasingly recognized as key drivers of structural complexity and biodiversity, rather than purely pathological (Hlásny et al., 2025). Moreover, landscape diversity resulting from bark beetle disturbances can dampen the continuation of large-scale outbreaks, as heterogeneous forests are less prone to epidemic spread (Sommerfeld et al., 2018). However, whether bark beetle impacts are viewed as beneficial or detrimental largely depends on the societal values assigned to forest resources (Hlásny, Zimová, et al., 2021).

2.3. Post-Disturbance Forest Recovery

After a bark beetle outbreak, a significant change in forest ecosystems is expected as the prevailing ecosystem structure and composition is disrupted, this releases resources and breaks the original cycle of the pre-disturbance systems (Seidl et al., 2024). The reorganization phase, which is the time immediately following a disturbance is considered important for the development of the forest in the future, this because there is great potential for fundamental change during this window (Seidl et al., 2024; Seidl & Turner, 2022). The trees that are successful in getting established at this point are often able to determine the structure and species composition of the forest in the following decades or even centuries (Seidl et al., 2024; Seidl & Turner, 2022). The sudden increase in tree mortality experienced in Central Europe between the period 2018 and 2020, reached unprecedented levels not seen in at least 170 years. Followoing such an outbreak, it is essential to study the reorganizationto gain an immediate indication of potential long-term trajectories of forests under climate change (Seidl et al., 2024; Seidl & Turner, 2022).

Figure 6: Post-disturbance forest landscape in central Czech Republic following drought-driven bark beetle infestation and subsequent salvage logging. The site is characterized by extensive canopy removal, exposed stumps, and early-stage natural regeneration, illustrating the pronounced structural simplification and heterogeneity typical of bark-beetle-affected spruce stands.

2.3.1. Ecosystem resilience and the importance of the recovery phase

After a disturbance, the release of resources such as light, nutrients, and space occurs. This stage is critical because it determines whether the ecosystem will renew itself demonstrating resilience or shift toward an altered developmental trajectory, indicating forest change.

Post-disturbance forest trajectories can range from full resilience to fundamental ecological regime shifts. Under a resilient trajectory, structural and compositional attributes return to pre-disturbance conditions, whereas regime shifts occur when disturbances push the system into an alternative state, such as conversion from forest to non-forest vegetation. However, Seidl, (2014) argue that this binary view obscures intermediate but ecologically important forms of reorganization. They propose four pathways capturing the continuum of post-disturbance change: resilience (structure and composition remain unchanged), restructuring (structural change without compositional turnover), reassembly (compositional change with structural continuity), and replacement (changes in both structure and composition). Applying this framework to post-2018 drought and bark beetle impacts in Central Europe, Seidl, (2014) found that only 36.3% of forest patches followed a resilient trajectory, while 63.7% showed early

forms of reorganization. Replacement was the most prevalent pathway (43.1%), followed by reassembly (33.4%), indicating that structural and compositional transformations are already reshaping large areas of Central Europe's forests.

2.3.2. Regeneration pathways

The prominent role of advanced regeneration trees that established prior to canopy disturbance has been increasingly recognized in post-disturbance forest recovery across Central Europe (Bače et al., 2015; Petrovska et al., 2023). Advanced regeneration serves as a crucial biological legacy, carrying forward the structural and spatial patterns of pre-disturbance stands into the succeeding generation (Bače et al., 2015). This legacy effect ensures continuity in forest structure and composition, thereby supporting resilience and aiding ecosystem recovery after major disturbance events (Seidl & Senf, 2024). The persistence of pre-disturbance spatial patterns strongly influences the organization of regenerating stands, contributing to the maintenance of structural complexity in early-seral forests (Bače et al., 2015).

Empirical studies have demonstrated that pre-disturbance spatial legacies play a decisive role in shaping post-disturbance forest structure, particularly in montane spruce forests (Bače et al., 2015; Seidl et al., 2024; Senf et al., 2019). For instance, surviving Norway spruce (Picea abies) and rowan (Sorbus aucuparia) individuals were frequently found clustered around the locations of former canopy trees, snags, and stumps indicating a strong overstory understory neighborhood effect (Wild et al., 2014). This spatial relationship is often mediated by microenvironmental factors such as the availability of suitable deadwood microsites and reduced competition from understory vegetation beneath residual canopy cover (Żywiec & Ledwoń, 2008). Together, these findings underscore the pivotal role of advanced regeneration and spatial legacies in determining the trajectory and structural complexity of post-disturbance forest development.

3. Study Area and Workflow of Methodology

3.1. Study Areas

The first study in the thesis examines all forested area in the Czech Republic (figure 7) (2.67 million ha; 34.1% forest cover). Norway spruce dominates (48.8%), followed by Scots pine (16.1%) and broadleaf species such as beech (9%) and oaks (7.5%). The current forest structure reflects two centuries of intensive spruce planting in ecologically unsuitable sites, resulting in homogenized stands with long rotation periods (>100 years) and increased vulnerability to disturbance. Historically, windthrows were the main initiators of *Ips typographus* outbreaks. After 2017, this regime shifted dramatically as severe multi-year drought, rather than wind, triggered an unprecedented, country-wide bark beetle outbreak.

The height-structure and recovery analyses focus on the most severely affected region (Figure 7). This region was defined as the most affected hotspot during the national-scale disturbance assessment. The hotspot spans ~9,000 km² 210–837 m a.s.l., with mean annual temperatures of 7.6–9.3 °C and annual precipitation of 670–887 mm (2000–2022). Forest cover is ~35%, dominated by Norway spruce (~70%) due to long-standing plantation forestry. These structural and climatic conditions, combined with recent drought, drove the extreme post-2018 mortality.

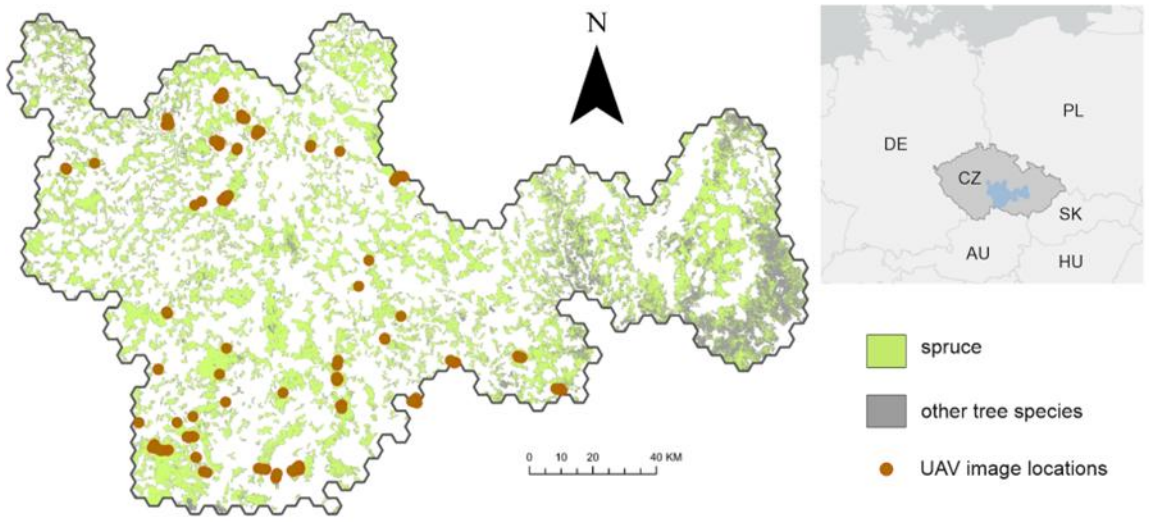

Figure 7: Study area representing major spruce mortality hotspots in Czechia (2016–2022). The map shows forest cover and the distribution of Norway spruce stands in 2015, prior to the outbreak. Locations of the 2023–2024 UAV acquisitions used as reference data for assessing post-disturbance landscape structure for height structure and recovery mapping are also shown. The inset indicates the study area's position within Czechia and Europe (Source: Washaya et al., 2025).

The fourth study (drought simulation) was conducted in a 40,928 ha landscape in the Czech Republic (figure 8), of which 45% (18,500 ha) is forested. Elevation ranges from 240 to 540 m a.s.l., with mean annual temperatures of 7.8–9.2 °C and precipitation of 604–683 mm (1961–2018). The forests are intensively managed, dominated by Norway spruce (57.7%) growing largely outside its ecological optimum. Other common species include Scots pine (10.7%), European beech (7.6%), and oaks (8.8%). Management follows a shelterwood system with ~120-year rotations.

Following prolonged drought, the area experienced a severe *Ips typographus* outbreak after 2018, which destroyed 40.6% of the spruce growing stock by 2021—its most extreme disturbance on record. These dynamics mirror the broader national-scale outbreak patterns described in the disturbance mapping study.

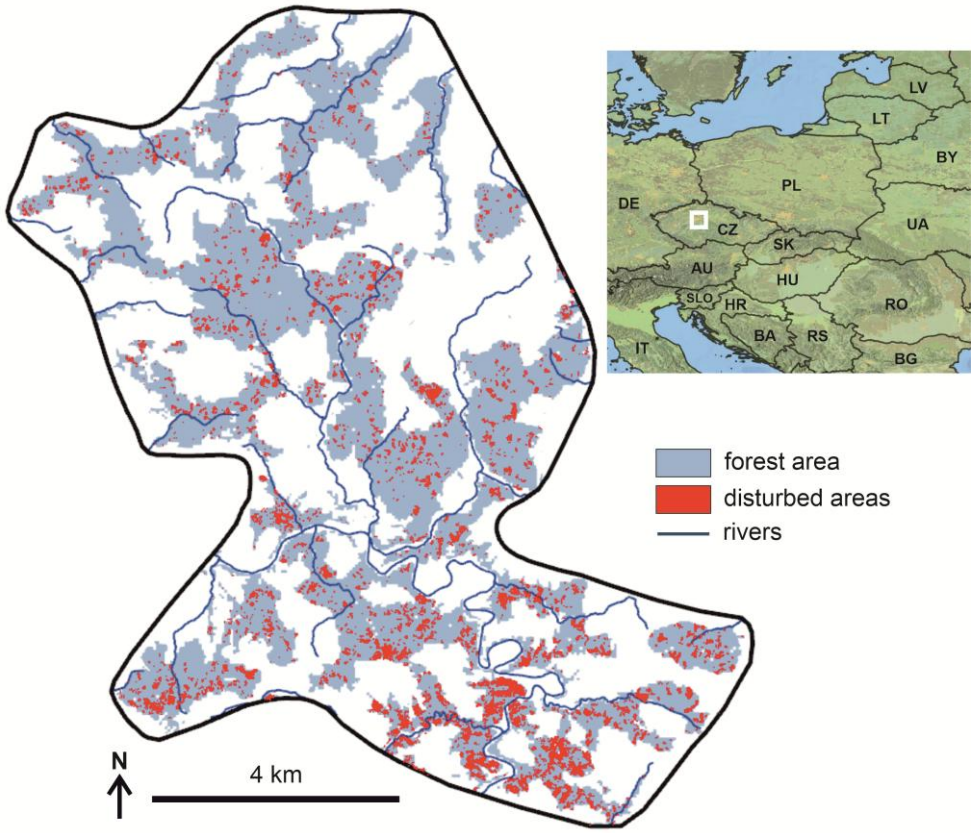

Figure 8: The position of the study landscape in Europe (a white square), forest cover of the landscape and the extent of bark beetle disturbance between 2018 and 2021 identified based on classification of satellite data. (Das et al., 2025)

3.2. Data Sources

3.2.1. Satellite Data for Disturbance, Recovery, and Height Mapping

All studies associated with this thesis, disturbance mapping, height structure mapping, recovery classification, and climate-disturbance simulation calibration, relied on multi-source remote sensing imagery. Across analyses, optical and SAR data were used to detect canopy disturbance, characterize vegetation height and recovery structure, and generate consistent annual time series.

Landsat 5 and Landsat 8 OLI imagery (2000–2022) formed the backbone of long-term disturbance mapping. Annual Landsat composites were used to derive NDVI, NBR, and NDWI, capturing canopy greenness, disturbance severity, and moisture stress. Sentinel-2 imagery (10 m) provided higher-resolution optical data for recovery and height mapping, supplying detailed spectral information during the post-disturbance period and we derived similar indices calculated with Landsat plus B3, B5, B11, B12, TCB, TCW).

Sentinel-1 VV, VH backscatter and sum variables were used for disturbance, recovery mapping and height due to their sensitivity to canopy structure, moisture, and debris removal, and for their ability to provide cloud-independent observations during peak disturbance years.

3.2.2. Reference Data for Disturbance, Recovery, and Height Mapping

Reference datasets from airborne and UAV platforms were used to train and validate the models for disturbance detection, post-disturbance recovery classification, and forest height estimation. The simulation analysis relied solely on the disturbance maps produced using the disturbance-mapping methodology and therefore required no additional reference data.

Airborne data for disturbance mapping.

High-resolution (25 cm) RGB stereo imagery from the national forest-change monitoring program provided reference data for canopy-loss detection. Photogrammetric nDSMs were differenced between annual survey campaigns to identify areas affected by disturbance. Data from 2019–2020—years dominated by salvage logging—were used, yielding ~235,000 polygons (76,000 ha) representing canopy loss primarily associated with bark beetle mortality.

UAV imagery for recovery and height mapping.

UAV surveys conducted in 2023–2024 provided very high-resolution RGB orthophotos (2–2.5 cm) across 40 representative sites in the main outbreak zone. These flights captured the full

gradient of post-disturbance conditions, from bare soil to dense regrowth, and supported both recovery and height reference datasets. For recovery classification, three vegetation states were manually delineated from the orthophotos: near-bare soil (<0.2 m), transient regrowth (≤2 m), and established regrowth (2–6 m), resulting in 600 polygons covering 123 ha. For height modelling, photogrammetric canopy height models (CHMs) were derived from the UAV imagery and resampled to 10 m resolution to align with satellite predictors, yielding 47,103 canopy height samples ranging from 0 to 40.82 m (figure 9).

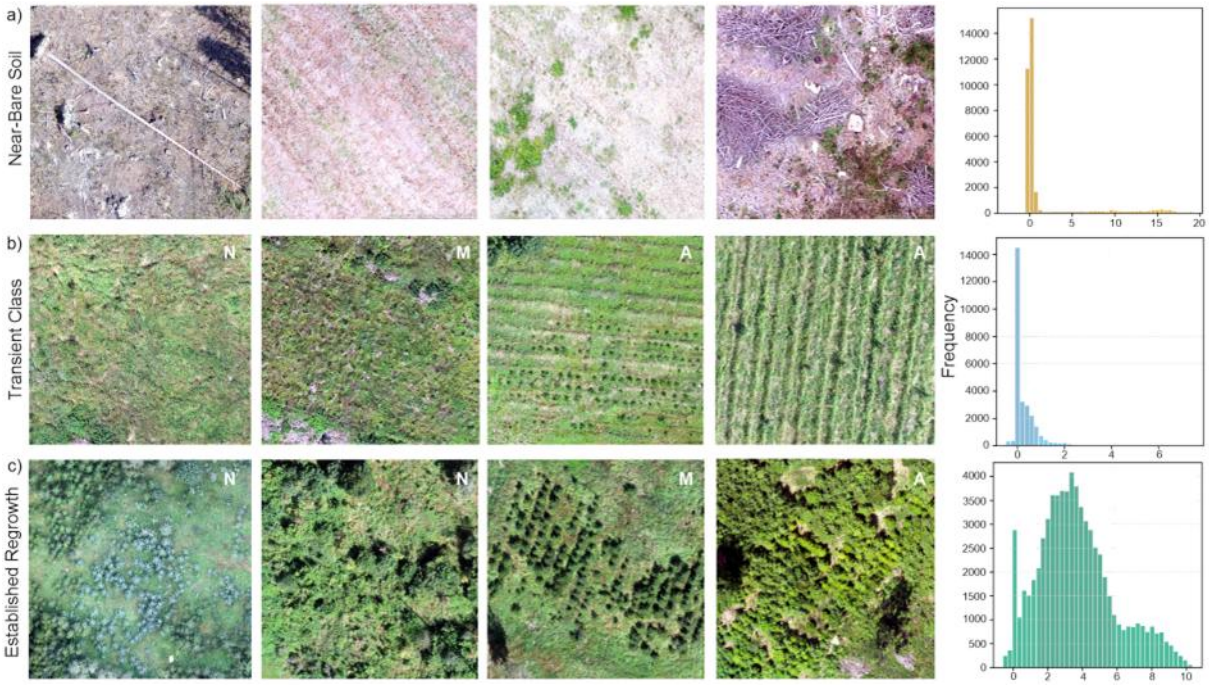

Figure 9: Representative examples of the three post-disturbance recovery classes derived from the UAV imagery across the study region: a) near-bare soil, b) transient class, and c) established regrowth. The transient class and established regrowth examples illustrate various vegetation structures resulting from replanting (characterized by regular tree spacing), from natural regeneration, or mixed approaches combining both pathways. Histograms represent the distribution of pixel-level vegetation heights (m), derived from Canopy Height Models from Drone imagery (Source: Washaya et al., 2025).

3.3. Data Pre-processing

Pre-processing procedures were standardized through the studies in this thesis to ensure consistency in disturbance mapping, height estimation, and recovery classification.

Landsat Collection 2 Surface Reflectance (SR) and Sentinel-2 Level-2A Surface Reflectance products were used. Clouds, cirrus, and shadows were masked using the respective QA bands, and annual cloud-free composites were generated for May–September. Spectral indices (NDVI, NBR, NDWI) were computed from these composites for all analyses. Sentinel-1 imagery underwent standard radiometric calibration, thermal noise removal, and terrain correction.

Annual VV and VH backscatter composites were produced from both ascending and descending orbits to capture structural changes across different viewing geometries.

For detecting canopy loss during peak outbreak years, interannual differences in optical and SAR predictors (dNDVI, dNBR, dNDWI, dVV, dVH) were computed by subtracting 2018 values from 2020 composites. These difference layers served as inputs to the disturbance model. Because reference data contained only disturbed samples, non-disturbed forest pixels were randomly sampled from areas outside mapped disturbance zones using the 2018 forest mask.

For recovery and height analyses, raw annual variables (rather than interannual differences) were used to better represent vegetation structure, height gradients, and temporal progression following disturbance. UAV-derived canopy height models were resampled to 10 m to align with satellite predictors.

3.4. Machine Learning and Deep Learning for Disturbance, Height, and Recovery Mapping

3.4.1. Random Forest (RF)

Machine learning methods were used for mapping Norway spruce distribution, post-disturbance recovery states, and vegetation height structure. Across all applications, Random Forest (RF) was chosen for its robustness to noisy predictors, limited training samples, and nonlinear relationships common in heterogeneous post-disturbance environments.

3.4.1.1. Spruce distribution and initial forest structure

RF classification was used to map the spatial distribution of Norway spruce for the reference year (2015) using optical indices (NDVI, NDWI). Training data were derived from airborne nDSM differencing, capturing mature spruce stands significantly affected during the outbreak. To reduce misclassification with visually similar conifers, polygons for Scots pine and Colorado blue spruce were manually digitized from high-resolution imagery. Additional broadleaf samples were taken from CORINE land cover. Stratified sampling generated 250,000 training and validation samples.

3.4.1.2. Post-disturbance recovery mapping

RF was used to classify three recovery states—near-bare soil, transient regrowth, and established regrowth—using non-differenced Sentinel-1 and Sentinel-2 predictors (NDVI, NBR, NDWI, VV, VH). Class imbalance was addressed by oversampling under-represented

classes and subsampling dominant ones. Data were split into training, validation, and testing subsets (70/15/15%). The trained model produced annual recovery maps capturing vegetation regrowth trajectories within the cumulative disturbance footprint.

3.4.1.3. Vegetation height structure modelling

RF regression was applied to estimate forest height using (i) selected optical/SAR predictors and (ii) AlphaEarth Foundations (AEF) embeddings. Samples were generated at 10 m resolution using UAV-derived canopy height models as reference data (47,860 samples). Stratified sampling ensured balanced height distributions. The RF model (100 trees) was implemented in scikit-learn and provided stable height estimates across a wide range of post-disturbance conditions.3.4.2. Convolutional Neural Networks (CNN)

Deep learning methods using U-Net architectures were employed to map forest disturbance and model vegetation height, leveraging their ability to capture spatial dependencies and multiscale patterns in optical and SAR imagery.

3.4.2.1. Disturbance mapping.

A U-Net convolutional neural network was used to classify disturbed and undisturbed forest pixels. Model inputs consisted of 256×256 patches of interannual difference layers (dNDVI, dNBR, dNDWI, dVV, dVH). The dataset was split into 70% training, 15% validation, and 15% testing. Encoder blocks used two 3×3 convolutions with ReLU activation followed by max pooling; decoder blocks mirrored this with bilinear upsampling and skip connections to recover spatial detail. A sigmoid-activated 1×1 output layer produced binary disturbance masks. This approach captured fine-scale disturbance patterns that are difficult to model using pixel-based machine learning methods.

3.4.2.2. Vegetation height estimation with U-Net.

For height mapping, a modified U-Net was implemented as a regression model. The architecture followed a standard contracting–expanding path, enabling extraction of both global and local features. Input channels varied depending on the predictor set: the traditional model used nine optical and SAR variables, while the AEF-based version used 64-channel feature embeddings. A softplus activation with a 0.1 m offset was applied in the output layer to ensure physically meaningful, non-negative height predictions. This model effectively captured the spatial heterogeneity of post-disturbance forest structure.

3.4.3. Accuracy metrics

Model performance was evaluated using a combination of classification and regression metrics to assess both disturbance detection and continuous forest structural predictions. Table 1 summarizes the evaluation metrics used, including measures of classification accuracy, error magnitude, and explained variance, providing a comprehensive assessment of model performance across tasks.

Table 1: Description of metrics used for the assessment of disturbance and spruce distribution classification

Metric	Equation	Description
Precision	TP / (TP + FP)	Accuracy of true positives calculated as the proportion of true positive and all positive predictions
Recall	TP / (TP + FN)	Accuracy of true positives calculated as the proportion of all correct predictions (TP and FN together)
F_1-Score	2 × (Precision × Recall) / (Precision + Recall)	Harmonic mean of the precision and recall
Overall Accuracy	(TP + TN) / (TP + TN + FP + FN)	The proportion of correct predictions reached across the entire dataset
RMSE	$\sqrt{[\Sigma(y_i - \hat{y}_i)^2 / n]}$	Root mean square error; measures the magnitude of prediction errors, with higher weight on larger errors
MAE	$\Sigma\lvert y_i - \hat{y}_i\rvert / n$	Mean absolute error; measures the average magnitude of prediction errors regardless of direction.
R^2	$1 - (SS_{res} / SS_{tot})$	Coefficient of determination; measures the proportion of variance in observed values explained by the model (0–1)

For vegetation height modelling, accuracy was quantified using 10-fold cross-validation, with model performance reported using root mean square error (RMSE), mean absolute error (MAE), and the coefficient of determination (R^2) between predicted and UAV-derived canopy heights. These metrics captured both absolute error and the strength of correspondence between predicted and observed height structure.

3.5. Analyses

3.5.1. Spatial and Temporal Disturbance Dynamics

To assess the spatial–temporal progression of bark beetle disturbances, annual disturbance maps were analyzed using a hexagonal grid covering the Czech Republic (500 m cell diameter, matching the typical mass-dispersal distance of *Ips typographus*). For each year, newly affected hexagons were classified into three categories: (i) emergence of new mortality clusters (no prior or adjacent disturbance), (ii) short-range spread (new disturbance within previously affected hexagons), and (iii) medium-range spread (disturbance in hexagons adjacent to those affected in the previous year). This classification distinguished local outbreak expansion from the appearance of new initiation zones. Temporal changes in spatial aggregation were evaluated using Ripley's G statistic, enabling detection of shifts in clustering intensity throughout the outbreak period.

3.5.2. Landscape-Scale Transformation

To assess the country-wide impact of the bark beetle outbreak, we applied a hexagonal grid with a 7 km cell size across the entire Czech Republic. The chosen cell size was determined based on an incremental spatial autocorrelation analysis of disturbance patch sizes, ensuring that the spatial scale captured meaningful clustering patterns of forest damage.

Within each hexagon, we evaluated the annual reduction of both total forest area and Norway spruce area, allowing us to identify temporal shifts in the distribution and intensity of forest damage. Subsequently, we quantified the cumulative disturbance impact for the period 2016–2022 by calculating, for each hexagon, the proportion of affected spruce area relative to the total spruce area.

Large-scale disturbance impacts were quantified using a 7 km hexagonal grid, selected based on incremental spatial autocorrelation of disturbance patch sizes to capture biologically meaningful clustering patterns. Within each hexagon, annual losses of total forest area and Norway spruce area were computed, followed by cumulative disturbance proportions for 2016–2022. Spatial hotspots of high disturbance intensity were identified using the Getis-Ord Gi* statistic, which evaluates whether local concentrations of disturbed area significantly exceed national-level expectations. Hotspot mapping served two purposes: (i) quantifying landscape transformation across the country and (ii) identifying the main outbreak zone used for subsequent recovery and height-structure analyses.

3.5.3. Forest Recovery Dynamics Analysis

Recovery trajectories were evaluated by analysing annual transitions among the three post-disturbance classes across the main outbreak zone between 2018 and 2024. Pixel-level transitions were examined under two definitions of recovery: (i) progression from bare soil to any vegetated state (transient or established regrowth), capturing early structural regeneration, and (ii) a stricter definition tracking transitions from bare soil to established regrowth (>2 m vegetation height), which excludes short-lived ruderal vegetation and better reflects long-term forest recovery. Reverse transitions were also quantified to identify regeneration failures and spatial instability.

To model recovery timing, a survival-analysis framework was applied. For each pixel, the number of years since initial disturbance and the occurrence (or absence) of recovery were recorded. Pixels that had not recovered by 2024 were treated as right-censored, ensuring that incomplete trajectories were retained without biasing recovery estimates. To minimize censoring effects from very recent disturbances, the analysis was restricted to pixels first disturbed between 2018 and 2021, ensuring at least three years of observation.

Recovery probability was then estimated using the Kaplan–Meier estimator, adapted to treat recovery, not mortality, as the event of interest. This non-parametric method provided cumulative recovery curves describing how quickly disturbed areas transitioned to vegetated states over time, while accounting for both observed and censored recovery pathways.

3.5.4. Patch-Level Recovery Structure

To characterize spatial structure during the recovery process, annual patch metrics were computed for all recovery classes using 8-neighbor connectivity. For each year, largest patch size and median patch size were calculated to quantify the persistence of bare-soil patches and the consolidation of regenerating vegetation. These metrics allowed assessment of structural homogenization versus diversification in post-disturbance landscapes.

3.6. Software Platforms and Packages

All pre-processing, processing, and analyses were conducted using Google Earth Engine (GEE), Python, and ArcGIS Pro.

Data pre-processing was performed primarily in GEE, where optical and SAR products were accessed, masked, composited, and resampled. GEE's Python API provided compatibility with local Python workflows and enabled the use of additional libraries. Within the Python

environment, NumPy supported numerical operations, scikit-learn was used for machine learning (Random Forest), TensorFlow for training CNN models, and Matplotlib for plotting. Pandas facilitated tabular data handling, rasterio supported raster I/O and manipulation, seaborn enabled statistical visualization, and the lifelines package was used for survival analysis of recovery trajectories.

ArcGIS Pro was used for spatial statistics, map production, and visualization of disturbance, recovery, and structural patterns.

4. Results

4.1. Disturbance mapping and bark beetle dynamics

Washaya, P., Modlinger, R., Tyšer, D., & Hlásny, T. (2024). Patterns and impacts of an unprecedented outbreak of bark beetles in Central Europe: A glimpse into the future? Forest Ecosystems, 11, 100243. https://doi.org/10.1016/j.fecs.2024.100243

Forest Ecosystems 11 (2024) 100243

Contents lists available at ScienceDirect

Forest Ecosystems

journal homepage: www.keaipublishing.com/cn/journals/forest-ecosystems

Patterns and impacts of an unprecedented outbreak of bark beetles in Central Europe: A glimpse into the future?

Prosper Washaya, Roman Modlinger, Daniel Tyšer, Tomáš Hlásny *

Czech University of Life Sciences in Prague, Faculty of Forestry and Wood Sciences Kamýcká 129, 165 00, Prague 6 – Suchdol, Czech Republic

ARTICLE INFO

Keywords:
Bark beetle disturbance
Remote sensing
Landscape transformation
Forest fragmentation
Central Europe

ABSTRACT

Natural disturbances have significantly intensified across European forests, with bark beetle outbreaks being the most rapidly escalating disturbance type. Since 2018, the Czech Republic (Central Europe) has become a Europe's disturbance epicentre due to the unprecedented outbreak of spruce bark beetle *Ips typographus* in the forests dominated by Norway spruce *Picea abies*. Here we provide novel insights into the impacts and dynamics of this disturbance from 2016 to 2022. The investigation is based on annual forest change maps developed by the classification of optical and Synthetic Aperture Radar satellite imagery. We identified seven major outbreak foci across the country, where the outbreaks culminated between 2018 and 2021. Most of the outbreak waves exhibited a symmetric shape, characterized by a three-year build-up phase, a single culmination year, and the subsequent decline. The substantial proportion of spruce remaining in the outbreak areas after the culmination point implies that resource depletion is an improbable cause for the outbreak's retreat. In the year of retreat, the proportion of spruce in the forest ranged between 26% and 36% in most of the outbreak areas. The disturbance dynamics manifested a transition from the emergence of new tree mortality spots in the early outbreak phase to their short-range expansion, suggesting density-dependent changes in bark beetle dispersal during the studied period. The core disturbance zone, pinpointed in 2022, covered an area of 9,000 km^2 and experienced a 38% loss in forest cover. Within this area, forest fragmentation increased significantly, leading to a greater forest patch complexity and reduced connectivity among the patches. The presented findings can serve as a glimpse into the future for other European regions, revealing the potential impacts of natural disturbances amplified by climate change.

1. Introduction

Natural disturbances are an important driver of ecosystem dynamics globally, with profound effects on forest demography, ecosystem functioning, and the provision of ecosystem services (Johnstone et al., 2016; Sommerfeld et al., 2018). Climate change amplifies most of the disturbances and modifies their interactions, which can result in regime shifts with hardly predictable societal and environmental consequences (Seidl et al., 2017; Turner and Seidl, 2023; Weed et al., 2013). In Europe, disturbance dynamics have significantly intensified during the last two decades (Patacca et al., 2023), with the major shift occurring after the series of hot and dry years that peaked in 2018 (Buras et al., 2020; Senf and Seidl, 2021a). This forest mortality wave was spatially aligned with soil moisture and vapor pressure deficit anomalies, implying an increasing role of drought in driving the disturbance dynamics (Senf et al., 2021; Senf and Seidl, 2021b). Strong drought legacy effects were detected in the following years, suggesting that the recovery processes were impaired and trees were prone to impacts from pests and pathogens (Schuldt et al., 2020).

Forest disturbances caused by insect pests and pathogens, intensified by high temperatures and extended droughts, are becoming increasingly significant (Huang et al., 2019; Netherer et al., 2019; Rouault et al., 2006). The processes involved are the compromised tree defence due to the aggravating climatic stress (Netherer et al., 2019), accelerated development of many insect pests, shortened generation time, increased fecundity and survival, and range expansion (Jactel et al., 2019). These effects have been particularly evident in spruce bark beetle *Ips typographus* (L.), which is the most significant outbreak species in Europe. *I. typographus* attacks Norway spruce *Picea abies* (L.) H. Karst. as its primary host (Biedermann et al., 2019) (Fig. 1), which constitutes ca 25% of the total forest growing stock in Europe (Hlásny et al., 2021a). In the past, outbreaks have been particularly severe in spruce forests planted outside

* Corresponding author.
E-mail address: hlasny@fld.czu.cz (T. Hlásny).

https://doi.org/10.1016/j.fecs.2024.100243
Received 1 May 2024; Received in revised form 6 August 2024; Accepted 12 August 2024

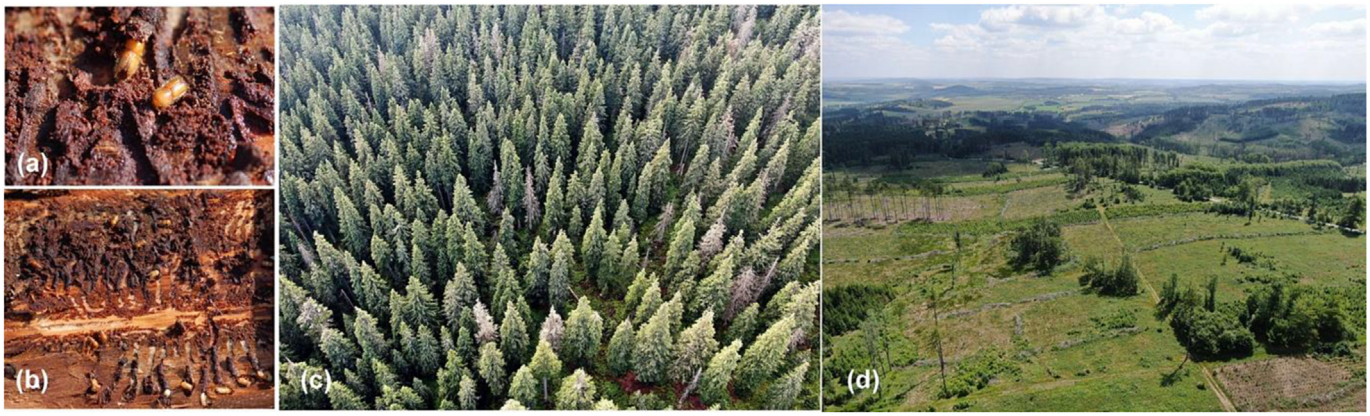

Fig. 1. Individual beetles (**a**) and breeding galleries of spruce bark beetle *Ips typographus* (**b**) created in spruce xylem and interrupting the transport of nutrients in a tree, leading to tree death; a single-tree mortality pattern that is typical of the endemic population phase (**c**); and a post-outbreak forest landscape treated by an extensive removal of dead trees in the central Czech Republic in 2023. Surviving host and non-host trees, and different phases of forest regeneration can be seen (**d**).

their natural distribution in Fennoscandia, the Baltic countries and European mountain ranges (DeVries et al., 2015; Spiecker et al., 2004). However, recently, there has been an increased outbreak intensity also in high latitudes, such as Sweden (Kärvemo et al., 2023), and in mountainous environments like the European Alps (Hallas et al., 2024).

Norway spruce poses efficient defences against bark beetles that include anatomical and chemical adaptations which are preformed or induced by the attack (Krokene, 2015). However, spruce, as an isohydric species, does not tolerate water potential dropping below a certain level and prevents water loss by closing its stomata (Netherer et al., 2021). This compromises the supply of non-structural carbohydrates, which play a central role in spruce defence to bark beetles (Hartmann et al., 2018; Huang et al., 2020). Intensifying climate change and spruce planting in suboptimal conditions are thus increasing spruce susceptibility to bark beetle attacks (Marini et al., 2017). Several thermal and photoperiod-regulated traits allow for the adjustment of *I. typographus* lifecycle across its distributional range, including overwintering mortality, spring swarming, generation timing, and voltinism (Baier et al., 2007; Bentz et al., 2019; Netherer and Hammerbacher, 2022). These traits make climate change a strong amplifier of bark beetle epidemics. The main underpinning effects include an increase in the annual number of generations, extended flight period, outbreak expansion to the previously thermally limited environments, and climatically-induced outbreak synchrony over large areas (Bentz et al., 2019; Hlásny et al., 2021a; Huang et al., 2020). The outbreaks of *I. typographus* are driven by cross-scale interactions that mainly include local host abundance and susceptibility, favourable weather, escape from natural enemies, and landscape-scale host distribution and connectivity (Raffa et al., 2008; Wermelinger, 2004). While the initial population build-up is typically associated with the increased abundance of windfelled or stressed trees, the ability to mass-attack trees is a key adaptation that enables the species to kill healthy trees once its populations have risen and sustain outbreaks in relatively healthy stands even after the inciting stress is relaxed (Hlásny et al., 2021a; Raffa et al., 2008). Outbreaks typically lose momentum after several years due to the depletion of local resources (Fig. 1d), unfavorable weather, intraspecific competition, the density-dependent build-up of natural enemies, defence priming, changes in symbiont communities, and different interactions of these factors (Biedermann et al., 2019; Wegensteiner et al., 2015). However, the mechanisms of epidemic downregulation and the possible alteration of these processes by climate change remain insufficiently understood (Biedermann et al., 2019).

Recent drought-driven outbreaks of *I. typographus* in Europe have differed from historical, mostly wind-driven dynamics, where drought predominantly acted as a modulating factor (Marini et al., 2017). A specific feature of these outbreaks was their large-scale spatial-temporal synchrony, which arose due to the effect of extreme weather conditions that affected large geographical areas (Senf and Seidl, 2018). The most distinct manifestation of these dynamics was the outbreak of *I. typographus* in the Czech Republic in 2017–2023 (Central Europe) that affected ca. 100 mil. m^3 of timber during the seven years of its duration (Hlásny et al., 2021b; Czech Forest Protection Service, internal data). The initiated cascade of impacts had severe social and economic implications, including timber price fluctuation due to the large amounts of harvested wood affected by bark beetles (Asada et al., 2023), which required active state intervention to stabilize the national forestry economy.

In this study, we investigated the patterns and impacts of this extensive outbreak across the country in 2016–2022. The addressed period encompassed the entire outbreak cycle, spanning from the initially scattered mortality pattern to the devastating culmination phase and the subsequent decline. By examining the full outbreak cycle at the scale of the country, we sought to gain insights into the ultimate impacts of such a natural disturbance amplified by climate change. First, we aimed to disentangle the overall disturbance dynamics and interpret its partial processes from the perspective of *I. typographus* ecology and population dynamics. Second, we sought to evaluate the overall degree of landscape transformation resulting from the outbreak. Given the extent of the affected area and the landscape-scale focus of the investigation, we employed spatial analyses of forest change maps produced by the classification of remote sensing data, which have been increasingly used in ecosystem disturbance research (Senf et al., 2017a, 2017b).

Acquiring this knowledge is crucial, as most of our current understanding of bark beetle dynamics and impacts originates from the outbreaks that occurred in a cooler past climate and were primarily associated with windthrows (Havašová et al., 2017; Mezei et al., 2017; Potterf et al., 2019). The dynamics of drought-driven outbreaks occurring in low-to-medium elevations, without the initial surplus of windfelled trees, can manifest different dynamics, mainly accounting for the different initial distribution of susceptible trees and stands (Kärvemo et al., 2023). Moreover, outbreak impacts on a uniform forest environment, such as that of planted spruce forests in Central Europe, may have long-lasting implications for the provision of ecosystem services and the post-disturbance recovery.

2. Materials and methods

2.1. Czech Republic as a study area

Forests of the Czech Republic cover 2.67 mil. ha, representing 34.1% of the land area. Norway spruce represents 48.8% of tree species composition, followed by Scots pine *Pinus sylvestris* L. – 16.1%. Broadleaf trees constitute 28.2% of the species composition, with the dominance of

the European beech *Fagus sylvatica* L. – 9% and oaks *Quercus* spp. – 7.5% (Ministry of the Environment of the Czech Republic, 2022). The Norway spruce mostly occurs in suboptimal conditions due to its widespread planting over the past two centuries. The historical focus of management on "simplicity and efficiency" (Messier et al., 2019) resulted in a homogenized forest structure that is particularly prone to bark beetle infestations and their uncontrolled spread. Additionally, the forest rotation period often exceeds 100 years, which further increases the forest's vulnerability to natural disturbances (Zimová et al., 2020).

The historical disturbance dynamics were dominated by windthrows that typically triggered local bark beetle epidemics. These cumulatively accounted for 29% of total harvests in 1982–2016. The disturbance regime has dramatically changed after 2017, with bark beetles becoming the dominant agent (Fig. 2). Contrary to the previous period, the outbreak was triggered by drought rather than wind and its pattern was spatially aligned with significantly low values of the standardized precipitation-evapotranspiration index (Hlásny et al., 2021b; Appendix A). While the majority of damage was caused by *I. typographus*, a certain proportion was attributed to the associated species such as *Pityogenes chalcographus* (L.), *Ips amitinus* (Eichh.) and *Ips duplicatus* (Sahl.). Notably, *I. duplicatus* contributed to the total bark beetle damage in 2015 by as much as 27% due to its regional outbreak in Silesia. By 2021, this damage decreased to 3%. The contribution of the remaining species was negligible.

2.2. Spruce distribution and disturbance mapping

The forest cover mask, which spatially constrained both disturbance and spruce distribution mapping, was based on the forest categories "broadleaved", "coniferous", and "mixed" of the seamless landcover classification of Europe Corine Landcover (European Environment Agency, 2020). This dataset demonstrated a high degree of accuracy when compared with national forest inventory data (Trombik and Hlásny, 2013).

The disturbance mapping was based on a supervised classification of the Landsat 8 OLI optical imagery and the Synthetic Aperture Radar (SAR) Sentinel-1 C-band data with the VH polarization. The optical data included the Surface Reflectance products corrected for the Top-of-the-Atmosphere effects. Clouded areas were masked and excluded from the analysis. The SAR data processing involved radiometric calibration, converting the raw data into the backscatter values, and speckle filtering. A geometric correction was applied to address spatial distortions inherent in radar images and ensure that SAR and optical data are spatially aligned. A terrain correction was applied to remove topographic effects. The optical variables used for disturbance mapping included the normalized difference vegetation index (NDVI), normalized burn ratio (NBR), and the normalized difference water index (NDWI). Optical and SAR imagery was taken from multiple dates between May 1 and July 15 each year, with less than 10 percent cloud cover in the optical data.

The training data, which provided an accurate description of disturbance occurrence, were based on the national airborne-based forest change mapping (Source: Forest Management Institute, Czech Republic). These data are collected annually for half of the country and consist of RGB stereo images with a resolution of 25 cm. Photogrammetric analysis of these images was used to create the normalized digital surface models (nDSM). Changes in forest cover, indicative of harvests and disturbances, are identified by comparing the nDSMs between consecutive mapping campaigns. Disturbance detection was thus based on changes in tree height. For our study, we aggregated data from the years 2017, 2018, and 2019, which were unaffected by planned harvesting, as it was prohibited during this period across most of the country.

A convolutional neural network (CNN) model was used to map the disturbed areas on an annual basis. The input layer of the model receives four channels representing the differences in three vegetation indices and SAR backscatter between 2016 and 2019. A stratified sampling approach was employed to generate 655,000 training data, which were randomly split into training, validation, and testing sets in the proportions 70:15:15. The CNN included several convolutional layers, followed by the batch normalization (Ioffe and Szegedy, 2015). The activation function in these layers was the Rectified Linear Unit (Agarap, 2018) The output layer uses a sigmoid activation function to generate values that indicate the presence or absence of the disturbance. To avoid model overfitting, the model was trained using a binary cross-entropy loss function, augmented with an L2 regularization term ($\lambda = 0.001$). Additionally, hyperparameter optimization was conducted to refine the model's settings and improve its performance.

That the planned harvesting was significantly reduced between 2018 and 2021 makes the attribution of the identified forest changes to the disturbance reliable. However, the effect of planned harvests and disturbance became intertwined outside this period. To further mitigate

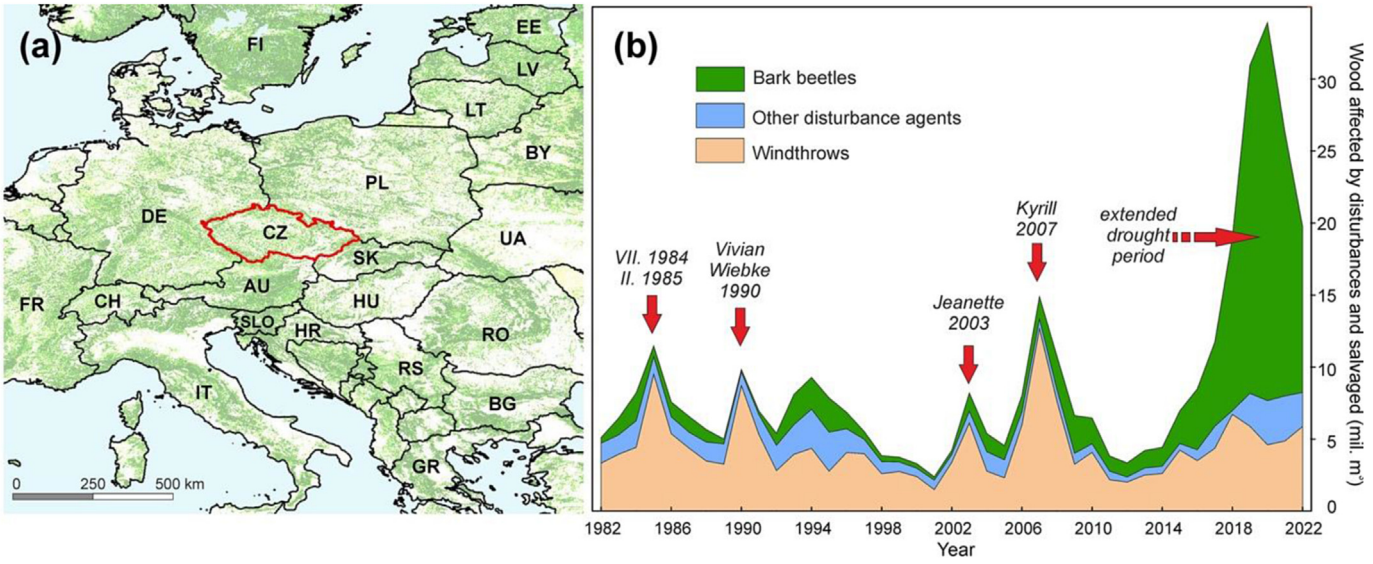

Fig. 2. (**a**) Position of the Czech Republic in Europe with forests in the background (Source: CORINE Land Cover, EEA, 2018). Country codes according to the European norm ISO-3166 Alpha-2 are displayed. (**b**) Development of disturbed and harvested wood in the Czech Republic attributed to the main disturbance types. The arrows indicate the major windthrows and the extended drought spell that initiated the most recent bark beetle outbreak. The 2018–2022 peak depicts the outbreak of *I. typographus* investigated here. Sources: Forest Management Institute of the Czech Republic, Czech Statistical Office.

the possible misattribution, the disturbance mapping was constrained by the spruce area, where most of the disturbance occurred across the entire study period.

The classification of Norway spruce distribution was conducted for the reference year 2015. The classification was based on the random forest classifier and used optical imagery only (NDVI, NDWI). The training data were represented by polygons obtained through the nDSM differencing from the period 2018–2020 (which marks the outbreak culmination phase), which involved almost exclusively mature Norway spruce stands. Due to a certain spectral mismatch of spruce with other conifers, we manually created training polygons for Colorado blue spruce *Picea pungens* Engelm. and Scots pine *P. sylvestris*, which locally prevailed in species composition. The species were visually identified by using a very high-resolution Google Earth imagery and digitized on-screen. The training data for the broadleaved species were defined based on the Corine Landcover category "broadleaved" (European Environment Agency, 2020). A stratified sampling was applied to generate 250,000 training data that were split into training and validation sets in the proportion 80:20. Although the training data included mature spruce stands only, the final classification may also include younger age classes which are not attractive for bark beetles.

The accuracy of all classifications was assessed based on four metrics including the overall accuracy, precision, recall, and the *F1*-score (see Appendix B; Table B1 for more detailed description). The SAR data were processed using the Python SNAPPY, which is based on the SNAP API (European Space Agency, 2015). The analysis of optical data and classifications was conducted using the Google Earth Engine (Gorelick et al., 2017).

2.3. Assessing spatial-temporal outbreak dynamics

The spatio-temporal dynamics of bark beetle infestations and the associated tree mortality were investigated using a hexagonal design covering the entire Czech Republic. Each individual hexagon had a diameter of 500 m, corresponding to the estimated distance of mass dispersal of *I. typographus* (Kautz et al., 2011; Ripley, 1981; Wermelinger, 2004; Wichmann and Ravn, 2001). This design was used to pool the overall spruce mortality in the studied period as follows.

i. Emergence of new mortality spots: These are disturbance occurrences within the hexagons that had not previously experienced any damage and do not neighbour any hexagons that experienced damage in the previous year.
ii. Mortality spots resulting from the short-range bark beetle dispersal: this includes mortality patches appearing within hexagons where damage was recorded in the preceding year.
iii. Mortality spots resulting from the medium-range bark beetle dispersal: this includes mortality patches appearing in hexagons adjacent to those where damage was recorded in the previous year.

This analysis was complemented by evaluating the temporal changes in spatial clustering of the disturbed areas using the Ripley's *G* statistics (Ripley, 1981).

$$G(r) = \frac{\text{number of pairs of data points within the distance} \leq r}{\text{total number of pairs of points}}$$

where r is a distance between the points. The statistic evaluates the deviation of a point process from spatial homogeneity, i.e., the theoretical random spatial distribution. The function thus describes the level of clustering or dispersion of the data. To facilitate the analysis, each pixel classified as a disturbance in the underlying disturbance maps was represented by a single point.

2.4. Assessing outbreak impacts

To assess the country-wide impact of the outbreak, a hexagonal grid with a 7-km cell size was designed with the cell size determined based on the evaluation of incremental autocorrelation of disturbance patch sizes. Within each hexagon, the reduction of the total forest area and the spruce area was evaluated on an annual basis and shifts in damage distribution were identified.

Next, the cumulative disturbance impact between 2016 and 2022 was evaluated for each hexagon in terms of the proportion of affected spruce area out of the total spruce area. These values were used to identify major disturbance hotspots across the country using the Getis-Ord Gi* statistics (Getis and Ord, 1992). The statistics identify clusters of points with values higher or lower in magnitude than expected by random chance. It considers neighbouring features and compares their local sum to the sum of all features. A statistically significant *z*-score results when the local sum significantly deviates from the expected value. Positive *z*-scores indicate hot spots (intense clustering of high values), while negative *z*-scores indicate cold spots (intense clustering of low values). The statistics is calculated as:

$$\text{Gi}^* = \frac{\sum_{j=1}^{n} w_{i,j}\, x_j - \overline{X} \sum_{j=1}^{n} w_{i,j}}{S \sqrt{\frac{\left[n \sum_{j=1}^{n} w_{i,j}^2 - \left(\sum_{j=1}^{n} w_{i,j}\right)^2\right]}{n-1}}}$$

where, i and j are the coordinates of the investigated spatial features (hexagons), x_j is the attribute value for the spatial unit j, and $w_{i,j}$ is the spatial weight between i and j. $\overline{X}$ is the mean and S is the standard deviation of the attribute values, and n is the total number of features.

2.5. Assessing landscape transformations

The degree of landscape transformations was evaluated within the largest disturbance hotspot (as identified through the Getis-Ord Gi* statistics) on an annual basis by using a suite of landscape metrics (Table 1). We separately investigated the properties of forest cover and disturbed areas, two defining characteristics of the studied system. Each year's assessment included impacts that occurred in all the preceding years. The calculations were conducted by means of the Python library Pylandstats (Bosch, 2019).

3. Results

3.1. Mapping spruce distribution and bark beetle disturbance

The classification of tree species composition (Fig. 3), with a focus on creating an accurate spruce map, demonstrated a fairly good performance in terms of all metrics. The precision achieved was 0.82, the recall 0.79, and the *F1*-score 0.81 (Table 2). Notably, the *F1*-score exceeded 0.81 for Norway spruce, Colorado blue spruce, and broadleaves, but reached 0.74 only for the Scots pine (Appendix B; Table B2). The mapped proportion of spruce area relative to the total forests in the country was 51.3%, which corresponds closely to the 48.8% of Norway spruce proportion out of the total growing stock reported in the national forestry statistics.

The overall accuracy of disturbance classification achieved was 0.81 (Table 2). Testing the prediction maps for the years 2016, 2017, 2018, and 2019 against the independent testing data demonstrated good performance as well; however, the accuracy varied across the years (Appendix B; Table B3). The overall accuracy ranged from 0.72 to 0.78, with the highest value attained in 2019. The precision was highest in 2019 (0.84) indicating that the model reliably identified true disturbance

Table 1
Landscape metrics used to characterize landscape transformations due to the bark beetle outbreak within the largest disturbance hotspot in the Czech Republic. The metrics are calculated on an annual basis for two landcover classes – forest and disturbed areas. Patch refers to a single forest or disturbance polygon. Landscape refers to the entire disturbance hotspot.

Metrics, abbreviation	Description	Type of metrics	Units
Total patch area (TA)	Total area covered by patches of a specified landcover class (i.e., forest or disturbed areas)	Landscape	ha
Patch density (PD)	Number of patches per unit area	Landscape	No·ha^{-1}
Euclidian nearest neighbour (EUCL)	Mean edge-to-edge distance to the nearest patch of the same class	Landscape	m
Effective mesh size (MESH)	A measure of landscape fragmentation. Value range: Area of a single cell – maximum fragmentation, where a class covers a single cell only. Total area of the landscape – maximum aggregation, where the landscape consists of a single patch only[a]	Landscape	ha
Largest patch area index (LPI)	The size of the largest patch relative to the total area of the landscape	Landscape	%
Median patch size (MA)	Median size of all patches of a specified class	Patch	ha
Patch shape index (SH)	A measure of complexity of patch shapes calculated as the ratio of patch perimeter and the square root of patch area. Range: 1– compact, >1 increasingly irregular	Patch	–

[a] see Appendix C for more information.

Table 2
Performance metrics of disturbance and spruce distribution mapping. Range of values for years 2016–2019 is indicated.

Metrics	Accuracy	Precision	Recall	*F*1-score
Tree species mapping (validation set, 20% of the training data)	0.83	0.82	0.79	0.81
Disturbance mapping (validation set, 15% of the training data)	0.81	0.88	0.75	0.80
Disturbance mapping (independent testing samples for years 2016, 2017, 2018, and 2019)	0.72–0.78	0.72–0.84	0.70–0.74	0.71–0.75

occurrences. On the contrary, the performance was lowest in 2016 (0.72). Recall peaked in 2018 at 0.74, indicating a fairly high model's performance in disturbances mapping compared to the remaining years, where the values ranged from 0.70 to 0.72. The *F*1-score approached 0.75 in all years except for 2016, where the metric was 0.71. This demonstrates a fairly good balance between the precision and recall, i.e., the balance between minimizing false positives and correctly identifying the true disturbance occurrences. The overall quality of disturbance mapping (Fig. 3) is supported by the fact that the cumulative loss of Norway spruce area during the studied period was 17%, which corresponds to ca. 20% loss of growing stock (ca. 100 mil. m^3) reported in the national forestry statistics.

3.2. Spatial-temporal disturbance patterns

The relative change in spruce area within the 7-km hexagonal grid (Fig. 4a) was inspected using Getis-Ord Gi* statistics to identify

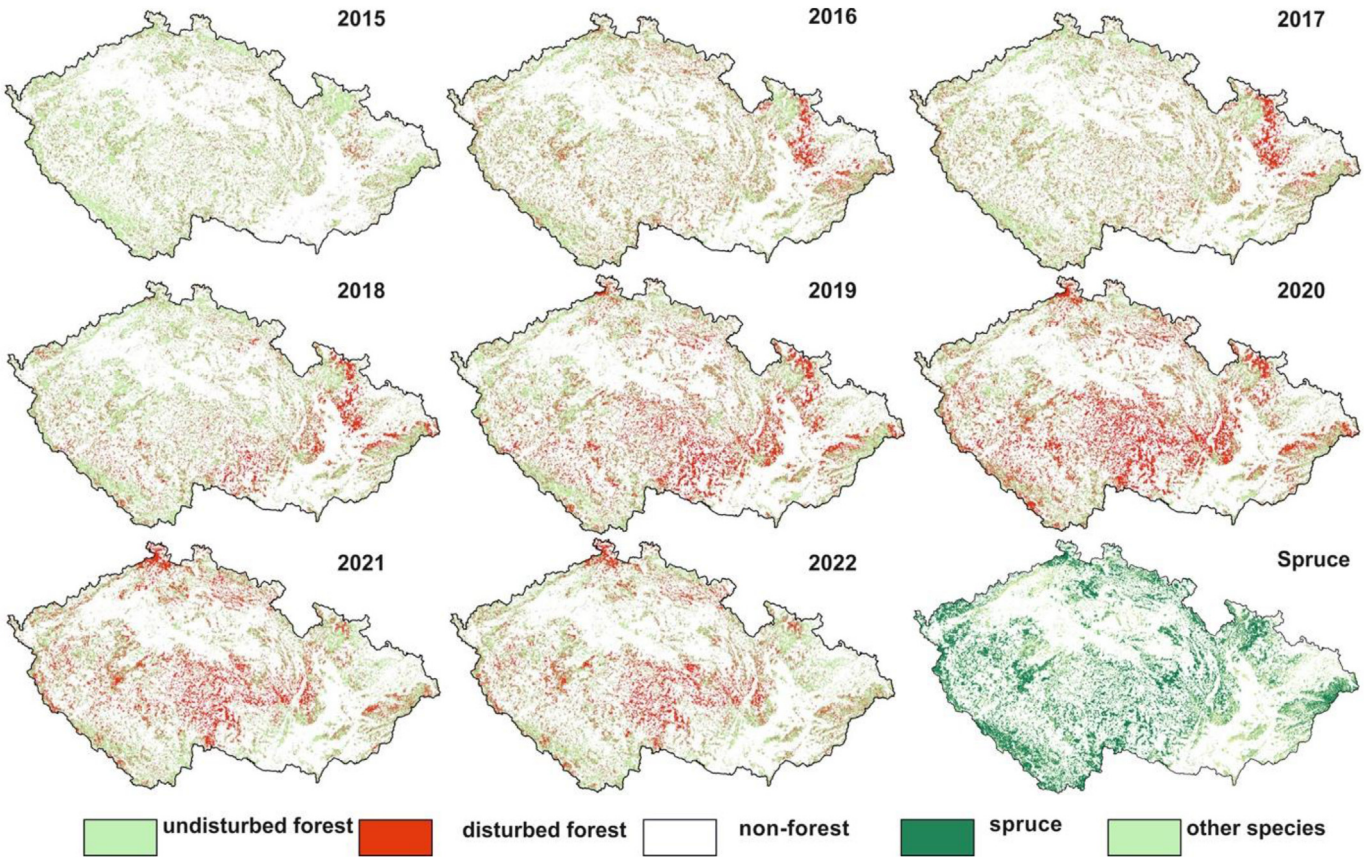

Fig. 3. The temporal progression of bark beetle disturbance in the Czech Republic mapped based on satellite imagery. The mapped distribution of spruce in the year 2015 is also presented.

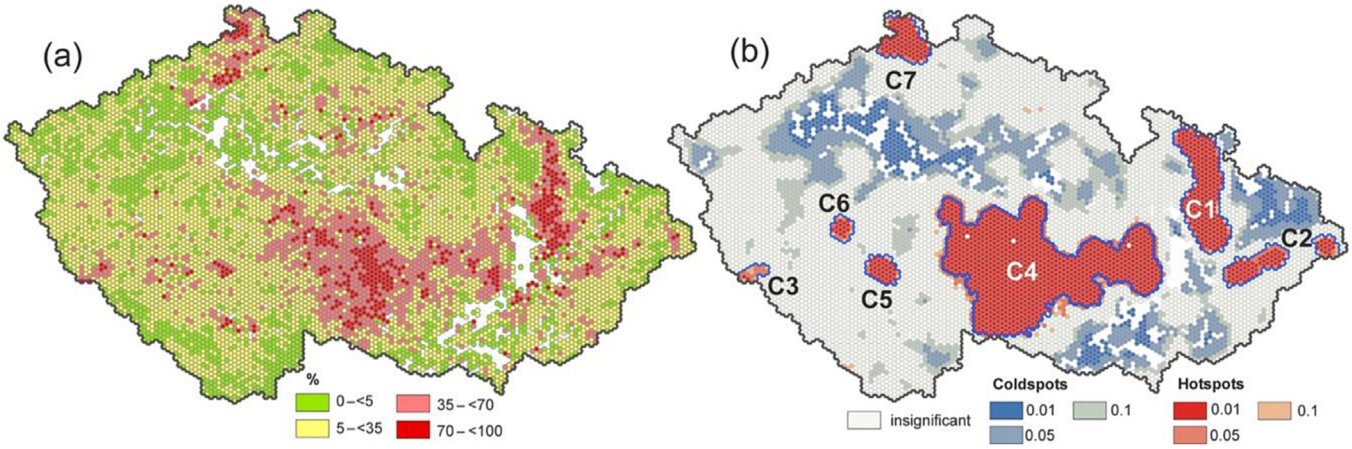

Fig. 4. (**a**) Cumulative loss of spruce area during 2016–2022 within the hexagonal grid with a 7-km cell size. (**b**) Disturbance hotspots identified by means of the Getis-Ord Gi* statistics. Alpha levels indicate the statistical significance of the identified features.

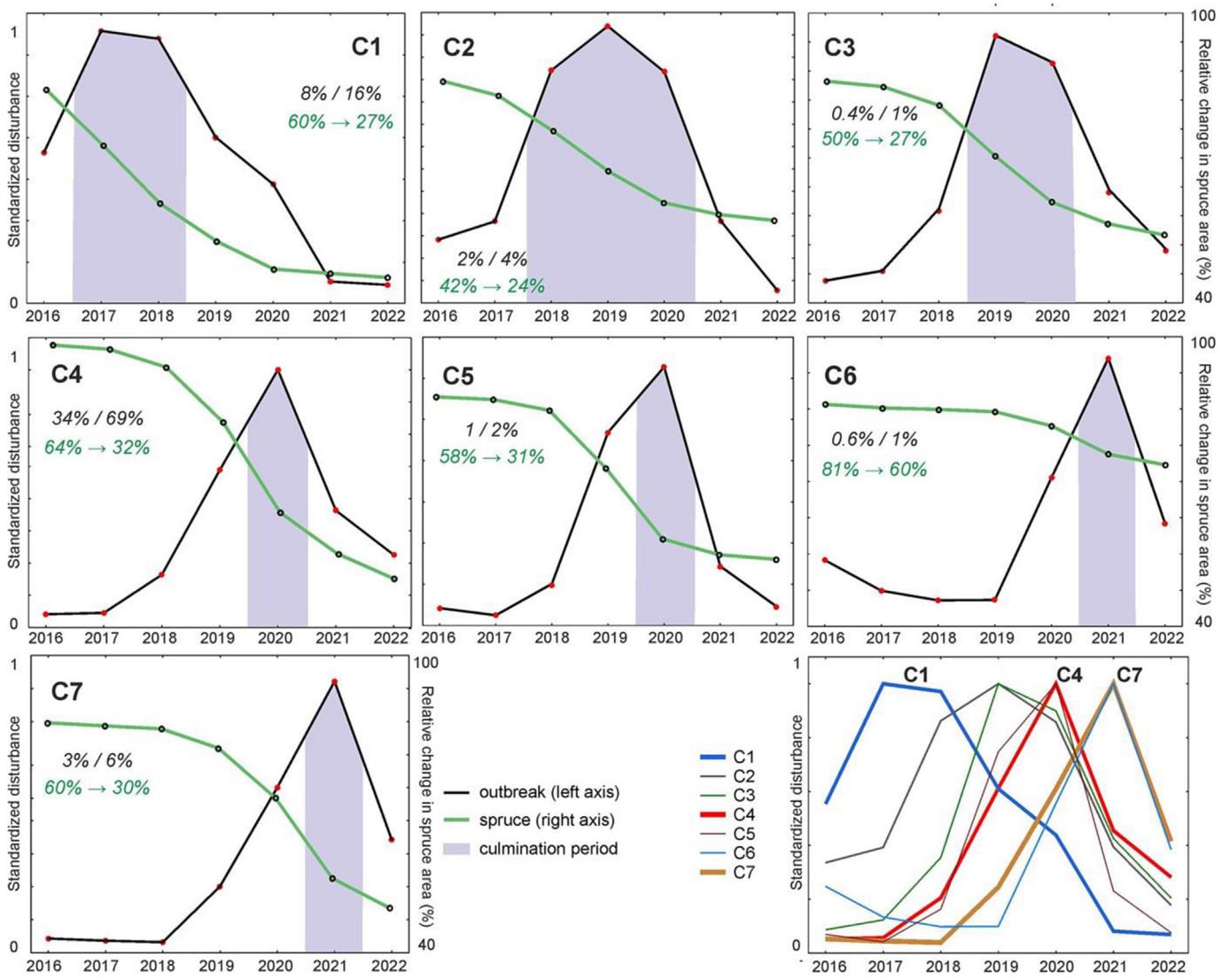

Fig. 5. The development of regional outbreaks within the main disturbance hotspots across the Czech Republic. Outbreak curves are scaled to 1 for comparability. The green line represents the reduction in spruce area relative to the initial value from 2015. Outbreak culmination phases are highlighted. The black values indicate the contribution of a given regional outbreak to the total disturbance level in the country (first number) and to the area covered by all disturbance hotspots (second number). The green values indicated the pre-outbreak (2015) and final (2022) spruce proportions in the forest. (For interpretation of the references to colour in this figure legend, the reader is referred to the Web version of this article.)

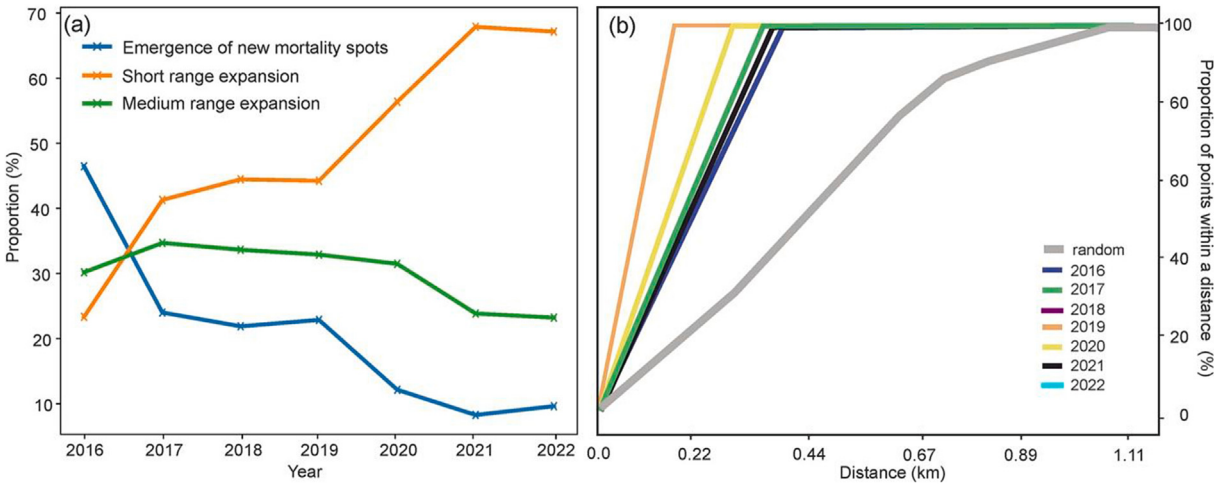

Fig. 6. (**a**) Decomposition of the overall outbreak dynamics into the emergence of new mortality spots, short-range, and medium-range dispersal; and (**b**) spatial autocorrelation of the disturbance patches represented by the Ripley *K* statistics. A hypothetical random distribution is also indicated. The analyses cover the entire Czech Republic.

significant disturbance hotspots at the 0.05 alpha level. In total, seven hotspots were detected, with C2 comprising two sub-areas (Fig. 4b). The primary disturbance pattern consisted of three distinct areas: one located in the north–east (C1–C2, Fig. 4b), another in the central part (C4), and a third in the north (C7). The south–east exhibited a scattered distribution of the disturbance, with three minor hotspots (C3, C5, C6). The total area covered by the hotspots was 15,324 km^2. Notably, the major hotspot C4 spanned 9,000 km^2. More detailed characteristics of the hotspots are provided in Appendix D; Table D2.

The outbreak dynamics within the hotspots exhibited variations in terms of the onset and duration of the main outbreak wave (Fig. 5). The northeastern hotspot C1 experienced an increased disturbance level as early as 2016, before the main country-wide outbreak wave began (Fig. 2). Here, the disturbance level peaked between 2017 and 2018. The adjacent hotspot C2 exhibited an extended culmination period 2018–2020. In the remaining hotspots, except for C3, the disturbance culminated in a single year, 2020 or 2021. Most of the outbreaks culminating after 2018 exhibited a symmetric shape, characterized by a three-year build-up phase, a single culmination year, and subsequent retreat. The retreat typically began when 15%–35% of the initial spruce area had been exhausted. In terms of the proportion of spruce within the entire forest area in the hotspots (Fig. 4, Appendix D; Table D3), the first year of retreat occurred when it accounted for 26%–35%. This was not the case for C6, where the proportion remained high at 60%. By the end of the investigated period, the remaining spruce area ranged between 45% and 60% of the initial stock, which corresponded to the spruce proportion in the forest 24% and 32% (except for C6).

3.3. Bark beetle dispersal range

The country-wide analysis of outbreak dynamics conducted within the flight range hexagons (500 m hexagonal cells) indicated that the emergence of new mortality spots dominated in 2016 (48% of the total) (Fig. 6a). Simultaneously, the contribution of short-range expansion (i.e., within the same hexagon where the previous-year disturbance was recorded) was minor (22%). The medium-range expansion, which involved disturbance occurrence in hexagons adjacent to the previous-year disturbance, accounted for 30% of the overall dynamics in 2016.

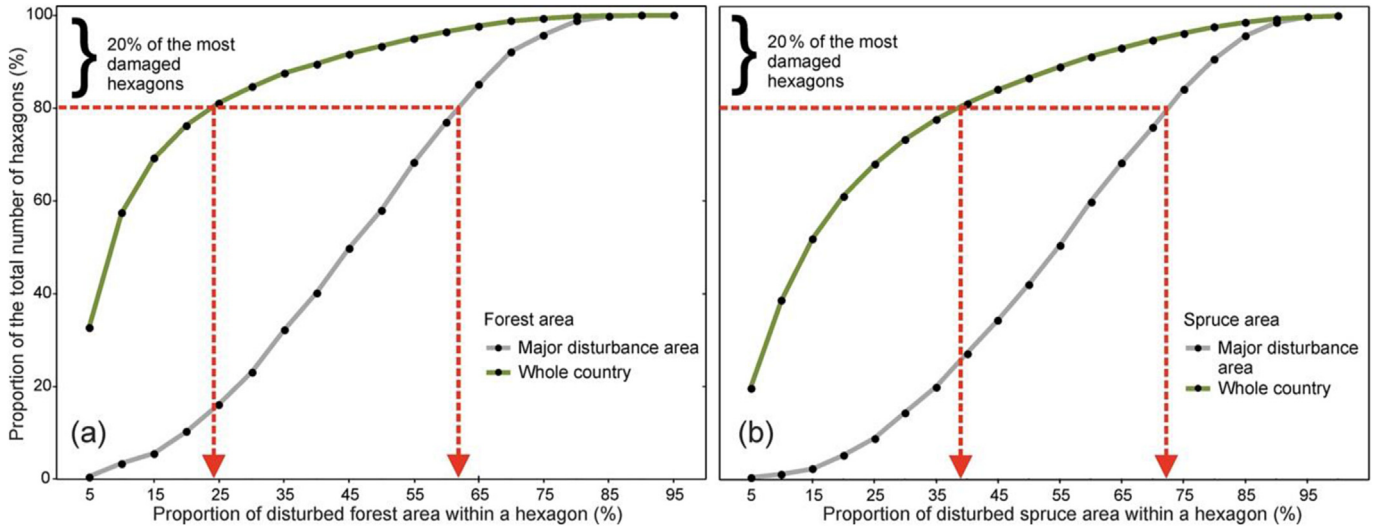

Fig. 7. The cumulative proportion of forest area (**a**) and spruce area (**b**) affected by the disturbance from 2016 to 2022 evaluated within a 7-km hexagonal grid. The values for the entire country and the main outbreak area (C4) are indicated. The red arrows highlight the lower disturbance threshold (*x*-axis) of 20% of the most affected hexagons (*y*-axis) (meaning, for example, that 20% of the most affected hexagons experienced disturbance > 24%). (For interpretation of the references to colour in this figure legend, the reader is referred to the Web version of this article.)

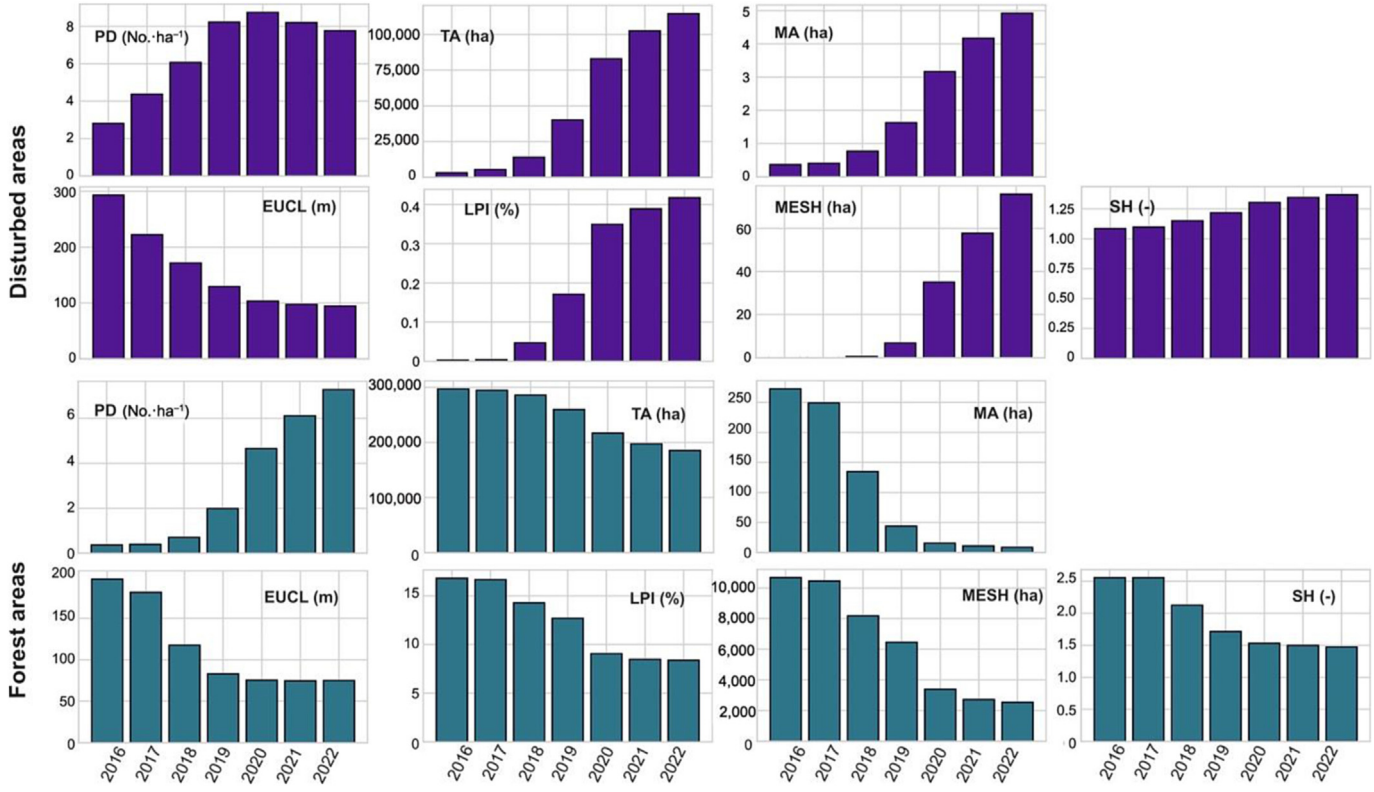

Fig. 8. Landscape metrics characterizing the spatial structure of forests and disturbed areas within the main outbreak area in the period 2016–2022 (Appendix D; Tables D3, D4). Abbreviations: PD – patch density, TA – total patch area, MA – mean patch area, EUCL – mean Euclidian distance between the patches, LPI – proportion of the landscape covered by the largest patch, MESH – effective mesh size characterizing landscape fragmentation, SH – a measure of patch shape complexity.

As the outbreak culminated, the proportion of emergence and medium-range dispersal decreased, while the short-range dispersal became the dominant process, accounting for 42%–48% of the total dynamics.

The Ripley *K* statistics indicated that disturbance patch clustering significantly deviated from random distribution throughout the studied period (Fig. 6b). It exhibited a distinct clustering pattern that was more pronounced during the outbreak culmination years in 2019 and 2020 than in the remaining years.

3.4. Disturbance impact and resultant landscape transformations

During the period 2016-2022, the disturbance affected 11% of the total forest area in the country and 17% of the initial spruce area. In the main outbreak area C4 (Fig. 4b), the forest area affected represented 38% of the total forest and 49% of the initial spruce cover. A closer look at the level of disturbance within the hexagonal grid (Fig. 7a, Appendix D; Table D1) indicates that 20% of the most affected hexagons (*y*-axis) in the country exhibited damage above 24% (*x*-axis) (in terms of the total forest area affected). In the core zone C4, the 20% of most affected hexagons showed damage above 62% (Fig. 7a). The impact was more pronounced in terms of spruce change (Fig. 7b), with the earlier mentioned values shifting to 38% and 72%, respectively.

The degree of landscape transformation in the C4 zone (see Fig. 4b and Appendix D; Table D4) exhibited several distinct tendencies (Fig. 8). The initial forest area decreased by 38%, from 296,860 ha in 2016 to 185,390 ha in 2022 (Fig. 8). This reduction was accompanied by significant fragmentation of the originally compact forest complexes. Specifically, the mean forest patch size decreased from 272 ha to 8 ha, while the patch density increased due to the fragmentation from 0.4 to 7.3 patches per ha. The largest forest patch, which initially covered 17% of the forest area, was reduced to 8% (from 64,296 to 30,257 ha). The patch shape index indicated a decrease in forest patch complexity during the studied period. Finally, forest connectivity on the landscape has been considerably reduced, as indicated by the 80% reduction in the effective mesh size (see Table 1 and Appendix C for the definition). Due to increased forest fragmentation, the mean distance between forest patches increased.

In the case of disturbed areas (Appendix D; Table D5), their total area (Fig. 8) increased from 3,000 to 114,000 ha during the study period, with the mean patch area growing from 0.4 ha to 4.9 ha. Simultaneously, the largest disturbed patch in 2022 covered 1,513 ha, representing 0.4% of the total forest area in the C4 zone. Initially, the patch density increased due to the escalating disturbance impacts. However, as the initially scattered patches merged into more compact areas, the patch density decreased. The patch shape index increased during the study period, indicating an increase in the complexity of disturbed areas. Regarding the indicators of connectivity, the mean Euclidean distance between patches decreased from 293 m to 94 m and the effective mesh size increased from 0.01 ha to 76 ha.

4. Discussion

Our investigation has focused on a drought-driven outbreak of spruce bark beetle in Central Europe, which encompassed novel features diverging from historical dynamics. We identified multiple regional outbreak foci across the Czech Republic and evaluated the degree of synchrony among them, including outbreaks' onset and culmination. Disentangling the overall disturbance dynamics into its partial processes has corroborated that the density-dependent dispersal patterns of infestation documented in the past are applicable to the investigated drought-driven outbreak type, despite the remarkably different distribution of resources. We have provided new insights into the landscape-scale transformations induced by the outbreak—a field that has not received much attention in the past but can be essential for understanding the

ongoing regime shifts and informing other outbreak-prone regions in Europe about the possible consequences.

4.1. Spatial and temporal dynamics of the outbreak

The beginning of the studied outbreak after 2018 coincided with the climatically driven tree mortality wave that affected much of Europe and drove disturbance dynamics beyond their historical variation (Senf and Seidl, 2021a). This wave was, *inter alia,* driven by the numerous outbreaks of *I. typographus*, which occurred, for example, in Germany, Sweden, France, and northern Italy (Gilles et al., 2024; Kärvemo et al., 2023). Despite the initial climatic trigger being identical across the Czech Republic, we identified seven outbreak foci which displayed certain asynchrony in their onset and culmination. The two eastern hotspots, C1 and C2, distinctly differed from the remaining areas. These outbreaks began earlier and culminated over multiple years: C1 in 2017–2018 and C2 in 2018–2021. Both C1 and C2 represented the continuation of an extended outbreak that started around 2010 driven by the combined effect of *I. typographus*, the double-spined bark beetle *I. duplicatus,* and the widespread tree infection the fungus *Armillaria* spp. (Hlásny and Sitková, 2010; Holuša and Liška, 2022). Most of the outbreaks in the remaining areas were characterized by a three-year build-up phase and a single culmination year (2019–2021), followed by a sharp retreat. The exceptions were C3 with a two-year culmination in 2019–2020, and C6 with a shorter two-year build-up phase. The likely explanation for this variation is differences in local forest and environmental conditions which pre-determine the size of the beetle population required to cross the epidemic threshold and trigger a self-sustaining outbreak (Raffa et al., 2008). Another factor can be management which encompasses heavy salvage and sanitary logging, which can exert a certain dampening effect on the outbreaks (Hlásny et al., 2021a; Wermelinger, 2004), yet its strength seems diminishing under climate change (Dobor et al., 2019). Still, spatially and temporally varying intensity of these operations due to logistic and labour limitations and ownership fragmentation, could have desynchronized the regional outbreaks.

A comparison of these dynamics with the documented wind-driven outbreaks indicates that both outbreak types share a 2–3-year long build-up phase, however, the culmination seems to be considerably longer in the wind-driven outbreaks. For example, Lieutier et al. (2004) identified a 2–3 build-up (gradation) phase followed by an outbreak lasting 5–7 years. An overview of historical outbreaks in the 20th century by Skuhravý (2002) suggested a wider span of 3–11 years, while the model proposed by Økland and Bjørnstad (2006) indicated an outbreak length of around 10 years. While this anecdotal comparison remains inconclusive, it highlights potential research avenues that should aim to uncover the defining features of the drought-driven outbreaks.

The evaluated outbreak resembled the dynamics of outbreaks observed in the past in terms of the transition from the emergence of new spots to their expansion to the local surroundings along the outbreak cycle (Hlásny and Turčáni, 2013; Kautz et al., 2011). The most distinct increase in the local expansion was aligned with the outbreak culmination in the years 2019–2020 (Fig. 6a), indicating that the enlarged beetle populations managed to efficiently consume local resources, without searching for a suitable host over longer distances. We identified only an indistinct change in the medium-range dispersal to the adjacent 500 m large hexagons. However, this finding should be interpreted cautiously due to the potentially intertwined processes of the emergence of new infestation spots (i.e., the increase in the local endemic population) and the expansion from the source hexagons to their surroundings. At the same time, the patterns we identified could have been influenced by changes in host distribution over time. However, the methodology we used did not allow us to isolate this effect.

An interesting finding was a relatively high proportion of Norway spruce that remained after the outbreak retreat, suggesting that resource depletion was not the primary cause of the collapse. In the first year of retreat, the initial spruce area was reduced by 40%–50% in most of the hotspots (Fig. 5, Appendix D; Table D2). This corresponded to the level of spruce proportion in the forest between 26% and 36 %. While these values are relatively high, the accompanying reduction in spruce connectivity may have exerted a significant dampening effect on the outbreak, resulting in the observed outbreak retreat (Honkaniemi et al., 2020; Raffa et al., 2008). Moreover, it is likely that at least a portion of the remaining spruce stands was younger than 40–50 years, rendering them less suitable for infestation (Wermelinger, 2004). Consequently, the degree of resource exhaustion, particularly in terms of mature spruce stands, was probably higher than what our study reported. This problem is difficult to overcome as the cycle of forest inventories, which could provide more details on forest structure and composition, is typically around 10 years. Therefore, it is not possible to keep up with the rapidly progressing forest change due to the disturbance. Another reason behind the outbreak's retreat can be wetter weather conditions in the springs of 2020 and 2021; however, establishing such a causal link would require further research. Generally, mechanisms driving outbreak collapses remain insufficiently understood (Huang et al., 2019); our current research suggests, at least, that resource depletion may not be the most pronounced one.

The latter finding also suggests that the post-outbreak areas may not be entirely on the "safe side". There remains a possibility of re-occurrence of outbreaks in these regions in the future because of the substantial proportion of unaffected spruce forests. However, the likelihood of such development remains unclear and requires assessing post-outbreak forest demography, host connectivity, and other factors that determine forest susceptibility to infestations (Netherer and Nopp-Mayr, 2005). Moreover, the identified increase in forest patch complexity and the overall forest fragmentation have resulted in the increased length of forest edges, which can significantly heighten forest susceptibility to windthrows (Zeng et al., 2010) and infestations by bark beetles (Kautz et al., 2013). These facts, together with the considerable proportion of spruce in the species composition, highlight the potential risk of recurring outbreaks in areas where the recent outbreak has retreated.

4.2. Outbreak impacts

The impacts of bark beetle outbreaks in Europe have traditionally been evaluated based on directly quantifiable indicators, including the volume of affected or salvaged timber, the extent of impacted areas, and the direct economic losses (Grégoire et al., 2015; Hlásny et al., 2021a). We suggest that outbreaks fuelled by climate change, affecting unprecedently large areas, require adopting a more comprehensive landscape-scale perspective. Such insights can be instrumental for better understanding the societal and biodiversity implications of the outbreaks, as well as the possible post-outbreak development trajectories, which depend largely on the amount and distribution of disturbance legacies (Turner and Seidl, 2023).

Altogether, our results suggested the loss of 17% of spruce during the studied period across the Czech Republic. This corresponds with the total volume of wood affected by bark beetles and salvaged (Fig. 2b), accounting for approximately 20% of the initial spruce growing stock (ca. 100 mil. m^3 of wood, Forest Management Institute, Czech Republic). Although this impact may not seem dramatic, the problem arises from its concentration in several zones, which cover 24% of all spruce forests in the country. The largest one spanned 9,000 km^2 and experienced a 38% loss of forest cover and 49% of the initial spruce area (Appendix D; Table D2). Such an extent of damage places the current outbreak among the largest and most severe natural disturbances in recent European history. It surpasses previous outbreaks, including the ones following the windthrow Kyrill in the Bohemian Forest in 2007 (Czech Republic, 9 mil. m^3 in 2007–2011 (Brázdil et al., 2022); Žofia in the Tatra Mountains in 2004 (Slovakia, 21 mil. m^3 in 2004–2013 (Kunca et al., 2019); and the outbreak after the storm Gudrun (southern Sweden, 3.5 mil. m^3).

Due to historical land use, the forest cover in the main outbreak zone was already fragmented before the outbreak occurred. In 2016, the forest

cover proportion was 42% in the main outbreak zone and the mean forest patch size was 272 ha (Appendix D; Table D5). The disturbance has led to a forest cover reduction by 38% that resulted in mean patch size reduction by 97% (from 272 ha to 8 ha) and the patch density increase by over 1,900%. Together with the expansion of disturbed areas (Appendix D; Table D4), these transformations have compromised traditional scenic values and affected habitat availability for different forest-dwelling species (see Hlásny et al., 2021a, b). Appraising such societal and ecological impacts requires increased research attention, however, this area has historically been neglected in Europe (but see, for example, Grégoire et al., 2015; Montagné-Huck and Brunette, 2018; Müller, 2011). The increasing disturbance activity will require more focused research appraising disturbance consequences, as identified in the current study, on cultural and biodiversity values and ecosystem services (Morris et al., 2018).

5. Conclusions

Bark beetle outbreaks across Europe are transitioning from the historical wind-driven dynamics to the dynamics driven by extreme climate events or a combination thereof. This disturbance type can generate specific and, until now, unrecognized disturbance patterns and impacts. Our current study provided one of the first insights into these new dynamics by focusing on the current outbreak epicenter in Europe, the Czech Republic. We discovered that local resource depletion is an unlikely cause of outbreak termination, although this conclusion requires further experimental research. Our assessment of landscape transformations has revealed the remarkable extent of the outbreak's epicentre characterized by a high degree of forest reduction and fragmentation. These changes could potentially lead to severe societal and ecological consequences, a type of impact that requires an increased research attention in the future. The findings we presented can be instrumental in informing about the potential impact of natural disturbances amplified by climate change, expanding our current understanding of bark beetle outbreak dynamics, and supporting the implementation of novel disturbance dynamics in ecosystem models.

Fundings

This work was supported by the project “EVA4.0”, No. CZ.02.1.01/0.0/0.0/16_019/0000803 financed by OP RDE of the Czech Republic, the project of the National Agency for Agriculture Research of the Czech Republic No. QK23020039l, and the Technology Agency of the Czech Republic under grant No. SS02030018.

Availability of data and materials

Data is available on request from the authors.

CRediT authorship contribution statement

Prosper Washaya: Writing – review & editing, Writing – original draft, Visualization, Validation, Software, Methodology, Data curation. **Roman Modlinger:** Writing – review & editing, Methodology, Formal analysis. **Daniel Tyšer:** Methodology, Data curation. **Tomáš Hlásny:** Writing – review & editing, Writing – original draft, Visualization, Resources, Methodology, Funding acquisition, Formal analysis, Conceptualization.

Declaration of generative AI and AI-assisted technologies in the writing process

During the preparation of this work the authors used GPT 4 to improve style and grammar of several paragraphs in the text. After using this tool, the authors reviewed and edited the content as needed and take full responsibility for the content of the publication.

Declaration of competing interest

The authors declare that they have no known competing financial interests or personal relationships that could have appeared to influence the work reported in this paper.

Appendix A. Supplementary data

Supplementary data to this article can be found online at https://doi.org/10.1016/j.fecs.2024.100243.

References

Agarap, A.F., 2018. Deep learning using rectified linear units (ReLU). https://doi.org/10.48550/arXiv.1803.08375 arXiv preprint.

Asada, R., Hurmekoski, E., Hoeben, A.D., Patacca, M., Stern, T., Toppinen, A., 2023. Resilient forest-based value chains? Econometric analysis of roundwood prices in five European countries in the era of natural disturbances. For. Policy Econ. 153, 102975. https://doi.org/10.1016/j.forpol.2023.102975.

Baier, P., Pennerstorfer, J., Schopf, A., 2007. PHENIPS-A comprehensive phenology model of *Ips typographus* (L.) (Col., Scolytinae) as a tool for hazard rating of bark beetle infestation. For. Ecol. Manag. 249, 171–186. https://doi.org/10.1016/j.foreco.2007.05.020.

Bentz, B.J., Jönsson, A.M., Schroeder, M., Weed, A., Wilcke, R.A.I., Larsson, K., 2019. *Ips typographus* and *Dendroctonus ponderosae* models project thermal suitability for intra- and inter-continental establishment in a changing climate. Front. For. Glob. Chang. 2, 1. https://doi.org/10.3389/ffgc.2019.00001.

Biedermann, P.H.W., Müller, J., Grégoire, J.C., Gruppe, A., Hagge, J., Hammerbacher, A., Hofstetter, R.W., Kandasamy, D., Kolarik, M., Kostovcik, M., Krokene, P., Sallé, A., Six, D.L., Turrini, T., Vanderpool, D., Wingfield, M.J., Bässler, C., 2019. Bark beetle population dynamics in the Anthropocene: Challenges and solutions. Trends Ecol. Evol. 34, 914–924. https://doi.org/10.1016/j.tree.2019.06.002.

Bosch, M., 2019. PyLandStats: an open-source Pythonic library to compute landscape metrics. PLoS One 14 (12), e0225734. https://doi.org/10.1371/journal.pone.0225734.

Brázdil, R., Zahradník, P., Szabó, P., Chromá, K., Dobrovolný, P., Dolák, L., Trnka, M., Řehoř, J., Suchánková, S., 2022. Meteorological and climatological triggers of notable past and present bark beetle outbreaks in the Czech Republic. Clim. Past 18, 2155–2180. https://doi.org/10.5194/cp-18-2155-2022.

Buras, A., Rammig, A., Zang, C.S., 2020. Quantifying impacts of the 2018 drought on European ecosystems in comparison to 2003. Biogeosciences 17, 1655–1672. https://doi.org/10.5194/bg-17-1655-2020.

DeVries, B., Verbesselt, J., Kooistra, L., Herold, M., 2015. Robust monitoring of small-scale forest disturbances in a tropical montane forest using Landsat time series. Remote Sens. Environ. 161, 107–121. https://doi.org/10.1016/j.rse.2015.02.012.

Dobor, L., Hlásny, T., Rammer, W., Zimová, S., Barka, I., Seidl, R., 2019. Is salvage logging effectively dampening bark beetle outbreaks and preserving forest carbon stocks? J. Appl. Ecol. 57, 67–76. https://doi.org/10.1111/1365-2664.13518.

European Environment Agency, 2020. Corine land cover 2018. EEA geospatial Catalogue. SNAP - ESA Sentinel Application Platform. European Space Agency, Denmark.

Getis, A., Ord, J.K., 1992. The analysis of spatial association by use of distance statistics. Geogr. Anal. 24, 189–206. https://doi.org/10.1111/j.1538-4632.1992.tb00261.x.

Gilles, A., Lisein, J., Cansell, J., Latte, N., Piedallu, C., Claessens, H., 2024. Spatial and remote sensing monitoring shows the end of the bark beetle outbreak on Belgian and north-eastern France Norway spruce (*Picea abies*) stands. Environ. Monit. Assess. 196, 226. https://doi.org/10.1007/s10661-024-12372-0.

Gorelick, N., Hancher, M., Dixon, M., Ilyushchenko, S., Thau, D., Moore, R., 2017. Google Earth engine: planetary-scale geospatial analysis for everyone. Remote Sens. Environ. 202, 18–27. https://doi.org/10.1016/j.rse.2017.06.031.

Grégoire, J.-C., Raffa, K.F., Lindgren, B.S., 2015. Economics and politics of bark beetles. In: Vega, F.E., Hofstetter, R.W. (Eds.), Bark Beetles – Biology and Ecology of Native and Invasive Species. Elsevier, London-San Diego-Waltham-Oxford, pp. 585–613. https://doi.org/10.1016/B978-0-12-417156-5.00015-0.

Hallas, T., Steyrer, G., Laaha, G., Hoch, G., 2024. Two unprecedented outbreaks of the European spruce bark beetle, *Ips typographus* L. (Col., Scolytinae) in Austria since 2015: different causes and different impacts on forests. Centr. Eur. For. J. 70. https://doi.org/10.2478/forj-2024-0014.

Hartmann, H., Moura, C.F., Anderegg, W.R.L., Ruehr, N.K., Salmon, Y., Allen, C.D., Arndt, S.K., Breshears, D.D., Davi, H., Galbraith, D., Ruthrof, K.X., Wunder, J., Adams, H.D., Bloemen, J., Cailleret, M., Cobb, R., Gessler, A., Grams, T.E.E., Jansen, S., Kautz, M., Lloret, F., O'Brien, M., 2018. Research frontiers for improving our understanding of drought-induced tree and forest mortality. New Phytol. 218, 15–28. https://doi.org/10.1111/nph.15048.

Havašová, M., Ferenčík, J., Jakuš, R., 2017. Interactions between windthrow, bark beetles and forest management in the Tatra national parks. For. Ecol. Manag. 391, 349–361. https://doi.org/10.1016/j.foreco.2017.01.009.

Hlásny, T., König, L., Krokene, P., Lindner, M., Montagné-Huck, C., Müller, J., Qin, H., Raffa, K.F., Schelhaas, M.-J., Svoboda, M., Viiri, H., Seidl, R., 2021a. Bark beetle outbreaks in Europe: state of knowledge and ways forward for management. Curr. For. Rep. 7, 138–165. https://doi.org/10.1007/s40725-021-00142-x.

Hlásny, T., Sitková, Z., 2010. Spruce Forests Decline in the Beskids. National Forest Centre, Czech University of Life Sciences, Forestry and Game Management Research Institute, Zvolen, Prague. Jíloviště.
Hlásny, T., Turčáni, M., 2013. Persisting bark beetle outbreak indicates the unsustainability of secondary Norway spruce forests: case study from Central Europe. Ann. For. Sci. 70, 481–491. https://doi.org/10.1007/s13595-013-0279-7.
Hlásny, T., Zimová, S., Merganičová, K., Štěpánek, P., Modlinger, R., Turčáni, M., 2021b. Devastating outbreak of bark beetles in the Czech Republic: drivers, impacts, and management implications. For. Ecol. Manag. 490, 119075. https://doi.org/10.1016/j.foreco.2021.119075.
Holuša, J., Liška, J., 2022. Hypothesis of spruce forests decline and dying in Silesia. Zpr. Lesn. Výzk. 47, 9–15.
Honkaniemi, J., Rammer, W., Seidl, R., 2020. Norway spruce at the trailing edge: the effect of landscape configuration and composition on climate resilience. Landsc. Ecol. 35, 591–606. https://doi.org/10.1007/s10980-019-00964-y.
Huang, J., Hammerbacher, A., Weinhold, A., Reichelt, M., Gleixner, G., Behrendt, T., van Dam, N.M., Sala, A., Gershenzon, J., Trumbore, S., Hartmann, H., 2019. Eyes on the future – evidence for trade-offs between growth, storage and defense in Norway spruce. New Phytol. 222, 144–158. https://doi.org/10.1111/nph.15522.
Huang, J., Kautz, M., Trowbridge, A.M., Hammerbacher, A., Raffa, K.F., Adams, H.D., Goodsman, D.W., Xu, C., Meddens, A.J.H., Kandasamy, D., Gershenzon, J., Seidl, R., Hartmann, H., 2020. Tree defence and bark beetles in a drying world: carbon partitioning, functioning and modelling. New Phytol. 225, 26–36. https://doi.org/10.1111/nph.16173.
Ioffe, S., Szegedy, C., 2015. Batch normalization: accelerating deep network training by reducing internal covariate shift. Proceedings of the 32nd International Conference on Machine Learning, Lille France,, pp. 448–456.
Jactel, H., Koricheva, J., Castagneyrol, B., 2019. Responses of forest insect pests to climate change: not so simple. Curr. Opin. Insect Sci. 35, 103–108. https://doi.org/10.1016/j.cois.2019.07.010.
Johnstone, J.F., Allen, C.D., Franklin, J.F., Frelich, L.E., Harvey, B.J., Higuera, P.E., Mack, M.C., Meentemeyer, R.K., Metz, M.R., Perry, G.L.W., Schoennagel, T., Turner, M.G., 2016. Changing disturbance regimes, ecological memory, and forest resilience. Front. Ecol. Environ. 14, 369–378. https://doi.org/10.1002/fee.1311.
Kärvemo, S., Huo, L., Öhrn, P., Lindberg, E., Persson, H.J., 2023. Different triggers, different stories: bark-beetle infestation patterns after storm and drought-induced outbreaks. For. Ecol. Manag. 545, 121255. https://doi.org/10.1016/j.foreco.2023.121255.
Kautz, M., Dworschak, K., Gruppe, A., Schopf, R., 2011. Quantifying spatio-temporal dispersion of bark beetle infestations in epidemic and non-epidemic conditions. For. Ecol. Manag. 262, 598–608. https://doi.org/10.1016/j.foreco.2011.04.023.
Kautz, M., Schopf, R., Ohser, J., 2013. The "sun-effect": microclimatic alterations predispose forest edges to bark beetle infestations. Eur. J. For. Res. 132, 453–465. https://doi.org/10.1007/s10342-013-0685-2.
Krokene, P., 2015. Conifer defense and resistance to bark beetles. In: Vega, F.E., Hofstetter, R.W. (Eds.), Bark Beetles – Biology and Ecology of Native and Invasive Species. Elsevier, London-San Diego-Waltham-Oxford, pp. 177–207. https://doi.org/10.1016/B978-0-12-417156-5.00005-8.
Kunca, A., Zúbrik, M., Galko, J., Vakula, J., Leontovyč, R., Konôpka, B., Nikolov, C., Gubka, A., Longauerová, V., Maľová, M., Rell, S., Lalík, M., 2019. Salvage felling in the Slovak Republic's forests during the last twenty years (1998–2017). Cent. Eur. For. J. 65, 3–11. https://doi.org/10.2478/forj-2019-0007.
Lieutier, F., Day, K.R., Battisti, A., Grégoire, J.-C., 2004. Bark and Wood Boring Insects in Living Trees in Europe, a Synthesis. Springer, Dordrecht.
Marini, L., Økland, B., Jönsson, A.M., Bentz, B., Carroll, A., Forster, B., Grégoire, J., Hurling, R., Nageleisen, L.M., Netherer, S., Ravn, H.P., Weed, A., Schroeder, M., 2017. Climate drivers of bark beetle outbreak dynamics in Norway spruce forests. Ecography 40, 1426–1435. https://doi.org/10.1111/ecog.02769.
Messier, C., Bauhus, J., Doyon, F., Maure, F., Sousa-Silva, R., Nolet, P., Mina, M., Aquilué, N., Fortin, M.J., Puettmann, K., 2019. The functional complex network approach to foster forest resilience to global changes. For. Ecosyst. 6, 21. https://doi.org/10.1186/s40663-019-0166-2.
Mezei, P., Jakuš, R., Pennerstorfer, J., Havašová, M., Škvarenina, J., Ferenčík, J., Slivinský, J., Bičárová, S., Bilčík, D., Blaženec, M., Netherer, S., 2017. Storms, temperature maxima and the Eurasian spruce bark beetle *Ips typographus*–An infernal trio in Norway spruce forests of the Central European High Tatra Mountains. Agric. For. Meteorol. 242, 85–95. https://doi.org/10.1016/j.agrformet.2017.04.004.
Ministry of the Environment of the Czech Republic, 2022. Report on the Environment of the Czech Republic 2022, Czech.
Montagné-Huck, C., Brunette, M., 2018. Economic analysis of natural forest disturbances: a century of research. J. For. Econ. 32, 42–71. https://doi.org/10.1016/j.jfe.2018.03.002.
Morris, J.L., Cottrell, S., Fettig, C.J., DeRose, R.J., Mattor, K.M., Carter, V.A., Clear, J., Clement, J., Hansen, W.D., Hicke, J.A., Higuera, P.E., Seddon, A.W.R., Seppä, H., Sherriff, R.L., Stednick, J.D., Seybold, S.J., 2018. Bark beetles as agents of change in social–ecological systems. Front. Ecol. Environ. 16, S34–S43. https://doi.org/10.1002/fee.1754.
Müller, M., 2011. How natural disturbance triggers political conflict: bark beetles and the meaning of landscape in the Bavarian Forest. Glob. Environ. Chang. 21, 935–946. https://doi.org/10.1016/j.gloenvcha.2011.05.004.
Netherer, S., Hammerbacher, A., 2022. The Eurasian spruce bark beetle in a warming climate: phenology, behavior, and biotic interactions. In: Gandhi, K., Hofstetter, R. (Eds.), Bark Beetle Management, Ecology, and Climate Change. Elsevier, London-San Diego-Waltham-Oxford, pp. 89–131. https://doi.org/10.1016/B978-0-12-822145-7.00011-8.
Netherer, S., Kandasamy, D., Jirosová, A., Kalinová, B., Schebeck, M., Schlyter, F., 2021. Interactions among Norway spruce, the bark beetle *Ips typographus* and its fungal symbionts in times of drought. J. Pest. Sci. 94, 591–614. https://doi.org/10.1007/s10340-021-01341-y.
Netherer, S., Nopp-Mayr, U., 2005. Predisposition assessment systems (PAS) as supportive tools in forest management – rating of site and stand-related hazards of bark beetle infestation in the High Tatra Mountains as an example for system application and verification. For. Ecol. Manag. 207, 99–107. https://doi.org/10.1016/j.foreco.2004.10.020.
Netherer, S., Panassiti, B., Pennerstorfer, J., Matthews, B., 2019. Acute drought is an important driver of bark beetle infestation in Austrian Norway spruce stands. Front. For. Glob. Chang. 2, 39. https://doi.org/10.3389/ffgc.2019.00039.
Økland, B., Bjørnstad, O.N., 2006. A resource-depletion model of forest insect outbreaks. Ecology 87, 283–290. https://doi.org/10.1890/05-0135.
Patacca, M., Lindner, M., Lucas-Borja, M.E., Cordonnier, T., Fidej, G., Gardiner, B., Hauf, Y., Jasinevičius, G., Labonne, S., Linkevičius, E., Mahnken, M., Milanovic, S., Nabuurs, G., Nagel, T.A., Nikinmaa, L., Panyatov, M., Bercak, R., Seidl, R., Ostrogović Sever, M.Z., Socha, J., Thom, D., Vuletic, D., Zudin, S., Schelhaas, M., 2023. Significant increase in natural disturbance impacts on European forests since 1950. Glob. Chang. Biol. 29, 1359–1376. https://doi.org/10.1111/gcb.16531.
Potterf, M., Nikolov, C., Kočická, E., Ferenčík, J., Mezei, P., Jakuš, R., 2019. Landscape-level spread of beetle infestations from windthrown- and beetle-killed trees in the non-intervention zone of the Tatra National Park, Slovakia (Central Europe). For. Ecol. Manag. 432, 489–500. https://doi.org/10.1016/j.foreco.2018.09.050.
Raffa, K.F., Aukema, B.H., Bentz, B.J., Carroll, A.L., Hicke, J.A., Turner, M.G., Romme, W.H., 2008. Cross-scale drivers of natural disturbances prone to Anthropogenic amplification: the dynamics of bark beetle eruptions. Bioscience 58, 501–517. https://doi.org/10.1641/B580607.
Ripley, B.D., 1981. Spatial Statistics. Wiley, Hoboken. https://doi.org/10.1002/0471725218.
Rouault, G., Candau, J.-N., Lieutier, F., Nageleisen, L.-M., Martin, J.-C., Warzée, N., 2006. Effects of drought and heat on forest insect populations in relation to the 2003 drought in Western Europe. Ann. For. Sci. 63, 613–624. https://doi.org/10.1051/forest:2006044.
Schuldt, B., Buras, A., Arend, M., Vitasse, Y., Beierkuhnlein, C., Damm, A., Gharun, M., Grams, T.E.E., Hauck, M., Hajek, P., Hartmann, H., Hiltbrunner, E., Hoch, G., Holloway-Phillips, M., Körner, C., Larysch, E., Lübbe, T., Nelson, D.B., Rammig, A., Rigling, A., Rose, L., Ruehr, N.K., Schumann, K., Weiser, F., Werner, C., Wohlgemuth, T., Zang, C.S., Kahmen, A., 2020. A first assessment of the impact of the extreme 2018 summer drought on Central European forests. Basic Appl. Ecol. 45, 86–103. https://doi.org/10.1016/j.baae.2020.04.003.
Seidl, R., Thom, D., Kautz, M., Martin-Benito, D., Peltoniemi, M., Vacchiano, G., Wild, J., Ascoli, D., Petr, M., Honkaniemi, J., Lexer, M.J., Trotsiuk, V., Mairota, P., Svoboda, M., Fabrika, M., Nagel, T.A., Reyer, C.P.O., 2017. Forest disturbances under climate change. Nat. Clim. Chang. 7, 395–402. https://doi.org/10.1038/nclimate3303.
Senf, C., Pflugmacher, D., Hostert, P., Seidl, R., 2017a. Using Landsat time series for characterizing forest disturbance dynamics in the coupled human and natural systems of Central Europe. ISPRS J. Photogramm. Remote Sens. 130, 453–463. https://doi.org/10.1016/j.isprsjprs.2017.07.004.
Senf, C., Sebald, J., Seidl, R., 2021. Increasing canopy mortality affects the future demographic structure of Europe's forests. One Earth 4, 749–755. https://doi.org/10.1016/j.oneear.2021.04.008.
Senf, C., Seidl, R., 2021a. Persistent impacts of the 2018 drought on forest disturbance regimes in Europe. Biogeosciences 18, 5223–5230. https://doi.org/10.5194/bg-18-5223-2021.
Senf, C., Seidl, R., 2021b. Storm and fire disturbances in Europe: distribution and trends. Glob. Chang. Biol. 27, 3605–3619. https://doi.org/10.1111/gcb.15679.
Senf, C., Seidl, R., 2018. Natural disturbances are spatially diverse but temporally synchronized across temperate forest landscapes in Europe. Glob. Chang. Biol. 24, 1201–1211. https://doi.org/10.1111/gcb.13897.
Senf, C., Seidl, R., Hostert, P., 2017b. Remote sensing of forest insect disturbances: current state and future directions. Int. J. Appl. Earth Obs. Geoinf. 60, 49–60. https://doi.org/10.1016/j.jag.2017.04.004.
Skuhravý, V., 2002. Spruce Bark Beetle (*Ips Typographus* L.) and its Calamities. Agrospoj, Prague.
Sommerfeld, A., Senf, C., Buma, B., D'Amato, A.W., Després, T., Díaz-Hormazábal, I., Fraver, S., Frelich, L.E., Gutiérrez, Á.G., Hart, S.J., Harvey, B.J., He, H.S., Hlásny, T., Holz, A., Kitzberger, T., Kulakowski, D., Lindenmayer, D., Mori, A.S., Müller, J., Paritsis, J., Perry, G.L.W., Stephens, S.L., Svoboda, M., Turner, M.G., Veblen, T.T., Seidl, R., 2018. Patterns and drivers of recent disturbances across the temperate forest biome. Nat. Commun. 9, 4355. https://doi.org/10.1038/s41467-018-06788-9.
Spiecker, H., Hansen, J., Klimo, E., Skovsgaardl, J.P., Sterba, H., von Teuffel, K., 2004. Norway spruce conversion – options and consequences. EFI Research Report vol. 18. Brill, Leiden, Boston, Köln.
Trombik, J., Hlásny, T., 2013. Free European data on forest distribution: overview and evaluation. J. For. Sci. 59, 447–457. https://doi.org/10.17221/58/2013-jfs.
Turner, M.G., Seidl, R., 2023. Novel disturbance regimes and ecological responses. Annu. Rev. Ecol. Evol. Syst. 54, 63–83. https://doi.org/10.1146/annurev-ecolsys-110421-101120.
Weed, A.S., Ayres, M.P., Hicke, J.A., 2013. Consequences of climate change for biotic disturbances in North American forests. Ecol. Monogr. 83, 441–470. https://doi.org/10.1890/13-0160.1.
Wegensteiner, R., Wermelinger, B., Herrmann, M., 2015. Natural enemies of bark beetles. In: Vega, F.E., Hofstetter, R.W. (Eds.), Bark Beetles – Biology and Ecology of Native

and Invasive Species. Elsevier, London-San Diego-Waltham-Oxford, pp. 247–304. https://doi.org/10.1016/B978-0-12-417156-5.00007-1.

Wermelinger, B., 2004. Ecology and management of the spruce bark beetle *Ips typographus*—a review of recent research. For. Ecol. Manag. 202, 67–82. https://doi.org/10.1016/j.foreco.2004.07.018.

Wichmann, L., Ravn, H.P., 2001. The spread of *Ips typographus* (L.) (Coleoptera, Scolytidae) attacks following heavy windthrow in Denmark, analysed using GIS. For. Ecol. Manag. 148, 31–39. https://doi.org/10.1016/S0378-1127(00)00477-1.

Zeng, H., Garcia-Gonzalo, J., Peltola, H., Kellomäki, S., 2010. The effects of forest structure on the risk of wind damage at a landscape level in a boreal forest ecosystem. Ann. For. Sci. 67, 111. https://doi.org/10.1051/forest/2009090.

Zimová, S., Dobor, L., Hlásny, T., Rammer, W., Seidl, R., 2020. Reducing rotation age to address increasing disturbances in Central Europe: potential and limitations. For. Ecol. Manag. 475, 118408. https://doi.org/10.1016/j.foreco.2020.118408.

4.2. Post-Disturbance Forest Recovery Dynamics

Washaya, P., Potterf, M., Modlinger, R., Hüttnerová, T., Melichová, Z., & Hlásny, T. (2025). Severely disturbed forests in Central Europe retain robust recovery capacity but face resilience loss due to spatial homogenization. Landscape Ecology. https://doi.org/10.1007/s10980-025-02264-0

Landsc Ecol (2026) 41:9
https://doi.org/10.1007/s10980-025-02264-0

RESEARCH ARTICLE

Severely disturbed forests in Central Europe retain robust recovery capacity but face resilience loss due to spatial homogenization

P. Washaya · M. Potterf · R. Modlinger · T. Hüttnerová · Z. Melichová · T. Hlásny

Received: 2 June 2025 / Accepted: 10 November 2025

Abstract

Context Following the hot and dry year of 2018, European forests underwent an unprecedented wave of disturbances. The subsequent recovery phase is indicative of ecosystem resilience and critical for long-term forest development; however, the landscape-scale manifestation of these processes remains poorly understood.

Objectives Quantify forest disturbance and early recovery dynamics across a 9000-km^2 forested landscape (Central Europe, Czech Republic) following an extensive outbreak of spruce bark beetle and subsequent treatment by extensive salvage logging and replanting.

Methods We integrated optical and Synthetic Aperture Radar remote sensing data with very high-resolution UAV imagery and derived vegetation height models to map disturbance impacts and post-disturbance recovery patterns from 2018 to 2024.

Results Between 2018 and 2024, 30.8% of the initial forest area was disturbed. Within the disturbed areas, bare soil dominated, indicating a lack of understory in the pre-disturbance forest and the high intensity of removal of disturbance legacies. Temporary regeneration failures, i.e., transitions back to bare soil represented a significant part of recovery dynamics. The average transition time from bare soil to regrowth > 2 m was 5.2 years and the net annual recovery rate (i.e., recovery corrected for failure) was 5.9%. By 2024, 25% of disturbed area was covered by vegetation taller than 2 m.

Conclusions Severely disturbed managed forests in Central Europe retain substantial recovery capacity, even under increasingly extreme climatic conditions. However, the predominance of non-vegetated landcover following disturbance may lead to structurally uniform forests with reduced resilience, suggesting the need for improved management practices.

Keywords Forest disturbance · Post-disturbance recovery · Remote sensing · Forest resilience · Landcover transition · Norway spruce forests

Supplementary Information The online version contains supplementary material available at https://doi.org/10.1007/s10980-025-02264-0.

P. Washaya · M. Potterf · R. Modlinger · T. Hüttnerová · Z. Melichová · T. Hlásny (✉)
Faculty of Forestry and Wood Sciences, Czech University of Life Sciences in Prague, Kamýcká 129, 16500 Prague 6 –Suchdol, Czech Republic
e-mail: hlasny@fld.czu.cz

P. Washaya
e-mail: washaya@fld.czu.cz

M. Potterf
e-mail: potterf@fld.czu.cz

R. Modlinger
e-mail: modlinger@fld.czu.cz

T. Hüttnerová
e-mail: huttnerova@fld.czu.cz

Z. Melichová
e-mail: melichova@fld.czu.cz

Published online: 25 November 2025

Introduction

The intensification of forest disturbance regimes driven by climate change is increasingly challenging forest resilience worldwide (Hartmann et al. 2022; Forzieri et al. 2022). At the same time, disturbed areas represent a window of opportunity to adapt forest structure and composition in response to climate change, emerging disturbance regimes, and shifting societal demands (Seidl and Turner 2022). This is particularly relevant in many intensively managed forest landscapes, which have undergone substantial homogenization in the past, for example, through the promotion of even-aged rotation forestry and the focus on a limited number of productive tree species (Bauhus et al. 2017; Jönsson 2024). Understanding these transformations is essential, as greater spatial heterogeneity and species diversity in regenerating vegetation can enhance future forest resilience (Meigs et al. 2017; Seidl and Turner 2022) and dampen cross-scale interactions that often drive catastrophic feedbacks and regime shifts (Peters et al. 2004; Seidl et al. 2024). In ecosystems prone to insect outbreaks, such heterogeneity may reduce the likelihood of a synchronous crossing of eruptive thresholds – critical points beyond which outbreaks are triggered – and thus limit the risk of large-scale disturbances (Raffa et al. 2008).

Central Europe has been hit after 2018 by the largest disturbance event in at least 170 years (Senf and Seidl 2021). The outbreak of the European spruce bark beetle (*Ips typographus*) initiated by extreme drought affected millions of cubic meters of forest growing stock and transformed traditionally forested landscapes (Hlásny et al. 2021a; Washaya et al. 2024; Das et al. 2025). The outbreak primarily, but not exclusively, affected managed production forests of Norway spruce (*Picea abies*), one of the cornerstones of regional forestry economies (Asada et al. 2023). The disturbed areas have been treated by a high-intensity salvage logging aimed to mitigate economic losses (Knoke et al. 2021) and slow the spread of infestation (Hlásny et al. 2021b; Leverkus et al. 2021). While such management is widely applied across Europe, the extreme disturbance extent combined with high intensity salvaging may impair recovery processes (Lindenmayer and Noss 2006; Leverkus et al. 2020). These effects can further be exacerbated by increasingly extreme weather conditions and the pressure of overpopulated ungulates, with adverse effects on forest recovery and resilience (Champagne et al. 2021; Dobor et al. 2024). Nevertheless, recent research has documented remarkably high regeneration densities shortly after large-scale drought-induced tree mortality in Germany (Central Europe, 2018–2022), largely driven by a vigorous cohort of advanced regeneration (Seidl et al. 2024). Similarly, high recovery capacity of vegetation cover and canopy height following bark beetle outbreaks has been observed across a range of Central European environments (Zeppenfeld et al. 2015; Macek et al. 2017; Senf et al. 2019). However, a body of evidence suggests that this resilience may be increasingly eroded by changing climate and disturbance regimes, particularly in areas prone to drought (Senf and Seidl 2021).

Important insights into these dynamics have been obtained through remote sensing, which became an essential tool for evaluating forest disturbance and recovery dynamics across a wide range of spatial and temporal scales (Frolking et al. 2009; Griffiths et al. 2014; Senf and Seidl 2021; White et al. 2022; Mandl et al. 2024). The recent surge in insect outbreaks across Europe has drawn research attention toward identifying optimal sensors and algorithms for mapping and monitoring this type of disturbance, which is characterized by a high variability in spectral responses, depending on insect and host species (Senf et al. 2017; Hollaus and Vreugdenhil 2019). Particularly challenging is disturbance and recovery mapping in actively managed forests, where differentiation between planned harvests and disturbances, natural and human-aided regeneration, and the effects of post-disturbance salvage logging, are yet to be satisfactorily resolved (Jarron et al. 2016; Sebald et al. 2021). The increasing extent and complexity of disturbance impacts, along with a growing recognition of the ecological significance of disturbance legacies (Johnstone et al. 2016; Storch et al. 2020), have highlighted the need for integrating multisource and multisensory remote sensing data (e.g., Chen et al. 2017). For example, the integration of optical and active sensors, such as LiDAR and Synthetic Aperture Radar (SAR), can enhance the detection of combined spectral and structural characteristics during the transition from canopy tree mortality to subsequent recovery (Liu et al. 2011; Hollaus and Vreugdenhil 2019).

In this study, we are focusing on disturbance and recovery dynamics in one of the most heavily disturbed forest landscapes in Europe, the central Czech Republic (Washaya et al. 2024). This landscape experienced after 2018 the most extensive disturbance in its recent history – a drought-initiated outbreak of spruce bark beetle – and now can offer unique insights into subsequent recovery processes. Our objectives are to: (i) develop a method for mapping the transition from the disturbance to early recovery phase, using the fusion of multisource remote sensing data – including satellite optical and SAR data, and UAV imagery; (ii) quantify recovery dynamics in disturbed areas, including transitions between specific recovery classes; and (iii) assess the implications of early post-disturbance patterns and dynamics for future forest resilience. We are addressing these objectives by testing the following hypotheses: (H1) The extensive scale and high severity of the disturbance, together with intensive post-disturbance salvage logging, resulted in significant spatial homogenization and a widespread prevalence of bare soil in the affected areas. (H2) Despite the high intensity of the disturbance and consistent with recent research on post-disturbance forest dynamics (e.g., Senf et al. 2019; Seidl et al. 2024), the studied forests retain a strong capacity for recovery with a general tendency toward full regeneration. (H3) Local and temporary regeneration failures represent a significant component of recovery dynamics, slowing the overall pace of regeneration.

Methodology

Study area

The study area is located in the Czech Republic (Central Europe), which experienced the most severe outbreak of spruce bark beetle (*I. typographus*) on record between 2018 and 2023, affecting approximately 100 million m^3 of growing stock. We focused on the country's most heavily affected region, covering 9000 km^2 (Fig. 1). The area was delineated using spatial analysis of outbreak progression identified based on remote sensing data (Washaya et al. 2024). Specifically, annual disturbance maps were overlaid on a hexagonal grid (7 km cell size) spanning the entire country. For each cell, the proportion of initial Norway spruce area (*P. abies*, the main host tree for *I. typographus*) affected by disturbance between 2017 and

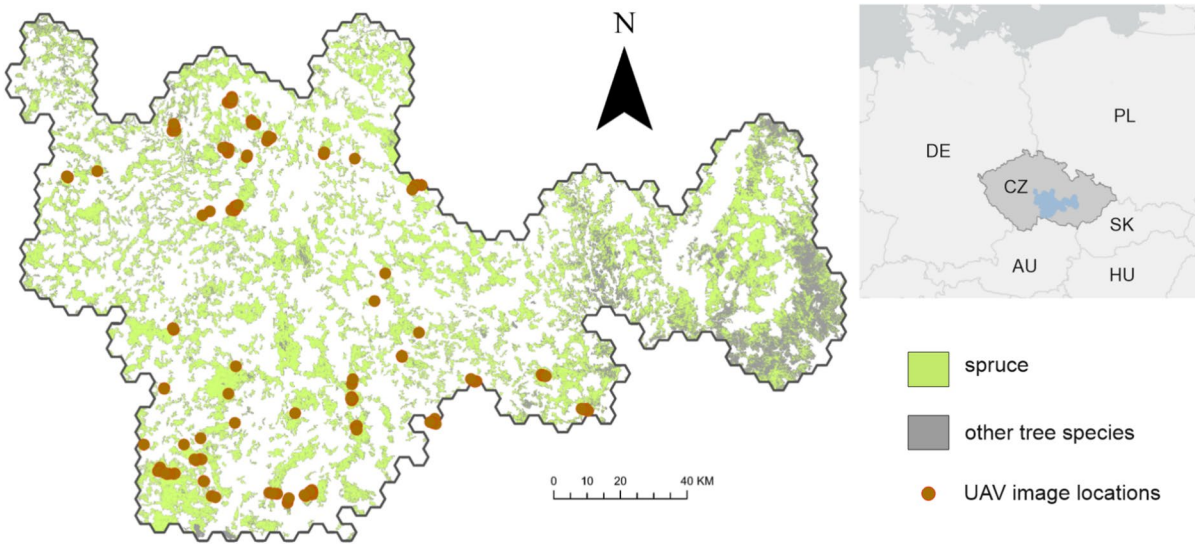

Fig. 1 Forest cover in the study area and the distribution of Norway spruce stands from 2017, prior to the large-scale spruce bark beetle outbreak. Locations of high-resolution UAV imagery acquired in 2023 and 2024, used as ground-truth data for assessing post-disturbance landscape structure, are also indicated. The inset map shows the position of the case study within the Czech Republic and Europe

2023 was calculated. The Getis-Ord Gi* statistic (Getis and Ord 1992) was then applied to identify statistically significant hotspots where disturbance intensity exceeded the country-wide average (i.e., calculated across all hexagons). The study area investigated here represent the major disturbance hotspot in the country (Fig. 1).

The area spans an elevation range of 210 to 837 m a.s.l., with an average annual air temperature range 7.6–9.3 °C and total annual precipitation range 670–887 mm (period 2000–2022). Forests represent 35% of the area, of which 70% consisted of Norway spruce (situation from 2017). Tree species composition has been substantially altered over the last two centuries, with originally dominant broadleaved forests replaced by commercially valuable conifers. The forests are intensively managed, with the prevalence of clearcutting and shelterwood management, with an average rotation period of 120 years. Historically strong focus on timber production characterized by long rotation periods, a limited number of productive tree species, and high growing stock levels, created vulnerable conditions contributing to an unprecedented level of tree mortality after 2018 (Hlásny et al. 2021a, b).

Disturbed areas are typically subjected to intensive salvage logging shortly after disturbance. Moreover, management involves precautionary (sanitary) removal of infested trees to slow the spread of the outbreak. Hence, the studied disturbance is a compound of natural (bark beetle) and anthropogenic (logging) disturbance, which is a frequent sequence across many European countries (Seidl and Senf 2024). While replanting is widely practiced on disturbed sites, natural regeneration is generally retained as part of the recovery strategy. Therefore, the studied disturbance and recovery dynamics contain a strong signal from both salvage removal of dead trees and subsequent replanting. However, due to different logistical and legal constraints (workforce and seedling availability, COVID-19-related restriction, etc.), management intensity varied in time. No nature conservation areas with constrained management interventions (e.g., obligatory dead tree retention) are present in the study area. The bark beetle outbreak 2018–2023 was the only natural disturbance that affected the region within the studied period.

Reference data for forest disturbance and recovery mapping

The disturbance mapping leveraged training data derived from national airborne forest change assessments (Source: Forest Management Institute, Czech Republic). The data collection strategy involves annual acquisition of RGB stereo imagery at a spatial resolution of 25 cm, covering approximately half of the country each year. A normalized Digital Surface Model (nDSM) was generated from these images using photogrammetric stereoscopy. Changes in forest structure, identified by comparing nDSMs from consecutive mapping campaigns, served as indicators of harvests and disturbances. For this study, we used data from the years 2019 and 2020 (see Fig. 2 for the time chart), when planned harvests were significantly reduced due to the large-scale post-disturbance salvage operations. As a result, observed changes can be attributed almost exclusively to bark beetle disturbance, typically followed by salvage logging. In total, 235,000 reference polygons, covering 76,000 ha across the country, were used as training data. Because the training data are derived from vegetation-height differences between the two acquisition campaigns, they mainly represent salvaged areas and stands with downed dead trees, rather than stands with snags. However, given the absence of designated nature conservation areas and the high intensity of salvage logging, unsalvaged stands are rare.

UAV imagery acquired in the study area in summers 2023 and 2024 served as training data for classifying post-disturbance forest recovery conditions (see Fig. 1 for scene locations). The UAV campaigns involved low-altitude (~100 m height) RGB imaging at a spatial resolution of 2–2.5 cm, covering representative recovery conditions across the study area. Altogether, 40 drone images covering 10–12 ha each were used. The images were taken using the DJI Phantom 4 Pro (©2022 SZ DJI Technology Co., Ltd., Shenzhen, China) with an integrated 20-megapixel RGB camera. The seamless orthophotographs were produced through georeferencing, triangulation, and mosaicking. Height information (Digital Surface Model, DSM) was acquired through the structure-from-motion techniques using the Agisoft software (Agisoft 2023). Finally, Canopy Height Models (CHMs) were calculated by subtracting the Digital

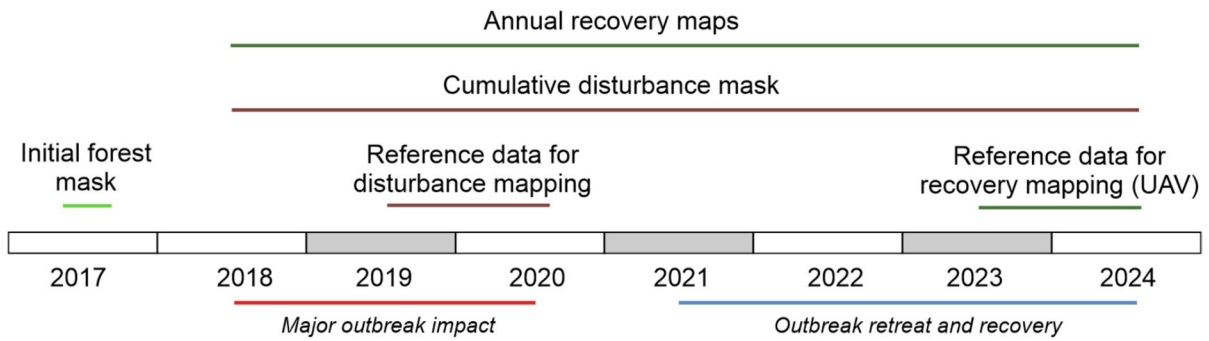

Fig. 2 Overview of experimental design. The study period spans the full outbreak cycle, from onset in 2017, through the peak in 2018–2020, to the subsequent retreat and recovery phase. The initial forest mask was derived from the pre-outbreak year 2017. Reference data for developing the disturbance-mapping algorithm (disturbance presence/absence) were taken from the peak period 2019–2020. Reference data for training the recovery mapping model (three recovery classes identified in UAV imagery) were taken from 2023 to 2024. Recovery was evaluated within a disturbance mask representing the cumulative disturbance impact in 2018–2024. Annual recovery maps were generated for this same period

Terrain Model from the DSM. The height accuracy of produced CHMs was ca 40 cm.

Manual on-screen digitization was used to prepare training data representing three post-disturbance recovery classes:

(i) Near-Bare Soil (NBS) – Disturbed areas lacking significant vegetation cover with height values below 0.2 m, as identified in the CHM (Fig. 3a). Sparse woody vegetation and grasses are likely to be present in the training data.
(ii) Transient class (TC) – Disturbed areas with continuous vegetation cover ≤ 2 m in height (median 0.7 m; Fig. 3b). The training polygons were defined to contain both natural and man-aided regeneration (with a regular spacing between individuals). Nevertheless, certain admixtures of ruderal vegetation (shrubs and grasses) may also be present.
(iii) Established regrowth (ER) – Disturbed areas continuously covered by vegetation between 2 and 6 m in height, with the median height of 4.35 m (Fig. 3c). This class almost exclusively includes trees. The 6 m threshold was set arbitrarily as the theoretical maximum height attainable within the study period in disturbed forest stands.

While the classes are clearly differentiated by their maximum height values, there is considerable overlap in their minimum heights (Fig. 3). This is due to the presence of gaps occurring within the TC and ER classes. In total, the three classes were represented by 600 polygons covering 123 ha, with 14.5% classified as NBS, 60.4% as TC, and 24.1% as ER (see Online Appendix C for more details).

Satellite data used for disturbance and recovery mapping

Sentinel-1 and Sentinel-2 data with 10 m spatial resolution were used for both disturbance mapping and post-disturbance classification. The Google Earth Engine platform was used to access the Sentinel-2 Level-2A surface reflectance product and the Sentinel-1 Level-1 GRD product. Optical indices, including the Normalized Difference Vegetation Index (NDVI), Normalized Burn Ratio (NBR), and Normalized Difference Water Index (NDWI), were derived from the Sentinel-2 data (see Online Appendix A for the respective formulas). Two SAR variables from the ascending and descending orbits of Sentinel-1 were used: Vertical Transmit – Vertical Receive (VV) and Vertical Transmit – Horizontal Receive (VH). These variables can support vegetation mapping: VV is sensitive to surface structure and moisture, while VH is effective in detecting volume scattering from vegetation canopies, making their combination useful for assessing vegetation structure (Tsyganskaya et al. 2018).

The preprocessing applied to Sentinel-2 data included using the Level-2A surface reflectance

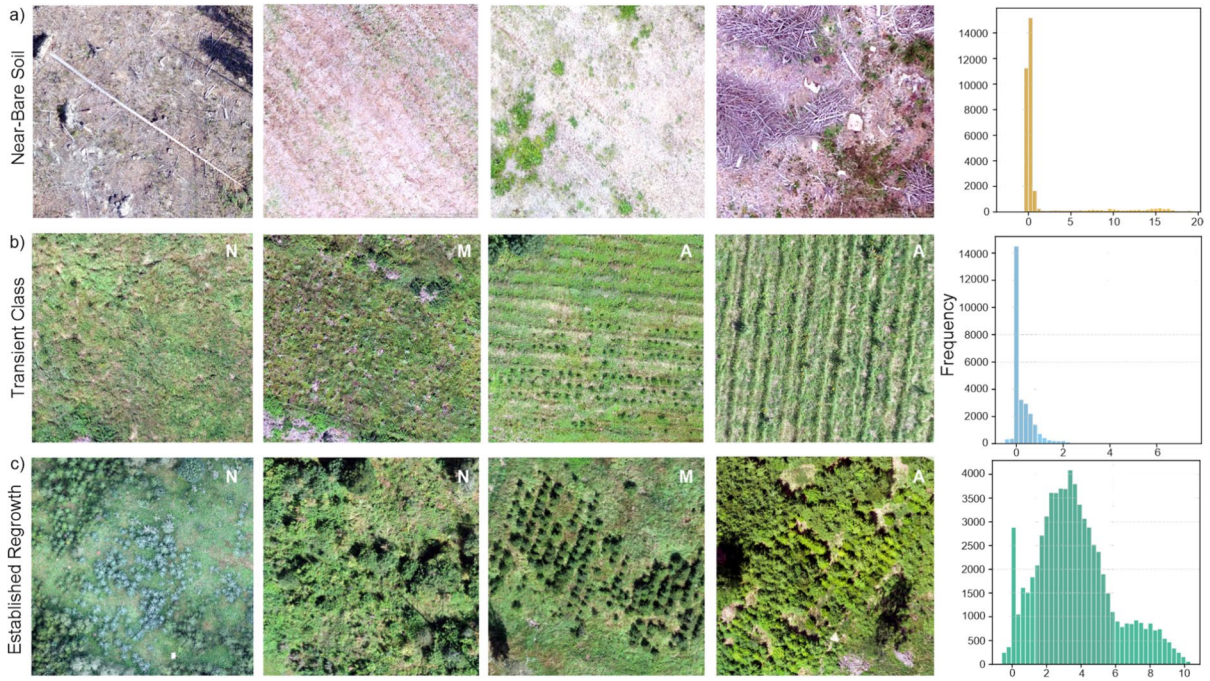

Fig. 3 Representative examples of the three post-disturbance recovery classes derived from the UAV imagery across the study region: **a** Near-Bare Soil, **b** Transient Class, and **c** Established Regrowth. The Transient Class and Established Regrowth examples illustrate various vegetation structures resulting from replanting (characterized by regular tree spacing), from natural regeneration, or mixed approaches combining both pathways. *N* natural regeneration, *A* artificial regeneration, *M* mixed regeneration. Histograms represent the distribution of pixel-level vegetation heights (m), derived from Canopy Height Models

product (atmospherically corrected), masking clouds and shadows using the SCL band, and generating annual cloud-free May–September composites. For Sentinel-1, we applied geometric-distortion and noise corrections and produced annual VV/VH composites for both ascending and descending orbits.

Disturbance mapping algorithm

To train the disturbance mapping model, inter-annual differences in optical and SAR data were calculated by subtracting 2018 from the 2020 values for each variable (dNDVI, dNBR, dNDWI, dVV, dVH). The difference variables were then used as predictors of the observed disturbance occurrence within the period 2019–2020, as defined by the reference data described in Sect. "Study area" (Fig. 3). Since the training data only represented disturbance presence, disturbance absence data were sampled from forest area outside of disturbed areas.

A Convolutional Neural Network (CNN) based on the U-Net architecture was used for disturbance mapping. This model is well-suited for capturing spatial dependencies between neighboring pixels, which is especially important for interpreting SAR imagery (Bueso-Bello et al. 2022). The U-Net configuration was optimized through hyperparameter tuning and consisted of four convolutional blocks in both the encoder and decoder. The input included tiled 256×256-pixel patches of all difference layers (dNDVI, dNBR, dNDWI, dVV, dVH), along with training labels indicating disturbance presence and absence. We split the dataset in the proportion of 70–15–15 into training, validation, and test sets. The training set was used to fit the CNN to distinguish disturbed from undisturbed classes; the validation set to optimize the U-Net configuration and prevent overfitting (i.e., hyperparameter tuning and early stopping); and the test set to provide an unbiased estimate of the model's performance on unseen data. Each encoder block contained two 3×3 convolutional

layers followed by ReLU activation, with downsampling via 2×2 max pooling. The output layer applied a 1×1 convolution with a sigmoid activation to predict annual binary classification of disturbed and undisturbed areas. Model performance was evaluated using a confusion matrix and class-wise metrics including precision, recall, and F1-score (see Online Appendix B for respective formulas). The developed model was used to predict annual disturbance maps for 2018–2024.

Forest recovery classification algorithm

To train the post-disturbance classification model, original (i.e., non-differenced) vegetation indices and SAR data from June 2024 were used as predictors (NDVI, NBR and NDWI from Sentinel-2 and VV and VH from Sentinel-1) for the three recovery classes (Fig. 3). The cumulative area disturbed between 2018 and 2024 (calculated based on annual disturbance maps, as described in Sect. "Disturbance mapping algorithm") was used as a mask for the classification of post-disturbance conditions (Fig. 3). A Random Forest classifier was used for mapping three forest recovery classes due to its proven effectiveness with smaller, imbalanced datasets (Han et al. 2021). The RF classifier was implemented on the Google Earth Engine platform using the ee.Classifier.smileRandomForest function, a server-side implementation of the SMILE (Statistical Machine Intelligence and Learning Engine) library (Li 2016). To address class imbalance in the training dataset (Sect. "Study area"), the less frequent NBS and ER classes were oversampled, while the dominant TC was under sampled. The dataset was then randomly split into training, testing, and validation sets in 70–15–15 proportions and used the same way as in the disturbance-mapping model. The final Random Forest model, optimized with 200 trees through hyperparameter tuning, was used to generate annual recovery maps. The trained model was used to predict annual forest recovery maps for 2018–2024 (Fig. 4).

Forest recovery dynamics

We analyzed inter-annual transitions among the three post-disturbance classes predicted for the entire study area (Fig. 1) over 2018–2024. First, we tracked pixel-level progression from NBS to the TC and ER combined (TC/ER). Second, we adopted a more conservative definition, evaluating only transitions from NBS/TC to ER, assuming that TC includes a certain proportion of ruderal vegetation that can confound the recovery signal. Finally, we evaluated the proportion of reverse transitions, indicating potential regeneration failures.

We used a survival analysis framework to quantify the probability of post-disturbance recovery as a function of time since disturbance. For each pixel, we recorded the number of years elapsed from the initial disturbance and noted whether transition occurred within the study period. If recovery had not occurred, the observation was considered right-censored, meaning that recovery could still occur, but was not observed within the available timeframe. By including both recovered and unrecovered (i.e., censored) pixels, we ensured that all valid recovery trajectories are incorporated (Klein and Moeschberger 2003).

We included only pixels that were first disturbed between 2018 and 2021 (Fig. 2), allowing a minimum of three years for potential recovery before the end of the observation period in 2024. This approach helped avoid potential censoring bias from very recent disturbances (e.g., 2022–2024).

We applied the Kaplan–Meier estimator to quantify the probability of recovery as a function of time since disturbance. Although traditionally used to estimate survival probabilities (i.e., the probability of not experiencing an event such as death or failure; Klein and Moeschberger 2003), we adapted the method to model cumulative recovery, treating recovery as the event of interest. The Kaplan–Meier recovery probability at a specific time, $R_{KM}(t)$, is given as:

$$R_{KM}(t) = 1 - \prod_{t_i \le t} \left(1 - \frac{d_i}{n_i}\right) \quad (1)$$

where t_i is the time of the i^{th} observed recovery event; d_i is the number of recoveries at time t_i; and n_i is the number of non-recovered pixels (i.e., still classified as bare soil) under observation prior to t_i .

Further, we used the log-normal survival model to describe the cumulative probability of recovery over time, assuming that recovery times follow a log-normal distribution. The function was also used to extrapolate recovery probability beyond actual observation period. The function $R_{LN}(t)$ is defined as:

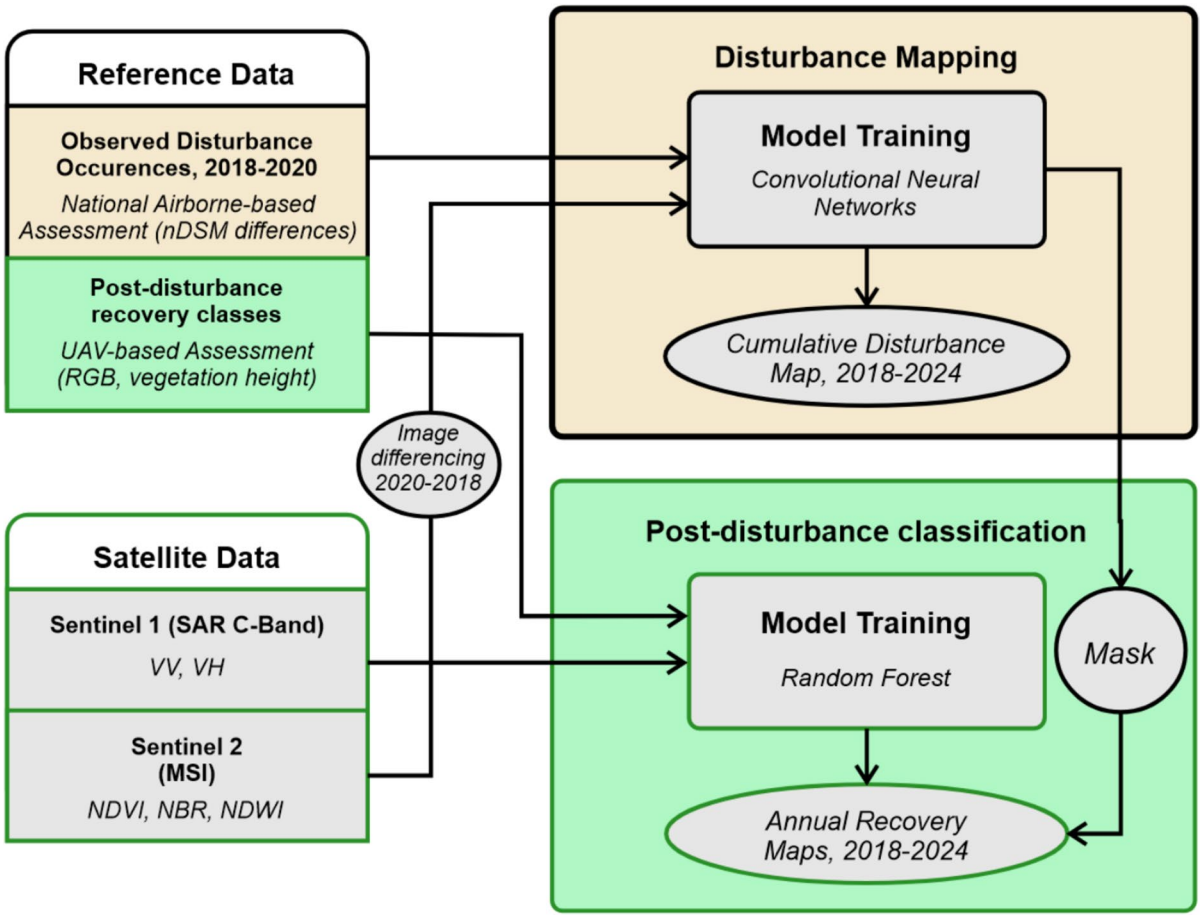

Fig. 4 Workflow for mapping forest disturbance and classifying post-disturbance recovery classes. Ground truth data from airborne (disturbance mapping) and UAV-based mapping (post disturbance forest recovery) were combined with Sentinel-1 and Sentinel-2 imagery. A convolutional neural network was used to generate a cumulative disturbance map (2018–2024), which served as a mask for post-disturbance classification. Recovery classes were mapped annually using a Random Forest model trained on UAV-derived data. *VV* vertical transmit–vertical receive, *VH* vertical transmit–horizontal receive (Synthetic Aperture Radar variables, SAR), *NDVI* normalized difference vegetation index, *NBR* normalized burn ratio, *NDWI* normalized difference water index

$$R_{LN}(t) = \varphi\left(\frac{\ln(t) - \mu}{\sigma}\right) \quad (2)$$

where μ (mu) and σ (sigma) are parameters of log-normal distribution, and Φ represents the standard normal cumulative distribution function. The model was implemented using the lifelines package v. 0.30.0. in Python (Davidson-Pilon 2024).

Finally, the median recovery time was approximated using the restricted mean survival time. This was derived by numerically integrating the Kaplan–Meier survival curve over a six-year period and by linearly interpolating the time point at which the survival probability exceeded 0.5.

Patch size dynamics analysis

To characterize spatial patterns of post-disturbance recovery, we computed patch-level metrics for three post-disturbance classes. Patches were defined as contiguous pixel groups of the same class, based on an 8-neighbor connectivity rule. For each year from 2018 to 2024, we calculated two metrics: the largest patch size (ha) and the median patch size (ha) for

Table 1 Classification performance metrics for disturbed and undisturbed forests mapping

Class	Precision	Recall	F1-score	Overall accuracy
Undisturbed forest	0.96	0.94	0.95	–
Disturbed forest	0.92	0.90	0.91	–
Overall accuracy	–	–	–	0.93

Table 2 Classification performance metrics for post-disturbance recovery mapping

Class	Precision	Recall	F1-score	Overall accuracy
Near-Bare Soil	0.92	0.85	0.84	–
Transient class	0.92	0.86	0.89	–
Established regrowth	0.80	0.82	0.82	–
Overall accuracy	–	–	–	0.85

each class. The analyses were conducted in Python v.3.9.19., using the libraries rasterio v. 1.3.6. and scikit-image v. 0.24.0. (der Walt et al. 2014).

Results

Classification performance

The overall accuracy of disturbance classification was 0.93, indicating that 93% of predictions matched the ground truth across the entire dataset (Table 1). At the class level, the undisturbed forest had a precision of 0.96 (the proportion of correctly identified undisturbed areas among all areas predicted as undisturbed), a recall of 0.94 (the proportion of correctly classified undisturbed areas relative to all actual undisturbed areas), and an F1-score of 0.95 (the harmonic mean of precision and recall). For the disturbed forest class, precision and recall were 0.92 and 0.90, respectively, resulting in an F1-score of 0.91.

The classification of post disturbance recovery reached a lower overall accuracy than the disturbance mapping, 0.85. At the class level, NBS and TC reached slightly higher metrics compared to ER (Table 2).

Disturbance impact and dynamics

The total area of undisturbed forest decreased from 6028 km^2 in 2018 to 4159 km^2 in 2024, representing 30.8% reduction. The most impacted region was located in the central part of the study area (Fig. 5a). Disturbance peaked in 2020, when it affected 551 km^2 of the forest, representing 13.2% of the initial forested area. Following this peak, disturbance levels declined sharply in subsequent years (Fig. 5b). The largest remaining unaffected forests were located in the eastern part of the study area, where tree species other than Norway spruce prevailed (Fig. 5a).

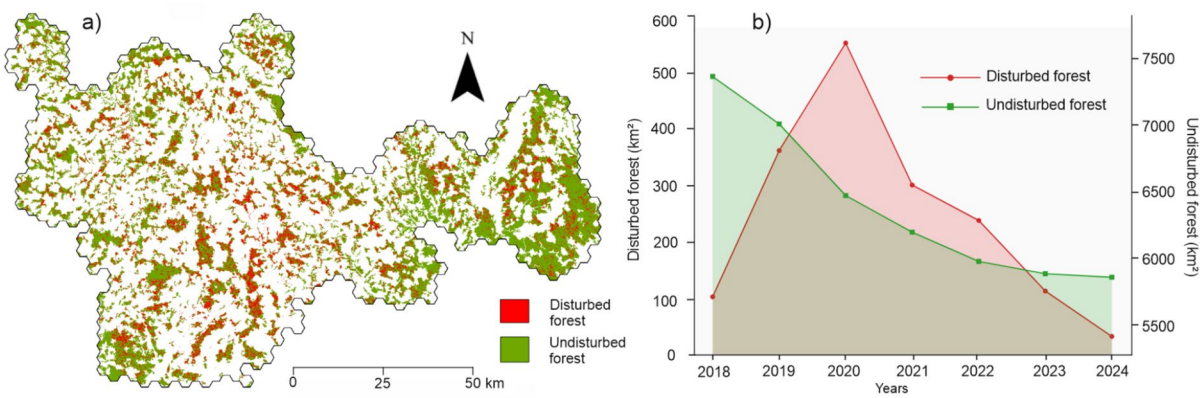

Fig. 5 Spatial and temporal patterns of forest disturbance between 2018 and 2024. **a** Spatial distribution of disturbed and undisturbed forest areas across the study region. **b** Temporal development of disturbed forest (left axis) and undisturbed forests (right axis)

Post-disturbance forest recovery

Between 2018 and 2023, NBS represented the dominant post-disturbance condition, gradually decreasing from 92% of the total disturbed area in 2018 to 45.8% in 2024 (Fig. 6, Online Appendix D). ER began to increase substantially in 2022 (15%) and continued to expand, representing 25% of the disturbed areas in 2024 (Fig. 6). TC first appeared as a distinct land-cover class in 2020, occupying 14% of the disturbed areas. By 2024, the combined area of TC and ER surpassed NBS, together accounting for 54% of the disturbed area.

Spatial dynamics of recovery patch sizes

NBS formed continuous patches of considerable size across the landscape (Fig. 7, Online Appendix F). Mean patch size ranged from 0.1 to 0.26 ha, while the largest patch reached 647 ha in 2021. In the remaining years, maximum NBS patch size ranged between 300 and 400 ha. Continuous patches of TC and ER exhibited comparable sizes, with mean patch sizes ranging from 0.02 ha to 0.08 ha and maximum patch sizes between 0.21 ha and 99.87 ha for TC and 0.26 ha and 41.4 ha for ER, respectively. Over time, NBS patch sizes followed a hump-shaped temporal trend, whereas the two vegetated classes showed a consistent increase, particularly in the mean patch size.

Post-disturbance forest recovery trajectories

We identified a full matrix of transition types among the three recovery classes (Fig. 8). The most common transition was NBS remaining as NBS, accounting for an average of 74.6% of all transitions throughout the study period (Online Appendix E). On average, 19.1% of NBS transitioned to TC annually, while 6.3% transitioned directly to ER. At the same time, we observed distinct transitions from both TC and ER back to NBS, suggesting potential regeneration

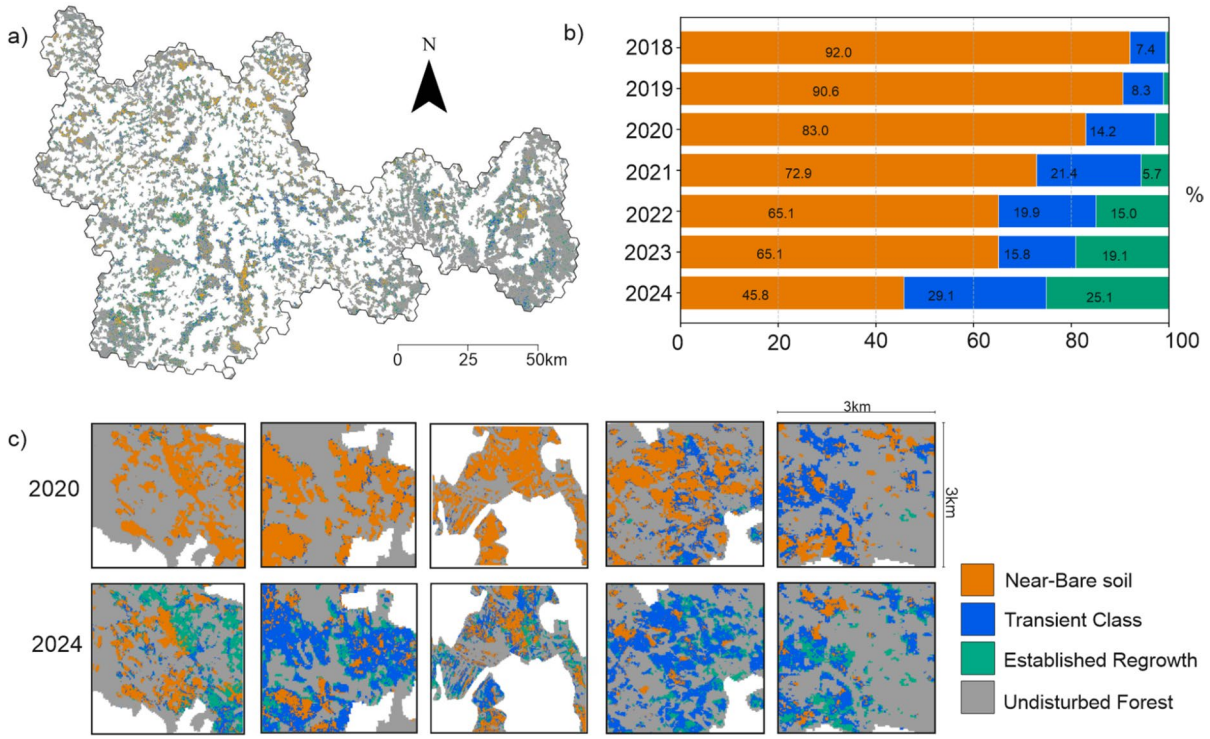

Fig. 6 Post-disturbance forest recovery patterns from 2018 to 2024. **a** Spatial distribution of post-disturbance recovery classes across the study area in 2024; **b** Annual changes in the relative proportions of recovery classes from 2018 to 2024, highlighting the decline in Near-Bare Soil class and the increase in vegetated classes over time; **c** Examples of local transitions among recovery classes between 2020 (outbreak peak) and 2024

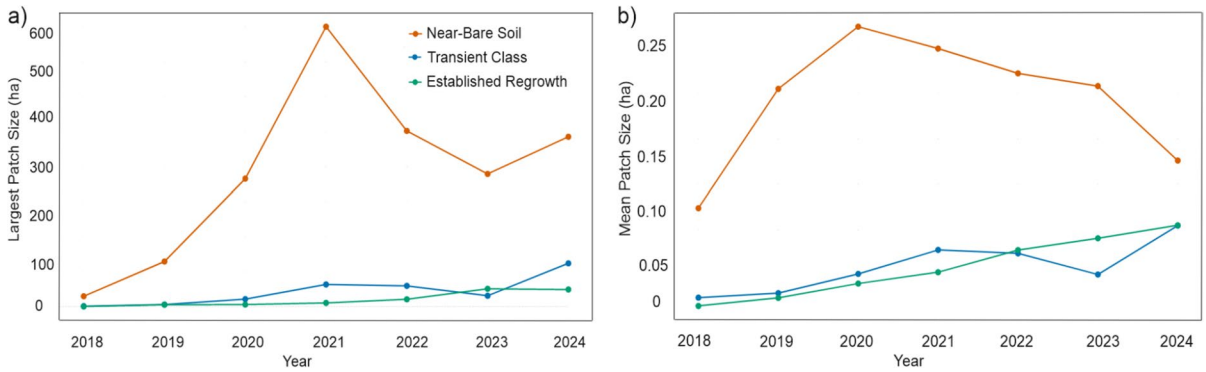

Fig. 7 Patch size dynamics of three post-disturbance forest recovery classes: **a** maximum patch size, and **b** mean patch size

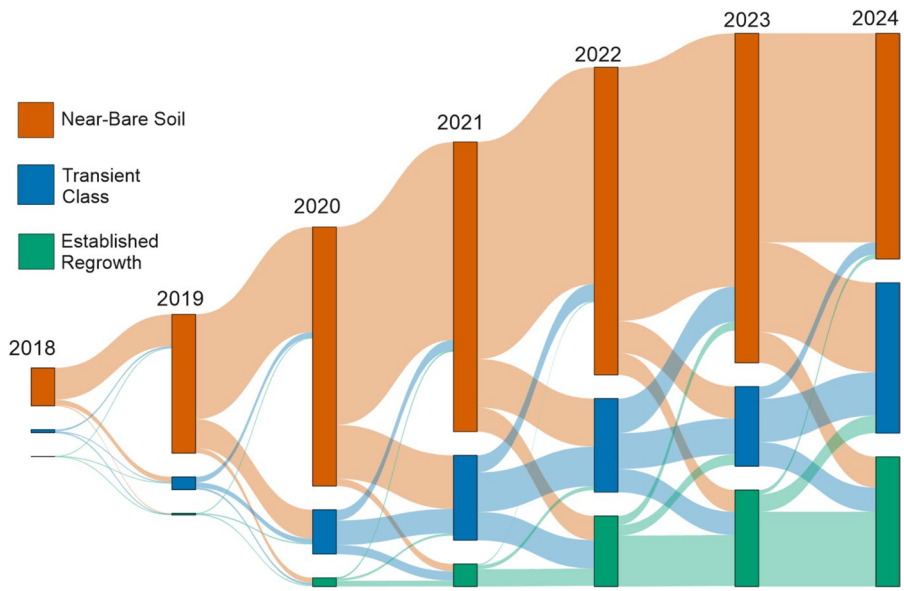

Fig. 8 Temporal transitions between three post-disturbance recovery classes from 2018 to 2024. The heights of each bar represent the total area occupied by a class each year, while the flow widths between bars indicate the magnitude and direction of transitions between classes over time. The cumulative height of all bars in each year reflects the total area affected by disturbance up to that year

failures. On average, 28.2% of TC and 8.6% of ER reverted to NBS each year.

The net annual recovery rate, defined as the transition from NBS to TC and ER combined, minus reverse transitions (i.e., regeneration failures), was 13.3%, with an interannual range of 2.2–20.5% (Table 3). A conservative estimate considering only the transition to ER yields a net recovery rate of 5.91% (2.8–11.9%; Table 3).

Recovery probability

The probability of transitioning from NBS to TC/ER and from NBS to ER was strongly dependent on the time since disturbance (Fig. 9). In the former case,

Table 3 Net annual recovery rates calculated as the difference between transitions from Near-Bare Soil (NMBS) to the Transient Class (TC) and Established Regrowth (ER) corrected for the reverse transitions from the vegetated classes back to NBS

Period	Net recovery rate NBS → TC/ER (%)	Net recovery rate NBS/TC → ER (%)
2018–2019	10.47	2.84
2019–2020	18.38	4.32
2020–2021	15.98	4.41
2021–2022	13.66	11.94
2022–2023	2.16	5.41
2023–2024	20.47	6.55
Average	13.52	5.91

Two transition types are presented: NBS to TC and ER combined (TC/ER) and NBS/TC to ER

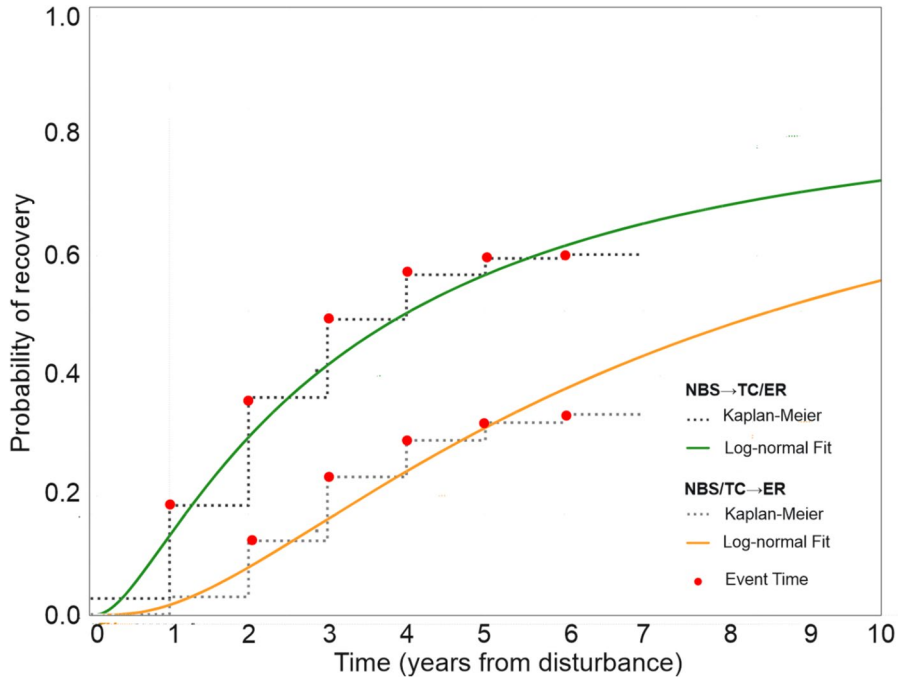

Fig. 9 Time-dependent probability of forest recovery following disturbance. The plot shows the transition probability from the Near-Bare Soil class to any vegetated recovery class (the Transitional Class and Established Regrowth, NBS → TC/ER) and to Established Regrowth only (NBS/TC → ER), expressed as a function of time since disturbance. A non-parametric Kaplan–Meier estimate, and a parametric log-normal survival model are fitted to the data. Red dots indicate time points at which transitions (recovery events) were evaluated. Given the large sample size ($n = 9{,}397{,}673$ pixels), confidence intervals were negligible

recovery increased most rapidly during the first two years, with cumulative probability reaching 22% after one year and 42% after two years. After this initial phase, the rate slowed, reaching 70% by year five. Although the curve approached 86% by year ten, this segment is extrapolated beyond the observed period and should be interpreted with caution. In the case of transitions from NBS to ER, the increase was slower, reaching 3% after one year and 15% after two years; in the extrapolated domain, the cumulative probability reached 66% by year ten. The estimated mean recovery time obtained from the Kaplan–Meier estimator was 3.8 years for the transition from NBS to TC/ER, and 5.2 years for the transition to ER alone.

Discussion

Central European forests have repeatedly demonstrated considerable capacity for recovery after disturbances (Senf et al. 2019; Seidl et al. 2024). However, the disturbance pulse after 2018 differed significantly from the past events (Senf and Seidl 2021; Das et al. 2025), generating concerns about these forests' resilience. In the current study, we found that 30.8% of the studied forest area was affected by disturbance within a six-year period, underscoring the enormous scale of the impact. This scale together with intensive post-disturbance management and increasingly extreme weather conditions may have impaired recovery processes and further increased the uncertainty of recovery trajectories.

Regarding our initial hypotheses, we confirmed that disturbed areas were dominated by bare soil shortly after the disturbance (H1), indicating a high degree of landscape homogenization with potentially adverse effects on recovery processes and future resilience (e.g., Johnstone et al. 2016; Storch et al. 2020). Next, we confirmed that despite the unfavorable conditions following the disturbance, there was a tendency toward full recovery (H2). Finally, we confirmed that temporary regeneration failures constituted a significant component of recovery dynamics, potentially signaling emerging vulnerabilities (H3). In the following, we are discussing the key drivers, implications, and limitations underlying the observed patterns.

Recovery dynamics

Although post-disturbance forest recovery processes are inherently complex, two distinct regeneration pathways have been identified in Central Europe: one driven by the presence of advance regeneration, a

cohort of trees already established in the understory prior to disturbance (e.g., Bače et al. 2015; Petrovska et al. 2023; Seidl et al. 2024); and another driven by post-disturbance regeneration, where the majority of trees establish after the disturbance (Winter et al. 2015; Macek et al. 2017; Schüle et al. 2023). A combination of both pathways may occur, for example, in multi-owner landscapes or landscapes composed of a mosaic of managed and unmanaged forests (Winter et al. 2015).

In the current study, the observed recovery dynamics aligned more closely with the second pathway. Specifically, NBS covered, on average, more than 80% of disturbed areas in the period 2018–2020, while the proportion of the two vegetated classes started to increase gradually after the disturbance, reaching 25% (ER) and 54% (TC/ER) of the initially disturbed areas by 2024. The presence of this pathway can be attributed, among other factors, to the legacy of historical rotation-based forest management with a lack of emphasis on promoting structurally complex forest stands that has been practiced across different regions in Europe (Bauhus et al. 2017). The structural homogenization (i.e., the dominance of NBS patches reaching as much as 600 ha; Fig. 7) was likely further amplified by extensive salvage operations. These primarily aimed to remove dead and infested trees but locally also included the removal of surviving individuals and understory vegetation (pers. obs.). However, this pattern should be generalized cautiously as it strongly depends on local forest condition, disturbance type and management practices. For example, forest recovery following the concurrent tree mortality in Germany (Central Europe), was predominantly driven by the presence of advance regeneration (Seidl et al. 2024).

We found distinctly different interannual dynamics among the three post-disturbance classes. On average, 74.6% of NBS and 71.5% of ER remained unchanged between years (Online Appendix E). By contrast, TC was remarkably less stable: on average, 28.2% was transitioning to NBS and 25.0% to ER per year. This instability is consistent with the class's transient nature and with generally high mortality in early regeneration (e.g., Bianchi et al. 2019; Collet et al. 2024), as well as the likely presence of short-lived ruderal vegetation in this class. On the contrary, the hight stability of ER suggests that mortality from competition, browsing, and other agents declined once vegetation reached the ER phase. Although a small share of regeneration failures occurred within ER (8.6% per year, on average), the probability of successful establishment in this class can be considered high.

We found that temporary regeneration failures, i.e., reverse transitions from vegetated classes back to NBS, accounted for 36.8% of total transitions (28.2% from TC and 8.6% from MR), representing a non-negligible component of the overall landscape dynamics (Fig. 7, Online Appendix E). We acknowledge that these dynamics need to be interpreted cautiously in the case of TC due to possible misclassification of vegetation composition. Still, the high proportion of such temporary failures corresponds to generally high mortality rate in forest regeneration: For example, Bianchi et al. (2019) identified only 36.7% survival of seedlings after the first season across ten tree species in an experiment from Central Europe. In the case of extensive disturbed areas without the sheltering effect of mature vegetation, combined with high herbivory from game and insects (mainly the weevil *Hylobius abietis*, which causes extensive regeneration mortality on clear-cuts across Europe; Nordlander et al. 2011), these effects can be even more severe. Although we did not focus on resolving the drivers of the observed reverse transitions, understanding them can be essential for identifying emerging vulnerabilities. Particular attention should be paid to the impacts of climatic stress, which is expected to aggravate with climate change (Petrie et al. 2017; Davis et al. 2019), and effects of high game populations, which is recognized to be one of the main adaptation barriers in many regions (Champagne et al. 2021; Dobor et al. 2024).

Survival analysis, together with the net recovery rate, provided a more integrative view of these dynamics. When recovery was defined as a transition from NBS to TC/ER, the net annual recovery rate was 13.5% and the mean recovery time was 3.8 years. Under the more conservative definition, i.e. considering the transition from NBS/TC to ER, the corresponding values were 5.9% and 5.2 years, respectively. In comparison with some previous studies, here identified recovery dynamics may seem slower: For example, high stem densities have been observed as early as two years post-disturbance in various contexts, including after fire (Schüle et al. 2023), after windthrow in unmanaged stands (Piazza et al. 2024), and following drought-induced tree mortality (Seidl

et al. 2024). However, direct comparison between our findings and those of field-based studies is limited by methodological differences, such as the coarser spatial resolution of the satellite data (10 m), a broader definition of our recovery classes, and differences in forest types and management. Nevertheless, these metrics together with the steadily decreasing size of NBS indicate robust recovery capacity of the studied forest. Importantly, we found no evidence of permanent regeneration failure, defined as a sustained inability to re-establish forest cover (Hansen et al. 2018; Stevens-Rumann et al. 2022).

The inter-annual variation in the transitions was significant, raising questions about the underlying drivers. For example, the net recovery rate calculated based on transitions from NBS to TC/ER peaked in 2023–2024 (20.47%) but was minimal in 2022–2023 (2.16%) (Table 3). Likely drivers include a mix of ecological and socio-economic factors typical of many managed forests, most notably weather, variable management intensity, and their interactions. Disentangling their relative contributions is difficult given the short study period that limits correlation analyses and the lack of socio-economic data. For instance, planting effort was constrained by labor and seedling shortages during the outbreak peak; the extent of planting and protection of regeneration from ungulates (fencing, repellents) could have depended on actual subsidy programs; and management operations were significantly reduced during the COVID-19 crisis. These effects are obviously context-specific, which limits how the identified patterns can be generalized. Nonetheless, the large variation in recovery metrics, though difficult to attribute, underscores the complexity of recovery dynamics in intensively managed landscapes, where one could expect more uniform, management-driven trajectories.

Methodological aspects and limitations

Forest recovery is commonly assessed using indicators such as forest cover, biomass, vegetation height, and species composition (Williams et al. 2012; Bolton et al. 2015; Dobor et al. 2018; Lloret et al. 2024). Here, we used an indicator that integrates vegetation presence and height, two key attributes of forest structure that could have been reliably derived from our reference data (UAV imagery and derived canopy height models). A limitation is that we did not consider tree species composition in regeneration, which is another key determinant of long-term forest function and resilience (Aquilué et al. 2020). This fact needs to be considered when interpreting our results, as the species composition of regenerating cohorts may diverge from pre-disturbance conditions due to factors such as climate change and adaptive forest management (Dieler et al. 2017; van Tiel et al. 2024). This trend is particularly evident in planted spruce forests across Central Europe (a forest type studied here), which demonstrate poor site suitability and their adaptation can be catalyzed by disturbances (Thom and Seidl 2016; Seidl et al. 2024).

Another limitation concerns the length of our study period (2018–2024), which may be considered too short to allow for robust inferences about longer-term recovery processes and their implications for future resilience. For instance, local regeneration failures may become more frequent in the coming years due to increasingly extreme climate, or forest managers might choose to remove parts of the regenerating cohort composed of early-successional species and replace them with more commercially valuable ones. Such effects may restart local recovery process and extend recovery times identified here. On the other hand, they may also increase spatial variation in vegetation structure across the landscape and, to some extent, alter the unfavorable outlook for future resilience suggested by the current results. Nevertheless, recent research has indicated the importance of early reorganization phase for future forest resilience as well as that early development pathways may remain locked for decades to centuries (Seidl and Turner 2022). Therefore, the presented results should be interpreted as robust insight into early recovery dynamics, while recognizing that longer-term implications may be context-dependent.

Our satellite-based approach provided novel insight into large-scale, early recovery dynamics. However, ecological important attributes remained beyond its resolution, such as tree-species composition of regeneration, the relative contributions of natural regeneration versus replanting, and the distribution of unsalvaged patches (e.g., Seidl et al. 2024; Cerioni et al. 2024). Interpretation is further constrained by classification accuracy and the use of simplified recovery classes that may not align with successional gradients commonly used in ecological studies (e.g., Taeroe et al. 2019; Cerioni et al. 2024).

Some model limitations are evident: for example, the 6.3% share of direct transitions from NBS to ER (Online Appendix E) is improbable, even for fast-growing early-seral species. Hence, further research is needed to identify options for large-scale recovery mapping that could resolve finer-scale, ecologically important features. At the same time, the system here studied was characterized by substantial homogeneity in pre- and post-disturbance conditions; therefore, the influence of data and algorithmic limitations on our main inferences is not severe.

Practical implications

Our findings reflect the legacy of long-term management focused on "simplicity and efficiency" rather than resilience (Bauhus et al. 2017; Messier et al. 2019) as well as the generally limited consideration of disturbance legacies in European forestry (Gustafsson et al. 2012; Seidl et al. 2014). Although these shortcomings have been well documented, the present study provides an important demonstration of possible ecological consequences on a landscape scale. Our results thus draw further attention to resilience-oriented strategies such as retention forestry (e.g., Gustafsson et al. 2012), natural-dynamics silviculture (Aszalós et al. 2022), and closer-to-nature forestry (Larsen et al. 2022), which has become a central strategy of the European Commission (European Commission 2023). Specifically, disturbed landscapes provide a window of opportunity to adapt forests to future conditions by enhancing species diversity and increasing structural and spatial complexity. Although the conditions we identified were unfavorable, management opportunities to create more resilient landscapes remain.

Conclusion

Despite the unprecedented scale of the recent disturbance pulse and the compounding effects of climatic stress, extensive tree mortality and salvage logging, our findings indicate that Central European forests retain a substantial capacity for recovery. However, the notable extent of temporary regeneration failures and delayed regeneration in some areas reveal emerging vulnerabilities, which may be amplified by climate change and improper management. These patterns underscore the need for science-based management approaches that exploit disturbance legacies and support structural complexity in regenerating forests. Future research should prioritize disentangling the drivers of early-stage regeneration, particularly those that may erode long-term resilience. A deeper understanding of these processes will be critical to ensuring the sustainability of forest ecosystems in the face of intensifying environmental changes.

Author contributions PW, MP, TH, and RM: formal analysis and methodology, conceptualization, writing, review and editing. THu, ZM: resources and validation. TH: research coordination and funding acquisition. All authors read and approved the final manuscript.

Funding Open access publishing supported by the institutions participating in the CzechELib Transformative Agreement. This work was supported by the projects of the National Agency for Agriculture Research of the Czech Republic no. QK23020039 and QL25020059. Prosper Washaya acknowledges support from the Internal Grant Agency (IGA A_36_24) of the Faculty of Forestry and Wood Sciences, Czech University of Life Sciences, Prague.

Data availability The datasets generated during and/or analyzed during the current study are available from the corresponding author at request.

Declarations

Competing interests The authors declare no competing interests.

References

Agisoft LLC (2023) Agisoft Metashape Professional (Version 2.0.2) [Computer software]. Agisoft LLC. https://www.agisoft.com

Aquilué N, Filotas É, Craven D, Fortin MJ, Brotons L, Messier C (2020) Evaluating forest resilience to global threats using functional response traits and network properties. Ecol Appl 30(5):e02095

Asada R, Hurmekoski E, Hoeben AD, Patacca M, Stern T, Toppinen A (2023) Resilient forest-based value chains? Econometric analysis of roundwood prices in five European countries in the era of natural disturbances. For Policy Econ 153:102975

Aszalós R, Thom D, Aakala T, Angelstam P, Brūmelis G, Gálhidy L, Gratzer G, Hlásny T, Katzensteiner K, Kovács B, Knoke T, Larrieu L, Motta R, Müller J, Ódor P, Roženbergar D, Paillet Y, Pitar D, Standovár T, Svoboda M, Szwagrzyk J, Toscani P, Keeton WS (2022) Natural disturbance regimes as a guide for sustainable forest management in Europe. Ecol Appl 32(5):e2596

Bače R, Svoboda M, Janda P et al (2015) Legacy of pre-disturbance spatial pattern determines early structural diversity following severe disturbance in Montane Spruce Forests. PLoS ONE 10:e0139214

Bauhus J, Forrester DI, Gardiner B et al (2017) Ecological stability of mixed-species forests. Mixed-species forests. Springer, Berlin Heidelberg, pp 337–382

Bianchi E, Bugmann H, Bigler C (2019) Early emergence increases survival of tree seedlings in Central European temperate forests despite severe late frost. Ecol Evol 9:8238–8252

Bolton DK, Coops NC, Wulder MA (2015) Characterizing residual structure and forest recovery following high-severity fire in the western boreal of Canada using Landsat time-series and airborne lidar data. Remote Sens Environ 163:48–60

Bueso-Bello J-L, Carcereri D, Martone M, González C, Posovszky P, Rizzoli P (2022) Deep learning for mapping tropical forests with TanDEM-X bistatic InSAR data. Remote Sens 14(16):3981

Cerioni M, Brabec M, Bače R, Bāders E, Bončina A, Brůna J, Chećko E, Cordonnier T, de Koning JHC, Diaci J, Dobrowolska D, Dountchev A, Engelhart J, Fidej G, Fuhr M, Garbarino M, Jansons Ā, Keren S, Kitenberga M, Klopčič M, Konôpka B, Kopecký M, Köster K, Kucbel S, Lacombe E, Laurent L, Leyman A, Lingua E, Macek M, Maciejewski Z, Malandra F, Marzano R, Metslaid M, Morresi D, Panayotov M, Pawlak B, Pittner J, Šebeň V, Socha J, Svoboda M, Szwagrzyk J, Tsvetanov N, Urbinati C, Vallet P, de Van Kerckhove P, Vandekerkhove K, Vencurik J, Vitali A, Vodde F, Wild J, Nagel TA (2024) Recovery and resilience of European temperate forests after large and severe disturbances. Glob Chang Biol 30(2):e17159

Champagne E, Raymond P, Royo AA et al (2021) A review of ungulate impacts on the success of climate-adapted forest management strategies. Curr Forestry Rep 7:305–320

Chen B, Huang B, Xu B (2017) Multi-source remotely sensed data fusion for improving land cover classification. ISPRS J Photogramm Remote Sens 124:27–39

Collet C, Agro C, Akroume E, Bello J, Berthelot A, Boulanger V, Calas A, Dumas N, Pitaud J, Puyal M, Vast F (2024) Mechanical site preparation severity mediates one-year-survival response to summer drought in planted tree seedlings. New For 55(5):1581–1594.

Das AK, Baldo M, Dobor L et al (2025) The increasing role of drought as an inciting factor of bark beetle outbreaks can cause large-scale transformation of Central European forests. Landsc Ecol 40:108

CDavidson-Pilon2024Lifelines: survival analysis in PythonZenodo10.5281/zenodo.4048819Davidson-Pilon C(2024) Lifelines: survival analysis in Python. Zenodo. https://doi.org/10.5281/zenodo.4048819

Davis KT, Dobrowski SZ, Higuera PE et al (2019) Wildfires and climate change push low-elevation forests across a critical climate threshold for tree regeneration. Proc Natl Acad Sci USA 116:6193–6198

Dieler J, Uhl E, Biber P et al (2017) Effect of forest stand management on species composition, structural diversity, and productivity in the temperate zone of Europe. Eur J Forest Res 136:739–766

Dobor L, Hlásny T, Rammer W, Barka I, Trombik J, Pavlenda P, Šebeň V, Štěpánek P, Seidl R (2018) Post-disturbance recovery of forest carbon in a temperate forest landscape under climate change. Agric for Meteorol 263:308–322

Dobor L, Baldo M, Bílek L, Barka I, Máliš F, Štěpánek P, Hlásny T (2024) The interacting effect of climate change and herbivory can trigger large-scale transformations of European temperate forests. Glob Chang Biol 30(2):e17194

European Commission (2023) Guidelines on closer-to-nature forest management. Publications Office of the European Union

Forzieri G, Dakos V, McDowell NG et al (2022) Emerging signals of declining forest resilience under climate change. Nature 608:534–539

Frolking S, Palace MW, Clark DB, Chambers JQ, Shugart HH, Hurtt GC (2009) Forest disturbance and recovery: a general review in the context of spaceborne remote sensing of impacts on aboveground biomass and canopy structure. J Geophys Res Biogeosci 114(G2):2008JG000911

Getis A, Ord JK (1992) The analysis of spatial association by use of distance statistics. Geogr Anal 24:189–206

Griffiths P, Kuemmerle T, Baumann M, Radeloff VC, Abrudan IV, Lieskovsky J, Munteanu C, Ostapowicz K, Hostert P (2014) Forest disturbances, forest recovery, and changes in forest types across the Carpathian ecoregion from 1985 to 2010 based on Landsat image composites. Remote Sens Environ 151:72–88

Gustafsson L, Baker SC, Bauhus J et al (2012) Retention forestry to maintain multifunctional forests: a world perspective. Bioscience 62:633–645

Han S, Williamson BD, Fong Y (2021) Improving random forest predictions in small datasets from two-phase sampling designs. BMC Med Inform Decis Mak 21:322

Hansen WD, Braziunas KH, Rammer W et al (2018) It takes a few to tango: changing climate and fire regimes can cause

regeneration failure of two subalpine conifers. Ecology 99:966–977
Hartmann H, Bastos A, Das AJ, Esquivel-Muelbert A, Hammond WM, Martínez-Vilalta J, McDowell NG, Powers JS, Pugh TAM, Ruthrof KX, Allen CD (2022) Climate change risks to global forest health: emergence of unexpected events of elevated tree mortality worldwide. Annu Rev Plant Biol 73(1):673–702
Hlásny T, Augustynczik ALD, Dobor L (2021a) Time matters: resilience of a post-disturbance forest landscape. Sci Total Environ. https://doi.org/10.1016/j.scitotenv.2021.149377
Hlásny T, Zimová S, Merganičová K, Štěpánek P, Modlinger R, Turčáni M (2021b) Devastating outbreak of bark beetles in the Czech Republic: drivers, impacts, and management implications. For Ecol Manage 490:119075
Hollaus M, Vreugdenhil M (2019) Radar satellite imagery for detecting bark beetle outbreaks in forests. Curr Forestry Rep 5:240–250
Jarron L, Hermosilla T, Coops N et al (2016) Differentiation of alternate harvesting practices using annual time series of Landsat data. Forests 8:15
Johnstone JF, Allen CD, Franklin JF et al (2016) Changing disturbance regimes, ecological memory, and forest resilience. Front Ecol Environ 14:369–378
Jönsson J (2024) Historical perspectives on forestry science and monocultures: ideas of rationality in Sweden during the early twentieth century. Ambio 53:933–940
Klein JP, Moeschberger ML (2003) Censoring and truncation: survival analysis: techniques for censored and truncated data, 2nd edn. Springer, New York, pp 63–90
Knoke T, Gosling E, Thom D et al (2021) Economic losses from natural disturbances in Norway spruce forests—a quantification using Monte-Carlo simulations. Ecol Econ 185:107046
Larsen JB, Angelstam P, Bauhus J, et al (2022) Closer-to-nature forest management: from science to policy 12. European Forest Institute, Joensuu. https://doi.org/10.36333/fs12
Leverkus AB, Gustafsson L, Lindenmayer DB et al (2020) Salvage logging effects on regulating ecosystem services and fuel loads. Front Ecol Environ 18:391–400
Leverkus AB, Polo I, Baudoux C et al (2021) Resilience impacts of a secondary disturbance: meta-analysis of salvage logging effects on tree regeneration. J Ecol 109:3224–3232
Li (2016) Statistical Machine Intelligence and Learning Engine (SMILE). https://haifengl.github.io/
Lindenmayer DB, Noss RF (2006) Salvage logging, ecosystem processes, and biodiversity conservation. Conserv Biol 20:949–958
Liu YY, de Jeu RAM, McCabe MF et al (2011) Global long-term passive microwave satellite-based retrievals of vegetation optical depth. Geophys Res Lett. https://doi.org/10.1029/2011GL048684
Lloret F, Hurtado P, Espelta JM et al (2024) ORF, an operational framework to measure resilience in social–ecological systems: the forest case study. Sustain Sci 19:1579–1593
Macek M, Wild J, Kopecký M et al (2017) Life and death of *Picea abies* after bark-beetle outbreak: ecological processes driving seedling recruitment. Ecol Appl 27:156–167
Mandl L, Viana-Soto A, Seidl R, Stritih A, Senf C (2024) Unmixing-based forest recovery indicators for predicting long-term recovery success. Remote Sens Environ 308:114194
Meigs GW, Morrissey RC, Bače R et al (2017) More ways than one: mixed-severity disturbance regimes foster structural complexity via multiple developmental pathways. For Ecol Manage 406:410–426
Messier C, Bauhus J, Doyon F et al (2019) The functional complex network approach to foster forest resilience to global changes. For Ecosyst 6:21
Nordlander G, Hellqvist C, Johansson K, Nordenhem H (2011) Regeneration of European boreal forests: effectiveness of measures against seedling mortality caused by the pine weevil *Hylobius abietis*. For Ecol Manage 262:2354–2363
Peters DPC, Pielke RA, Bestelmeyer BT et al (2004) Cross-scale interactions, nonlinearities, and forecasting catastrophic events. Proc Natl Acad Sci USA 101:15130–15135
Petrie MD, Bradford JB, Hubbard RM et al (2017) Climate change may restrict dryland forest regeneration in the 21st century. Ecology 98:1548–1559
Petrovska R, Bugmann H, Hobi ML, Brang P (2023) Replace me if you can: abundance of advance regeneration under canopy trees in a primeval beech forest. For Ecol Manage 537:120939
Piazza N, Bebi P, Vacchiano G, Rigling A, Wohlgemuth T, Bottero A (2024) Post-windthrow forest development in spruce-dominated mountain forests in Central Europe. For Ecol Manage 561:121884
Raffa KF, Aukema BH, Bentz BJ et al (2008) Cross-scale drivers of natural disturbances prone to anthropogenic amplification: the dynamics of bark beetle eruptions. Bioscience 58:501–517
Schüle M, Domes G, Schwanitz C, Heinken T (2023) Early natural tree regeneration after wildfire in a Central European Scots pine forest: forest management, fire severity and distance matters. For Ecol Manage 539:120999
Sebald J, Senf C, Seidl R (2021) Human or natural? Landscape context improves the attribution of forest disturbances mapped from Landsat in Central Europe. Remote Sens Environ 262:112502
Seidl R, Senf C (2024) Changes in planned and unplanned canopy openings are linked in Europe's forests. Nat Commun 15:4741
Seidl R, Turner MG (2022) Post-disturbance reorganization of forest ecosystems in a changing world. Proc Natl Acad Sci USA. https://doi.org/10.1073/pnas.2202190119
Seidl R, Rammer W, Spies TA (2014) Disturbance legacies increase the resilience of forest ecosystem structure, composition, and functioning. Ecol Appl 24:2063–2077
Seidl R, Potterf M, Müller J, Turner MG, Rammer W (2024) Patterns of early post-disturbance reorganization in Central European forests. Proc R Soc Lond B Biol Sci 291(2031):20240625
Senf C, Seidl R (2021) Persistent impacts of the 2018 drought on forest disturbance regimes in Europe. Biogeosciences 18:5223–5230

Senf C, Seidl R, Hostert P (2017) Remote sensing of forest insect disturbances: current state and future directions. Int J Appl Earth Obs Geoinf 60:49–60

Senf C, Müller J, Seidl R (2019) Post-disturbance recovery of forest cover and tree height differ with management in Central Europe. Landsc Ecol 34:2837–2850

Stevens-Rumann CS, Prichard SJ, Whitman E et al (2022) Considering regeneration failure in the context of changing climate and disturbance regimes in western North America. Can J for Res 52:1281–1302

Storch I, Penner J, Asbeck T, Basile M, Bauhus J, Braunisch V, Dormann CF, Frey J, Gärtner S, Hanewinkel M, Koch B, Klein A-M, Kuss T, Pregernig M, Pyttel P, Reif A, Scherer-Lorenzen M, Segelbacher G, Schraml U, Staab M, Winkel G, Yousefpour R (2020) Evaluating the effectiveness of retention forestry to enhance biodiversity in production forests of Central Europe using an interdisciplinary, multi-scale approach. Ecol Evol 10(3):1489–1509

Taeroe A, de Koning JHC, Löf M et al (2019) Recovery of temperate and boreal forests after windthrow and the impacts of salvage logging: a quantitative review. For Ecol Manage 446:304–316

Thom D, Seidl R (2016) Natural disturbance impacts on ecosystem services and biodiversity in temperate and boreal forests. Biol Rev Camb Philos Soc 91:760–781

Tsyganskaya V, Martinis S, Marzahn P, Ludwig R (2018) SAR-based detection of flooded vegetation—a review of characteristics and approaches. Int J Remote Sens 39:2255–2293

van der Walt S, Schönberger JL, Nunez-Iglesias J, Boulogne F, Warner JD, Yager N, Gouillart E, Yu T (2014) scikit-image: image processing in Python. PeerJ 2:e453

van Tiel N, Fopp F, Brun P et al (2024) Regional uniqueness of tree species composition and response to forest loss and climate change. Nat Commun 15:4375

Washaya P, Modlinger R, Tyšer D, Hlásny T (2024) Patterns and impacts of an unprecedented outbreak of bark beetles in Central Europe: a glimpse into the future? For Ecosyst 11:100243

White JC, Hermosilla T, Wulder MA, Coops NC (2022) Mapping, validating, and interpreting spatio-temporal trends in post-disturbance forest recovery. Remote Sens Environ 271:112904

Williams CA, Collatz GJ, Masek J, Goward SN (2012) Carbon consequences of forest disturbance and recovery across the conterminous United States. Global Biogeochem Cycles. https://doi.org/10.1029/2010GB003947

Winter M-B, Baier R, Ammer C (2015) Regeneration dynamics and resilience of unmanaged mountain forests in the Northern Limestone Alps following bark beetle-induced spruce dieback. Eur J for Res 134:949–968

Zeppenfeld T, Svoboda M, DeRose RJ et al (2015) Response of mountain *Picea abies* forests to stand-replacing bark beetle outbreaks: neighbourhood effects lead to self-replacement. J Appl Ecol 52:1402–1411

4.3. Forest Height Structure Mapping

Karim, M. F., **Washaya, P.,** Potterf, M., Modlinger, R., & Hlásny, T. (submitted). AlphaEarth Foundations provides superior accuracy in forest height mapping across severely disturbed areas. Remote Sensing of Environment.

AlphaEarth Foundations provide superior accuracy in vegetation height mapping across severely disturbed forest areas

Md Fazlul Karim [a], Prosper Washaya [a], Maria Potterf [a], Roman Modlinger [a], Karel Kuželka [a], Tomáš Hlásny [a] *

[a] Faculty of Forestry and Wood Sciences, Czech University of Life Sciences in Prague, Kamýcká 129, 165 00 Prague 6–Suchdol, Czech Republic

Abstract

Large-scale forest height mapping remains a key challenge in remote sensing, with implications for harvest planning, carbon accounting, and habitat assessment. Despite recent advances, limitations persist, including signal saturation in high-biomass stands and high preprocessing demands for multi-sensor harmonization. AlphaEarth Foundations (AEF; Google DeepMind, 2025) integrates multi-source Earth observation data into compact representations that may alleviate some of these constraints. Yet its performance relative to traditional approaches remains unclear.

We systematically reviewed research published from 2017 to 2025 to identify predictors (bands and indices) used for forest height mapping using optical and SAR sensors and the accompanying performance metrics, resulting in 487 initial papers. We then built vegetation height-prediction models using Random Forest and U-Net, leveraging the top-ranked predictors identified in the previous studies. Concurrently, we developed prediction models using the AEF combined with both Random Forest and the U-NET classifiers. We used vegetation height models derived from drone-acquired stereoscopic imagery (40 images aproximately 500 ha, in total) as the ground truth data.

AEF consistently outperformed traditional variable sets across both Random Forest and U-Net models, yielding higher explained variance (R^2 increased from 0.61 to 0.90) and reduced bias (from –0.01 to 0.07 m) . Moreover, the use of AEF substantially simplified the workflow, reduced the dimensionality and the need for cross-sensor preprocessing. Therefore, the use of AEF data with combination of U-Net architecture proved its overall superiority over traditional band-based approaches in vegetation height mapping.

Key words:

Vegetation height, Alpha Earth Foundations, machine learning, U-Net, SAR, optical, UAV data fusion.

1. Introduction

Accurate vegetation height mapping at regional to global scales characterizes a fundamental challenge in Earth observation, with inferences spanning carbon cycle modeling, biodiversity assessment, forest management, and climate change mitigation (Dubayah et al., 2020; H. Li et al., 2024; Potapov et al., 2021). Vegetation height serves as a critical structural variable relating above-ground biomass, habitat complexity, and ecosystem function, yet its prediction from satellite observations remains constrained by sensor limitations, modeling approaches, and the growing structural heterogeneity led by natural disturbances and land-use change (Lang et al., 2022). Large-scale disturbances are rapidly altering canopy cover by mortality of mature trees and demographic shifts into younger cohorts, creating spatially and vertically heterogenous post-disturbance structure (Seidl & Turner, 2022). Estimation of vegetation height in these complex landscapes is crucial for evaluating natural regeneration potential, planning forest restoration and identifying spatial distribution of remaining vegetation over harvested areas for ecosystem management.

The satellite-based vegetation height mapping has relied on physical satellite extracted input representations from optical and synthetic aperture radar (SAR) sensors, particularly since the launch of operational satellite constellations such as Landsat, Sentinel-1, and Sentinel-2 (Drusch et al., 2012; Torres et al., 2012). Optical sensors capture spectral variation through multispectral bands and derived vegetation indices, typically achieving correlations around $R^2 = 0.60$ with field-measured heights (Torres de Almeida et al., 2022). Complementary SAR backscatter contributes structure-sensitive information independent of cloud cover, with C-band systems providing sensitivity to vertical structure through co-polarized returns and volume scattering (Ghosh et al., 2020; Y. Liu et al., 2019). Multi-frequency SAR fusion, combining C-band Sentinel-1 with L-band ALOS-2, further enhances sensitivity to canopy and subcanopy elements, yielding R^2 values up to 0.72 in conifer forests (Xi et al., 2022). These multi-sensor approaches emerged in response to the limitations of single-sensor systems in capturing forest structural complexity, with integration efforts demonstrating that combining optical spectral information and SAR structural sensitivity substantially improves predictive accuracy compared to individual sensor streams (Chen et al., 2025; A. Liu et al., 2024; C. Liu et al., 2025; Y. Liu et al., 2019; Morin et al., 2022).

Despite documented improvements, multi-sensor workflows remain constrained by fundamental limitations. Feature engineering requires calculation of vegetation indices, backscatter metrics, and coherence measures tailored to specific sensors and ecological contexts, limiting model transferability across regions and sensor configurations (Fassnacht et al., 2016; Potapov et al., 2021). Cross-sensor preprocessing demands extensive radiometric calibration, geometric co-registration, and temporal harmonization before data fusion, introducing preprocessing complexity that constrains operational scalability (Senf & Seidl, 2022). Additionally, both optical and SAR signals exhibit saturation effects in tall or high-biomass vegetation, with C-band backscatter saturating beyond 20–25 m canopy height and even L-band systems showing reduced sensitivity above 30 m (Mermoz et al., 2015; Santoro et al., 2021) (). In addition, traditional vegetation indices (NDVI, EVI, SAVI) perform poorly in structurally heterogeneous

landscapes, particularly in post-disturbance environments dominated by low vegetation and bare ground where spectral signals saturate rapidly at low biomass levels (Morin et al., 2022).

Advancements in satellite-based vegetation height mapping have occurred at multiple levels. At the data level, incorporation of spaceborne LiDAR systems, especially GEDI (Global Ecosystem Dynamics Investigation) and ICESat-2, has provided direct 3D structural measurements that improve vegetation height model accuracy when fused with optical and SAR predictors (Dubayah et al., 2020; Lei et al., 2024; Sothe et al., 2022). Studies repeatedly demonstrate that combining spaceborne LiDAR metrics with optical and SAR predictors outperforms any individual sensor – for example, correlations between predicted and observed vegetation heights were found to rise from <0.50 for single-sensor approaches to 0.60–0.70 for fused systems (Lei et al., 2024; W. Li et al., 2020; J. Wang et al., 2024; W. Zhu et al., 2023).

At the methodological level, machine learning and deep learning architecture have progressively replaced traditional regression approaches. Random Forest remains widely adopted due to its robustness, interpretability, and suitability for large-scale multi-sensor datasets, achieving 0.53–0.72 and RMSE of 2.9–5.8 m across diverse forest types (Y. Liu et al., 2019; Morin et al., 2022; Tsutsumida et al., 2023). Complementary models such as Support Vector Machines and symbolic regression report correlations around ~0.60 with RMSE values of 1.5–3.1 m (Ghosh et al., 2020; W. Li et al., 2020). However, a shift from classical methods to deep architectures, particularly the Convolutional Neural Networks (CNNs), capture hierarchical spatial structure unavailable to tree-based methods, outperform classical approaches when trained on multi-sensor datasets with R2≈0.64-0.78 (Deng et al., 2025; A. Liu et al., 2024; C. Wang et al., 2025; W. Zhu et al., 2023). U-Net architectures have extended these advances to pixel-level height mapping with superior spatial detail through encoder-decoder structures and skip connections that integrate multi-scale features, achieving correlations exceeding 0.75-0.85 in optimised implementations (Deng et al., 2025; Ge et al., 2022; Yu & Jung, 2023). Hyperparameter optimization, i.e., systematic evaluation of model configurations including filter depth, kernel size, dropout rate, learning rate, batch size, and regularization strength through randomized grid search, has been found to further improves mapping performance across model families (Lei et al., 2024; Torres de Almeida et al., 2022). The integration of advanced data sources with sophisticated algorithmic approaches represents the current state-of-the-art, though workflows remain task-specific and require substantial domain expertise for feature engineering and model design. Still, the transferability of models across regions and sensors remained limited (Fassnacht et al., 2016; Potapov et al., 2021; Senf et al., 2017).

Earth observation foundation models (FMs) represent an emerging approach to addressing these limitations by learning generalizable, multi-sensor representations from massive global datasets through self-supervised pre-training (Zhu et al., 2026). Foundation models such as Prithvi-EO-2.0 (IBM–NASA) (Szwarcman et al., 2024) and TESSERA (Feng et al., 2025) achieve state-of-the-art performance in classification and segmentation tasks by learning representations that transfer across diverse applications (Szwarcman et al., 2024). The Google's AlphaEarth Foundation (AEF, 2017-present) model represents a major step forward, integrating Sentinel-1

SAR, Sentinel-2 optical imagery, GEDI spaceborne LiDAR, ALOS PALSAR-2 L-band radar, ERA5-Land climate reanalysis spanning 2017-2024 into, and auxiliary geospatial datasets into a unified 10 m global grid (Brown et al., 2025). The model outputs compact 64-dimensional embeddings that encode multi-sensor and temporal information without requiring cloud masking, cross-sensor preprocessing, or manual feature engineering. While the original AEF publication demonstrated superior performance across diverse mapping tasks including land cover classification and agricultural monitoring (Fang et al., 2025; Houriez et al., 2025), applications to continuous vegetation height prediction—particularly in structurally heterogeneous landscape - remain limited in peer-reviewed literature.

In this study, we evaluate the potential of Alpha Earth Foundation (AEF) embeddings for vegetation height mapping by systematically comparing AEF embedding approaches against traditional multi-sensor methods. For reference data, we used early post-disturbance landscapes in Central Europe, heavily affected by bark-beetles and anthropogenic disturbances since 2018. Specific objectives are: (1) systematically review current literature to identify the best performing bands, sensors, and modelling methods as candidate predictors to predict vegetation heights; (2) use univariate analysis to test performance power of the candidate predictors; (3) compare the performance among four modeling configurations: combining two input representations (physical satellite extracted inputs vs. virtual embeddings with two algorithmic paradigms (Random forest and U-Net); (4) Systematically quantify prediction accuracy, bias, and variability across approaches using comprehensive regression metrics (R^2, RMSE, MAE, MBE) and height-stratified performance analysis. This approach allowed us systematically evaluate the performance of tradition band-based input vs novel AEF databases and evaluate performance of the traditionally used prediction models (here, random forests) to novel deep learning algorithms (U-Net).

2. Materials and methods

2.1. Experimental design

The workflow comprises four main components for vegetation height prediction: (i) predictors derived from physical satellites – Sentinel-1 (SAR) and Sentinel-2 (optical); (ii) virtual satellite representations provided by AlphaEarth Foundations (AEF) embeddings; (iii) UAV-derived canopy height models used as ground-truth reference data; and (iv) machine- and deep-learning modelling frameworks (Fig. 1).

First, candidate optical and SAR predictor variables are identified through a systematic literature review covering the period 2019–2025. Using UAV-based height data as reference, candidate variables are subsequently screened through univariate linear correlation analyses to retain the most informative predictors. AEF embeddings are retrieved directly from Google Earth Engine and used without additional preprocessing.

Second, four experimental configurations are evaluated: Random Forest and U-Net models trained either on predictors derived from physical satellite data (Physical/RF, Physical/U-Net) or on AEF virtual embeddings (Virtual/RF, Virtual/U-Net). Third, the performance of these

configurations is assessed to identify the most effective approach for generating wall-to-wall vegetation height maps. Model performance is evaluated using multiple metrics, both across the full dataset and within specific vegetation height strata

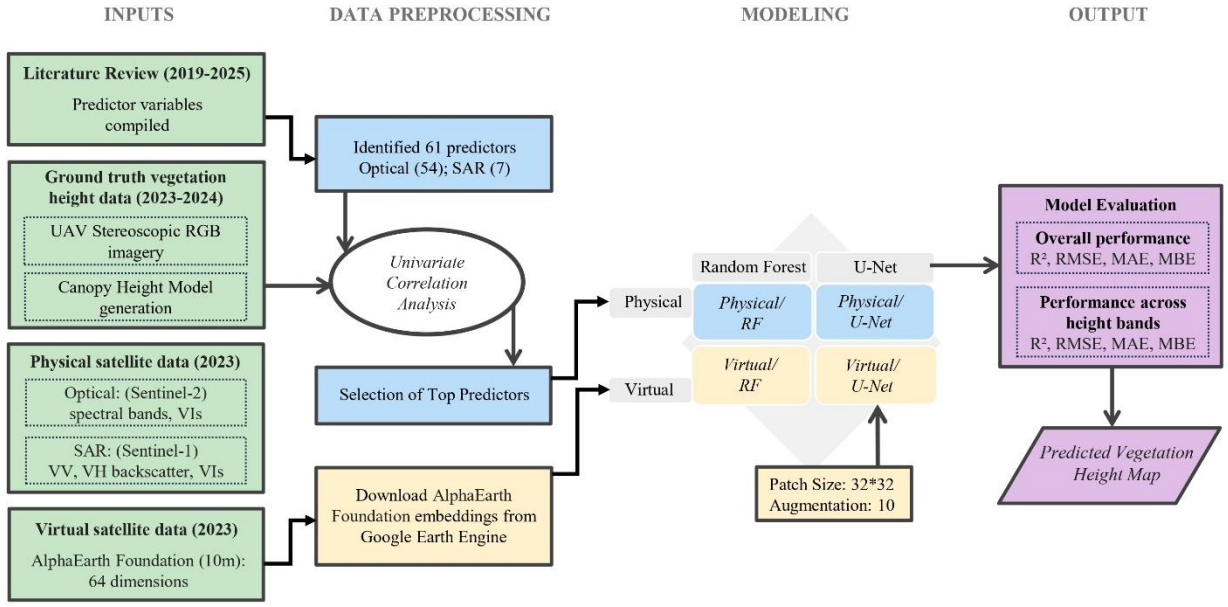

Fig. 1. Workflow for vegetation height prediction using physical (optical and SAR) and virtual (AlphaEarth Foundations) remote sensing data and two model types (Random Forests and U-NET).

2.2. Study region

The research was conducted across a 9,000 km² forested in the Czech Republic, Central Europe (Fig. 2) that was severely affected by bark beetle outbreaks between 2018 and (Washaya et al., 2024, 2025). Forests cover approximately 35% of the region, with Norway spruce (Picea abies) representing 70% of canopy cover. Approximately 38% of total forest areas and 49% of initial spruce cover experienced mortality due to the outbreak and were subsequently harvested (Washaya et al., 2024). Together with the subsequent recovery dynamics, the disturbance created highly complex spatial and height vegetation structure.

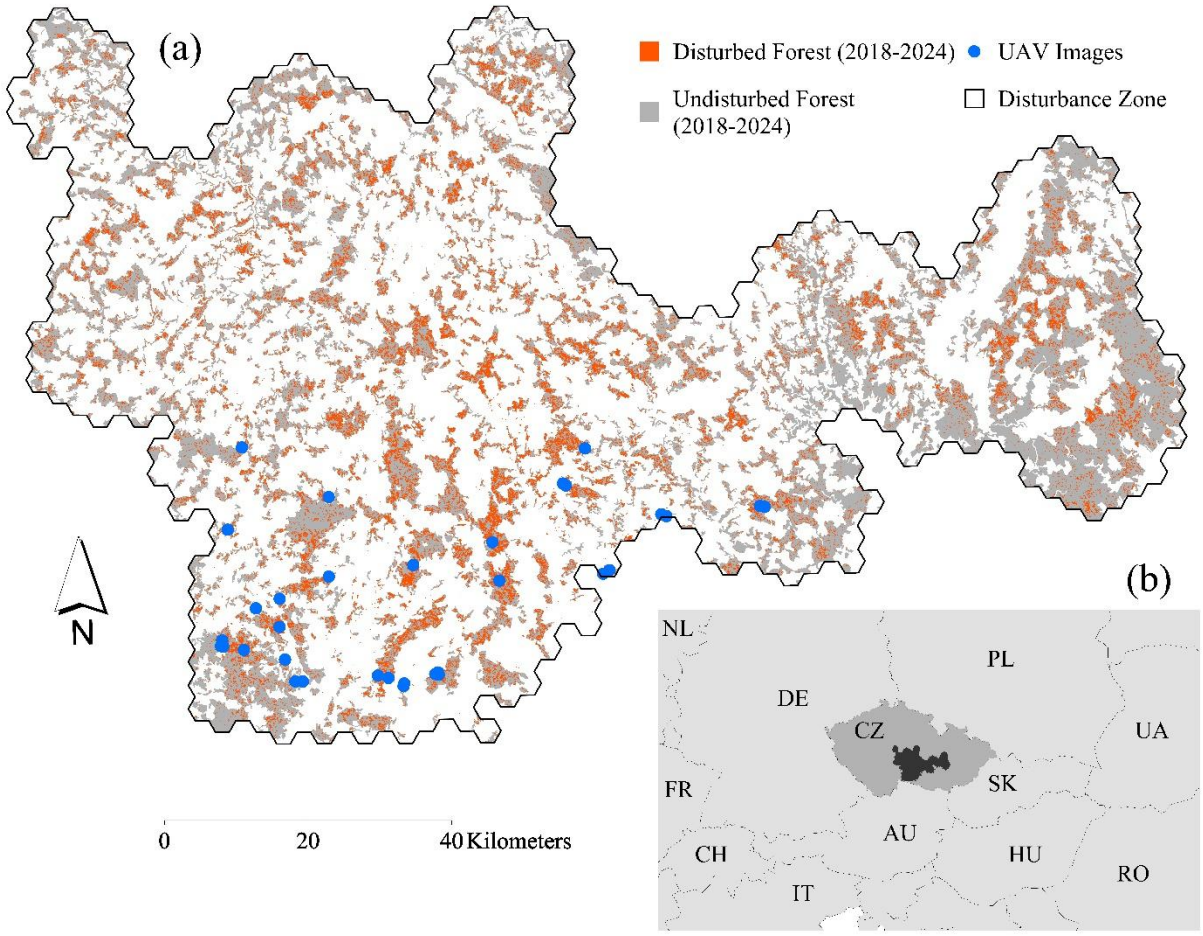

Fig. 2. Study area with the positions of high-resolution UAV imagery acquired in 2023 and 2024 (blue dots) (a) and location of the study area within the Czech Republic and Europe (b).

2.3. Ground truth vegetation height data

High-resolution canopy height model (CHM) derived from UAV imagery acquired during summers 2023 and 2024 served as reference data for model training and validation (Fig. 3). The UAV campaigns involved low-altitude flights (approximately 100 m above ground level) using a DJI Phantom 4 Pro equipped with an integrated 20-megapixel RGB camera, capturing imagery at 2–2.5 cm spatial resolution. A total of 40 flight missions were conducted, each covering 10–12 hectares and representing diverse post-disturbance conditions. The captured images were processed using Agisoft Metashape software and structure-from-motion photogrammetry techniques to generate georeferenced orthophotographs. The workflow involved aligning UAV imagery to produce sparse point clouds, subsequently densified through multi-view stereo matching. Ground filtering algorithms classified ground points, enabling Digital Terrain Model (DTM) generation. Digital Surface Models (DSMs) were derived from all point cloud data.

Canopy height models were calculated by subtracting DTMs from DSMs (Yu & Jung, 2023)(Yu & Jung, 2023).

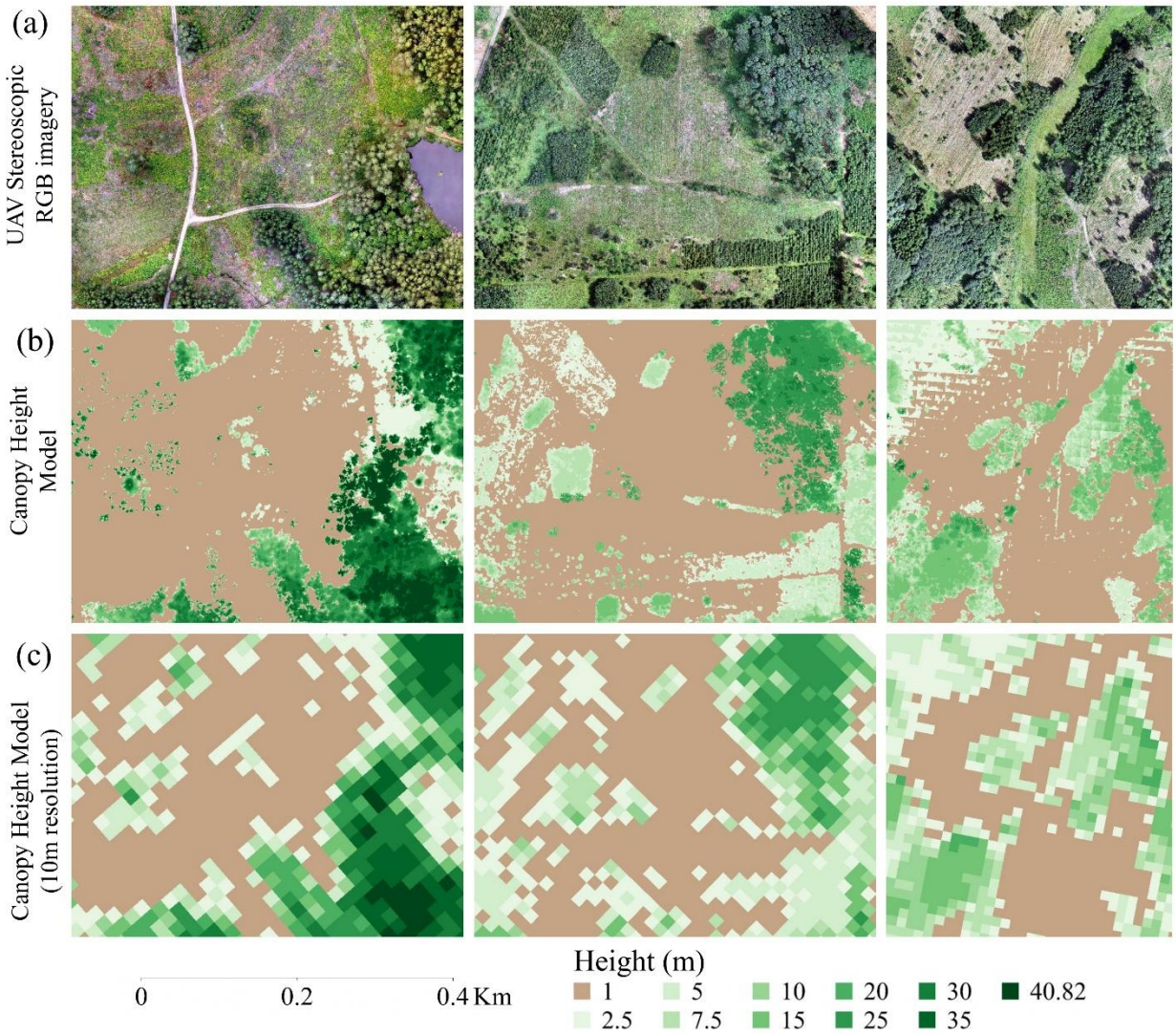

Fig. 3. Multi-scale representation of reference vegetation height data. (a) Original UAV RGB orthophotographs at ~2.5 cm resolution for three representative sites. (b) Structure-from-motion-derived Canopy Height Models showing continuous height distribution. (c) Reference data resampled to a 10 m resolution grid aligned to the used satellite imagery. Brown colors represent bare soils (vegetation height <1m).

To align resolution of the reference data with the used satellite imagery, a 10 m × 10 m fishnet grid was imposed over each UAV-derived CHM, geometrically matching satellite imagery grid. Mean height was calculated for each grid cell and used as reference for model training. The resulting dataset comprised 47,103 reference height samples ranging from 0.00 to 40.82 m (mean: 2.37 m, median: 0.59 m, standard deviation: 4.42 m) (Fig 4). The data exhibits strongly right-skewed distribution, characterizing the heavily disturbed forest landscape.

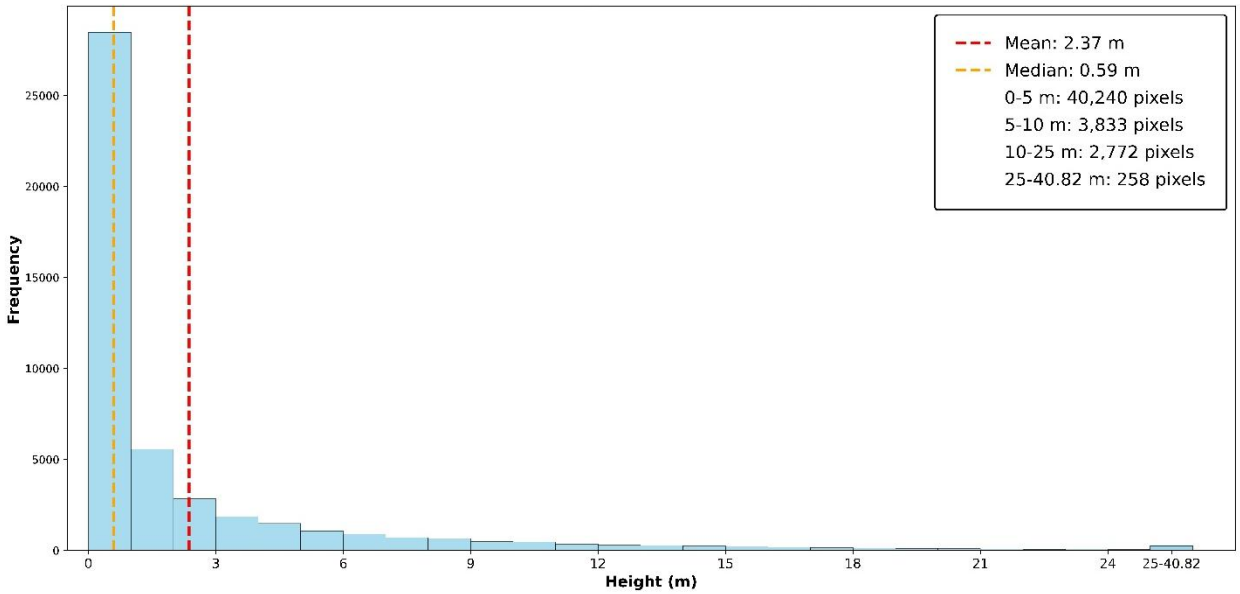

Fig. 4. Frequency distribution of reference vegetation height samples (n = 47,103) extracted from UAV-derived canopy height models and resampled to a 10 m spatial resolution of the used satellite imagery.

2.4. Literature review

To identify candidate input features commonly used in multi-sensor satellite-based vegetation height mapping, we conducted a systematic literature review following the PRISMA (Preferred Reporting Items for Systematic Reviews and Meta-Analyses) framework (Page et al., 2021)(Page et al., 2021). The search addressed three major academic databases (Web of Science, Scopus, and Google Scholar) using keyword combinations: ("vegetation height" OR "canopy height" OR "forest height") AND ("Sentinel-1" OR "Sentinel-2" OR "SAR" OR "optical") AND ("machine learning" OR "random forest" OR "deep learning" OR "U-Net" OR "neural network", OR "CNN").

Searches were restricted to peer-reviewed journal articles published in English between 2019 and 2025. Studies were included if they: (1) utilized Sentinel-1 and/or Sentinel-2 satellite imagery for vegetation height estimation, (2) employed machine learning or statistical modeling approaches, (3) clearly documented predictor variables used, and (4) reported quantitative performance metrics (RMSE, R^2, MAE). Studies were excluded if they relied exclusively on airborne platforms, focused solely on categorical classification rather than continuous height estimation, or lacked sufficient methodological detail for replication. From each included study, we extracted information on geographic location, modeling methods, input features employed with their mathematical formulations, reference data sources, spatial resolution, and reported accuracy metrics. All identified input features were compiled into a comprehensive candidate list for empirical evaluation (see Table 1).

2.5. AlphaEarth Foundations dataset

The AlphaEarth Foundation (AEF) embeddings represent learned feature representations generated by a deep learning foundation model pre-trained on diverse global satellite observation data (Brown et al., 2025). The foundation model was trained on multiple data sources including Sentinel-1 SAR (Torres et al., 2012), Sentinel-2 optical imagery (Drusch et al., 2012), GEDI spaceborne LiDAR (Dubayah et al., 2020), ALOS PALSAR-2 L-band radar (Rosenqvist et al., 2014), and ERA5-Land climate reanalysis (Muñoz-Sabater et al., 2021), spanning the period from 2017 to 2024 with global coverage. This pre-training enables the model to learn generalizable representations of vegetation structure, biomass, moisture content, and phenological characteristics encoded within complex spectral-structural-temporal patterns (Houriez et al., 2025). Unlike feature-based predictors requiring explicit mathematical formulation (such as vegetation indices), the AEF embeddings are data-driven representations optimized to encode information relevant for diverse Earth observation tasks (Brown et al., 2025).

We accessed the AEF embeddings of 2023 (a year of acquisition of most ground truth data) at 10 m spatial resolution through GEE Python API using the image collection identifier "GOOGLE/SATELLITE_EMBEDDING/V1/ANNUAL". Each pixel is represented by a 64-dimensional embedding vector (bands A00–A63), where each dimension captures latent features learned during model training. We extracted AEF embeddings for all 47,103 ground truth sample locations, forming virtual satellite input feature dataset.

2.6 Height prediction models

We developed four modeling configurations combining physical and virtual satellite input features with two algorithmic paradigms – machine learning represented by Random Forest (RF) and deep learning represented by the U-Net algorithm.

2.6.1. Random Forest model

RF is an ensemble machine learning methods that combines predictions from multiple decision trees, where each tree is trained on random subsets of features and samples to reduce overfitting and improve generalization (Breiman, 2001). RF models operated on individual 10 m × 10 m pixels as independent point samples, with each pixel represented as a feature vector paired with reference height. Training data comprised 47,103 samples extracted using Google Earth Engine's sampleRegions() function, partitioned into training (70%, n=32,973) and testing (30%, n=14,130) subsets via stratified random sampling. Physical/RF utilized selected predictor variables identified through systematic literature review, where Virtual/RF utilized all 64 AEF embedding dimensions. Both models were implemented in scikit-learn (Pedregosa et al., 2018)(Pedregosa et al., 2018) with standard hyperparameters: 100 trees (n_estimators=100), unlimited depth (max_depth=None), and sqrt feature selection (max_features='sqrt'). Model performance was evaluated using 10-fold cross-validation on training data, with final assessment on the held-out test set using Coefficient

of Determination (R2), Root Mean Square Error (RMSE), Mean Absolute Error (MAE), and Mean Bias Error (MBE).

2.6.2. U-Net model

U-Net, a convolutional neural network architecture originally designed for biomedical image segmentation (Ronneberger et al., 2015), features an encoder-decoder structure with skip connections for multi-scale feature integration. The model performed pixel-wise regression on 32×32 patches at 10 m resolution (320 m ground coverage). The three-level encoder extracted hierarchical features through successive 3×3 convolutions with ReLU activation and 2×2 max pooling: Level 1 (32×32, F filters), Level 2 (16×16, 2F filters), and Level 3 (8×8, 4F filters). The bottleneck applied dual convolutional layers with 8F filters and spatial dropout at 8×8 resolution. The decoder reconstructed spatial resolution through three upsampling blocks, each performing 2×2 bilinear upsampling, concatenating encoder features via skip connections to preserve fine spatial details, and applying dual 3×3 convolutions with decreasing filter counts (4F→2F→F). A final 1×1 convolutional layer with ReLU activation produced single channel output (32×32×1), ensuring non-negative height predictions. Physical/U-Net processed selected predictor variables identified through literary search, while Virtual/U-Net utilized 64-dimensional embeddings; all other architectural components remained identical.

Training patches were extracted from 40 UAV-derived height models (10-12 ha each) and augmented 10-fold through spatial transformations (90° rotations, horizontal/vertical flips) and spectral perturbations (brightness adjustment, contrast enhancement, Gaussian noise). Virtual/U-Net and Physical/U-Net training datasets comprised 572 and 336 patches, respectively, partitioned through stratified random sampling into training (70%; n=400 and 236), validation (15%; n=86 and 59), and testing (15%; n=86 and 50) subsets. Channel-wise normalization applied using training set statistics (mean and standard deviation per band) to prevent information leakage. Systematic grid search (20) evaluated hyperparameter configuration: base filter count $F \in \{24, 32, 40\}$, kernel size $\in \{3, 5\}$, dropout rate $\in \{0.15, 0.2\}$, learning rate $\in \{0.0005, 0.001\}$, batch size $\in \{2, 4\}$, and L2 regularization $\in \{5\times10^{-5}, 8\times10^{-5}\}$. The training employed Adam optimizer (Kingma & Ba, 2017) (β_1=0.9, β_2=0.999) with early stopping (patience=20 epochs) and adaptive learning rate reduction (factor=0.5) upon validation loss plateaued, with 200 epoch maximum duration. For operational deployment, we implement a sliding-window strategy processing 32×32-pixel patches with 50% overlap (stride=16) to minimize boundary artifacts. Each patch receives Gaussian-weighted blending (σ=8) with center-weighted decay toward boundaries, reducing visible seams when aggregating overlapping predictions. This approach, similar to techniques employed in large-scale geospatial inference (Houriez et al., 2025), enables seamless wall-to-wall mapping while maintaining prediction consistency across patch boundaries.

3. Results

3.1. Predictor identification through systematic literature review

The database searches yielded 484 articles from Web of Science, 202 articles from Scopus, and 500 from Google Scholar, totaling 1186 articles. Following duplication removal, 573 unique articles remained for screening. Title and abstract screening of all 573 articles was conducted to identify studies focused on vegetation or canopy or forest height mapping. The screening resulted in 103 articles being retained for full-text assessment. Additional 79 articles were excluded during full-text assessment for the following reasons: (1) studies where continuous vegetation height estimation was not the primary research objective but rather a secondary attribute alongside biomass mapping, forest structure characterization, or land cover classification; (2) studies that did not incorporate Sentinel-1 and/or Sentinel-2 data as part of their methodological framework, despite initial abstract indications; and (3) studies that lacked sufficient detail in their methodology sections regarding predictor variable selection, feature engineering processes, or model implementation procedures, thereby preventing independent replication of the proposed approaches. Following this assessment, 23 articles were included in the final review (Table 1).

Table 1 Selected vegetation height mapping studies using different physical remote sensing products (SAR, optical, spaceborne LiDAR such as GEDI and ICESat-2) and different methods. Performance metrics are root mean square error (RMSE), coefficient of determination (R^2), and the mean absolute error (MAE). Implemented techniques: K-Nearest Neighbors (KNN), Random Forest (RF), Support Vector Machine (SVM), eXtreme Gradient Boosting (XGB), Multi-scale Adaptive Residual Segmentation Network (MARSNet), Visual Geometry Group-Adaptive Bins (VGG-AdaBins), AutoGluon Automated Machine Learning (AAML), Light Gradient Boosting Machine (LightGBM), Categorical Boosting (CatBoost), Gradient Boosting (GB), Classification and Regression Trees (CART), Gradient Boosting Decision Tree (GBDT), Symbolic Regression (SR), Linear Regression (LR), Deep Learning (DL), Convolutional Neural Network (CNN), 1-Dimensional Convolutional Neural Network (1D CNN), Artificial Neural Network (ANN), BP Neural Network Inversion Model (BP NNIM), Fully Convolutional Network (FCN). Input data sensor: Sentinel-1 (S1), Sentinel-2 (S2), Landsat-8 (L8), Landsat-9 (L9), Airborne Laser Scanning (ALS). Ground truth (Response): GEDI: Relative Height (RH) which represents canopy height percentiles; ICEsat-2: ATL08 which represents surface type land/vegetation.

Location & Citation	**Methods**	**Variables**		**Map Accuracy**	
		Predictor	Response	Pixel size	Metrics: RMSE (R2)
USA (Wang et al., 2025)	KNN; RF; SVM; XGB	**Optical:** S2 (B2-B8A, B11, B12, NDVI, EVI); **SAR:** S1 **(**VV, VH	Spaceborne LiDAR: GEDI L2A (RH98)	10m	4.85m (0.55)

		backscatter, InSAR coherence); ALOS-2: (HH, HV backscatter)			
China (Chen et al., 2025)	DL: MARSNet	**Optical:** S2 (B2-B8A, B11, B12, NDVI); **SAR:** S1 (VV, VH, ratio (VV/VH)); ALOS-2 (HV, HH, ratio (HV/HH))	Spaceborne LiDAR: GEDI L2A (RH 95; RH98)	10m	2.82m (0.62)
China (Li et al., 2025)	RF	**Optical:** S2 (RVI, NDVI, EVI, LAI, Cab, FVC); **SAR:** S1 (VV, VH)	Spaceborne LiDAR: GEDI L2B (RH 98)	10m	2.56m (0.71)
Canada (C. Liu et al., 2025)	DL: VGG-AdaBins	**Optical:** S2 (B2-B8A, 11, 12, NDVI); **SAR:** S1 (VV, VH, VV-VH, VV+VH, RVI); ALOS-2 (HH, HV, HH/HV, HH-HV)	ICESat-2 (ATL08)	30m	2.27m (0.76)
Indonesia (Pickstone et al., 2025)	RF	**Optical:** S2 (B2-8A, 11, 12, NDRE, CIRE, GNDVI, AVI)	Airborne LiDAR	10m	3.52 (0.68)
China (Deng et al., 2025)	UNet	**Optical:** S2 (B2-8A, 11, 12); SAR: S1 (VV, VH)	Spaceborne LiDAR: GEDI L2A (RH 98)	10m	5.54 (0.55)
China (Guo et al., 2024)	RF	**Optical:** S2 (B2-8, 11, 12, NDVI, EVI, LSWI); **SAR:** S1 (VV and VH backscatter)	Spaceborne LiDAR: ICESat2 ATL08	30m	2.99m (0.73)
Brazil (A. Liu et al., 2024)	AAML (RF, XGB, LightGBM, CatBoost)	**Optical:** L8 (B2-B7, NDVI, TCG, KNDVI); **SAR:** ALOS-2**:** (HH, HV backscatter)	Spaceborne LiDAR:: GEDI L2A (RH90, 95, 98, 100); ICSSat-2: ATL08	30m	4.81m (0.72)
China (J. Wang et al., 2024)	1D CNN, ANN, and RF	**Optical:** S2 (B2-B8, B11-B12, ARI, CIG, CIRE, CVI, EVI, EVI2, MSAVI, MSI, NDVI, NDVI705, RVI, SAVI, Tasseled Cap (3))	Spaceborne LiDAR: GEDI L2A (RH 98)	10m	4.59m (0.64)

Italy (Alvites et al., 2024)	RF, GB, and CART	**Optical:** S2 (B2-7); **SAR:** S-1 (VV, VH backscatter, ascending and descending)	Spaceborne LiDAR: GEDI L2A (RH90, 95, 98, 100)	10m	nRMSE: 16-27% (0.61-0.93)
China (Lei et al., 2024)	RF, and FCN	**Optical:** L8 (B2-B7, NDVI, NDWI, EVI, SAVI, NBR, NDMI, RVI, DVI, NDSI, TCT (3)); **SAR:** S-2 (B1-B9, NDVI, NDWI, EVI, SAVI, NBR, NDMI, RVI, DVI, NDSI, TCT (3))	Spaceborne LiDAR: GEDI L2A (RH95)	10m	6.93m (MAE: 5.65m)
Japan (Tsutsumi da et al., 2023)	RF	**Optical:** S2 (B2-8A, 11, 12); **SAR:** S1 (VV, VH backscatter, ascending and descending**)**	Spaceborne LiDAR: GEDI L2A: (RH 98)	10 m	5.80m (0.63)
China (W. Zhu et al., 2023)	BP NNIM model	**Optical:** L8 and L9: (SLAVI, TCB, VI3, EVI, ARVI, TCG, TCW, DVI, PVI)	Spaceborne LiDAR: GEDI L2A (RH95); ICSSat-2: ATL08	30m	3.11m (0.75)
Brazil (Torres de Almeida et al., 2022)	LR, CART, and RF	**Optical:** S2 (B2-8A, 11, 12, SR, NDVI, GNDVI, VIgreen, RENDVI, SRRE, RRI1, IRECI, MSI, NDII, NBR, SLAVI); **SAR:** S1 (VV, VH backscatter, ratio, NDI, RVI)	Airborne LiDAR Canopy height	10m	4.86m (0.60)
China (Xi et al., 2022)	RF, and GBDT	**Optical:** S2 (B2-4, B8, LAI, FAPAR, FCOVER, RVI, EVI, DVI, MSAVI, NDVI)**; SAR:** S1 (VV, VH backscatter)	Spaceborne LiDAR: ICESat-2 (ATLO8)	250 m	3.37m (0.59)
Canada	RF	**Optical:** S2 (B4 and B8); **SAR:** S1 (VV, VH	Spaceborne LiDAR: ICESat-2	250 m	5.4m (0.60)

(Sothe et al., 2022)		backscatter); ALOS-2 (HH and HV)	ATL08; GEDI L2A: (RH98)		
France (Morin et al., 2022)	SVM	**Optical:** S2 (B4, 8, 8A, 11, NDVI, BI, NDWI); **SAR:** S1 (VV, VH backscatter); ALOS-2: (HH and HV Polarization)	Spaceborne LiDAR: GEDI L2A (RH95)	10m	3.3m (nRMSE: 0.23%)
Finland (Ge et al., 2022)	UNet	**Optical:** S2 (B2-B4, B8); **SAR:** S1 (VV, VH)	ALS	20m	1.72m (0.75)
Paraguay (Kacic et al., 2021)	RF	**Optical:** S-2 (B2-B8A, B11, B12, NDVI, EVI, NDWI, NDMI, Tasseled Cap, IPVI, GNDVI, ARVI2, DVI, LCI, Band Ratios); **SAR:** S-1 (VV and VH backscatter)	Spaceborne LiDAR: GEDI L2A and L2B (RH95)	10m	1.6m (0.64)
China (W. Li et al., 2020)	CNN and RF	**Optical:** S-2 (B2-B8A, B11, B12, NDVI, EVI, MSAVI, NDVIredEdge1-4, NDVI); L8 (B2-B7, NDVI, EVI, MSAVI)**; SAR:** S1 (VV and VH backscatter)	Spaceborne LiDAR: ICESat-2 (ATLO8)	250 m	2.68m (0.78)
India (Ghosh et al., 2020)	RF and SR	**Optical:** S2 (LAI and FVC); **SAR:** S1-Coherence	Field-plot CH	20m	1.48m (0.62)
Gabon/Switzerland (Lang et al., 2019)	DL: CNN	**Optical: S2 (**B2-B8A, B11, B12**)**	Airborne LiDAR	10m	3.4m (MAE: 1.7m)
China (Liu et al., 2019)	RF	**Optical:** S2 (RVI, EVI, DVI, NDVI78a, NDVI67, NDVI58a, NDVI56, NDVI57, NDVI68a, NDVI48, LAI, Cab, FVC, FAPAR, CWC)**; SAR:** S1 (VV and VH backscatter)	Field-plot Mean Height	10m	2.92m (0.53)

The geographic distribution of identified studies showed a concentration in Asia, with remaining studies distributed across North America, South America, Europe, and Africa (Fig. 5a). Since 2019, the number of studies meeting the defined criteria has been increasing (Fig. 5b), though the annual number of studies was limited. The reported performance metrics varied substantially: RMSE ranged from 1.48–6.93 m (mean across the studies 3.72 m) and R^2 from 0.23–0.78 (mean 0.63). Studies employing airborne LiDAR or field-plot reference data achieved superior accuracy RMSE ranged from 1.48–4.86 m (mean: 2.98 m) compared to those using spaceborne LiDAR reference data 1.60–6.93 m (mean: 4.0 m). Analysis of modeling approaches identified Random Forest as the predominant method, followed by deep learning architectures, traditional machine learning algorithms including SVM and SR, and advanced ensemble methods such as XGBoost, Gradient Boosting, LightGBM, CatBoost (Fig. 5c). Multi-sensor fusion of optical and SAR data, particularly Sentinel-1 and Sentinel-2 integration, characterized the majority of implementations (Fig. 5d).

We identified 61 candidate predictor variables for evaluation: 54 optical-derived variables from Sentinel-2 (9 spectral bands, 40 vegetation indices, 5 biophysical parameters) and 7 SAR-derived variables from Sentinel-1 (2 backscatter polarizations, 5 SAR vegetation indices). Complete variable list with mathematical formulations is provided in Appendix Table A1.

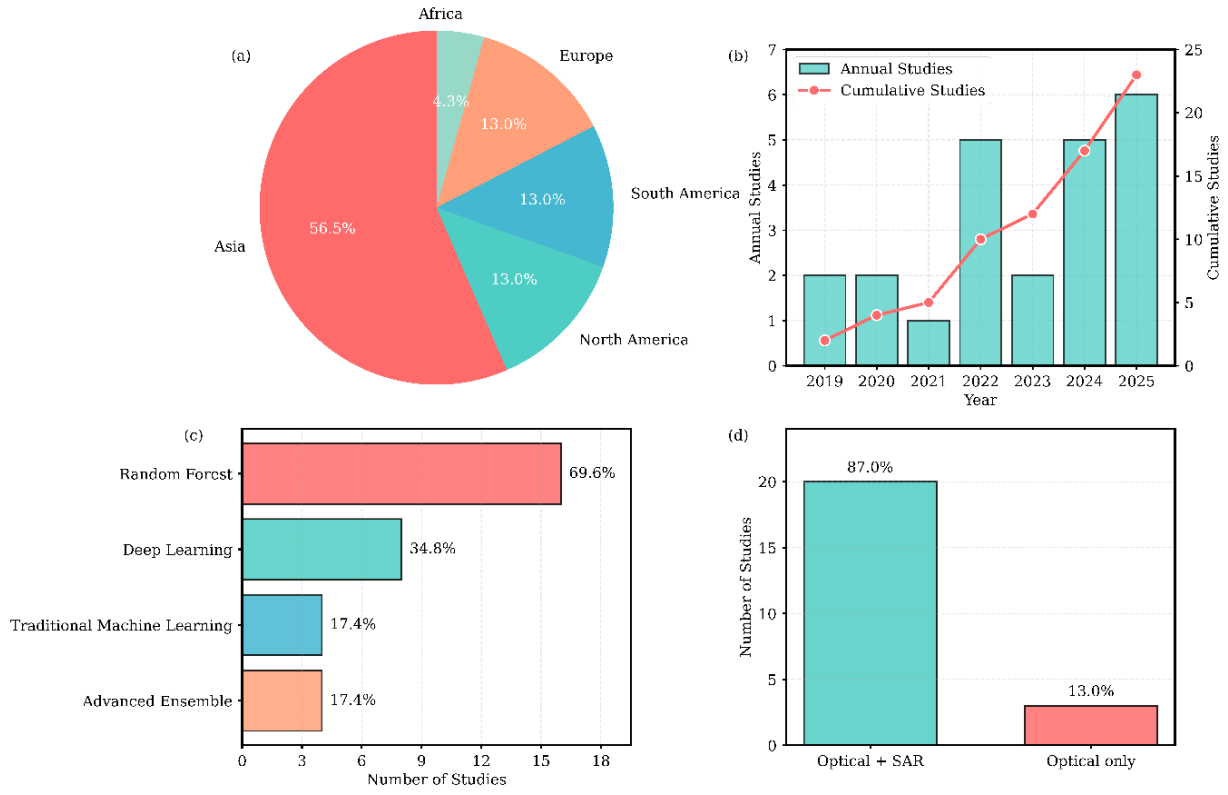

Fig. 5. Results of the systematic literature review of vegetation height mapping studies (2019-2025, n=23). (a) Geographic distribution of the selected studies by continent; (b) Annual (bars) and

cumulative (line) temporal trends in the number of studies; (c) Distribution of modeling approaches; and (d) Sensor integration strategies.

3.2. Reduction of candidate input features

Univariate linear regression analysis between 61 candidate predictor variables and the UAV-derived reference heights ranked variables by their predictive powers (R^2 values) (Fig. 6, Table A1). We found nine bands that with the strongest predictive power ($R^2 \geq 0.20$) dominated by SAR-derived metrics and red-edge/SWIR optical bands. SAR variables demonstrated the strongest overall predictive power, with VV and VH polarizations (both individual and combined) achieving R^2 values of 0.22-0.24. Among optical variables, Band 5 (Red Edge) emerged as the single best predictor (R^2=0.26), followed by SWIR bands (B11, B12: R^2=0.20-0.24) and Band 3 (Green: R^2=0.21). Tasseled Cap transformations matched the predictive strength of individual spectral bands, with TCW (R^2=0.24) and TCB (R^2=0.20). These nine variables were used for training height prediction models. The moderate performance group ($0.10 \leq R^2 < 0.20$) contained 13 variables, including various vegetation indices (SLAVI, NDSI, NDMI, etc.) and additional spectral bands (B2, B4, B6). The low-performance bands ($R^2 < 0.10$) encompassed the remaining 39 variables, predominantly consisting of vegetation indices (NDVI, EVI, SAVI, GNDVI, etc.) and derived biophysical parameters (LAI, FAPAR, FVC, CAB).

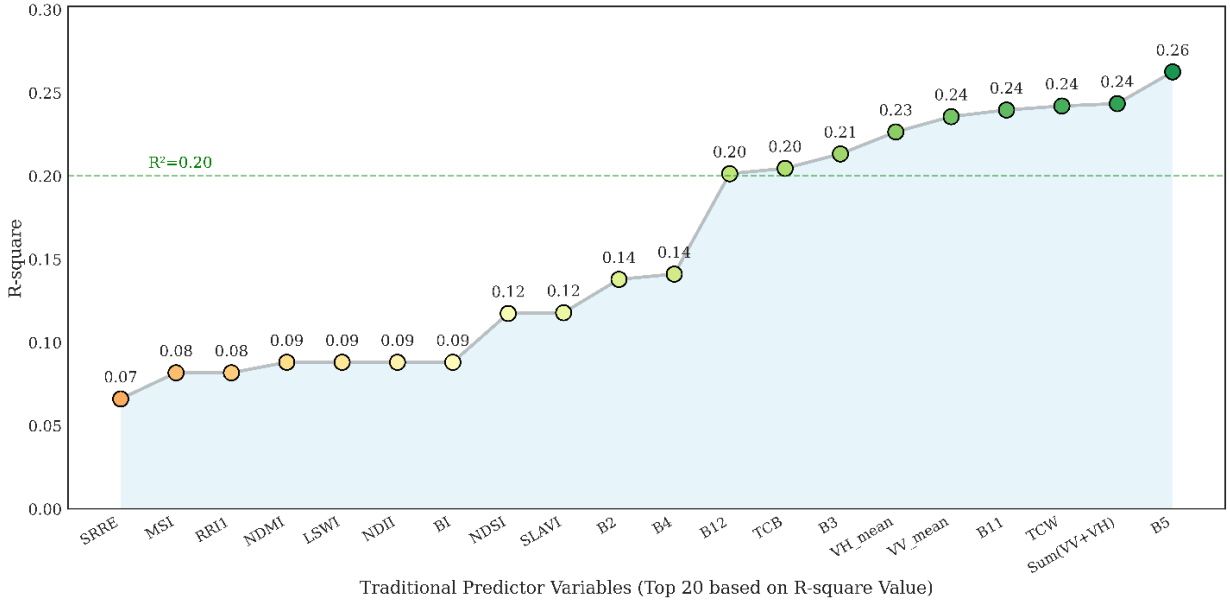

Fig. 6. Univariate regression performance of predictor variables. The top 20 variables are ranked by R^2 values calculated between each predictor and the UAV-derived reference vegetation heights.

3.3. Performance of tested model-dataset configurations

Model performance revealed that both input feature representation (physical vs. virtual) and modeling approach (RF vs. U-Net) contributed to prediction accuracy (Table 3). Virtual satellite

embeddings consistently outperformed physical satellite extracted features across both modeling approaches (RF and U-Net). At the same time, U-Net demonstrated higher performance than RF regardless of input feature type.

Table 3. Performance metrics for vegetation height prediction models evaluated on held-out (testing) datasets (Virtual/U-Net, Physical/U-Net, Virtual/RF and Physical/RF). Metrics include coefficient of determination (R^2), root mean square error (RMSE), mean absolute error (MAE), and mean bias error (MBE). Four model configurations combine two modeling approaches (U-Net and RF) with two input types (physical and virtual satellite features).

Model	R^2	RMSE (m)	MAE (m)	MBE (m)
Virtual/U-Net	0.90	1.26	0.68	0.07
Physical/U-Net	0.81	1.55	0.80	-0.01
Virtual/RF	0.78	2.05	1.04	0.03
Physical/RF	0.61	2.75	1.46	0.07

Virtual/U-Net configuration achieved the highest performance (R^2=0.90, RMSE=1.19 m), followed by a clear hierarchy: Physical/U-Net > Virtual/RF> Physical/RF (R^2: 0.81 > 0.78 > 0.60; RMSE: 1.55 m > 2.05 m > 2.75 m) (Table 3). Transitioning from RF to U-Net with identical input features reduced RMSE by 44% for physical satellite derived features (2.75 m → 1.55 m) and 39% for virtual embeddings (2.05 m → 1.26 m), indicating that spatial context modeling provides advantages across different feature representation types. Notably, Physical/U-Net outperformed Virtual/RF embeddings by 24% in RMSE. Similarly, transitioning from physical satellite extracted features to virtual satellite embeddings reduced RMSE by 26% for RF (2.75 m → 2.05 m) and 19% for U-Net (1.55 m → 1.26 m).

Scatter plots of observed versus predicted vegetation heights (Fig. 7) and the corresponding residual distributions indicate that the Virtual/U-Net configuration achieved the smallest dispersion and the closest agreement with the 1:1 line (Fig. 7a). In contrast, the Physical/RF configuration (Fig. 7d) exhibited the largest dispersion, particularly at higher vegetation heights. None of the tested models showed a zero trend in the residuals, indicating systematic underestimation in the upper vegetation height classes.

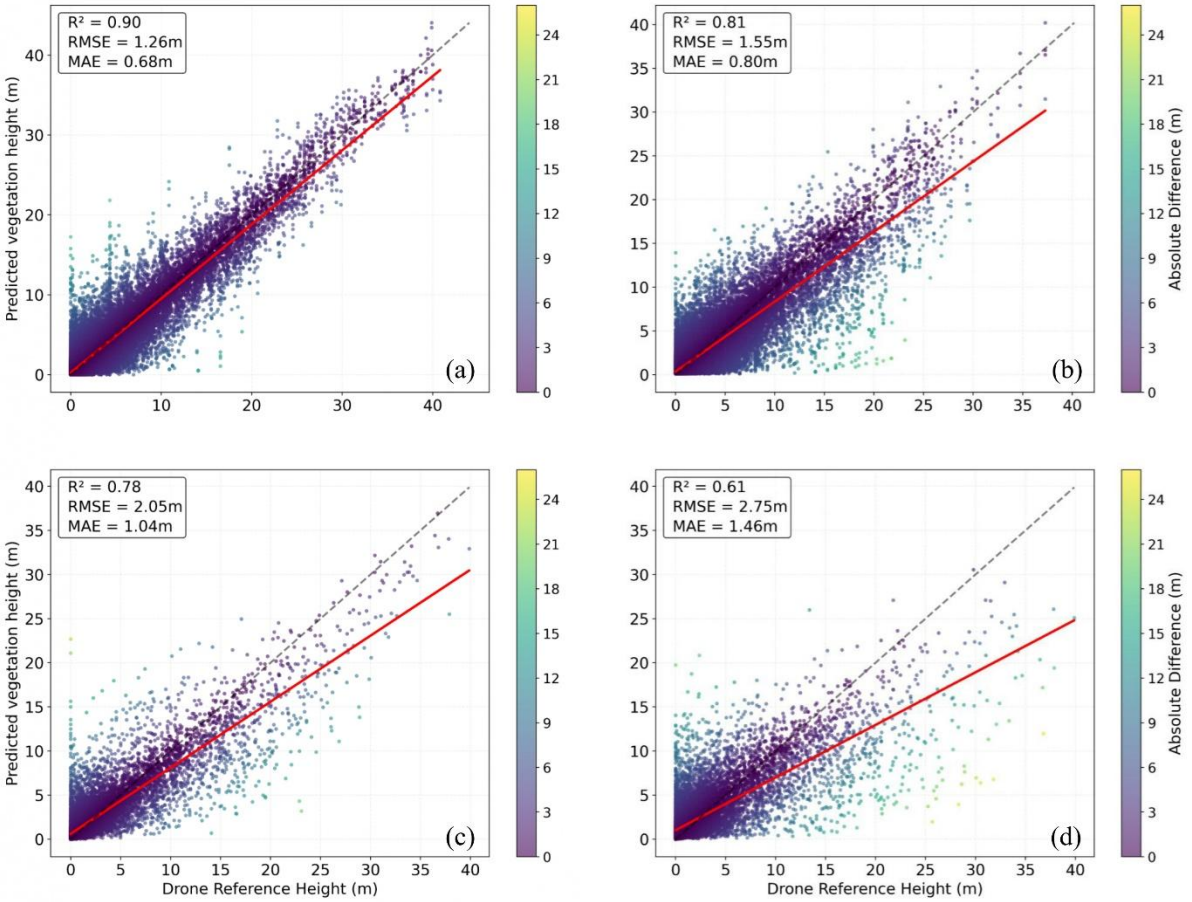

Fig. 7. Observed (held-out test sets) versus predicted vegetation height for four model configurations: (a) Virtual/U-Net, (b) Physical/U-Net, (c) Virtual/RF, and (d) Physical/RF. Point colors represent absolute error magnitude. Red solid lines show linear regression fits; dashed black lines represent an ideal 1:1 correspondence.

Spatial prediction maps from the best-performing Virtual/U-Net model (Fig. 8) demonstrated its ability to capture fine-scale vegetation height variability across three representative test areas. The predicted height maps (Fig. 8b) closely reproduced the reference patterns (Fig. 8a), delineating both tall and sparse vegetation areas. The spatial distribution of prediction errors (Fig. 8c) revealed that the largest absolute errors (5–18 m overestimation, up to 31 m underestimation) occurred primarily in tall vegetation areas, while predictions remained accurate across most of the landscape.

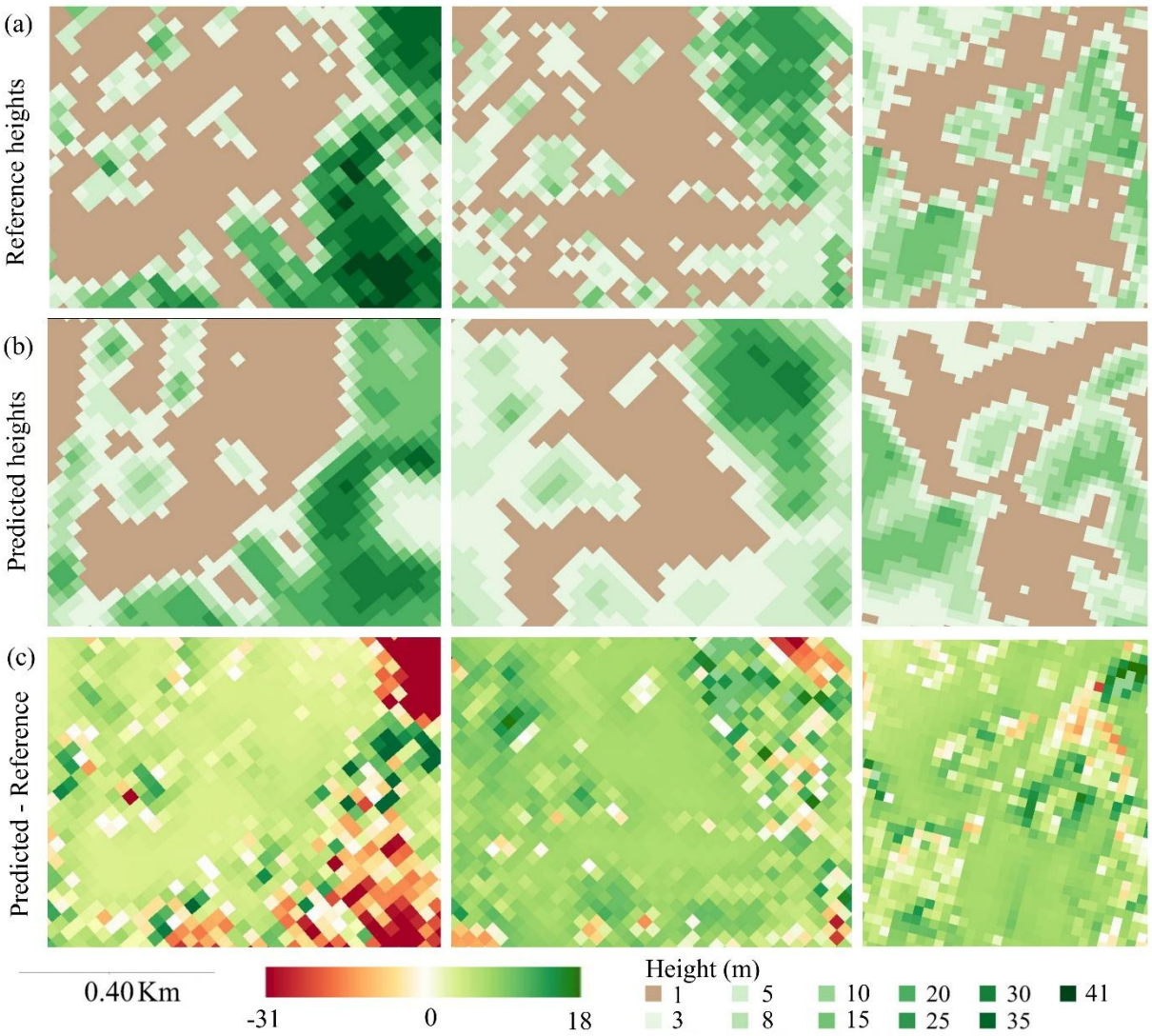

Fig. 8. Spatial predictions of vegetation height for the Virtual/U-Net model across three representative test areas. (a) UAV-derived reference heights, (b) predicted heights, and (c) prediction errors. Brown colors (vegetation height <1m represent bare soils – lack of vegetation).

3.4. Models' performance across height strata

Height-stratified error analysis (Fig. 9, Table A2) revealed distinct patterns across five tested height classes (0-5, 5-10, 10-20, 20-30, and 30-41 m). All models achieved comparable RMSE for low vegetation (0-5 m), but relative errors (nRMSE) varied substantially across models. Differences in model performance were more pronounced at higher vegetation heights than at lower heights.

Absolute error patterns differed fundamentally between model types (Fig. 9). Virtual/U-Net maintained relatively stable RMSE across height strata (0.98-3.11 m), whereas Physical/RF exhibited continuous error increase, particularly beyond 20 m (1.76 m to 15.29 m). The tallest

vegetation stratum (30-41 m) exhibited the largest performance differences, with Physical/RF RMSE exceeding Virtual/U-Net by a factor of 6.5.

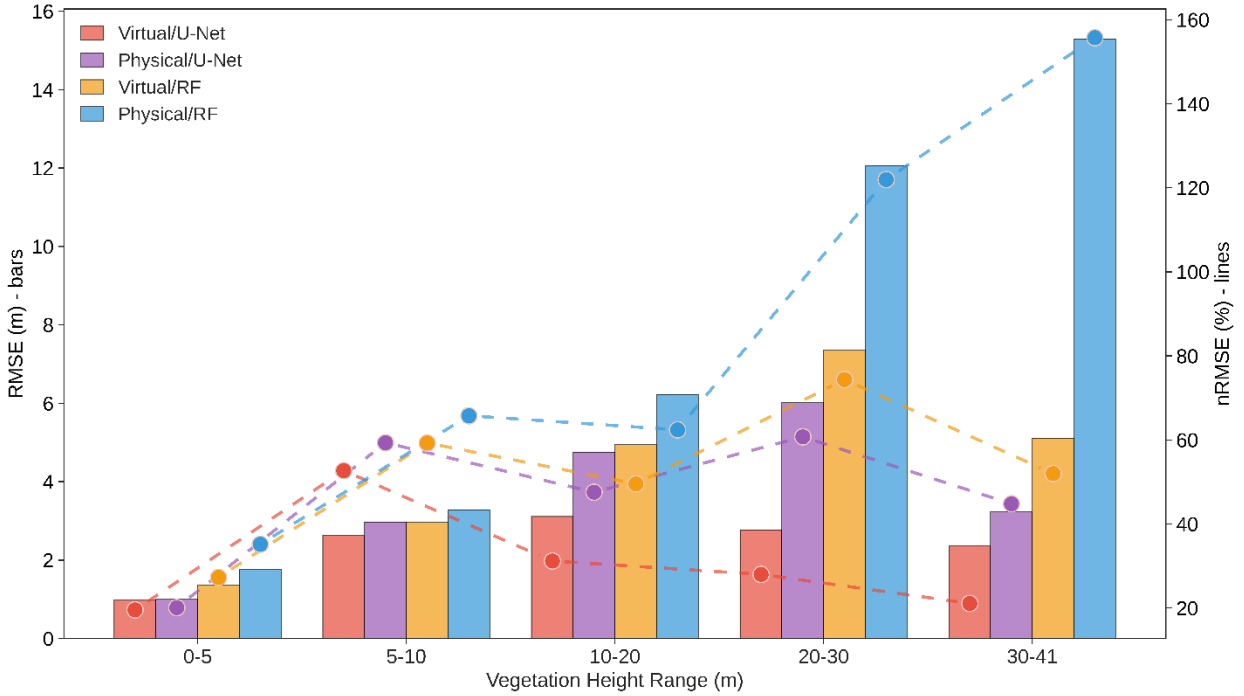

Fig. 9. Root Mean Square Error (RMSE) and normalized RMSE (nRMSE) across five vegetation height strata for four modeling approaches. Bars represent absolute RMSE (left y-axis); lines with markers represent nRMSE (right y-axis).

Virtual/U-Net showed relatively stable normalized relative errors across all height ranges (20%- 53%), with a slight increase in mid-height vegetation before stabilizing again in the tallest stratum. In contrast, Physical/RF maintained consistently elevated normalized relative errors as vegetation height increased, reaching 156% in the tallest stratum. This difference became most pronounced in tall vegetation, where Virtual/U-Net maintained stable performance below 22% relative errors while Physical/RF exceeded 156%.

The advantage of virtual embeddings over physical satellite extracted input features increased with vegetation height. For low vegetation (0–5 m), virtual embeddings improved performance by 3% (U-Net) and 22% (RF). For the tallest vegetation (30–41 m), improvements increased to 53% (U-Net) and 67% (RF). Similarly, U-Net outperformed RF across all height ranges, with advantages increasing from 28% in low vegetation to 62% in the 20–30 m range.

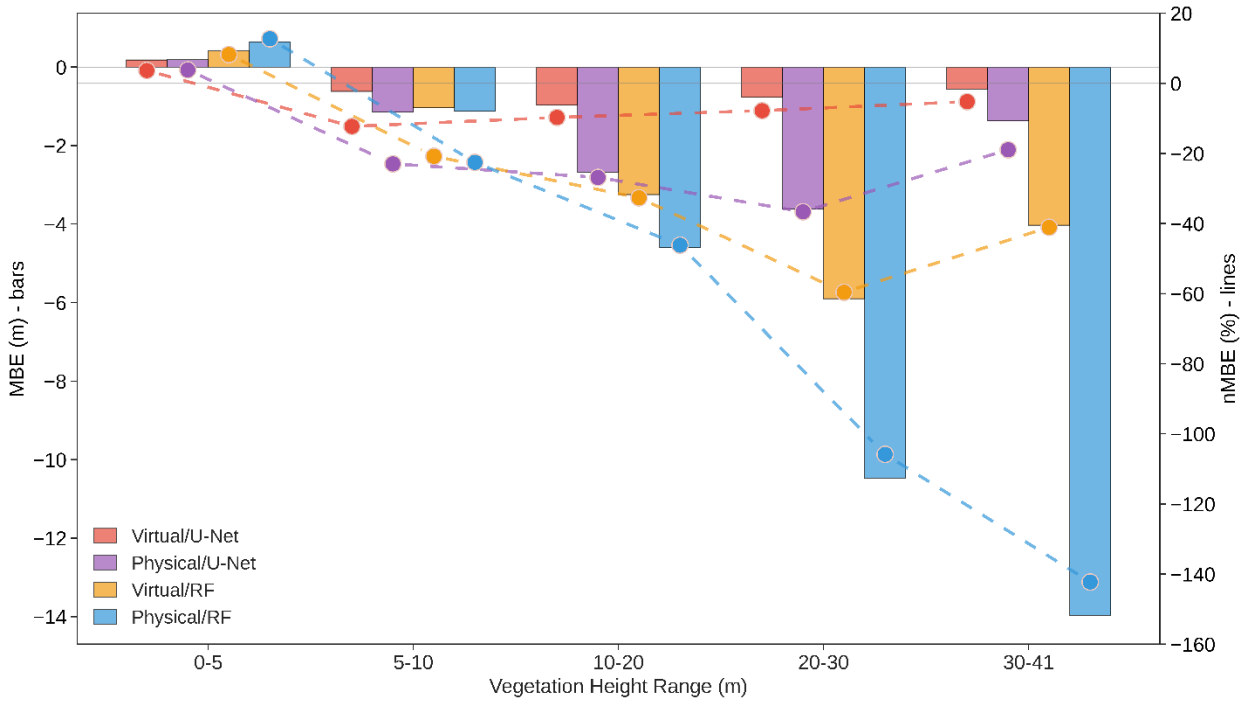

Fig. 10. Mean Bias Error (MBE) and normalized MBE (nMBE) across five vegetation height strata for four modeling approaches. Bars represent absolute MBE (left y-axis); lines with markers represent nMBE (right y-axis).

Bias patterns revealed systematic height-dependent underestimation across all models beyond the shortest vegetation stratum. Virtual/U-Net exhibited relatively small biases ranging from 0.18 m overestimation in short vegetation to -0.97 m underestimation in mid-height vegetation, before stabilizing around -0.56 m in the tallest stratum. In contrast, Physical/RF showed severe bias escalation with height, transitioning from 0.64 m overestimation at low vegetation to -13.97 m underestimation at tall trees. The tallest vegetation stratum exhibited the largest bias differences, with Physical/RF underestimating by nearly 14 m while Virtual/U-Net maintained bias below 1 m.

Virtual/U-Net demonstrated relatively stable normalized bias across height strata (ranging from 3.67% to -12.29%), with the most pronounced underestimation occurring in mid-height vegetation before improving in taller strata. Physical/RF exhibited increasing negative bias with vegetation height. This divergence became most severe in tall vegetation, where Virtual/U-Net maintained normalized bias below -6% while Physical/RF exceeded -142%, indicating systematic underestimation that worsened proportionally with increasing vegetation height.

The advantage of virtual embeddings in reducing systematic bias increased substantially with vegetation height. For low vegetation (0-5 m), virtual embeddings reduced normalized bias by 3% (U-Net) and 36% (RF). For the tallest vegetation (30-41 m), bias reductions increased to 72% (U-Net) and 71% (RF). Similarly, U-Net outperformed RF in bias control across all height ranges, with advantages increasing from 55% in low vegetation to 87% in the tallest stratum.

4. Discussion

4.1. Physical satellite extracted predictor variable selection and implications for multi-sensor vegetation height mapping

Our systematic literature review revealed substantial growth in satellite-based vegetation height mapping studies since 2019, with annual studies rising from 2 (2019) to 6 (2025) studies (Fig. 5b). This reflects growing recognition of vegetation height as a critical biodiversity variable (Lang et al., 2022). The geographic concentration in Asia (56.5%) and Europe (13.0%) likely reflects extensive forest resources and disturbance prevalence—tropical cyclones, bark beetle outbreaks, and land-use changes—necessitating vegetation monitoring (Lang et al., 2019; W. Li et al., 2020; A. Liu et al., 2024; Senf et al., 2019, 2021; Senf & Seidl, 2021; Torres de Almeida et al., 2022).

Studies employing airborne LiDAR or field-plot reference data achieved substantially higher accuracy (RMSE: 1.48–4.86 m, mean = 2.98 m) compared to those using spaceborne LiDAR (RMSE: 1.60–6.93 m, mean = 4.0 m). This pattern indicates that reference data quality determines maximum achievable model accuracy. Spaceborne LiDAR footprints (25–100 m diameter) introduce geo-location uncertainties (Roy et al., 2021), waveform processing errors (Dubayah et al., 2020), and terrain-induced biases (Potapov et al., 2021) that constrain downstream model performance. Our UAV-derived canopy height models (2.5 cm resolution) position this study among those with higher-quality ground truth.

Univariate analysis identified SAR-derived variables (VV, VH polarizations, and VV+VH) and optical blue/red-edge/SWIR bands and indices (B3, B5, B11, B12, TCW, TCB) as the most explanatory individual predictors (R^2 = 0.20–0.26), substantially outperforming traditional vegetation indices like NDVI (R^2 = 0.02). This SAR superiority aligns with established principles: C-band radar penetrates canopies with co-polarized VV returns sensitive to vertical structure through trunk-ground double-bounce scattering, while cross-polarized VH captures volume scattering from three-dimensional architectures (Ghosh et al., 2020; Y. Liu et al., 2019; Torres de Almeida et al., 2022). However, C-band backscatter saturates beyond 20–25 m (Santoro, Cartus, & Fransson, 2021), with even L-band systems showing reduced sensitivity above 30 m (Mermoz et al., 2015). Sentinel-2's Red-edge band B5 (R^2 = 0.26) demonstrates sensitivity to canopy density gradients and leaf area variations (Pickstone et al., 2025), while SWIR bands maintain sensitivity to moisture content and structural complexity. Tasseled Cap transformations (TCW, TCB) effectively captured structural variance without advantage over individual bands.

Traditional indices (NDVI, EVI, SAVI: $R^2 < 0.10$) performed poorly in our disturbed landscape versus mature forests, this is in line with literature (F. Li et al., 2025; Y. Liu et al., 2019). This discrepancy reflects data composition differences: our reference data dominated by low-height pixels (median = 0.59 m, 66.1% in 0–5 m) versus mature continuous canopies in prior studies. In disturbance-dominated landscapes, traditional indices saturate rapidly at low biomass (Morin et al., 2022), whereas SAR backscatter and red-edge reflectance maintain sensitivity across

disturbance-recovery gradients. This compositional difference limits direct comparability with literature focusing on structurally mature forests.

4.2. Virtual satellite embeddings (AlphaEarth Foundation) versus physical satellite extracted input representation: Multi-source learning

Virtual/U-Net achieved the highest unseen test set performance (R^2 = 0.90, RMSE = 1.19 m), demonstrating that learned embeddings from the AlphaEarth Foundation substantially outperformed physical satellite extracted input representations. To our knowledge, this study represents the first application of AEF embeddings for continuous vegetation height prediction. While the original AEF publication (Brown et al., 2025) demonstrated superior performance across diverse mapping tasks including land cover classification and agricultural monitoring, no peer-reviewed studies have yet applied AEF to vegetation height estimation in disturbed forest landscapes. AEF's superiority likely stems from its training methodology integrating GEDI spaceborne LiDAR canopy height metrics alongside optical (Sentinel-2, Landsat 8/9) and SAR (Sentinel-1, ALOS PALSAR-2) observations spanning 2017–2024 with global coverage (Brown et al., 2025). This multi-source pre-training enables the model to learn implicit relationships between spectral-structural patterns and three-dimensional forest structures that are difficult to capture through physical satellite extracted vegetation indices.

Virtual embeddings provided consistent advantages across both U-Net (23% RMSE reduction) and RF (26% RMSE reduction), suggesting complementary information regardless of modeling approach. However, diminishing relative improvement in U-Net (23% vs. 26%) indicates convolutional architectures partially compensate for limited spectral-SAR information through spatial pattern extraction, particularly valuable in heterogeneous post-disturbance landscapes where neighborhood information disambiguates spectrally similar but structurally distinct vegetation types. An unexpected finding was high variability in predicted heights for zero or near-zero reference areas (0–5 m: nRMSE = 41–74%). One might assume that detecting bare ground or sparse grass would be straightforward, yet this proved challenging for all models. Temporal mismatch between UAV acquisition (summers 2023–2024) and AEF embedding year (2023 annual composite) may contribute. In rapidly recovering post-disturbance sites, herbaceous vegetation and early successional shrubs establish within single growing seasons, creating asynchrony between reference and satellite observations. Additionally, low vegetation exhibits high spectral variability due to soil background influence, residual woody debris, and phenological dynamics not fully captured by annual composites (Senf et al., 2017, 2019; Senf & Seidl, 2022) . This limits post-disturbance monitoring applications where accurate early regeneration mapping is critical for assessing recovery trajectories. Despite challenges at low heights, Virtual/U-Net maintained stable absolute errors (RMSE: 0.98–3.11 m) and declining relative errors (nRMSE: 41% to 6.5%) across height strata. This performance consistency encourages potential applications in mature forests, suggesting AEF-based approaches may generalize beyond disturbed landscapes dominating our training data.

4.3. Height-stratified performance and operational challenges

Height stratification analysis revealed that modeling architecture choice became increasingly critical with vegetation height (Fig. 9). U-Net's advantage over RF increased substantially across strata: 28% RMSE reduction in low vegetation (0-5 m) expanding to 62% in mid-height vegetation (20-30 m). This escalating performance gap, from 0.38 m (0-5 m) to 4.58 m (20-30 m) absolute difference for Virtual embeddings, demonstrates that spatial context integration becomes indispensable for tall vegetation prediction. Convolutional architectures like U-Net analyze neighborhoods of pixels together, capturing spatial patterns such as canopy texture, vegetation edges, and how nearby areas relate to each other which is unavailable to Random Forest and examines each pixel independently (Ge et al., 2022). This neighborhood context becomes increasingly important for tall vegetation, where continuous tree canopies create homogeneous patches with distinct boundaries. Random Forest's pixel-by-pixel approach struggles in these situations because it cannot distinguish between spectrally similar vegetation types that differ in their spatial arrangement and context. The contrasting error trajectories between architectures—Virtual/U-Net maintained stable RMSE (0.98-3.11 m) while Physical/RF exhibited continuous escalation beyond 20 m (1.76-15.29 m)—underscore this fundamental architectural difference. In the tallest stratum (30-40.82 m), Physical/RF RMSE exceeded Virtual/U-Net by factor 6.5, demonstrating complete breakdown of pixel-based prediction in tall, structurally complex vegetation.

Despite strong unseen test set performance, operational deployment across 9,000 km² revealed systematic height-dependent bias not captured by test evaluation. Pixel-wise comparison with UAV reference data showed pronounced underestimation in tall stands (reaching -31 m) and minor overestimation in disturbed areas (up to +18 m), representing critical limitations for precise absolute height estimation across heterogeneous post-disturbance landscapes. Two interrelated factors explain the observed bias patterns. First, the training data was heavily imbalanced toward low vegetation. Nearly two-thirds of training samples (66.1%) came from areas with vegetation below 5 m height, while only 0.3% represented vegetation above 25 m (Fig. 4). This imbalance reflects the disturbed nature of our study area but created a critical limitation: only 161 training pixels (0.34%) captured vegetation exceeding 25 m, with just 2 pixels representing the maximum height of 41 m. With so few examples of tall vegetation, the model struggled to learn accurate predictions for tall trees, despite its sophisticated architecture designed to capture complex spatial patterns (Buda et al., 2018).

Second, satellite sensors have physical limitations at detecting tall, dense vegetation. Both radar (C-band SAR) and optical satellite signals become saturated—meaning they can no longer distinguish differences—once canopy heights exceed approximately 20-25 m (Potapov et al., 2021; Santoro, Cartus, & Fransson, 2021). While AEF embeddings incorporate spaceborne LiDAR data (GEDI) that partially overcome this limitation, the global dataset used to train AEF may not adequately represent severely disturbed temperate forests with scattered tall remnant trees. As a

result, even our best model (Virtual/U-Net) systematically underestimated heights in the tallest vegetation category (30-40.82 m: MBE = -0.81 m). These systematic biases pose significant limitations for carbon stock estimation in disturbed forests, where accurate quantification of both remnant tall trees and regeneration dynamics is essential (Bustamante et al., 2016; Senf et al., 2017).

The systematic height-dependent bias observed in operational deployment represents a well-documented challenge in remote sensing that can be effectively addressed through quantile mapping bias correction. This distribution-based technique, which adjusts predicted values to match the statistical distribution of reference data while preserving spatial patterns, has demonstrated success in correcting satellite-derived vegetation estimates across multiple applications including global forest canopy height (Lang et al., 2022; Potapov et al., 2021), GEDI lidar biomass predictions (Duncanson et al., 2022), and ICESat GLAS height retrievals (Simard et al., 2011).

The method operates by establishing transfer functions between the cumulative distribution functions of predicted and observed values following (Piani et al., 2010), effectively creating systematic corrections that account for model saturation effects at high values and noise sensitivity at low values.

For our application, we propose implementing height-stratified quantile mapping calibrated against independent UAV reference data, with corrections developed separately for distinct height classes (0-5 m, 5-10 m, 10-20 m, 20-30 m, 30-40.82 m) to explicitly address the non-linear bias patterns observed across the height gradient. However, several methodological considerations require careful attention for operational implementation.

First, temporal stability of correction functions must be validated across multiple growing seasons and years, as phenological variations and atmospheric conditions may affect transferability (Piani et al., 2010). Second, geographic stratification by structural class may be necessary to account for regional variations in canopy and species composition (Duncanson et al., 2022). Third, maintaining strict independence between model training, correction calibration, and validation datasets is essential to avoid circular validation (Olofsson et al., 2014).

While bias correction represents a scientifically rigorous pathway to improving operational accuracy, it should be implemented as an integral component of the mapping system to ensure reproducibility and appropriate interpretation of corrected products in downstream applications.

5. Conclusion

This study demonstrates that AlphaEarth Foundations (AEF) embeddings substantially advance satellite-based vegetation height mapping in structurally complex, severely disturbed forest landscapes. Across all experiments, AEF consistently outperformed traditional band- and index-based multi-sensor predictors, while also reducing workflow complexity by eliminating manual feature engineering and cross-sensor harmonization. In parallel, deep learning clearly surpassed classical machine learning: U-Net models outperformed Random Forests regardless of

input representation, highlighting the importance of spatial context for height prediction in heterogeneous post-disturbance environments.

The combination of AEF embeddings with a U-Net architecture achieved the highest overall accuracy (R^2 = 0.90, RMSE ≈ 1.3 m), outperforming state-of-the-art physical-feature-based approaches by a wide margin. Performance gains were particularly pronounced in taller vegetation strata, where traditional methods exhibited strong saturation effects, escalating errors, and severe negative bias. In contrast, the AEF–U-Net configuration maintained comparatively stable errors and low bias across the full height range, demonstrating improved robustness to structural complexity and canopy height extremes.

Beyond accuracy, AEF offers a conceptual shift for vegetation height mapping: compact, transferable representations replace task-specific predictor design, enabling scalable and operationally efficient modeling. These results indicate that foundation-model-derived embeddings, when paired with spatially explicit deep learning architectures, represent a robust and generalizable solution for large-area vegetation height mapping, especially in disturbance-driven landscapes where conventional optical–SAR approaches struggle. As foundation models mature and expand temporally and spatially, they are likely to become a cornerstone of next-generation forest structure monitoring and ecosystem assessment.

References

Alvites, C., O'Sullivan, H., Francini, S., Marchetti, M., Santopuoli, G., Chirici, G., Lasserre, B., Marignani, M., & Bazzato, E. (2024). High-Resolution Canopy Height Mapping: Integrating NASA's Global Ecosystem Dynamics Investigation (GEDI) with Multi-Source Remote Sensing Data. *Remote Sensing*, *16*(7). https://doi.org/10.3390/rs16071281

Breiman, L. (2001). *Random Forests* (Vol. 45).

Brown, C. F., Kazmierski, M. R., Pasquarella, V. J., Rucklidge, W. J., Samsikova, M., Zhang, C., Shelhamer, E., Lahera, E., Wiles, O., Ilyushchenko, S., Gorelick, N., Lydia Zhang, L., Alj, S., Schechter, E., Askay, S., Guinan, O., Moore, R., Boukouvalas, A., Kohli, P., … DeepMind, G. (2025). *AlphaEarth Foundations: An embedding field model for accurate and efficient global mapping from sparse label data*.

Buda, M., Maki, A., & Mazurowski, M. A. (2018). A systematic study of the class imbalance problem in convolutional neural networks. *Neural Networks*, *106*, 249–259. https://doi.org/10.1016/j.neunet.2018.07.011

Bustamante, M. M. C., Roitman, I., Aide, T. M., Alencar, A., Anderson, L. O., Aragão, L., Asner, G. P., Barlow, J., Berenguer, E., Chambers, J., Costa, M. H., Fanin, T., Ferreira, L. G., Ferreira, J., Keller, M., Magnusson, W. E., Morales-Barquero, L., Morton, D., Ometto, J. P. H. B., … Vieira, I. C. G. (2016). Toward an integrated monitoring framework to assess the effects of tropical forest degradation and recovery on carbon stocks and biodiversity. In

Global Change Biology (Vol. 22, Issue 1, pp. 92–109). Blackwell Publishing Ltd. https://doi.org/10.1111/gcb.13087

Chen, M., Dong, W., Yu, H., Woodhouse, I. H., Ryan, C. M., Liu, H., Georgiou, S., & Mitchard, E. T. A. (2025). Multimodal deep learning enables forest height mapping from patchy spaceborne LiDAR using SAR and passive optical satellite data. *International Journal of Applied Earth Observation and Geoinformation*, *143*. https://doi.org/10.1016/j.jag.2025.104814

Deng, X., Zhu, X., Tang, Z., & You, Y. (2025). A Novel Canopy Height Mapping Method Based on UNet++ Deep Neural Network and GEDI, Sentinel-1, Sentinel-2 Data. *Forests*, *16*(11). https://doi.org/10.3390/f16111663

Drusch, M., Del Bello, U., Carlier, S., Colin, O., Fernandez, V., Gascon, F., Hoersch, B., Isola, C., Laberinti, P., Martimort, P., Meygret, A., Spoto, F., Sy, O., Marchese, F., & Bargellini, P. (2012). Sentinel-2: ESA's Optical High-Resolution Mission for GMES Operational Services. *Remote Sensing of Environment*, *120*, 25–36. https://doi.org/10.1016/j.rse.2011.11.026

Dubayah, R., Blair, J. B., Goetz, S., Fatoyinbo, L., Hansen, M., Healey, S., Hofton, M., Hurtt, G., Kellner, J., Luthcke, S., Armston, J., Tang, H., Duncanson, L., Hancock, S., Jantz, P., Marselis, S., Patterson, P. L., Qi, W., & Silva, C. (2020). The Global Ecosystem Dynamics Investigation: High-resolution laser ranging of the Earth's forests and topography. *Science of Remote Sensing*, *1*. https://doi.org/10.1016/j.srs.2020.100002

Duncanson, L., Kellner, J. R., Armston, J., Dubayah, R., Minor, D. M., Hancock, S., Healey, S. P., Patterson, P. L., Saarela, S., Marselis, S., Silva, C. E., Bruening, J., Goetz, S. J., Tang, H., Hofton, M., Blair, B., Luthcke, S., Fatoyinbo, L., Abernethy, K., … Zgraggen, C. (2022). Aboveground biomass density models for NASA's Global Ecosystem Dynamics Investigation (GEDI) lidar mission. *Remote Sensing of Environment*, *270*. https://doi.org/10.1016/j.rse.2021.112845

Fang, J., Wu, M., Zhang, Z., & Luo, W. (n.d.). *Leveraging AlphaEarth Foundations Embeddings for High-Accuracy County-Scale Corn and Soybean Yield Estimation*.

Fassnacht, F. E., Latifi, H., Stereńczak, K., Modzelewska, A., Lefsky, M., Waser, L. T., Straub, C., & Ghosh, A. (2016). Review of studies on tree species classification from remotely sensed data. In *Remote Sensing of Environment* (Vol. 186, pp. 64–87). Elsevier Inc. https://doi.org/10.1016/j.rse.2016.08.013

Feng, Z., Atzberger, C., Jaffer, S., Knezevic, J., Sormunen, S., Young, R., Lisaius, M. C., Immitzer, M., Jackson, T., Ball, J., Coomes, D. A., Madhavapeddy, A., Blake, A., & Keshav, S. (2025). *TESSERA: Temporal Embeddings of Surface Spectra for Earth Representation and Analysis*. http://arxiv.org/abs/2506.20380

Ge, S., Gu, H., Su, W., Praks, J., & Antropov, O. (2022). Improved Semisupervised UNet Deep Learning Model for Forest Height Mapping With Satellite SAR and Optical Data. *IEEE Journal of Selected Topics in Applied Earth Observations and Remote Sensing*, *15*, 5776–5787. https://doi.org/10.1109/JSTARS.2022.3188201

Ghosh, S. M., Behera, M. D., & Paramanik, S. (2020). Canopy height estimation using sentinel series images through machine learning models in a Mangrove Forest. *Remote Sensing*, *12*(9). https://doi.org/10.3390/RS12091519

Guo, L., Zhang, Y., Xu, M., Yan, J., Zhang, H., Zou, Y., & Gao, J. (2024). A Novel Workflow for Mapping Forest Canopy Height by Synergizing ICESat-2 and Multi-Sensor Data. *Forests*, *15*(12). https://doi.org/10.3390/f15122139

Houriez, L., Pilarski, S., Vahedi, B., Ahmadalipour, A., Scully, T. H., Aflitto, N., Andre, D., Jaffe, C., Wedner, M., Mazzola, R., Jeffery, J., Messinger, B., McGinley-Smith, S., & Russell, S. (2025). *Scalable Geospatial Data Generation Using AlphaEarth Foundations Model*. http://arxiv.org/abs/2508.11739

Kacic, P., Hirner, A., & Da Ponte, E. (2021). Fusing sentinel-1 and-2 to model gedi-derived vegetation structure characteristics in gee for the paraguayan chaco. *Remote Sensing*, *13*(24). https://doi.org/10.3390/rs13245105

Kingma, D. P., & Ba, J. (2017). *Adam: A Method for Stochastic Optimization*. http://arxiv.org/abs/1412.6980

Lang, N., Kalischek, N., Armston, J., Schindler, K., Dubayah, R., & Wegner, J. D. (2022). Global canopy height regression and uncertainty estimation from GEDI LIDAR waveforms with deep ensembles. *Remote Sensing of Environment*, *268*. https://doi.org/10.1016/j.rse.2021.112760

Lang, N., Schindler, K., & Wegner, J. D. (2019). Country-wide high-resolution vegetation height mapping with Sentinel-2. *Remote Sensing of Environment*, *233*. https://doi.org/10.1016/j.rse.2019.111347

Lei, Y., Wang, Y., Wang, G., Song, C., Cao, H., & Xiao, W. (2024). Estimating Forest Canopy Height based on GEDI Lidar Data and Multi-source Remote Sensing Images. *International Archives of the Photogrammetry, Remote Sensing and Spatial Information Sciences - ISPRS Archives*, *48*(1), 297–303. https://doi.org/10.5194/isprs-archives-XLVIII-1-2024-297-2024

Li, F., Jiang, Y., Long, Y., Li, W., & He, Y. (2025). Forest Height Estimation in Jiangsu: Integrating Dual-Polarimetric SAR, InSAR, and Optical Remote Sensing Features. *Remote Sensing*, *17*(21). https://doi.org/10.3390/rs17213620

Li, H., Hiroshima, T., Li, X., Hayashi, M., & Kato, T. (2024). High-resolution mapping of forest structure and carbon stock using multi-source remote sensing data in Japan. *Remote Sensing of Environment*, *312*. https://doi.org/10.1016/j.rse.2024.114322

Li, W., Niu, Z., Shang, R., Qin, Y., Wang, L., & Chen, H. (2020). High-resolution mapping of forest canopy height using machine learning by coupling ICESat-2 LiDAR with Sentinel-1, Sentinel-2 and Landsat-8 data. *International Journal of Applied Earth Observation and Geoinformation*, *92*. https://doi.org/10.1016/j.jag.2020.102163

Liu, A., Chen, Y., & Cheng, X. (2024). Evaluating ICESat-2 and GEDI with Integrated Landsat-8 and PALSAR-2 for Mapping Tropical Forest Canopy Height. *Remote Sensing*, *16*(20). https://doi.org/10.3390/rs16203798

Liu, C., Gong, W., Shi, S., Wang, T., Xu, T., Shi, Z., & Niu, J. (2025). Deep learning-driven forest canopy height mapping in boreal regions through multi-source remote sensing fusion: Integrating Sentinel-1/2, PALSAR, and ICESat-2/LVIS data. *International Journal of Applied Earth Observation and Geoinformation*, *143*. https://doi.org/10.1016/j.jag.2025.104766

Liu, Y., Gong, W., Xing, Y., Hu, X., & Gong, J. (2019). Estimation of the forest stand mean height and aboveground biomass in Northeast China using SAR Sentinel-1B, multispectral Sentinel-2A, and DEM imagery. *ISPRS Journal of Photogrammetry and Remote Sensing*, *151*, 277–289. https://doi.org/10.1016/j.isprsjprs.2019.03.016

Mermoz, S., Réjou-Méchain, M., Villard, L., Le Toan, T., Rossi, V., & Gourlet-Fleury, S. (2015). Decrease of L-band SAR backscatter with biomass of dense forests. *Remote Sensing of Environment*, *159*, 307–317. https://doi.org/10.1016/j.rse.2014.12.019

Morin, D., Planells, M., Baghdadi, N., Bouvet, A., Fayad, I., Le Toan, T., Mermoz, S., & Villard, L. (2022). Improving Heterogeneous Forest Height Maps by Integrating GEDI-Based Forest Height Information in a Multi-Sensor Mapping Process. *Remote Sensing*, *14*(9). https://doi.org/10.3390/rs14092079

Muñoz-Sabater, J., Dutra, E., Agustí-Panareda, A., Albergel, C., Arduini, G., Balsamo, G., Boussetta, S., Choulga, M., Harrigan, S., Hersbach, H., Martens, B., Miralles, D. G., Piles, M., Rodríguez-Fernández, N. J., Zsoter, E., Buontempo, C., & Thépaut, J. N. (2021). ERA5-Land: A state-of-the-art global reanalysis dataset for land applications. *Earth System Science Data*, *13*(9), 4349–4383. https://doi.org/10.5194/essd-13-4349-2021

Olofsson, P., Foody, G. M., Herold, M., Stehman, S. V., Woodcock, C. E., & Wulder, M. A. (2014). Good practices for estimating area and assessing accuracy of land change. In *Remote Sensing of Environment* (Vol. 148, pp. 42–57). Elsevier Inc. https://doi.org/10.1016/j.rse.2014.02.015

Page, M. J., McKenzie, J. E., Bossuyt, P. M., Boutron, I., Hoffmann, T. C., Mulrow, C. D., Shamseer, L., Tetzlaff, J. M., Akl, E. A., Brennan, S. E., Chou, R., Glanville, J., Grimshaw, J. M., Hróbjartsson, A., Lalu, M. M., Li, T., Loder, E. W., Mayo-Wilson, E., McDonald, S., … Moher, D. (2021). The PRISMA 2020 statement: an updated guideline for reporting systematic reviews. *Systematic Reviews*, *10*(1). https://doi.org/10.1186/s13643-021-01626-4

Pedregosa, F., Varoquaux, G., Gramfort, A., Michel, V., Thirion, B., Grisel, O., Blondel, M., Müller, A., Nothman, J., Louppe, G., Prettenhofer, P., Weiss, R., Dubourg, V., Vanderplas, J., Passos, A., Cournapeau, D., Brucher, M., Perrot, M., & Duchesnay, É. (2018). *Scikit-learn: Machine Learning in Python*. http://arxiv.org/abs/1201.0490

Piani, C., Haerter, J. O., & Coppola, E. (2010). Statistical bias correction for daily precipitation in regional climate models over Europe. *Theoretical and Applied Climatology*, *99*(1–2), 187–192. https://doi.org/10.1007/s00704-009-0134-9

Pickstone, B. J., Graham, H. A., & Cunliffe, A. M. (2025). Estimating canopy height in tropical forests: Integrating airborne LiDAR and multi-spectral optical data with machine learning. *Sustainable Environment*, *11*(1). https://doi.org/10.1080/27658511.2025.2469406

Potapov, P., Li, X., Hernandez-Serna, A., Tyukavina, A., Hansen, M. C., Kommareddy, A., Pickens, A., Turubanova, S., Tang, H., Silva, C. E., Armston, J., Dubayah, R., Blair, J. B., & Hofton, M. (2021). Mapping global forest canopy height through integration of GEDI and Landsat data. *Remote Sensing of Environment*, *253*. https://doi.org/10.1016/j.rse.2020.112165

Ronneberger, O., Fischer, P., & Brox, T. (2015). U-net: Convolutional networks for biomedical image segmentation. *Lecture Notes in Computer Science (Including Subseries Lecture Notes in Artificial Intelligence and Lecture Notes in Bioinformatics)*, *9351*, 234–241. https://doi.org/10.1007/978-3-319-24574-4_28

Rosenqvist, A., Shimada, M., Suzuki, S., Ohgushi, F., Tadono, T., Watanabe, M., Tsuzuku, K., Watanabe, T., Kamijo, S., & Aoki, E. (2014). Operational performance of the ALOS global systematic acquisition strategy and observation plans for ALOS-2 PALSAR-2. *Remote Sensing of Environment*, *155*, 3–12. https://doi.org/10.1016/j.rse.2014.04.011

Roy, D. P., Kashongwe, H. B., & Armston, J. (2021). The impact of geolocation uncertainty on GEDI tropical forest canopy height estimation and change monitoring. *Science of Remote Sensing*, *4*. https://doi.org/10.1016/j.srs.2021.100024

Santoro, M., Cartus, O., Carvalhais, N., Rozendaal, D. M. A., Avitabile, V., Araza, A., De Bruin, S., Herold, M., Quegan, S., Rodríguez-Veiga, P., Balzter, H., Carreiras, J., Schepaschenko, D., Korets, M., Shimada, M., Itoh, T., Moreno Martínez, Á., Cavlovic, J., Gatti, R. C., … Willcock, S. (2021). The global forest above-ground biomass pool for 2010 estimated from

high-resolution satellite observations. *Earth System Science Data*, *13*(8), 3927–3950. https://doi.org/10.5194/essd-13-3927-2021

Santoro, M., Cartus, O., & Fransson, J. E. S. (2021). Integration of allometric equations in the water cloud model towards an improved retrieval of forest stem volume with L-band SAR data in Sweden. *Remote Sensing of Environment*, *253*. https://doi.org/10.1016/j.rse.2020.112235

Seidl, R., & Turner, M. G. (2022). Post-disturbance reorganization of forest ecosystems in a changing world. *Proceedings of the National Academy of Sciences of the United States of America*, *119*(28). https://doi.org/10.1073/pnas.2202190119

Senf, C., Müller, J., & Seidl, R. (2019). Post-disturbance recovery of forest cover and tree height differ with management in Central Europe. *Landscape Ecology*, *34*(12), 2837–2850. https://doi.org/10.1007/s10980-019-00921-9

Senf, C., Sebald, J., & Seidl, R. (2021). Increasing canopy mortality affects the future demographic structure of Europe's forests. *One Earth*, *4*(5), 749–755. https://doi.org/10.1016/j.oneear.2021.04.008

Senf, C., & Seidl, R. (2021). Persistent impacts of the 2018 drought on forest disturbance regimes in Europe. *Biogeosciences*, *18*(18), 5223–5230. https://doi.org/10.5194/bg-18-5223-2021

Senf, C., & Seidl, R. (2022). Post-disturbance canopy recovery and the resilience of Europe's forests. *Global Ecology and Biogeography*, *31*(1), 25–36. https://doi.org/10.1111/geb.13406

Senf, C., Seidl, R., & Hostert, P. (2017). Remote sensing of forest insect disturbances: Current state and future directions. In *International Journal of Applied Earth Observation and Geoinformation* (Vol. 60, pp. 49–60). Elsevier B.V. https://doi.org/10.1016/j.jag.2017.04.004

Simard, M., Pinto, N., Fisher, J. B., & Baccini, A. (2011). Mapping forest canopy height globally with spaceborne lidar. *Journal of Geophysical Research: Biogeosciences*, *116*(4). https://doi.org/10.1029/2011JG001708

Sothe, C., Gonsamo, A., Lourenço, R. B., Kurz, W. A., & Snider, J. (2022). Spatially Continuous Mapping of Forest Canopy Height in Canada by Combining GEDI and ICESat-2 with PALSAR and Sentinel. *Remote Sensing*, *14*(20). https://doi.org/10.3390/rs14205158

Szwarcman, D., Roy, S., Fraccaro, P., Gíslason, Þ. E., Blumenstiel, B., Ghosal, R., de Oliveira, P. H., Almeida, J. L. de S., Sedona, R., Kang, Y., Chakraborty, S., Wang, S., Gomes, C., Kumar, A., Truong, M., Godwin, D., Lee, H., Hsu, C.-Y., Asanjan, A. A., … Moreno, J. B. (2024). *Prithvi-EO-2.0: A Versatile Multi-Temporal Foundation Model for Earth Observation Applications*. https://doi.org/10.1109/TGRS.2025.3642610

Torres de Almeida, C., Gerente, J., Rodrigo dos Prazeres Campos, J., Caruso Gomes Junior, F., Providelo, L. A., Marchiori, G., & Chen, X. (2022). Canopy Height Mapping by Sentinel 1 and 2 Satellite Images, Airborne LiDAR Data, and Machine Learning. *Remote Sensing*, *14*(16). https://doi.org/10.3390/rs14164112

Torres, R., Snoeij, P., Geudtner, D., Bibby, D., Davidson, M., Attema, E., Potin, P., Rommen, B. Ö., Floury, N., Brown, M., Traver, I. N., Deghaye, P., Duesmann, B., Rosich, B., Miranda, N., Bruno, C., L'Abbate, M., Croci, R., Pietropaolo, A., … Rostan, F. (2012). GMES Sentinel-1 mission. *Remote Sensing of Environment*, *120*, 9–24. https://doi.org/10.1016/j.rse.2011.05.028

Tsutsumida, N., Kato, A., Osawa, T., & Doi, H. (2023). *Mapping Forest Vertical Structure Attributes with GEDI, Sentinel-1, and Sentinel-2*. 538–541. https://doi.org/10.1109/igarss52108.2023.10283403

Wang, C., Song, C., Schroeder, T. A., Woodcock, C. E., Pavelsky, T. M., Han, Q., & Yao, F. (2025). Interpretable Multi-Sensor Fusion of Optical and SAR Data for GEDI-Based Canopy Height Mapping in Southeastern North Carolina. *Remote Sensing*, *17*(9). https://doi.org/10.3390/rs17091536

Wang, J., Shen, X., & Cao, L. (2024). Upscaling Forest Canopy Height Estimation Using Waveform-Calibrated GEDI Spaceborne LiDAR and Sentinel-2 Data. *Remote Sensing*, *16*(12). https://doi.org/10.3390/rs16122138

Washaya, P., Modlinger, R., Tyšer, D., & Hlásny, T. (2024). Patterns and impacts of an unprecedented outbreak of bark beetles in Central Europe: A glimpse into the future? *Forest Ecosystems*, *11*. https://doi.org/10.1016/j.fecs.2024.100243

Washaya, P., Potterf, M., Modlinger, R., Hüttnerová, T., Melichová, Z., & Hlásny, T. (2025). Severely disturbed forests in Central Europe retain robust recovery capacity but face resilience loss due to spatial homogenization. *Landscape Ecology*. https://doi.org/10.1007/s10980-025-02264-0

Xi, Z., Xu, H., Xing, Y., Gong, W., Chen, G., & Yang, S. (2022). Forest Canopy Height Mapping by Synergizing ICESat-2, Sentinel-1, Sentinel-2 and Topographic Information Based on Machine Learning Methods. *Remote Sensing*, *14*(2). https://doi.org/10.3390/rs14020364

Yu, J. W., & Jung, H. S. (2023). Forest Vertical Structure Mapping Using Multi-Seasonal UAV Images and Lidar Data via Modified U-Net Approaches. *Remote Sensing*, *15*(11). https://doi.org/10.3390/rs15112833

Zhu, W., Yang, F., Qiu, Z., He, N., Zhu, X., Li, Y., Xu, Y., & Lu, Z. (2023). Enhancing Forest Canopy Height Retrieval: Insights from Integrated GEDI and Landsat Data Analysis. *Sustainability (Switzerland)*, *15*(13). https://doi.org/10.3390/su151310434

Zhu, X. X., Xiong, Z., Wang, Y., Stewart, A. J., Heidler, K., Wang, Y., Yuan, Z., Dujardin, T., Xu, Q., & Shi, Y. (2026). On the foundations of Earth foundation models. *Communications Earth & Environment*. https://doi.org/10.1038/s43247-025-03127-x

4.4. The role of drought in bark beetle outbreaks

Das, A. K., Baldo, M., Dobor, L., Seidl, R., Rammer, W., Modlinger, R., **Washaya, P.,** Merganičová, K., & Hlásny, T. (2025). The increasing role of drought as an inciting factor of bark beetle outbreaks can cause large-scale transformation of Central European forests. Landscape Ecology, 40, 108. https://doi.org/10.1007/s10980-025-02125-w

Landsc Ecol (2025) 40:108
https://doi.org/10.1007/s10980-025-02125-w

RESEARCH ARTICLE

The increasing role of drought as an inciting factor of bark beetle outbreaks can cause large-scale transformation of Central European forests

Agnish Kumar Das · Marco Baldo · Laura Dobor · Rupert Seidl · Werner Rammer · Roman Modlinger · Prosper Washaya · Katarína Merganičová · Tomáš Hlásny

Received: 22 February 2025 / Accepted: 5 May 2025 / Published online: 23 May 2025

Abstract

Context Historically, large-scale outbreaks of the European spruce bark beetle were initiated mainly by windthrows. However, after 2018, a severe drought triggered the hitherto largest bark beetle outbreak observed in Europe, signalling a major shift in the disturbance regime.

Objectives Develop and test an approach that allows simulating this novel disturbance dynamics and evaluate landscape-scale compound impacts of wind- and drought-initiated outbreaks throughout the twenty-first century.

Methods We incorporated drought-initiated outbreaks into the forest landscape simulation model iLand, using critical values of vapour pressure deficit as the outbreak trigger. Forest management records and remote sensing-based disturbance maps were used to derive model parameters and evaluate simulated dynamics in a Central European forest landscape (41,000 hectares). The period 1961–2021 was used for model evaluation, and the years until 2100 for scenario analysis.

Results **I**ncorporating drought as outbreak trigger led to a notable decoupling of wind and bark beetle disturbances, which have historically formed a typical disturbance cascade in European forests. While forest growing stock and species composition were resilient to a wind-dominated disturbance regime, this resilience diminished under the compounded impact

Supplementary Information The online version contains supplementary material available at https://doi.org/10.1007/s10980-025-02125-w.

A. K. Das · M. Baldo · L. Dobor · R. Modlinger · P. Washaya · K. Merganičová · T. Hlásny (✉)
Faculty of Forestry and Wood Sciences, Czech University of Life Sciences in Prague, Kamýcka 129, 165 00, Prague 6, Suchdol, Czech Republic
e-mail: hlasny@fld.czu.cz

A. K. Das
e-mail: kumar_das@fld.czu.cz

M. Baldo
e-mail: baldo@fld.czu.cz

L. Dobor
e-mail: dobor@fld.czu.cz

R. Modlinger
e-mail: modlinger@fld.czu.cz

P. Washaya
e-mail: washaya@fld.czu.c

K. Merganičová
e-mail: merganicova@fld.czu.cz

R. Seidl · W. Rammer
Ecosystem Dynamics and Forest Management, Technical University of Munich, TUM School of Life Sciences, Hans-Carl-Von-Carlowitz-Platz 2, 85354 Freising, Germany
e-mail: rupert.seidl@tum.de

W. Rammer
e-mail: werner.rammer@tum.de

of wind- and drought-triggered disturbances. The new disturbance regime caused a persistent decline in Norway spruce and resulted in an overall decrease in landscape-level growing stock.
Conclusions Our findings underscore the urgent need for new approaches to evaluate increasingly complex disturbance dynamics and suggest that the future impacts of bark beetles on forest landscapes may be greater than previously anticipated.

Keywords Forest disturbance · Climate change · iLand model · *Ips typographus* · Norway spruce

Introduction

After 2018, Europe has experienced an unprecedented wave of tree mortality that significantly departed from the historical dynamics in many regions (Senf and Seidl 2021). This disturbance pulse was spatially aligned with soil moisture and vapour pressure deficit anomalies, implying an increasing role of drought in disturbance regimes (Senf et al. 2020). Drought legacy effects observed in the following years suggest that physiological recovery processes were impaired, and trees were prone to secondary impacts from pests and pathogens (Schuldt et al. 2020).

The most severe and widespread disturbances in European forests have been caused by the European spruce bark beetle (*Ips typographus* L.), which primarily affects Norway spruce (*Picea abies* (L.) H. Karst.), a species constituting approximately 25% of the total growing stock in Europe's forests (Hlásny et al. 2021). *I. typographus* belongs to the subfamily Scolytinae (Coleoptera: Curculionidae) and is one of the few bark beetle species exhibiting eruptive population dynamics, capable of rapidly increasing in number and causing extensive tree mortality (Raffa et al. 2008). During outbreaks, enlarged beetle populations overwhelm tree defences through mass attacks, coordinated by chemical signalling that guides individuals to specific host trees (Raffa et al. 2016). The beetle typically targets trees older than 60 years and with diameter exceeding 20 cm (Wermelinger 2004). Under outbreak conditions and high population densities, smaller and younger trees may also be colonized. Factors such as a high proportion of spruce, high stand density, advanced stand age, and the presence of forest edges are among the key conditions that predispose bark beetle infestation on the stand level (Netherer and Nopp-Mayr 2005).

I. typographus possesses several traits regulated by temperature and photoperiod, such as spring swarming, generation timing, and voltinism, which allow it to adapt its life cycle across a broad geographic range (Baier et al. 2007; Bentz et al. 2019). In many parts of Europe, where the annual heat sum is sufficient, *I. typographus* can produce more than one generation per year (Jönsson et al. 2009). While warmer climate increases the number of annually completed bark beetle generations and extends the beetles` flight period (Jakoby et al. 2019), heat and drought spells compromise the defence mechanisms of host trees (Huang et al. 2020), Netherer et al. 2021. Specifically, spruce cannot tolerate a drop in plant water potential below a certain limit (Schumann et al. 2024), at which point it closes stomata to prevent further water loss. This stomatal closure, typical of spruce's isohydric strategy, helps protect the tree against hydraulic failure, but also limits photosynthesis and thus the production of defence compounds against bark beetles (Hartmann et al. 2018; Huang et al. 2020). Hot and dry conditions can thus boost population growth of *I. typographus*.

Historically, large outbreaks of *I. typographus* were mainly initiated by windthrows, which generated pulses of breeding material that boosted beetle population growth (Wermelinger 2004). Upon successful colonization of windfelled trees, the enlarged beetle populations typically expanded into the surrounding forests and caused tree mortality that often exceeded the impact of the initial windthrow (Mezei et al. 2017). The outbreaks triggered by windthrows typically declined after several years due to the exhaustion of local resources and other mechanisms, such as decreasing fitness of individual beetles, intraspecific competition, increasing levels of antagonists, defence priming of host trees and changes in symbiont communities (Biedermann et al. 2019).

The recent emergence of drought-initiated outbreaks occurring in the absence of windthrows represents a distinct change away from the historical disturbance regime. Such drought-induced outbreaks have occurred across a range of environments and forest types in recent years, including lowland and montane forests of Czechia, Germany, Austria, France, Italy, and Sweden (Hlásny et al. 2021; Kärvemo et al. 2023; Washaya et al. 2024). They have severe

ecological and socio-economic consequences, including accelerated species turnover, reduced forest carbon stocks and increased rate of carbon release to the atmosphere, compromised cultural ecosystem values and increased timber price fluctuations (Buras et al. 2020; Hlásny et al. 2021; Asada et al. 2023). While climate projections do not indicate any clear trend in windspeed (Seneviratne et al. 2021), suggesting a relatively stable frequency of outbreaks induced by windthrows, a strong trend in climate aridification throughout the distribution of Norway spruce (Vicente-Serrano et al. 2013) suggests an increasing frequency of drought-induced outbreaks. The amplifying effect of climate change on outbreak size and severity together with the increased incidence of triggering events can thus lead to a substantial increase in forest disturbance by bark beetles. However, the possible future trajectories and their implications for the provisioning of ecosystem services remain unclear.

Dynamic vegetation models are important tools for understanding ecosystem dynamics under climate change (Blanco and Lo 2023; Rammer et al. 2024). However, models are challenged by the emergence of novel process interactions and feedbacks, which require a continuous evaluation of model structure. In the context of *I. typographus* dynamics, models exist for simulating the interaction between windthrows and outbreaks, for example, PICUS, iLand, and LandClim (Temperli et al. 2013; Maroschek et al. 2015; Rammer et al. 2024). Water limitation typically serves as predisposing or amplifying factor in these models but is not considered as an inciting factor (sensu Manion 1981) of large-scale outbreaks. Given the experiences of years following 2018 and the expected future increase in drought frequency and severity, this design element of current models could lead to a considerable underestimation of bark beetle dynamics under climate change. Considering drought as predisposing, amplifying, and inciting factor of outbreaks explicitly could thus significantly improve simulations of climate change-induced shifts in disturbance regimes.

Here, our objectives were to (i) develop an approach that incorporates drought-induced bark beetle outbreaks into the forest landscape and disturbance model iLand (Seidl et al. 2012; Rammer et al. 2024); (ii) test whether this approach is able to capture important characteristics of the recent bark beetle outbreak in Central Europe; (iii) analyze simulations incorporating the compound effects of wind- and drought-initiated outbreaks throughout the twenty-first century considering scenarios of climate change; and (iv) assess their impact on forest species composition and growing stock.

Methods

Simulation model

iLand is a process-based forest landscape model that simulates forest dynamics at the level of individual trees for landscapes spanning several thousands of hectares (Seidl et al. 2012; Rammer et al. 2024). The model accounts for continuous processes such as tree growth, mortality, and regeneration, and discontinuous processes such as natural disturbances and forest management. iLand operates in a multiscale hierarchical framework, with large-scale processes forming constraints for processes at finer scales, and the dynamics at fine scales feeding into processes at higher scales.

iLand dynamically simulates the regeneration, growth and mortality of individual trees, as influenced by climate, soil, initial state of the vegetation and disturbance. The spatial resolution of forest dynamics simulations is 2×2 m, while element cycles and environmental constrains related to energy, water and nutrients are considered at the scale of 100×100 m. iLand is driven by daily climate data, i.e., minimum and maximum air temperature, precipitation, radiation, and vapour pressure deficit. Production physiology is modelled using a light-use efficiency approach, driven by environmental conditions and species traits (Landsberg and Waring 1997). Carbohydrate allocation in trees is calculated annually based on allometric ratios and is sensitive to a tree's competitive status. Tree regeneration is modelled at an annual time step in 2×2 m^2 grid cells. Seed dispersal, climate-dependent establishment, and seedling and sapling growth are driven by species-specific traits. The mortality probability of a tree is influenced by its carbon balance, size, and age.

Management is simulated using iLand's Agent-Based Management Engine (Rammer and Seidl 2015), which employs so-called Stand Treatment Programs (STPs) to execute a series of silvicultural operations throughout the course of stand development.

STPs include planting, thinning and harvesting of trees. The adaptive elements of STPs include modifying the timing of thinning based on the actual stand density, replanting disturbed sites depending on the state of natural regeneration, and resetting the sequence of operations if a stand experiences severe disturbance.

Wind disturbances are simulated based on maximum wind speed, wind direction, and storm duration (Seidl et al. 2014). Impacts are simulated with a dose–response model, accounting for the vertical wind profile and resulting turning moment (Gardiner et al. 2000), and for local sheltering by neighbouring trees as well as the size of upwind gaps. Wind disturbances are initiated in locations where vertical differences between the top heights of neighbouring grid cells exceed 10 m, i.e., at forest edges (Blennow and Sallnäs 2004). Critical wind speeds are calculated separately for stem breakage and uprooting based on Gardiner et al (2000). Wind impacts are simulated iteratively during an individual event, with forest structure being updated after each iteration. The model was tested, for example, in Sweden following the storm Gudrun (2005), displaying good correspondence of observed and predicted wind damage patterns (Seidl et al. 2014).

iLand includes an advanced submodule for simulating European spruce bark beetle (*Ips typographus* L.) dynamics. The module considers the phenology and development of beetles, their spatially explicit dispersal, host tree colonization and defence, and temperature-related overwintering success (Seidl and Rammer 2017). Beetle development is simulated using a phenology-based process model (Baier et al. 2007), accounting for life-stage specific thermal requirements for beetle development and determining the number of generations and sister broods the insect can complete per year. Host trees are Norway spruce trees with a diameter at breast height of > 15 cm. Concerning dispersal, the model tracks beetle cohorts defined as the minimum number of beetles needed to colonize a tree. Every brood tree disperses a number of beetle cohorts determined by the reproductive rate of the beetles, estimated to range between 4 and 24 (Wermelinger and Seifert 1999). Dispersal consists of two stages: a passive flight simulated with a symmetrical dispersal kernel and an active flight where beetles look for suitable host trees within a 30 × 30 m search window (Kautz et al. 2014). Host colonization success depends on the defense capacity of the host tree that is approximated by non-structural carbohydrate reserves (Huang et al. 2020). While bark beetle population size fluctuates depending on meteorological conditions, outbreaks are mainly triggered by windthrows, which provide a surplus of breeding material (Wermelinger 2004). Removal of windfelled trees can thus exert a strong dampening effect on bark beetle outbreaks (Dobor et al. 2020a; Augustynczik et al. 2021). Model simulations were previously tested against independent data by Sommerfeld et al. (2021), who found good correspondence of simulated levels of infestation and spatial infestation patterns. The model code and executable as well as an extensive online documentation are available at https://iland-model.org/.

Implementation and testing of drought-initiated outbreaks

In the absence of windthrow, bark beetle infestations are initiated in iLand based on a parameter determining the probability of a forest patch to be infested, represented as the annual outbreak probability per hectare. This initial probability (IP) is a user parameter with a default value of 0.000685, which has been estimated based on an empirically determined disturbance rotation period of 365 years and a mean disturbance size of 4 ha (Thom et al. 2013; Thom and Seidl 2016). The IP is modified by a climate-sensitive modifier that represents the deviation of summer precipitation in the actual year from the historical average conditions for which the IP has been specified (Seidl et al. 2016). While these fluctuations can mimic the variation in the size of endemic bark beetle populations (i.e., in a non-outbreak phase), they are unable to initiate large-scale outbreaks.

We build on the existing iLand bark beetle module – as described above – for incorporating drought as an inciting factor of bark beetle outbreaks. Since research on drought-induced outbreaks of spruce bark beetle remains scarce (but see Hlásny et al. 2021; Kärvemo et al. 2023; Washaya et al. 2024), we used a semi-empirical model formulation, combining fundamental ecological understanding with limited observational data (Jorgensen and Bendoricchio 2001). Specifically, we introduced a mechanism for drought-initiated outbreaks using Vapour Pressure Deficit (VPD) as an indicator for drought, as VPD

is a strong driver of tree mortality (Park Williams et al. 2013; Hartmann et al. 2018). Moreover, VPD is readily available within iLand, as it affects stomatal conductance and primary production in the model (Rammer et al. 2024). We introduced a new function to the module, the *OutbreakClimateMultiplier* (OCM), which increases IP during heavy droughts. Specifically, the function transforms VPD into an OCM value, which is then used to scale IP multiplicatively (Fig. 1, Eq. 1). Rather than using mean annual VPD, we used the biologically more relevant June-July mean VPD (*VPDjj*), roughly corresponding to the time of year when the second bark beetle generation emerges in Central Europe (Holuša et al. 2012), i.e., during a period when increased climatic stress to trees can critically boost beetles` colonization success and population growth. As the interannual fluctuations in *VPDjj* led to unrealistic model behaviour and to consider the effect of multi-year droughts we applied a weighted *VPDjj*, using 70% from the current year and 30% from the previous year ($VPDjj = 0.7 * VPDjj_{year\ i} + 0.3 * VPDjj_{year\ i-1}$). This aligns with documented effects of multiyear droughts on tree defence, although critical drought duration thresholds remain unclear (Peltier et al. 2023; Netherer et al. 2024). The modification of IP by the OCM is applied in a spatially explicit manner at the level of iLand resource units (i.e., 1-ha grid cells seamlessly defining environmental conditions across the study landscape). Once an outbreak is initiated, its further development is governed by the processes described earlier. Hence, once triggered, drought-induced outbreaks in the model follow a development pattern similar to wind-induced outbreaks.

The transformation of VPDjj into the OCM is conducted by means of a sigmoidal function:

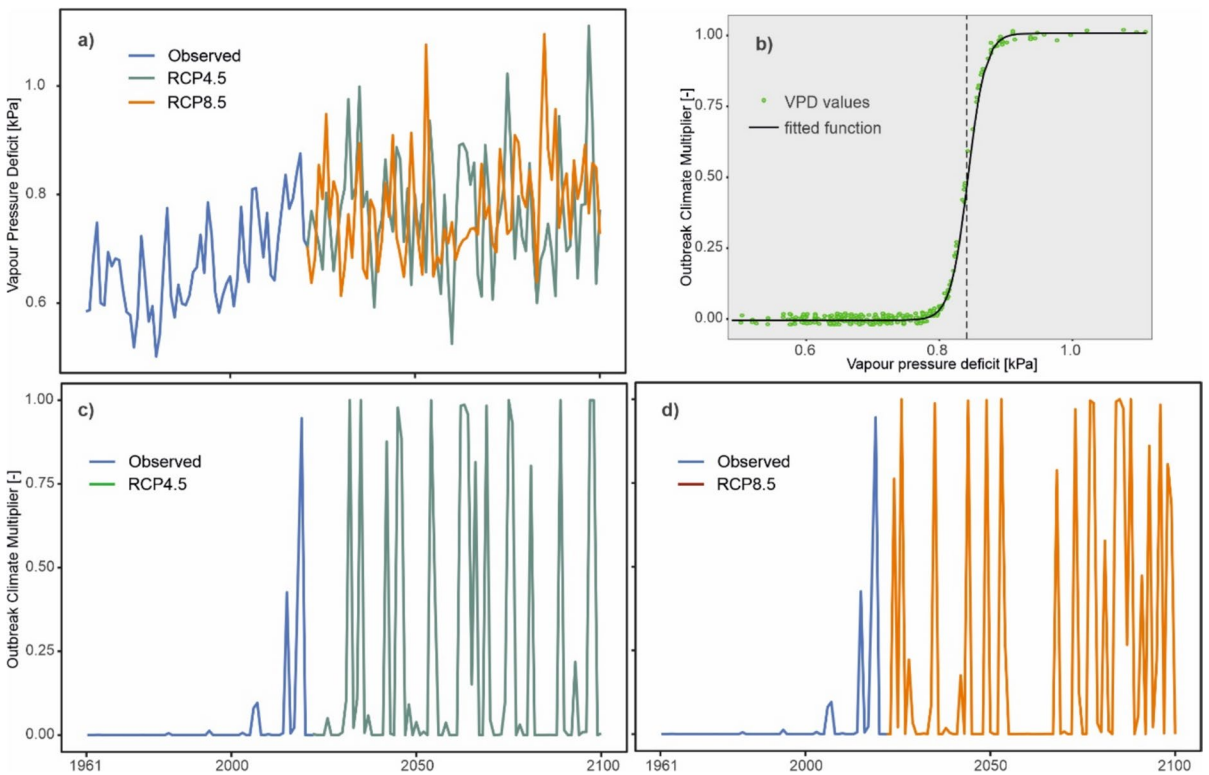

Fig. 1 A scheme for calculating the Outbreak Climate Multiplier (OCM) used to initiate bark beetle outbreaks in iLand. **a** Time series of mean June-July vapour pressure deficit (VPDjj) for the period 1961–2100, consisting of observed data until 2021 and climate projections produced by the model EC-EARTH_RACMO22E driven by greenhouse gas concentration scenarios RCP4.5 and RCP8.5 afterwards. **b** A sigmoidal function transforming VPDjj into the OCM. The vertical dashed line represents the critical VPDjj value initiating the outbreaks, here set to 0.84 kPa. **c**, **d** Resulting OCM time series indicating conditions with elevated potential for the outbreaks

$$OCM = k\frac{1}{1 + e^{-a(x-b)}} \quad (1)$$

where OCM is the *Outbreak Climate Multiplier*, *b* is a critical VPD value defining the function`s inflection point, *a* is the slope of the function (Fig. 1), *k* is a multiplier to scale OCM to result in a maximum outbreak probability that corresponds to that of windfelled trees, and *x* is *VPDjj*.

To address the uncertainty of parameter definitions, we represented each parameter in Eq. 1 as a distribution function:

$$k \sim N(\mu_k,\ \sigma_k^2),\ a \sim N(\mu_a,\ \sigma_a^2),\ b \sim N(\mu b,\ \sigma_b^2)$$

where $N(\mu_k, \sigma_k^2)$ represents a normal distribution of parameter *k,* with μ_k as the mean and σ_k^2 as the variance. The same notation applies to the parameters *a* and *b*. In each simulation, a parameter value is randomly drawn from the corresponding distribution and translated into the OCM. This procedure is applied individually to each 1-hectare resource unit, for which environmental constraints, including climate, are defined.

The function parameters were estimated based on an analysis of observed bark beetle disturbance data from our study region (see Fig. 2 and details below), specifically: (i) the annual timber volume of trees killed by bark beetles and salvaged during the period 2000–2021, and (ii) forest area affected by bark beetles identified through the classification of remote sensing data for the period 2000–2021 (Washaya et al. 2024) (Fig. 3). By iteratively comparing simulations to observed data we determined a *VPDjj* of 0.84 kPa to result in the best model performance (parameter *b* in Eq. 1). As the slope parameter *a* had only minor effects on simulated outbreak dynamics (see sensitivity analysis in Online appendix E), we arbitrarily set it to -80 (Fig. 1). Finally, we set *k* to 438, which, after multiplying with the baseline infestation probability of 0.000685, yields the value of 0.3. This represents the upper limit of infestation probability, indicating that drought-stressed trees were equally susceptible to infestation as windfelled trees. As the data required to parameterize distribution functions of the parameters of Eq. 1 are currently lacking, we demonstrated the effect of parameter uncertainty by using the earlier described parameter values as μ_k, μ_a, and μ_b, and

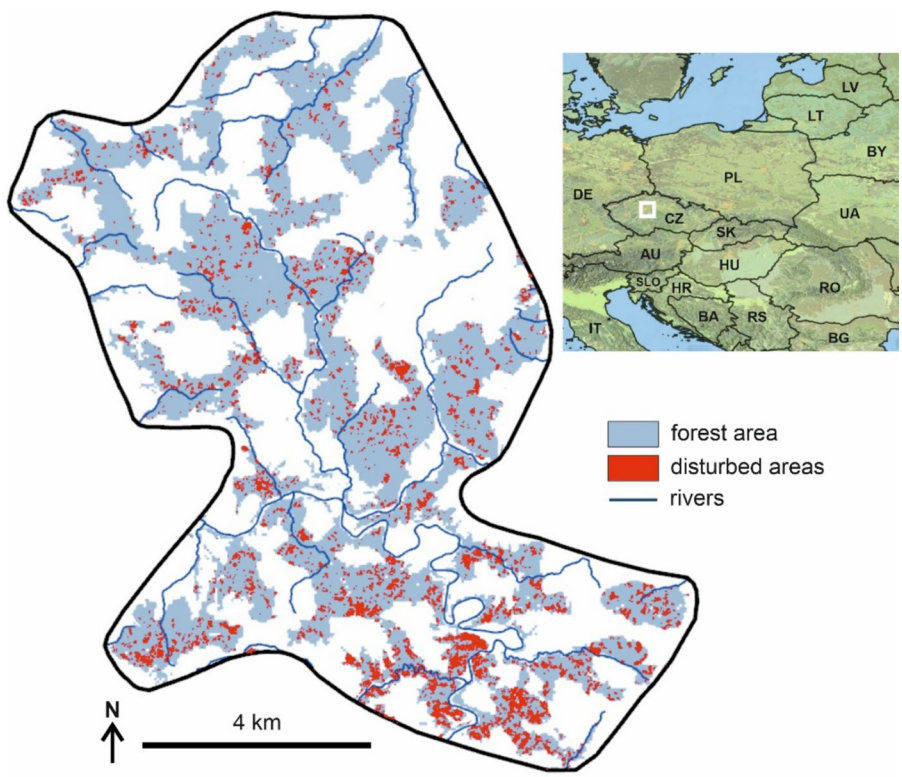

Fig. 2 The position of the study landscape in Europe (a white square), forest cover of the landscape and the extent of bark beetle disturbance between 2018 and 2021 identified based on classification of satellite data

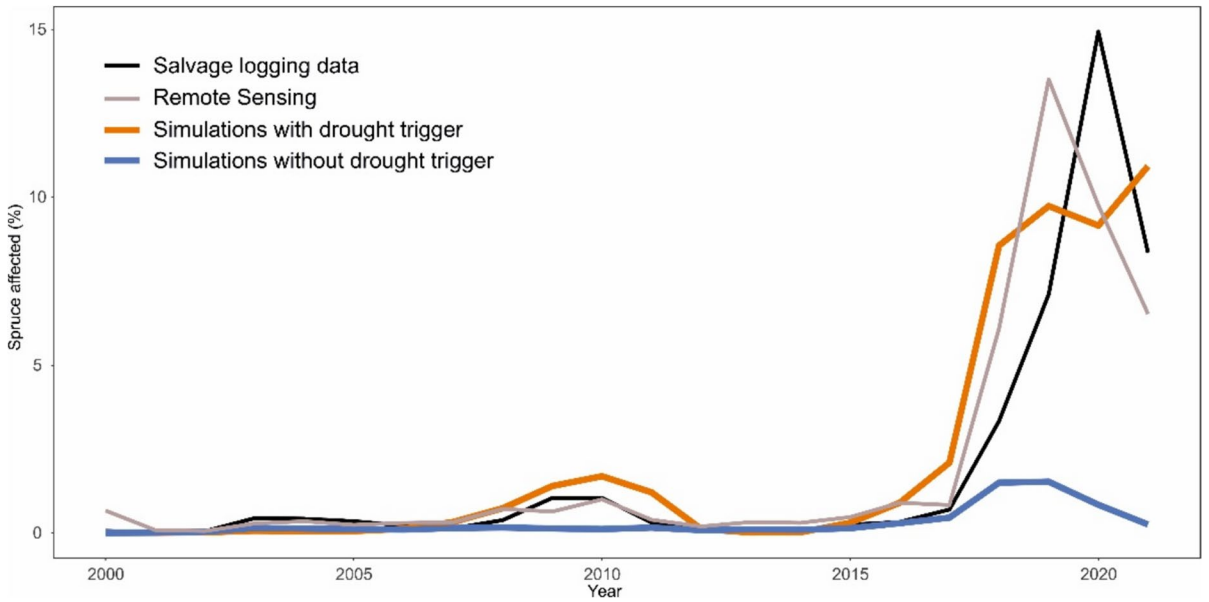

Fig. 3 Comparison of simulated bark beetle disturbance data with observed disturbance data. Two simulation outcomes are presented: one considering only wind-incited outbreaks (original model implementation, blue), and another considering both wind- and drought-related outbreaks (orange). The observed disturbance data are based on remote sensing (forest area affected) and field assessments (growing stock affected by bark beetles and salvage logged) in the study area. The annual percentage of spruce growing stock (from simulations and ground data) and of spruce area (from remote sensing data) affected by bark beetles is presented. The simulations were driven by observed climate data from the study landscape

defining the σ_k, σ_a, and σ_b as 10% of the respective μ value.

To understand how individual parameters affect simulated bark beetle dynamics, we conducted a sensitivity analysis (Online appendix E) evaluating spruce mortality under a broad range of parameter values. Simulations for the sensitivity analysis did not assume any windthrows and were driven by a set of climatic scenarios from 1961–2100 (Table 1). The response variable used was the total spruce growing stock affected by bark beetles during the simulation. We calculated the first derivative of the resulting response functions (i.e., disturbed growing stock over the range of considered parameter values) to evaluate which parameter value produces the greatest effect.

The simulated dynamics was tested against the earlier described disturbance data, aiming at the ability of the model to reproduce the forest mortality wave

Table 1 Projected changes in climate for 2051–2100 according to three climate models driven by two Representative Concentration Pathway scenarios relative to average climatic conditions for the study landscape in period 1961–1990 (Mean temperature (MT): 8.05 °C; Mean annual precipitation sum (AP): 650 mm; Mean annual Vapour Pressure Deficit (VPD): 0,62 kPa)

Climatic Models / (2051–2100) vs. (1961–1990)	MT - RCP4.5 (℃)	MT - RCP8.5 (℃)	AP - RCP4.5 (%)	AP - RCP8.5 (%)	VPD - RCP4.5 (%)	VPD - RCP8.5 (%)
EC-EARTH-RACMO22E-r1 (hot-wet)	+ 2.5	+ 3.8	− 3.7	+ 1.1	+ 23	+ 27
HadGEM2-CCLM (hot-dry)	+ 3.4	+ 5.0	− 7.9	− 6.8	+ 34	+ 53
MPI-CCLM (cool-dry)	+ 2.4	+ 3.7	− 3.1	− 2.4	+ 24	+ 31
Average	+ 2.8	+ 4.2	− 4.9	− 2.7	+ 27	+ 47

triggered after 2018 (Fig. 2) in terms of its onset, duration and termination as well as the total proportion of spruce growing stock and area affected. Although independent data would be desirable for model testing, they were not available here. We, however, note that only the critical VPD value (parameter *b*) was estimated based on observations, and the remaining metrics analysed in the evaluation are emergent properties of the simulation.

Climate data and pattern of outbreak-triggering drought events

To simulate the transition from historical climatic conditions (i.e., without the occurrence of outbreak-triggering droughts) to future climates (with a more prominent role of drought) we conducted simulations for the period 1961–2100. Climate data representing the period 1961–2021 (including daily minimum and maximum temperature, and precipitation) were measured at a meteorological station located in the study landscape (Source: Czech Hydrometeorological Institute). The measured data were downscaled to the 100 × 100m grid cells using the MT-CLIM software (Hungerford 1989), applying lapse rate calculated from twelve weather stations in the surrounding of the study region. Vapour pressure deficit was calculated based on temperature and relative humidity data (Murray 1967). Solar radiation was derived using MT-CLIM for each grid cell based on geographical position and topography.

Climate for the period 2022–2100 was extracted from the FORESEE 4.0 database (Kern et al. 2024), which provides bias corrected climate projections for Central Europe based on the CORDEX initiative (Jacob et al. 2014). The daily data from the nearest grid cell (0.1° × 0.1°) were downscaled to each 100 × 100m grid cell. Future climate was represented by the result of 14 climate models driven by two Representative Concentration Pathways, RCP4.5 and RCP8.5 (Moss et al. 2010). To drive the simulations with iLand, we selected three of the original 14 climate models that captured significant proportion of temperature–precipitation conditions projected in the ensemble (Online appendix B). As each model was driven by two RCP forcings, we considered a total of six distinct climatic trajectories (Table 1). To understand the evolution of outbreak triggering conditions across the twenty-first century, we examined the frequency of critical VPD anomalies (i.e., with *VPDjj* exceeding 0.84 kPa) across all 14 climate models. Specifically, we calculated the proportion of above-threshold climate models for each year from 2022 to 2100, which represent the probability of occurrence of outbreak-triggering conditions.

Study landscape

The study landscape is located in the Czech Republic, Central Europe (Fig. 2). The size of the landscape is 40,928 ha with 45% forest cover (18 500 ha). The elevation range is 240–540 m a.s.l., and the mean annual air temperature and precipitation sum ranges are 7.8–9.2 °C and 604–683 mm, respectively (1961–2018 data). Forests in the study landscape have been intensively managed for timber production, which resulted in a widespread occurrence of Norway spruce, mostly growing outside of its realized niche. Except for Norway spruce (57.7%), the current tree species composition mainly consists of Scots pine (*Pinus sylvestris* L.; 10.7%), European beech (*Fagus sylvatica* L., 7.6%), and oaks (*Quercus spp.;* 8.8%). The dominant management system is shelterwood (i.e., an even-aged silvicultural system that harvests trees in several progressive steps, leading to the establishment of a new cohort of trees under the shelter of the remaining mature trees) with an average rotation length of 120 years.

After 2018, the landscape was affected by a severe outbreak of spruce bark beetle that was initiated by an extended period of drought (Fig. 2) (Washaya et al. 2024). The outbreak affected 40.6% of spruce growing stock between 2018 and 2021, representing the most severe disturbance in the recorded history of the landscape. The recent disturbance dynamics of the study landscape aligns well with the dynamics observed across the entire country (Washaya et al. 2024) and parts of Europe (Patacca et al. 2023).

Experimental design

Initial forest conditions were defined based on stand-scale data seamlessly covering the landscape (Source: Forest Management Institute, Czech Republic), which were recorded in the field between 2010 and 2014. The data include the average characteristics of forest stands (i.e., polygons with an average size of 1.04 ha), specifically tree species composition, stand age, and

basal area (see Dobor et al. 2024, for more details). To evaluate the transient change in forest dynamics from 1961 to 2100, we used these forest conditions as a starting point for simulations. Simulated management closely resembled the practices applied by managers in the landscape over the past 30 years. It involved a shelterwood cutting system with rotation lengths of 80–140 years, depending on site conditions and tree species. Management was implemented through five site-specific STPs (Rammer and Seidl 2015), which included sequences of operations such as planting after harvests and disturbances, a series of thinning operations, and final harvesting. Unlike current management practices, we did not apply any salvage logging of windfelled trees which serve as breeding substrate for bark beetles (Dobor et al. 2020b, a).

To discern the effect on simulated disturbances resulting from the introduction of drought-induced outbreaks, we compared simulated forest dynamics under wind-induced outbreaks (previous model version) with the new regime that contained the combination of wind- and drought-initiated outbreaks. Given the high climatic sensitivity of bark beetle outbreaks and the anticipated increase in drought conditions under climate change, we assessed simulated disturbance dynamics under climate change in scenarios derived from three climate models for two RCP scenarios (Table 1). Because the parameters in Eq. 1 are represented as probability distributions, each simulation was replicated 30 times with randomly drawn parameter values from these distributions. Altogether, the simulation experiment consisted of 186 runs: [(simulation containing wind trigger only) + (simulation containing drought and wind triggers × 30 replicates of the Eq. 1 parameters)] × (3 RCMs × 2 RCPs).

All simulations were driven by an identical wind sequence representing the timing of windstorms, wind speed, wind direction, and windstorm duration (Seidl et al. 2014). The 140-year long sequence (1961–2100) consisted of a number of minor wind events and six more significant storms (Online appendix D). Wind speed and wind duration parameters were iteratively adjusted to reach the average impact of around 0.5% of the growing stock affected annually within the simulation period 1961–2021, which was the observed level of disturbance in the period 1980–2010. The most severe windstorm occurred in the year 2070, serving to assess the effects of previous forest development driven by different climates and outbreak dynamics on future wind vulnerability of forest growing stock. We note that although all simulations were exposed to the same wind sequence, the simulated impact differs between scenarios because it is an emergent property of the interaction of wind and vegetation conditions.

Results

Model testing

There was no significant windthrow in the study landscape during the period 2000–2021 (Fig. 3). After 2017, both remote sensing-based forest change maps and salvage logging data indicated a substantial increase in tree mortality associated with bark beetle outbreaks. During the peak period from 2018 to 2021, between 9 and 13% of spruce growing stock (according to salvage logging data) or spruce area (as indicated by remote sensing) was affected annually. Cumulatively, 44 and 46% of the initial spruce growing stock and spruce area, respectively, were affected between 2000 and 2021.

In simulations using the previous model version (wind-triggered outbreaks only), spruce mortality due to bark beetles slightly increased between 2017 and 2020, peaking at 1.8% of spruce growing stock affected by bark beetles annually. However, this increase was not sufficient to initiate an outbreak, and tree mortality declined as soon as the climatic stress was alleviated. The total affected spruce growing stock between 2000 and 2021 was 6.6% in these simulations. In contrast, spruce mortality caused by bark beetles exhibited a sharp increase post-2018 in simulations which involved a drought trigger (new model version), closely aligning with observed mortality patterns (Fig. 3). The total affected spruce growing stock between 2000 and 2021 was 47.5%, which closely corresponds to observations. Despite substantial difference in the total outbreak impact between the two simulations, the correlations of annual values of simulated tree mortality with observed tree mortality were high in both cases: The R^2 was of 0.72 without drought trigger and 0.86 with drought trigger.

Finally, while the observed outbreak collapsed after a single culmination year, the simulated outbreak culminated over several years. This is likely

the result of the specified outbreak duration in iLand (Kautz et al. 2011; Lausch et al. 2013; Seidl et al. 2016), but could also result from active risk management measures that were not considered in the simulation.

Temporal pattern of future droughts inciting bark beetle outbreaks

The distribution of *VPDjj* values differed significantly between the observed climate of the past and climate projections, as well as between RCP scenarios. Under RCP4.5, the median projected *VPDjj* for 2021–2050 (0.77 kPa) was similar to that for 2071–2100 (0.76 kPa) but higher than the observed median of 0.62 kPa for 1961–1990 (Fig. 4a, b). In contrast, under RCP8.5, the median *VPDjj* for 2071–2100 (0.83 kPa) was higher than for 2021–2050 (0.75 kPa). In the period 1961–1990, no year exceeded the outbreak threshold of 0.84 kPa. Under RCP4.5, an average of 24% of years (inter-model range: 7–38%) during 2021–2050 and 19% (0–47%) during 2071–2100 surpassed this threshold. Under RCP8.5, these proportions were 18% (7–27%) and 46% (17–83%), respectively.

Based on agreement across the 14 climate models (Online appendix B), the annual probability of exceeding the outbreak threshold of 0.84 kPa differed between RCP scenarios (Fig. 4c, d). Under RCP4.5, the probability peaked around 2060 at an average of 25%, with some years reaching up to 50%. Under RCP8.5, this proportion steadily increased after 2021, reaching 50% by 2100.

Simulated disturbance dynamics

In simulations considering only wind as outbreak trigger, bark beetle outbreaks were closely related to windthrows (Fig. 5). Outbreak peaks were higher under RCP8.5 than under RCP4.5 in the second half of the century, when the difference in warming levels between the two RCPs was more pronounced (Online appendix A). The cumulative disturbance impact from 1961 to 2100 ranged between 5,909 and 7,631 thousand m^3, depending on the climate model (6,323 thousand m^3, on average) (Fig. 6).

In simulations considering drought as outbreak inciting factor, outbreak size increased, mainly between 2020 and 2060, and outbreaks become distinctly decoupled from wind disturbances. The cumulative disturbance impact exceeded the wind-only scenario by 36.1%, with damage ranging from 8,140.8 to 9,638.8 thousand m^3. Although outbreak-triggering droughts were more frequent under RCP8.5 than under RCP4.5 (Fig. 4), the difference in outbreak dynamics between the RCP scenarios was only moderate. This is the result of a rapid depletion of host trees for bark beetles even under RCP4.5 (see Sect. "Disturbance effects on growing stock and tree species composition"), constraining disturbance activity across both scenarios, particularly in the second half of the century.

The combined wind- and drought-induced outbreaks reduced wind impacts in the second half of the twenty-first century (Fig. 5) by depleting wind-prone mature spruce trees, which were replaced by more wind-resistant species (Fig. 9). This suggests a transition from wind- to drought-driven disturbance dynamics in the twenty-first century. This transition was also confirmed by the substantially smaller impact of the major windthrow event simulated in 2070 and the subsequent outbreak (in the years 2070–2075) in simulations considering wind- and drought-induced outbreaks compared to those with wind-induced outbreaks only (Fig. 7).

Disturbance effects on growing stock and tree species composition

While the proportion of Norway spruce was relatively stable between 1961 and 2022, it declined in the remaining period under simulations with both model versions. In the wind-only case, the reduction was significantly accelerated after 2050, when progressive climate change amplified the outbreaks initiated by windthrows (Fig. 8a). The mean spruce reduction by 2100 was 43.1% relative to initial conditions, with an inter-climate model range of 10.2 – 72.1%. This represents a decrease from the initial spruce growing stock of 188 $m^3\ ha^{-1}$ to 106.9 $m^3\ ha^{-1}$ (52.4 – 168.8 $m^3\ ha^{-1}$ range). The variation between climate models was substantial. The most extreme scenario, represented by the hot-dry HadGEM2_CCLM model under RCP8.5, led to a sharp reduction in spruce after two consecutive windthrows around 2050, i.e., already before the major windthrow in 2070 (Online appendix C). This reduction persisted until the end of the simulation period. In the less extreme climate

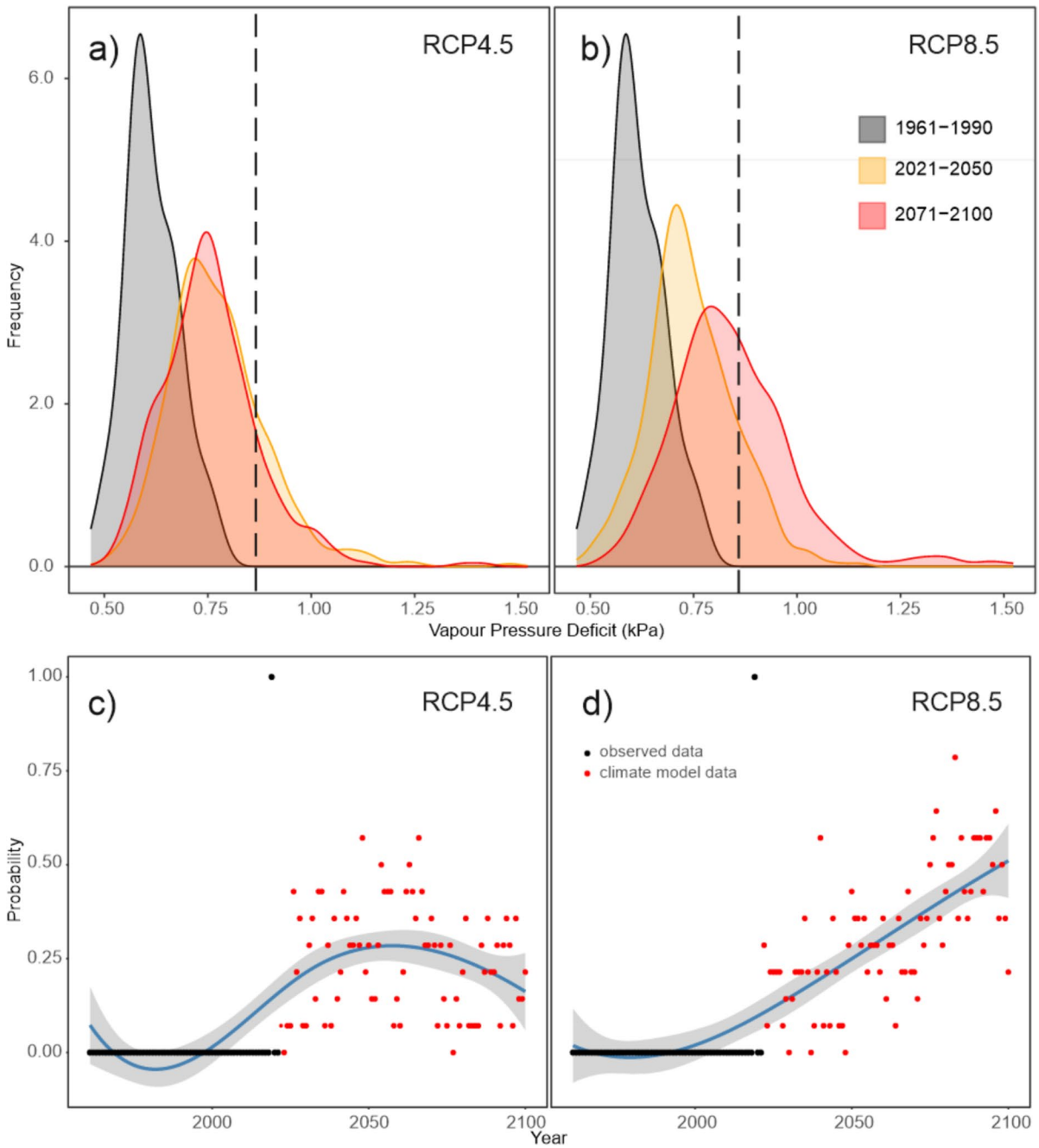

Fig. 4 Distribution of two-year weighted mean June-July Vapour Pressure Deficit (VPD_{jj}) values across three time periods and two RCP scenarios. The past period 1961–1990 is represented by observed data, while periods 2021–2050 and 2071–2100 are represented by fourteen climate models. Vertical dashed lines indicate the outbreak threshold of 0.84 kPa (**a**, **b**). Panels **c**, **d** give the annual probability of VPDjj values exceeding the outbreak threshold. During 1961–2021, probabilities are binary (0 or 1), while for 2022–2100, they are calculated based on the proportion of climate model runs (n=14) above threshold. A spline function with a 95% confidence band is included to aid the visual interpretation of the data

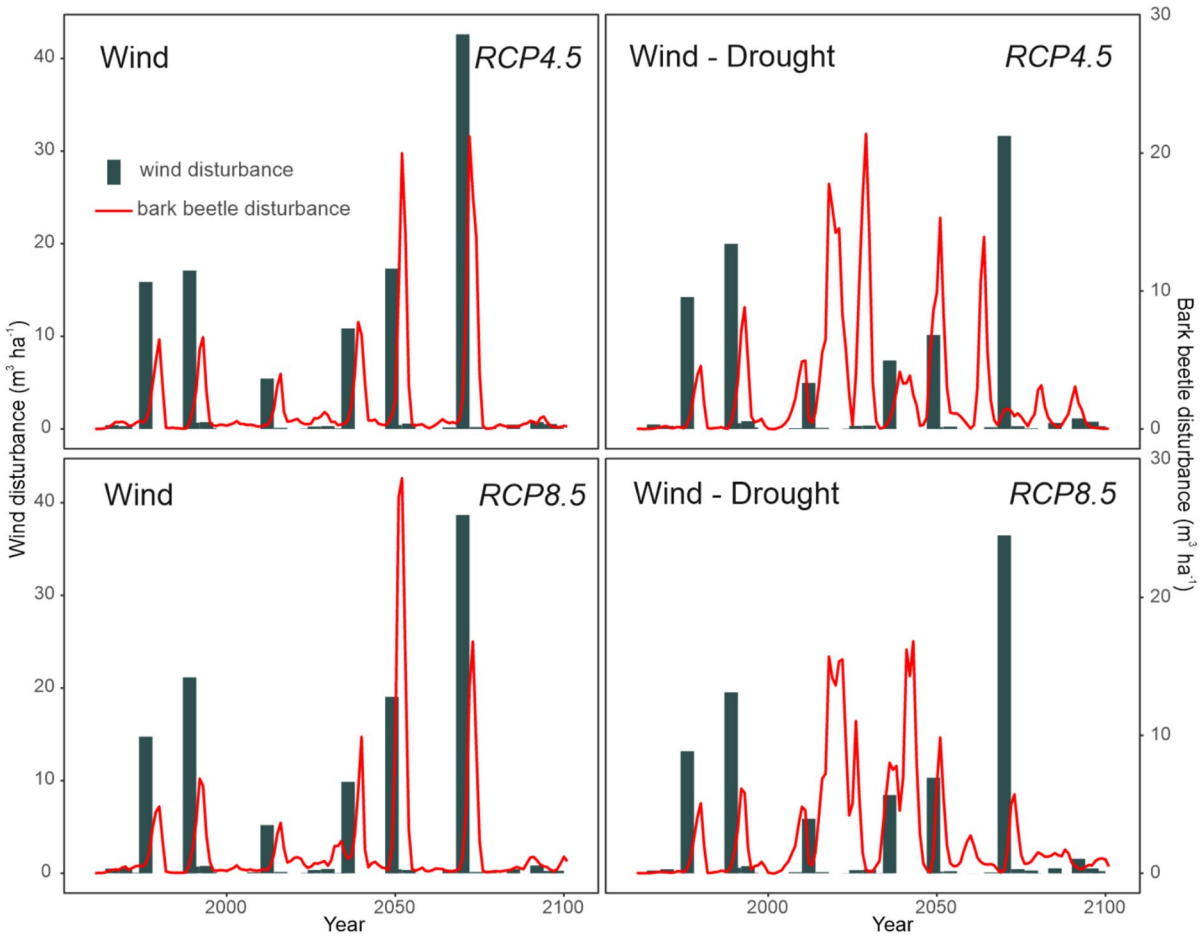

Fig. 5 Simulated disturbance dynamics in the period 1961–2100. Two simulations are presented: 'Wind,' which includes only wind-initiated bark beetle outbreaks, and 'Wind-Drought,' which combines wind and drought as outbreak triggers. In 'Wind-Drought', bark beetle activity is increasingly independently from windthrows as triggers. Climate in the period 1961–2021 was defined based on local meteorological data. Climate in the period 2021–2100 was defined based on the climate model HadGEM2_CCLM (hot-dry) driven by the greenhouse gas concentration pathways RCP4.5 and RCP8.5. Simulations driven by other climate model projections can be found in online Online appendix C

scenarios the reduction in spruce was effectively offset by the ingrowth of other tree species, notably European beech and Scots pine, maintaining the overall growing stock at a stable level (Fig. 9). This compensatory dynamic was pronounced under RCP8.5, supported by the stronger fertilization effect of elevated atmospheric CO_2 concentrations.

Simulations also considering drought-incited bark beetle outbreaks (Fig. 8, 9) caused an abrupt reduction of spruce already between 2018–2027, when the first outbreaks triggered by drought emerged. By 2100, 91.7% (range of 88.8—95.5%) of the initial spruce growing stock was lost. Despite the high climate sensitivity of bark beetle disturbances and higher frequency of VPD events above the outbreak threshold under RCP8.5 (Fig. 4), there was no significant difference between the RCP scenarios (Fig. 8b). This can be attributed to the already severe disturbance conditions under RCP4.5, which led to rapid spruce depletion and thus negative feedbacks on disturbance activity. In these simulations, the landscape was transformed into the beech-pine ecosystem, with admixed spruce, larch, and oaks (Fig. 9).

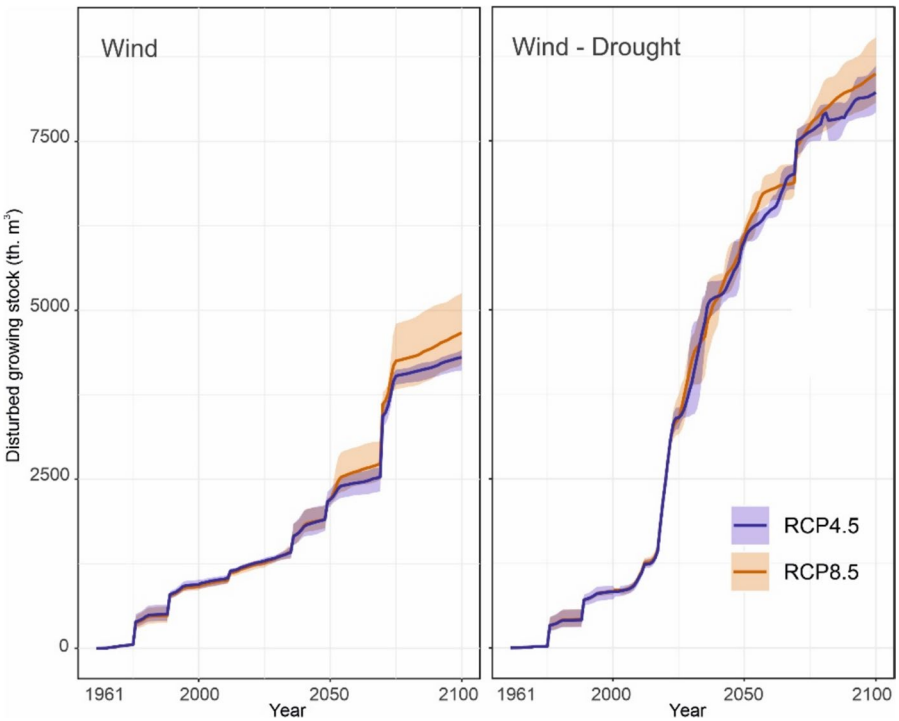

Fig. 6 Cumulative disturbed growing stock in the period 1961–2100 under different disturbance and climatic scenarios. 'Wind,' includes only wind-initiated bark beetle outbreaks. 'Wind-Drought' considers both wind and drought as outbreak triggers. Minimum–maximum envelopes arise from the combination of three climate models nested within RCP4.5 and RCP8.5 climate forcings. In the case of the Wind-Drought scenario, a portion of variability is attributed to the twenty replicates representing parameter uncertainty in the outbreak triggering function (Eq. 1)

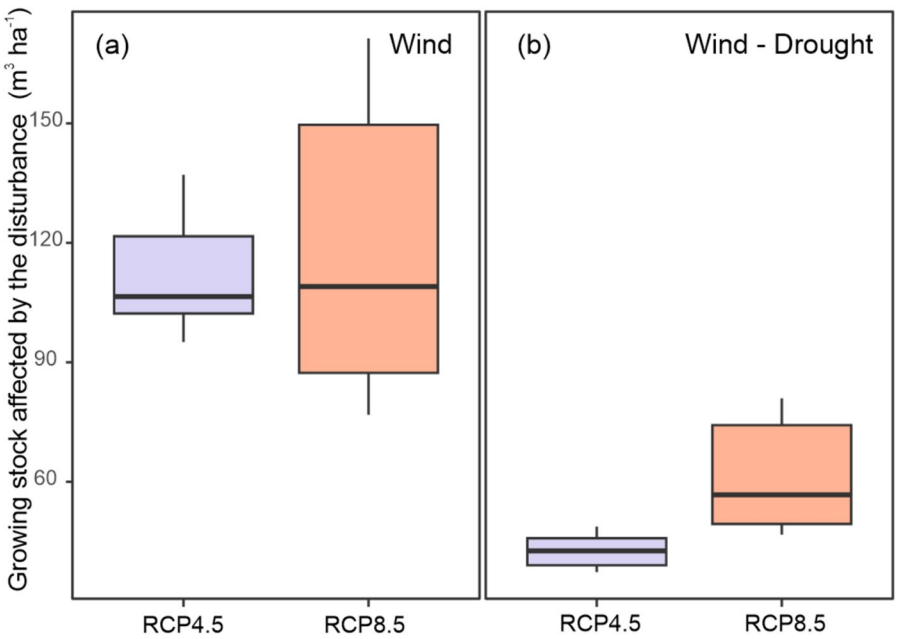

Fig. 7 Level of disturbed growing stock during the period 2070–2075 encompassing the major windthrow in year 2070 and the subsequent outbreak. Median, 25–75% and the minimum–maximum ranges are presented. 'Wind,' includes only wind-initiated bark beetle outbreaks. 'Wind-Drought' combines wind and drought as outbreak triggers. The variation arises from the combination of three climate projections and twenty replicates of each

Discussion

Here, we developed a parsimonious approach that enables the simulation of transitions from wind- to drought-driven bark beetle outbreak dynamics within the forest landscape model iLand (Rammer et al. 2024). The proposed approach can be used to explore, for example, the compounding effects of outbreaks initiated by wind and drought, an interaction expected to become increasingly frequent in

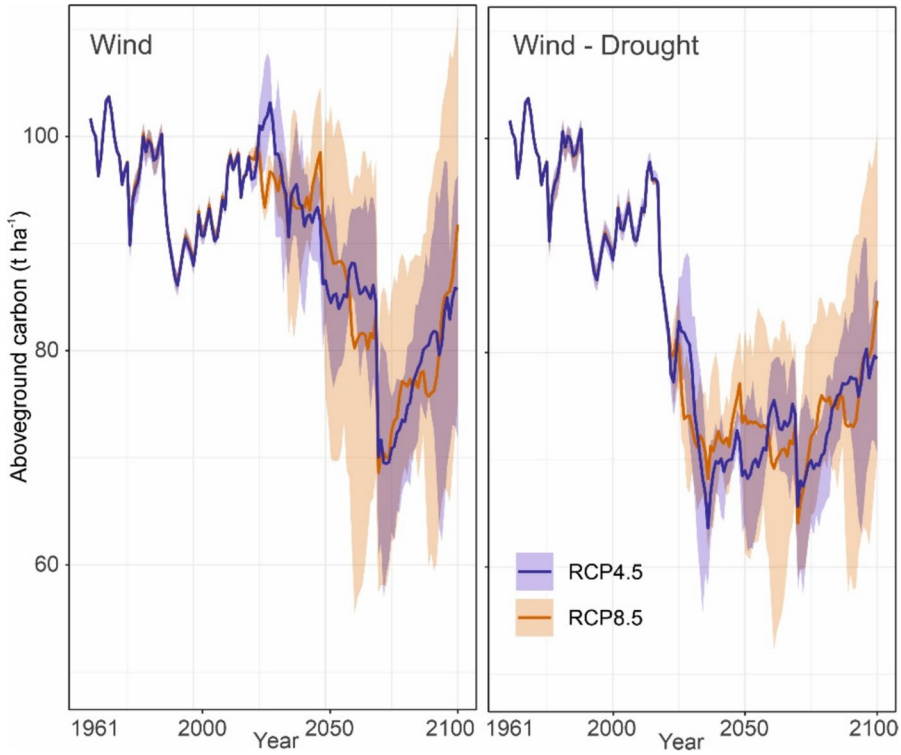

Fig. 8 Development of spruce growing stock under different disturbance and climatic scenarios. Mean and minimum–maximum envelopes of simulations driven by three climate models within each RCP scenario (2022–2100) are indicated. 'Wind' considers only wind-initiated bark beetle outbreaks. 'Wind-Drought' considers both wind and drought as outbreak triggers

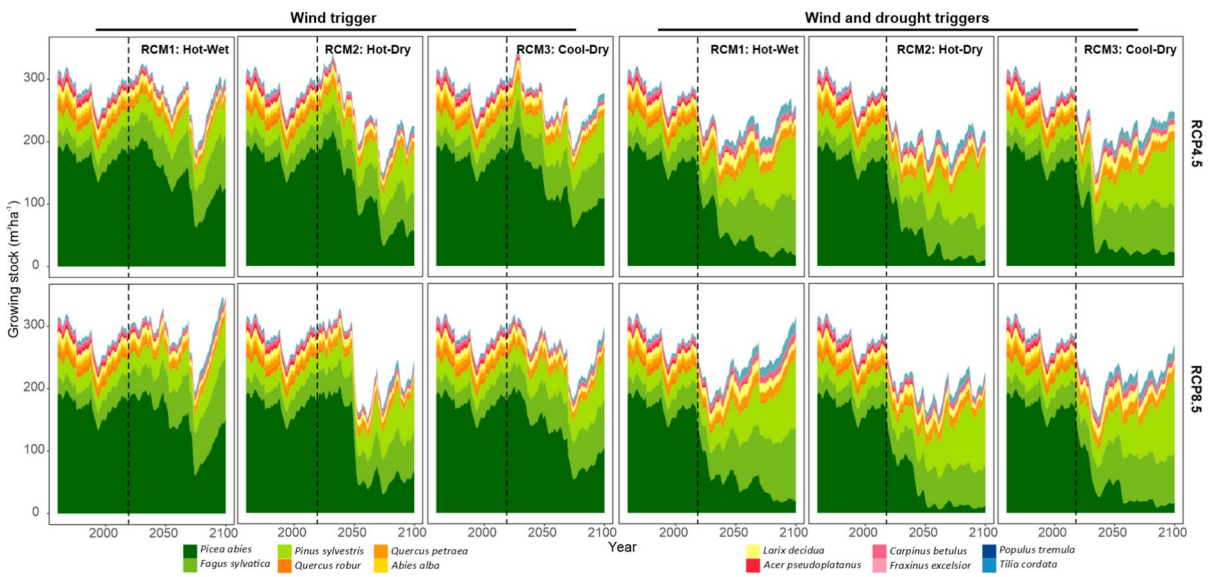

Fig. 9 Development of tree species composition simulated with different model versions under different climatic scenarios. 'Wind,' considers only wind-initiated bark beetle outbreaks. 'Wind-Drought' considers both wind and drought as outbreak triggers. Vertical dashed lines indicate the transition from observed climate data (1961–2021) to climate projections. RCM1: EC_EARTH_RACMO22E_r1, RCM2: HadGEM2_CCLM, RCM3: MPI_CCLM (Table 1)

the future. We demonstrated that the improved bark beetle module can reliably reproduce observed local outbreak dynamics and generate plausible outcomes in decadal-scale simulations. Given the projected increase in drought conditions under climate change, our approach represents an important contribution to more robust simulations of future disturbance dynamics. In the following, we discuss the limitations of the proposed framework and the potential ecological implications of the presented simulation outcomes.

Simulation of bark beetle outbreaks

Like several other ecosystem models simulating spruce bark beetle dynamics (Temperli et al. 2013; Maroschek et al. 2015), iLand includes windthrows as an inciting factor for outbreaks. Drought, on the other hand, has typically acted as amplifying factor for bark beetle infestations, modulating disturbance severity rather than triggering large-scale, self-sustaining outbreaks. However, the recent surge in drought-initiated bark beetle outbreaks across Europe underscored the emerging role of severe drought as a primary trigger. In response, we developed and tested a modelling approach capable of initiating outbreaks following such extreme drought events. We chose VPD as an outbreak trigger due to the growing evidence for its significant effects on tree physiology and mortality (Park Williams et al. 2013; Hartmann et al. 2018). Additionally, VPD is employed in iLand to modulate stomatal conductance and primary production, which ultimately determine the availability of non-structural carbohydrate reserves and hence tree defence against bark beetles (Rammer et al. 2024). Although inciting factors, as defined by Manion (1981), operate on a short time scale, such as windthrows, we utilized a two-year weighted average of June-July VPD as outbreak trigger in the simulations. This allowed us to capture the effect of multi-year droughts, which can impair tree physiological processes, including production of secondary metabolites essential for tree defence (Gely et al. 2020). Nonetheless, we note that the degree to which biotic mortality agents are linked to stress physiology is highly variable and insufficiently understood (Trugman et al. 2021), limiting the implementation of these interactions in ecosystem models. For example, legacy effects of previous drought exposure, gradual depletion of non-structural carbohydrate reserves under multiyear droughts, and the relationships between primary and secondary metabolism and their responses to drought, remain insufficiently understood, yet they are essential for improving the modelling of tree–bark beetle interactions (Netherer et al. 2015; Huang et al. 2020). Advances in empirical understanding of these interactions are essential for replacing prevalent, simplified representations (such as the one presented here) with more sophisticated, process-based approaches (Huang et al. 2020). Unless such knowledge is available, the proposed approach, which substitutes complex process understanding with an empirical relationship between changing climate and outbreak risk, provides a practical means to simulate transient disturbance dynamics, with potential applicability beyond bark beetle outbreaks.

We fitted parameter values of the function translating VPD to infestation probabilities, achieving a good match between observed and simulated outbreak dynamics. We note, however, that this parameterization mainly focused on high local accuracy, and that its ability to generalize should be tested in future works. The fact that the dynamics observed for our study landscape aligns well with developments observed across the Czech Republic (Washaya et al. 2024) and Central Europe (Senf et al. 2020) could be a first indication for broader applicability of the approach presented here. Future work should focus especially on refining the VPD outbreak threshold, identified as the most influential parameter in our sensitivity analysis (Online appendix E). To account for uncertainty in outbreak-triggering conditions due to factors such as variable forest age structure, spruce proportion and distribution, and site conditions, we represented each parameter using probability distributions. Due to limited empirical data, these distributions were defined arbitrarily in the current study. However, recent advancements in the use of remote sensing for research on biotic disturbances in forests (Senf et al. 2017) could help identify drought-initiated bark beetle outbreaks across Europe and thus improve the generality of model parameterizations, including parameter uncertainty ranges.

Uncertainty remains regarding the duration of drought-driven bark beetle outbreaks, which may differ from that of wind-driven outbreaks due to different resource distributions (Kärvemo et al. 2023). Moreover, our understanding of the underlying processes causing outbreaks to subside remains insufficient,

even for wind-initiated outbreaks (Biedermann et al. 2019). While the outbreak observed in our study landscape peaked in a single year (2019), the simulated tree mortality level remained high until the end of the simulation in 2021. An improved process-based understanding of processes driving the collapse of bark beetle outbreaks could further improve the robustness of simulated trajectories of bark beetle disturbance. In this context, future research should specifically examine how drought- and wind-triggered outbreaks differ in terms of the mechanisms that dampen outbreak dynamics (Biedermann et al. 2019; Schroeder et al. 2025).

Despite the limitations of the proposed framework, our results demonstrate the applicability of iLand and the improved bark beetle module to simulate local developments with high accuracy, and make meaningful decadal-scale projections of landscape trajectories. Although the changes made to the model are parsimonious, they are embedded in a complex simulation framework that incorporates climate-sensitive bark beetle development and tree defence, community level vegetation feedbacks, and possible interactions with other disturbance agents (Honkaniemi et al. 2021), and is thus able to simulate dynamic feedbacks between climate, vegetation and disturbances.

Effect of drought-initiated outbreaks on forest dynamics

The consideration of drought-induced bark beetle outbreaks significantly amplified simulated bark beetle disturbances after 2018, as the critical VPD threshold was increasingly exceeded. Considering wind- and drought-triggered outbreaks jointly resulted in a persistent reduction of growing stock already in the coming decades. This suggests that while growing stock was resilient to a wind-dominated disturbance regime, this resilience diminished under the compounded impact of wind- and drought-triggered disturbances, even under the moderate climate change represented by RCP4.5. This result aligns with previous studies which indicated low resilience of forest carbon and biomass to novel disturbance regimes under climate change (Turner and Seidl 2023), with potentially strong consequences for bioeconomy and climate change mitigation (Dye et al. 2024; Hetemäki et al. 2024). The simulated magnitude of bark beetle impact also corresponds well to recent observations from Central Europe: For instance, spruce growing stock in the Czech Republic declined by approximately 20% from 2017 to 2022, with certain regions experiencing reductions of 40 to 60% (Washaya et al. 2024).

Incorporating drought as a trigger for bark beetle outbreaks led to a notable decoupling of wind and bark beetle disturbances. Moreover, we observed an overall transition from wind- to drought-driven dynamics in the twenty-first century, with a notably smaller impact of the 2070 windthrow under the combined effect of wind and drought-initiated outbreaks (Fig. 5 and 7). The underlying mechanisms were complex, involving an increasing frequency of critical VPD conditions while windthrow frequency remained stable (Seneviratne et al. 2021), and vegetation feedback characterized by an increase in species which are less wind-prone than spruce (Wallentin and Nilsson 2014), and which are not suitable hosts for the European spruce bark beetle. These findings confirm the ability of our new module to simulate transient ecosystem dynamics and help understand changes in disturbance regimes in Europe caused by climate change.

Regarding tree species composition, spruce remained dominant when solely considering wind-driven bark beetle outbreaks, except in the most severe scenarios of climate change (Fig. 9). The incorporation of drought-incited outbreaks significantly reduced spruce on the landscape, with the major drop occurring between 2030 and 2040, even under the moderate climate scenario represented by RCP4.5. Subsequently, species such as European beech and Scots pine gained dominance. The direction of this transformation aligns well with previous empirical and modelling studies, which indicated the increase in drought tolerant and warm-adapted tree species under climate change, such as European beech at the expense of Norway spruce (Hanewinkel et al. 2013; Kasper et al. 2022). Nevertheless, the high pace of the transition identified here suggests that previous studies may have underestimated the impact of natural disturbances amplified by climate change and their catalyzing effect on forest transformation (Thom & Seidl 2016).

Finally, the two model variants (i.e., with and without considering drought-induced bark beetle outbreaks) resulted in distinctly different variability in simulation outcomes, driven primarily

by differences among climatic scenarios. In the wind-only simulations, variability remained high because a substantial amount of mature spruce stands persisted throughout the simulation period, allowing for varied disturbance dynamics under different climatic conditions. Conversely, under the compounding impacts of wind- and drought-initiated outbreaks, spruce growing stock was rapidly depleted—even under RCP4.5—thereby narrowing the simulated range of variability. Hence, while simulations with outbreaks triggered by wind-only suggest that spruce could be maintained and related management objectives achieved under certain conditions, simulations considering both wind and drought as outbreak triggers invariably predict a critical decline of spruce. Since the compounding impacts of wind and drought-triggered outbreaks are likely to become the new normal in the future, these outcomes warrant critical consideration in management planning in spruce dominated forests of Central Europe.

Conclusion

Modelling novel disturbance dynamics is among the key challenges for current ecosystem modelling, as it is essential for both projecting future ecosystem trajectories and for robustly informing ecosystem management and forestry policy-making. Here, we developed and tested an approach addressing one of the most distinct examples of such an emerging disturbance regime change in Europe: The transition from wind-driven to drought-driven dynamics of the European spruce bark beetle. We introduced this novel outbreak type into an existing simulation framework, and demonstrated that our approach simulates the compound impact of the historically dominating wind-initiated outbreaks and the emerging drought-initiated outbreaks as well as their feedbacks and interactions. While our study contributed a novel approach to simulate bark beetle outbreaks, it also revealed severe limitations in data and system understanding that limit process-based bark beetle modelling. Our work highlighted that the structure of process-based models needs to be continuously evaluated and potentially updated as novel process-interactions emerge under climate change.

Author contributions All authors contributed to the study's conception and design. Formal analysis and methodology were performed by AKD, MB, and LD. Conceptualization and software development were carried out by WR. RS and SM contributed to conceptualization, writing, review and editing. PW and RM were responsible for resources and validation. Writing, review, editing and research coordination was conducted by TH. All authors read and approved the final manuscript.

Funding Open access publishing supported by the institutions participating in the CzechELib Transformative Agreement. This work was supported by the H2020 project RESONATE under grant agreement No. 101000574 and project of the National Agency for Agriculture Research of the Czech Republic no. QK23020039. RS acknowledges support from the European Research Council under the European Union's Horizon 2020 research and innovation program (Grant Agreement 101001905, FORWARD). Agnish Kumar Das acknowledges support from the Internal Grants Commission (IGA A_35_24) at the Faculty of Forestry and Wood Sciences, Czech University of Life Sciences, Prague.

Data availability The datasets generated during and/or analysed during the current study are available from the corresponding author at request.

Declarations

Conflict of interests The authors declare no competing interests.

References

Asada R, Hurmekoski E, Hoeben AD et al (2023) Resilient forest-based value chains? Econometric analysis of roundwood prices in five European countries in the era of natural disturbances. For Policy Econ 153:102975

Augustynczik ALD, Dobor L, Hlásny T (2021) Controlling landscape-scale bark beetle dynamics: Can we hit the right spot? Landsc Urban Plan 209:104035

Baier P, Pennerstorfer J, Schopf A (2007) PHENIPS—a comprehensive phenology model of Ips typographus (L.)

(Col., Scolytinae) as a tool for hazard rating of bark beetle infestation. For Ecol Manage 249:171–186
Bentz BJ, Jönsson AM, Schroeder M et al (2019) *Ips typographus* and *Dendroctonus ponderosae* models project thermal suitability for intra-and inter-continental establishment in a changing climate. Front for Global Change 2:1
Biedermann PHW, Müller J, Grégoire J-C et al (2019) Bark beetle population dynamics in the Anthropocene: challenges and solutions. Trends Ecol Evol 34:914–924
Blanco JA, Lo Y-H (2023) Latest trends in modelling forest ecosystems: new approaches or just new methods? Curr for Rep 9:219–229
Blennow K, Sallnäs O (2004) WINDA—a system of models for assessing the probability of wind damage to forest stands within a landscape. Ecol Model 175:87–99
Buras A, Rammig A, Zang CS (2020) Quantifying impacts of the 2018 drought on European ecosystems in comparison to 2003. Biogeosciences 17:1655–1672
Dobor L, Hlásny T, Rammer W et al (2020a) Is salvage logging effectively dampening bark beetle outbreaks and preserving forest carbon stocks? J Appl Ecol 57:67–76
Dobor L, Hlásny T, Rammer W et al (2020b) Spatial configuration matters when removing windfelled trees to manage bark beetle disturbances in Central European forest landscapes. J Environ Manage 254:109792
Dobor L, Baldo M, Bílek L et al (2024) The interacting effect of climate change and herbivory can trigger large-scale transformations of European temperate forests. Glob Chang Biol 30:e17194
Dye AW, Houtman RM, Gao P et al (2024) Carbon, climate, and natural disturbance: a review of mechanisms, challenges, and tools for understanding forest carbon stability in an uncertain future. Carbon Balance Manag 19:1–25
Gardiner B, Peltola H, Kellomäki S (2000) Comparison of two models for predicting the critical wind speeds required to damage coniferous trees. Ecol Modell 129:1–23
Gely C, Laurance SGW, Stork NE (2020) How do herbivorous insects respond to drought stress in trees? Biol Rev 95:434–448
Hanewinkel M, Cullmann DA, Schelhaas M-J et al (2013) Climate change may cause severe loss in the economic value of European forest land. Nat Clim Chang 3:203–207
Hartmann H, Moura CF, Anderegg WRL et al (2018) Research frontiers for improving our understanding of drought-induced tree and forest mortality. New Phytol 218:15–28
Hetemäki L, D'Amato D, Giurca A, Hurmekoski E (2024) Synergies and trade-offs in the European forest bioeconomy research: State of the art and the way forward. For Policy Econ 163:103204
Hlásny T, König L, Krokene P et al (2021) Bark beetle outbreaks in Europe: state of knowledge and ways forward for management. Curr for Rep 7:138–165
Holuša J, Lukášová K, Lubojacký J (2012) Comparison of seasonal flight activity of *Ips typographus* and *Ips duplicatus*. Sci Agric Bohem 43:109–115
Honkaniemi J, Rammer W, Seidl R (2021) From mycelia to mastodons–a general approach for simulating biotic disturbances in forest ecosystems. Environ Model Softw 138:104977
Huang J, Kautz M, Trowbridge AM et al (2020) Tree defence and bark beetles in a drying world: carbon partitioning, functioning and modelling. New Phytol 225:26–36
Hungerford RD (1989) MTCLIM: A mountain microclimate simulation model. US Department of Agriculture, Forest Service, Intermountain Research Station
Jacob D, Petersen J, Eggert B et al (2014) EURO-CORDEX: new high-resolution climate change projections for European impact research. Reg Environ Change 14:563–578
Jakoby O, Lischke H, Wermelinger B (2019) Climate change alters elevational phenology patterns of the European spruce bark beetle (*Ips typographus*). Glob Chang Biol 25:4048–4063
Jönsson AM, Appelberg G, Harding S, Bärring L (2009) Spatio-temporal impact of climate change on the activity and voltinism of the spruce bark beetle, *Ips typographus*. Glob Chang Biol 15:486–499
Jorgensen SE, Bendoricchio G (2001) Fundamentals of ecological modelling. Elsevier
Kärvemo S, Huo L, Öhrn P et al (2023) Different triggers, different stories: Bark-beetle infestation patterns after storm and drought-induced outbreaks. For Ecol Manage 545:121255
Kasper J, Leuschner C, Walentowski H et al (2022) Winners and losers of climate warming: Declining growth in Fagus and Tilia vs. stable growth in three Quercus species in the natural beech–oak forest ecotone (western Romania). For Ecol Manage 506:119892
Kautz M, Dworschak K, Gruppe A, Schopf R (2011) Quantifying spatio-temporal dispersion of bark beetle infestations in epidemic and non-epidemic conditions. For Ecol Manage 262:598–608
Kautz M, Schopf R, Imron MA (2014) Individual traits as drivers of spatial dispersal and infestation patterns in a host–bark beetle system. Ecol Modell 273:264–276
Kern A, Dobor L, Hollós R, et al (2024). Seamlessly combined historical and projected daily meteorological datasets for impact studies in Central Europe: The FORESEE v4. 0 and the FORESEE-HUN v1. 0. Clim Serv. 33:100443
Landsberg JJ, Waring RH (1997) A generalised model of forest productivity using simplified concepts of radiation-use efficiency, carbon balance and partitioning. For Ecol Manage 95:209–228
Lausch A, Heurich M, Fahse L (2013) Spatio-temporal infestation patterns of Ips typographus (L.) in the Bavarian Forest National Park. Germany Ecol Indic 31:73–81
Manion PD (1981) Tree Disease Concepts
Maroschek M, Rammer W, Lexer MJ (2015) Using a novel assessment framework to evaluate protective functions and timber production in Austrian mountain forests under climate change. Reg Environ Change 15:1543–1555
Mezei P, Jakuš R, Pennerstorfer J et al (2017) Storms, temperature maxima and the Eurasian spruce bark beetle *Ips typographus*—An infernal trio in Norway spruce forests of the Central European High Tatra Mountains. Agric Meteorol 242:85–95
Moss RH, Edmonds JA, Hibbard KA et al (2010) The next generation of scenarios for climate change research and assessment. Nature 463:747–756
Murray FW (1967) On the computation of saturation vapor pressure. J Appl Meteorol Climatol 6:203–204

Netherer S, Nopp-Mayr U (2005) Predisposition assessment systems (PAS) as supportive tools in forest management—rating of site and stand-related hazards of bark beetle infestation in the High Tatra Mountains as an example for system application and verification. For Ecol Manage 207:99–107

Netherer S, Kandasamy D, Jirosová A et al (2004) (2021) Interactions among Norway spruce, the bark beetle Ips typographus and its fungal symbionts in times of drought. J Pest Sci 94:591–614

Netherer S, Matthews B, Katzensteiner K et al (2015) Do water-limiting conditions predispose N orway spruce to bark beetle attack? New Phytol 205:1128–1141

Netherer S, Lehmanski L, Bachlehner A et al (2024) Drought increases Norway spruce susceptibility to the Eurasian spruce bark beetle and its associated fungi. New Phytol 242:1000–1017

Park Williams A, Allen CD, Macalady AK et al (2013) Temperature as a potent driver of regional forest drought stress and tree mortality. Nat Clim Chang 3:292–297

Patacca M, Lindner M, Lucas-Borja ME et al (2023) Significant increase in natural disturbance impacts on European forests since 1950. Glob Chang Biol 29:1359–1376

Peltier DMP, Carbone MS, McIntire CD et al (2023) Carbon starvation following a decade of experimental drought consumes old reserves in Pinus edulis. New Phytol 240:92–104

Raffa KF, Aukema BH, Bentz BJ et al (2008) Cross-scale drivers of natural disturbances prone to anthropogenic amplification: the dynamics of bark beetle eruptions. Bioscience 58:501–517

Raffa KF, Andersson MN, Schlyter F (2016) Host selection by bark beetles: playing the odds in a high-stakes game. In: Advances in insect physiology. Elsevier, pp 1–74. https://doi.org/10.1016/bs.aiip.2016.02.001

Rammer W, Seidl R (2015) Coupling human and natural systems: Simulating adaptive management agents in dynamically changing forest landscapes. Glob Environ Chang 35:475–485

Rammer W, Thom D, Baumann M et al (2024) The individual-based forest landscape and disturbance model iLand: Overview, progress, and outlook. Ecol Modell. https://doi.org/10.1016/j.ecolmodel.2024.110785

Schroeder M, Knape J, Kärvemo S (2025) Rise and fall of a spruce bark beetle outbreak–Importance of colonisation density and reproductive success. For Ecol Manage 586:122695

Schuldt B, Buras A, Arend M et al (2020) A first assessment of the impact of the extreme 2018 summer drought on Central European forests. Basic Appl Ecol 45:86–103

Schumann K, Schuldt B, Fischer M et al (2024) Xylem safety in relation to the stringency of plant water potential regulation of European beech, Norway spruce, and Douglas-fir trees during severe drought. Trees 38:607–623

Seidl R, Rammer W (2017) Climate change amplifies the interactions between wind and bark beetle disturbances in forest landscapes. Landsc Ecol 32:1485–1498

Seidl R, Rammer W, Scheller RM, Spies TA (2012) An individual-based process model to simulate landscape-scale forest ecosystem dynamics. Ecol Modell 231:87–100

Seidl R, Rammer W, Blennow K (2014) Simulating wind disturbance impacts on forest landscapes: tree-level heterogeneity matters. Environ Model Softw 51:1–11

Seidl R, Müller J, Hothorn T et al (2016) Small beetle, large-scale drivers: How regional and landscape factors affect outbreaks of the European spruce bark beetle. J Appl Ecol 53:530–540

Seneviratne SI, Zhang X, Adnan M, et al (2021) Weather and climate extreme events in a changing climate. https://doi.org/10.1017/9781009157896.013

Senf C, Seidl R (2021) Persistent impacts of the 2018 drought on forest disturbance regimes in Europe. Biogeosciences 18:5223–5230

Senf C, Seidl R, Hostert P (2017) Remote sensing of forest insect disturbances: Current state and future directions. Int J Appl Earth Obs Geoinf 60:49–60

Senf C, Buras A, Zang CS et al (2020) Excess forest mortality is consistently linked to drought across Europe. Nat Commun 11:6200

Sommerfeld A, Rammer W, Heurich M et al (2021) Do bark beetle outbreaks amplify or dampen future bark beetle disturbances in Central Europe? J Ecol 109:737–749

Temperli C, Bugmann H, Elkin C (2013) Cross-scale interactions among bark beetles, climate change, and wind disturbances: A landscape modeling approach. Ecol Monogr 83:383–402

Thom D, Seidl R (2016) Natural disturbance impacts on ecosystem services and biodiversity in temperate and boreal forests. Biol Rev 91:760–781

Thom D, Seidl R, Steyrer G et al (2013) Slow and fast drivers of the natural disturbance regime in Central European forest ecosystems. For Ecol Manage 307:293–302

Trugman AT, Anderegg LDL, Anderegg WRL et al (2021) Why is tree drought mortality so hard to predict? Trends Ecol Evol 36:520–532

Turner MG, Seidl R (2023) Novel disturbance regimes and ecological responses. Annu Rev Ecol Evol Syst 54:63–83

Vicente-Serrano SM, Gouveia C, Camarero JJ et al (2013) Response of vegetation to drought time-scales across global land biomes. Proc Natl Acad Sci 110:52–57

Wallentin C, Nilsson U (2014) Storm and snow damage in a Norway spruce thinning experiment in southern Sweden. Forestry 87:229–238

Washaya P, Modlinger R, Tyšer D, Hlásny T (2024) Patterns and impacts of an unprecedented outbreak of bark beetles in Central Europe: A glimpse into the future? For Ecosyst 11:100243

Wermelinger B (2004) Ecology and management of the spruce bark beetle Ips typographus—a review of recent research. For Ecol Manage 202:67–82

Wermelinger B, Seifert M (1999) Temperature-dependent reproduction of the spruce bark beetle Ips typographus, and analysis of the potential population growth. Ecol Entomol 24:103–110

Terms and Conditions

Springer Nature journal content, brought to you courtesy of Springer Nature Customer Service Center GmbH (“Springer Nature”).
Springer Nature supports a reasonable amount of sharing of research papers by authors, subscribers and authorised users (“Users”), for small-scale personal, non-commercial use provided that all copyright, trade and service marks and other proprietary notices are maintained. By accessing, sharing, receiving or otherwise using the Springer Nature journal content you agree to these terms of use (“Terms”). For these purposes, Springer Nature considers academic use (by researchers and students) to be non-commercial.
These Terms are supplementary and will apply in addition to any applicable website terms and conditions, a relevant site licence or a personal subscription. These Terms will prevail over any conflict or ambiguity with regards to the relevant terms, a site licence or a personal subscription (to the extent of the conflict or ambiguity only). For Creative Commons-licensed articles, the terms of the Creative Commons license used will apply.
We collect and use personal data to provide access to the Springer Nature journal content. We may also use these personal data internally within ResearchGate and Springer Nature and as agreed share it, in an anonymised way, for purposes of tracking, analysis and reporting. We will not otherwise disclose your personal data outside the ResearchGate or the Springer Nature group of companies unless we have your permission as detailed in the Privacy Policy.
While Users may use the Springer Nature journal content for small scale, personal non-commercial use, it is important to note that Users may not:

1. use such content for the purpose of providing other users with access on a regular or large scale basis or as a means to circumvent access control;
2. use such content where to do so would be considered a criminal or statutory offence in any jurisdiction, or gives rise to civil liability, or is otherwise unlawful;
3. falsely or misleadingly imply or suggest endorsement, approval , sponsorship, or association unless explicitly agreed to by Springer Nature in writing;
4. use bots or other automated methods to access the content or redirect messages
5. override any security feature or exclusionary protocol; or
6. share the content in order to create substitute for Springer Nature products or services or a systematic database of Springer Nature journal content.

In line with the restriction against commercial use, Springer Nature does not permit the creation of a product or service that creates revenue, royalties, rent or income from our content or its inclusion as part of a paid for service or for other commercial gain. Springer Nature journal content cannot be used for inter-library loans and librarians may not upload Springer Nature journal content on a large scale into their, or any other, institutional repository.
These terms of use are reviewed regularly and may be amended at any time. Springer Nature is not obligated to publish any information or content on this website and may remove it or features or functionality at our sole discretion, at any time with or without notice. Springer Nature may revoke this licence to you at any time and remove access to any copies of the Springer Nature journal content which have been saved.
To the fullest extent permitted by law, Springer Nature makes no warranties, representations or guarantees to Users, either express or implied with respect to the Springer nature journal content and all parties disclaim and waive any implied warranties or warranties imposed by law, including merchantability or fitness for any particular purpose.
Please note that these rights do not automatically extend to content, data or other material published by Springer Nature that may be licensed from third parties.
If you would like to use or distribute our Springer Nature journal content to a wider audience or on a regular basis or in any other manner not expressly permitted by these Terms, please contact Springer Nature at

onlineservice@springernature.com

5. Discussion

This thesis demonstrates how multisensor remote sensing enables assessment of drought-driven bark beetle disturbances and early forest recovery in both space and time. By integrating optical, SAR, airborne nDSMs, and UAV data, the workflow mapped forest disturbances annually at a national scale (Czech Republic), delineated outbreak hotspots, characterized emerging post-disturbance vertical and horizontal structure and quantified recovery trajectories with the main disturbance zone. The unified remote sensing framework enabled consistent temporal tracking of disturbances and regeneration across the entire study period, while also providing a coherent interpretation of structural change from national-scale (Czech Republic) disturbance progression to regional (landscape-scale) forest structure in the main outbreak zone. It further introduced methodological advances, including machine learning-based disturbance mapping and multisensor predictor integration for vegetation height modelling. Together, the findings illustrate how remote sensing can capture both the pulse (disturbance) and response (recovery and structural reorganization) of forests experiencing an unprecedented climate-driven regime shift.

The results revealed a disturbance regime fundamentally different from historically wind-driven dynamics. The large-scale drought-induced outbreak exhibited multiple asynchronous foci across the Czech Republic, yet retained spatial spread patterns consistent with documented bark beetle dispersal processes. The mapping further captured the magnitude and spatial concentration of forest loss that triggered abrupt landscape transformation, an aspect of disturbance ecology that remains understudied despite its implications for ecosystem resilience, habitat configuration, and long-term forest trajectories.

Central European forests are often regarded as resilient to natural disturbances (Seidl et al., 2024; Senf et al., 2022), yet the 2018–2022 drought-driven bark beetle outbreak exceeded historical benchmarks and challenged this assumption (Senf & Seidl, 2021b). In our study area, nearly one-third (38%) of forests were affected within six years, with impacts further intensified by extensive salvage logging and repeated drought events. These interacting pressures created structurally simplified post-disturbance landscapes and introduced substantial uncertainty regarding the capacity, variability, and pace of natural regeneration under compounded climatic and management stressors.

The thesis tests its central hypotheses across the four research objectives. First, integrating multisource remote sensing data, including optical imagery, SAR, and airborne nDSMs,

improves the accuracy of mapping drought-driven bark beetle disturbances and enables reliable quantification of their spatial extent and temporal progression (H1). Second, the severity and spatial concentration of these disturbances, combined with intensive salvage logging, lead to measurable increases in landscape homogenization and fragmentation, as indicated by changes in landscape-structure metrics (H2). Third, fused optical–SAR predictors allow robust classification of post-disturbance vegetation into distinct structural stages and reveal quantifiable temporal recovery trajectories, including identifiable regeneration delays or failures (H3). Finally, vegetation height and vertical structure in heterogeneous post-disturbance landscapes can be predicted more accurately using multisource satellite predictors and learned feature embeddings than with single-sensor approaches (H4).

5.1. Remote Sensing Framework for Large-Scale Disturbance and Recovery Assessment

Combining multiple sensors was essential to the thesis because no single data source could provide the spatial–spectral detail, temporal frequency, and structural sensitivity required to track disturbance, vertical structure, and post-disturbance recovery reliably. Optical imagery alone is limited by cloud cover, illumination constraints, and shallow structural sensitivity (Hirschmugl et al., 2017; Trisasongko, 2010). Time-series approaches such as LandTrendr (Kennedy et al., 2010; Senf & Seidl, 2021b), while effective for long-term continuity, rely largely on optical reflectance trajectories and are therefore less suited to capturing the abrupt and spatially heterogeneous mortality patterns characteristic of drought-induced bark beetle outbreaks. Integrating Sentinel-1 SAR mitigated these limitations by providing cloud-independent observations and sensitivity to canopy moisture and structural change (Bouvet et al., 2018; Kobayashi et al., 2000), thereby complementing optical indicators of canopy decline and enabling a more reliable and comprehensive characterization of disturbance and early recovery.

Integrating Sentinel-1 SAR backscatter, Sentinel-2 optical indices, airborne nDSMs, and UAV-derived canopy height data enabled the workflow to leverage the complementary strengths of each sensor class: optical indices captured spectral signals of canopy decline, SAR provided cloud-independent sensitivity to structural and moisture changes, and airborne/UAV data supplied high-resolution reference information for disturbance attribution and post-disturbance height. This multisensor strategy reflects a broader shift in forest monitoring toward fusion-based approaches that address the limitations of single-sensor systems (Hirschmugl et al., 2020; Lehmann et al., 2015; Ye et al., 2019). While large-scale products such as Global Forest Change (Hansen et al., 2013b) and the European Disturbance Atlas (Senf & Seidl, 2020) rely primarily

on optical time series, this study builds on their approach by incorporating SAR data to address limitations in cloud-affected regions and capture vertical canopy change. In this context, fusion was not optional but necessary to map mortality in cloud-affected regions, capture both horizontal and vertical structural change, and produce disturbance and recovery metrics at meaningful scales.

5.1.1 Regional patterns and temporal dynamics

The 2018–2022 mortality wave coincided with a continent-wide surge in drought-driven tree mortality that pushed disturbance dynamics beyond historical variability (Senf & Seidl, 2021a). Central Europe experienced synchronous Ips typographus outbreaks in Germany, Sweden, France, and northern Italy (Arthur et al., 2024; Kärvemo et al., 2023) , reflecting the broader climatic anomaly. Using a multisensor image-to-image framework that fused Sentinel-2 optical data, Sentinel-1 SAR, and airborne imagery, the analysis identified seven distinct outbreak foci across Czechia. Despite being triggered by the same climatic event, these foci showed marked spatial asynchrony in onset and culmination.

Most other regions exhibited a three-year build-up followed by a short, intense culmination (2019–2021). Deviations from this pattern likely reflect local variation in forest structure, environmental conditions, and management intensity, which collectively influence population thresholds required for epidemic spread (Raffa et al., 2008). Although salvage and sanitary logging may have moderated growth in some areas, their effectiveness decreases under warming conditions (Dobor et al., 2018), and operational constraints introduce further spatial variability.

Compared with historical wind-driven outbreaks, the drought-induced event followed a similar 2–3-year build-up but a noticeably shorter culmination phase, contrasting earlier observations of multi-year epidemic plateaus lasting 5–10 years (Økland & Bjørnstad, 2006). This suggests that drought-triggered outbreaks may operate on compressed temporal scales. Spatially, the outbreak conformed to previously documented patterns of local initiation and short-range expansion (Hlásny & Turčáni, 2013; Kautz et al., 2011), with the strongest local spread occurring during 2019–2020. Medium-range expansion remained limited, likely reflecting a combination of host depletion and high local infestation pressure.

5.1.2 Drivers of Outbreak Variation and Collapse

A notable result identified after analysis of mapped spruce was the unexpectedly high proportion of Norway spruce remaining after the outbreak. Even after severe mortality, 26–

36% of the original spruce cover persisted across most hotspots, despite a 40–50% decline during the first retreat year. The ability to consistently distinguish spruce stands from mixed or non-forest areas enabled a precise assessment of host availability before and after the event. Although this decline substantially reduced stand connectivity, likely contributing to epidemic collapse by limiting the spatial continuity of susceptible hosts (Honkaniemi et al., 2021; Raffa et al., 2008), the remaining spruce area was still ecologically significant. Many surviving stands were younger (<40–50 years) and therefore less susceptible (Wermelinger, 2004), yet the true extent of host loss was probably underestimated because decadal forest inventory updates could not track rapid disturbance turnover. Improved moisture conditions in spring 2020–2021 may also have facilitated suppression of beetle populations, though this remains conjectural. Overall, these results indicate that resource depletion alone did not drive outbreak cessation and illustrate the utility of multisensor mapping for separating host depletion from climatic control mechanisms.

The persistence of substantial spruce cover also indicates that affected regions are not insulated from future outbreaks. Renewed susceptibility will depend on post-disturbance stand demography, residual host connectivity, and local predisposition factors (Netherer & Hammerbacher, 2022). Moreover, disturbance-driven fragmentation, manifested as increased edge density and patch disaggregation (Zeng et al., 2010), may heighten exposure to subsequent windthrow and secondary infestations. These structural and compositional legacies suggest that, although the 2018–2022 outbreak has subsided, the landscape remains vulnerable to recurrent disturbances under a warming climate.

5.1.3. Landscape Transformation and its Ecological Significance

Beyond its immediate ecological causes, the 2018–2022 outbreak fundamentally reconfigured the Central European forest landscape. Whereas past bark beetle impacts were typically quantified in economic or biophysical terms, such as timber loss or damaged area (Hlásny, Augustynczik, et al., 2021), the unprecedented scale of this event requires a broader landscape-scale perspective. Large disturbances reshape spatial configuration, biodiversity potential, and ecosystem service provision (Turner & Seidl, 2023), and thus must be evaluated not only in terms of mortality but also in terms of structural transformation.

Using disturbance maps derived from the multisensor workflow, the thesis quantified both the magnitude and spatial distribution of forest loss. Seventeen percent of spruce forest nationwide was affected, corresponding to roughly 20% of the initial spruce growing stock (≈100 million

m³; Forest Management Institute, Czech Republic). Although moderate as a national percentage, the spatial concentration of mortality intensified ecological and social impacts: nearly one-quarter of all spruce forests occurred within high-impact zones. The largest continuous outbreak region (≈9,000 km²) lost 38% of its forest cover and 49% of its spruce area—placing this event among the most severe natural disturbances in recent European history, exceeding the combined impacts of other areas in Europe in the past in terms of cumulative landscape transformation (Brázdil et al., 2022; Kunca et al., 2019).

5.2. Early Recovery Dynamics and Emerging Vulnerabilities

Building on the national disturbance mapping, the thesis quantified post-disturbance recovery by integrating Sentinel-1, Sentinel-2, and UAV-derived height data. Disturbances were mapped with a U-Net model, while recovery stages were classified using a Random Forest trained on multisensor predictors and vegetation indices. The use of Sentinel imagery provided 10 m spatial detail, substantially improving upon traditional 30 m Landsat-based approaches, and enabled finer discrimination of early regeneration processes. The results showed that high-severity mortality combined with extensive salvage logging produced widespread landscape homogenization, consistent with patterns reported across other regions affected by large-scale disturbances in Europe (Seidl & Senf, 2024; Senf et al., 2019).

Central European forests typically recover through two pathways: persistence of advance regeneration (Bače et al., 2015; Petrovska et al., 2023; Seidl et al., 2024) or post-disturbance colonization (Macek et al., 2017; Schüle et al., 2023; Winter et al., 2015). Our recovery maps indicated that colonization dominated, likely due to the legacy of rotation-based management and intensive salvage logging that removed standing deadwood and surviving understory. Consequently, near-bare soil covered >80% of disturbed areas between 2018 and 2020, with vegetation cover rising steadily to 79% by 2024.

The temporal stability of mapped classes reflected contrasting ecological dynamics. Near-bare-soil (NBS) and transient class (TC) were relatively stable (74.6% and 71.5%), while transient cover exhibited high turnover, with more than half transitioning annually to NBS or TC. These fluctuations likely represent early successional mortality, short-lived vegetation pulses, and temporary regeneration failures, processes widely documented in exposed post-disturbance environments (Bianchi et al., 2019; Nordlander et al., 2011). Overall, temporary failures accounted for 36.8% of transitions but did not accumulate into long-term collapse.

Across the landscape, the mean annual recovery rate was 13.5%, with a mean recovery time of 3.8 years (NBS → TC/ER). Under a more conservative definition (NBS/TC → ER), recovery averaged 5.9% per year with a 5.2-year recovery time. Although these rates are slower than field-based observations following fire or windthrow (Piazza et al., 2024; Schüle et al., 2023), they are consistent with the methodological scale and the homogenized post-disturbance conditions. Critically, there was no evidence of persistent, large-scale regeneration failure (Hansen et al., 2018; Stevens-Rumann et al., 2022), indicating that despite extreme disturbance magnitude and management-driven simplification, the system retained strong inherent recovery capacity.

5.3. Methodological Considerations and Limitations

The thesis established a multisensor framework for forest disturbance, height structure and recovery mapping. First, a national-scale disturbance mapping framework was developed using fused Sentinel-1 SAR and Sentinel-2/ Landsat optical data, enabling annual detection of drought-driven bark beetle mortality. The fusion of SAR and optical then adapted for height-structure mapping in the main outbreak zone, where two modelling strategies were compared: one using conventional Sentinel-1/2 predictors (hand-crafted) and another using Alpha-Earth feature embeddings. The Alpha-Earth embedding model consistently achieved higher accuracy than models based solely on multispectral and SAR inputs, demonstrating the value of learned multisensor representations for capturing complex post-disturbance vertical structure. The multisensor approach was further extended in the recovery analysis, where Sentinel-1/2 predictors and UAV-derived canopy height models enabled quantification of early regeneration trajectories across a highly disturbed landscape.

Accuracy levels in the study were generally high (85% to 94% overall accuracies) and aligned with, or exceeded, those reported in comparable European disturbance and recovery studies. The CNN-based disturbance mapping achieved strong detection performance at 10 m resolution, comparing favourably with Landsat-based time-series frameworks such as LandTrendr (Kennedy et al., 2010; Senf & Seidl, 2020), which operate at coarser spatial resolution and depend on long spectral trajectories. Recovery classification accuracies were consistent with other Sentinel-1/2–based regeneration studies, despite the structural heterogeneity of the outbreak zone. In the height-mapping task, the Alpha-Earth embedding model achieved the lowest RMSE and highest R^2 among tested configurations, outperforming traditional optical-SAR feature sets and demonstrating the advantage of embedding-based predictors in complex post-disturbance environments.

Several limitations should be noted. The 2018–2024 observation period captures only the initial stages of forest recovery, limiting inference about long-term resilience trajectories that may diverge due to replanting, extreme climatic events, or subsequent disturbance cycles. Recovery indicators measured vegetation presence and height but not species composition, an essential determinant of functional recovery and future vulnerability (Aquilué et al., 2020; Dieler et al., 2017; Van Tiel et al., 2024). The 10 m resolution constrained detection of fine-scale heterogeneity, including differentiation between natural regeneration and planting. Additionally, a small number of transitions, such as the 6.3% direct shift from near-bare soil to early regrowth, likely reflect classification uncertainty or compositing artefacts.

Despite these constraints, the integrated multisensor framework provided a robust characterization of early structural reorganization across one of Europe's most heavily impacted forest landscapes. The demonstrated performance of the Alpha-Earth embeddings and the Sentinel-1/2 disturbance, recovery pipeline underscores the value of multisensor integration for monitoring disturbance, recovery interactions at regional to national scales, particularly in cloud-prone, rapidly changing, and intensively managed forest systems.

6. Conclusion

This thesis demonstrates that multisensor remote sensing provides a powerful and scalable foundation for analysing drought-driven bark beetle disturbances and early post-disturbance forest recovery across Central Europe. By integrating Sentinel-1 SAR, Sentinel-2 optical indices, airborne nDSMs, UAV canopy height models, and learned feature embeddings, the work established unified pipelines capable of detecting annual disturbance, quantifying regeneration trajectories, and mapping vertical structure in heterogeneous post-disturbance landscapes.

The national-scale disturbance maps captured the spatial and temporal unfolding of the 2018–2022 outbreak, revealing strong regional asynchrony and substantial homogenization of forest structure in the main impact zones. Recovery analyses showed that, despite extensive canopy loss and widespread salvage logging, forests in the region retain considerable regeneration potential, though with clear spatial heterogeneity and transient failures. Height modelling demonstrated that combining multisensor predictors markedly improves the estimation of vertical structure, with Alpha-Earth embeddings providing the highest accuracy.

Together, these findings highlight both the vulnerability and resilience of Central European forests under compounding climatic and biotic pressures. They also illustrate the value of multisensor fusion for monitoring disturbance–recovery interactions at management-relevant scales. The framework developed here provides a transferable basis for long-term resilience assessment, supports more informed planning in disturbance-prone regions, and underscores the importance of integrating complementary Earth Observation datasets as forests transition toward novel structural and compositional states under climate change.

References:

Akca, D., Stylianidis, E., Smagas, K., Hofer, M., Poli, D., Gruen, A., Sanchez Martin, V., Altan, O., Walli, A., Jimeno, E., & Garcia, A. (2016). VOLUMETRIC FOREST CHANGE DETECTION THROUGH VHR SATELLITE IMAGERY. *The International Archives of the Photogrammetry, Remote Sensing and Spatial Information Sciences*, *XLI-B8*, 1213–1220. https://doi.org/10.5194/isprs-archives-XLI-B8-1213-2016

Aquilué, N., Filotas, É., Craven, D., Fortin, M., Brotons, L., & Messier, C. (2020). Evaluating forest resilience to global threats using functional response traits and network properties. *Ecological Applications*, *30*(5). https://doi.org/10.1002/eap.2095

Arthur, G., Jonathan, L., Juliette, C., Nicolas, L., Christian, P., & Hugues, C. (2024). Spatial and remote sensing monitoring shows the end of the bark beetle outbreak on Belgian and north-eastern France Norway spruce (Picea abies) stands. *Environmental Monitoring and Assessment*, *196*(3), 226. https://doi.org/10.1007/s10661-024-12372-0

Bače, R., Svoboda, M., Janda, P., Morrissey, R. C., Wild, J., Clear, J. L., Čada, V., & Donato, D. C. (2015). Legacy of Pre-Disturbance Spatial Pattern Determines Early Structural Diversity following Severe Disturbance in Montane Spruce Forests. *PLOS ONE*, *10*(9), e0139214. https://doi.org/10.1371/journal.pone.0139214

Baier, P., Pennerstorfer, J., & Schopf, A. (2007). PHENIPS—A comprehensive phenology model of Ips typographus (L.) (Col., Scolytinae) as a tool for hazard rating of bark beetle infestation. *Forest Ecology and Management*, *249*(3), 171–186. https://doi.org/10.1016/j.foreco.2007.05.020

Banskota, A., Kayastha, N., Falkowski, M. J., Wulder, M. A., Froese, R. E., & White, J. C. (2014). Forest Monitoring Using Landsat Time Series Data: A Review. *Canadian Journal of Remote Sensing*, *40*(5), 362–384. https://doi.org/10.1080/07038992.2014.987376

Bentz, B. J., Régnière, J., Fettig, C. J., Hansen, E. M., Hayes, J. L., Hicke, J. A., Kelsey, R. G., Negrón, J. F., & Seybold, S. J. (2010). Climate Change and Bark Beetles of the Western United States and Canada: Direct and Indirect Effects. *BioScience*, *60*(8), 602–613. https://doi.org/10.1525/bio.2010.60.8.6

Beudert, B., Bässler, C., Thorn, S., Noss, R., Schröder, B., Dieffenbach-Fries, H., Foullois, N., & Müller, J. (2015). Bark Beetles Increase Biodiversity While Maintaining Drinking Water Quality. *Conservation Letters*, *8*(4), 272–281. https://doi.org/10.1111/conl.12153

Bianchi, E., Bugmann, H., & Bigler, C. (2019). Early emergence increases survival of tree seedlings in Central European temperate forests despite severe late frost. *Ecology and Evolution*, *9*(14), 8238–8252. https://doi.org/10.1002/ece3.5399

Bouvet, A., Mermoz, S., Ballère, M., Koleck, T., & Le Toan, T. (2018). Use of the SAR Shadowing Effect for Deforestation Detection with Sentinel-1 Time Series. *Remote Sensing*, *10*(8), 1250. https://doi.org/10.3390/rs10081250

Brázdil, R., Zahradník, P., Szabó, P., Chromá, K., Dobrovolný, P., Dolák, L., Trnka, M., Řehoř, J., & Suchánková, S. (2022). Meteorological and climatological triggers of notable past and present bark beetle outbreaks in the Czech Republic. *Climate of the Past*, *18*(9), 2155–2180. https://doi.org/10.5194/cp-18-2155-2022

Brown, C. F., Kazmierski, M. R., Pasquarella, V. J., Rucklidge, W. J., Samsikova, M., Zhang, C., Shelhamer, E., Lahera, E., Wiles, O., Ilyushchenko, S., Gorelick, N., Zhang, L. L., Alj, S., Schechter, E., Askay, S., Guinan, O., Moore, R., Boukouvalas, A., & Kohli, P. (2025). *AlphaEarth Foundations: An embedding field model for accurate and efficient global mapping from sparse label data*. http://arxiv.org/abs/2507.22291

Bryk, M., Kołodziej, B., & Pliszka, R. (2020). Changes of Norway Spruce Health in the Białowieża Forest (CE Europe) in 2013–2019 during a Bark Beetle Infestation, Studied with Landsat Imagery. *Forests*, *12*(1), 34. https://doi.org/10.3390/f12010034

Chen, Li, C., Ghamisi, P., Jia, X., & Gu, Y. (2017). Deep Fusion of Remote Sensing Data for Accurate Classification. *IEEE Geoscience and Remote Sensing Letters*, *14*(8), 1253–1257. https://doi.org/10.1109/LGRS.2017.2704625

Chen, S., Woodcock, C. E., Bullock, E. L., Arévalo, P., Torchinava, P., Peng, S., & Olofsson, P. (2021). Monitoring temperate forest degradation on Google Earth Engine using Landsat time series analysis. *Remote Sensing of Environment*, *265*, 112648. https://doi.org/10.1016/j.rse.2021.112648

Chuvieco, E., Martín, M. P., & Palacios, A. (2002). Assessment of different spectral indices in the red-near-infrared spectral domain for burned land discrimination. *International Journal of Remote Sensing*, *23*(23), 5103–5110. https://doi.org/10.1080/01431160210153129

Cohen, W. B., Healey, S. P., Yang, Z., Stehman, S. V, Brewer, C. K., Brooks, E. B., Gorelick, N., Huang, C., Hughes, M. J., Kennedy, R. E., Loveland, T. R., Moisen, G. G., & Schroeder, T. A. (2017). *How Similar Are Forest Disturbance Maps Derived from Different Landsat Time Series Algorithms ?* 1–19. https://doi.org/10.3390/f8040098

Dalponte, M., Solano-Correa, Y. T., Frizzera, L., & Gianelle, D. (2022). Mapping a European Spruce Bark Beetle Outbreak Using Sentinel-2 Remote Sensing Data. *Remote Sensing*, *14*(13), 3135. https://doi.org/10.3390/rs14133135

DeVries, B., Verbesselt, J., Kooistra, L., & Herold, M. (2015). Robust monitoring of small-scale forest disturbances in a tropical montane forest using Landsat time series. *Remote Sensing of Environment*, *161*, 107–121. https://doi.org/10.1016/j.rse.2015.02.012

Dieler, J., Uhl, E., Biber, P., Müller, J., Rötzer, T., & Pretzsch, H. (2017). Effect of forest stand management on species composition, structural diversity, and productivity in the temperate zone of Europe. *European Journal of Forest Research*, *136*(4), 739–766. https://doi.org/10.1007/s10342-017-1056-1

Dobor, L., Hlásny, T., Rammer, W., Barka, I., Trombik, J., Pavlenda, P., Šebeň, V., Štěpánek, P., & Seidl, R. (2018). Post-disturbance recovery of forest carbon in a temperate forest landscape under climate change. *Agricultural and Forest Meteorology*, *263*, 308–322. https://doi.org/10.1016/j.agrformet.2018.08.028

Donato, D. C., Campbell, J. L., & Franklin, J. F. (2012). Multiple successional pathways and precocity in forest development: can some forests be born complex? *Journal of Vegetation Science*, *23*(3), 576–584. https://doi.org/10.1111/j.1654-1103.2011.01362.x

Einzmann, K., Haarpaintner, J., & Larsen, Y. (2012). Forest monitoring in Congo Basin with combined use of SAR C- & L-band. *2012 IEEE International Geoscience and*

Remote Sensing Symposium, 6573–6576. https://doi.org/10.1109/IGARSS.2012.6352093

Fassnacht, F. E., Latifi, H., Stereńczak, K., Modzelewska, A., Lefsky, M., Waser, L. T., Straub, C., & Ghosh, A. (2016). Review of studies on tree species classification from remotely sensed data. *Remote Sensing of Environment*, *186*, 64–87. https://doi.org/10.1016/j.rse.2016.08.013

Fernandez-Carrillo, A., Patočka, Z., Dobrovolný, L., Franco-Nieto, A., & Revilla-Romero, B. (2020). Monitoring Bark Beetle Forest Damage in Central Europe. A Remote Sensing Approach Validated with Field Data. *Remote Sensing*, *12*(21), 3634. https://doi.org/10.3390/rs12213634

Forzieri, G., Girardello, M., Ceccherini, G., Spinoni, J., Feyen, L., Hartmann, H., Beck, P. S. A. A., Camps-Valls, G., Chirici, G., Mauri, A., & Cescatti, A. (2021). Emergent vulnerability to climate-driven disturbances in European forests. *Nature Communications*, *12*(1), 1081. https://doi.org/10.1038/s41467-021-21399-7

Fransson, J. E. S., Smith, G., Askne, J., & Olsson, H. (2001). Stem volume estimation in boreal forests using ERS-1/2 coherence and SPOT XS optical data. *International Journal of Remote Sensing*, *22*(14), 2777–2791. https://doi.org/10.1080/01431160010006872

Gao, X. (2000). Optical–Biophysical Relationships of Vegetation Spectra without Background Contamination. *Remote Sensing of Environment*, *74*(3), 609–620. https://doi.org/10.1016/S0034-4257(00)00150-4

Gao, Gao, L., & Li, X. (2023). A hierarchical training-convolutional neural network with feature alignment for steel surface defect recognition. *Robotics and Computer-Integrated Manufacturing*, *81*, 102507. https://doi.org/10.1016/j.rcim.2022.102507

Gazzea, M., Solheim, A., & Arghandeh, R. (2023). High-resolution mapping of forest structure from integrated SAR and optical images using an enhanced U-net method. *Science of Remote Sensing*, *8*, 100093. https://doi.org/10.1016/j.srs.2023.100093

Gomez, D. F., Ritger, H. M. W., Pearce, C., Eickwort, J., & Hulcr, J. (2020). Ability of Remote Sensing Systems to Detect Bark Beetle Spots in the Southeastern US. *Forests*, *11*(11), 1167. https://doi.org/10.3390/f11111167

Hanewinkel, M., Breidenbach, J., Neeff, T., & Kublin, E. (2008). Seventy-seven years of natural disturbances in a mountain forest area — the influence of storm, snow, and insect damage analysed with a long-term time series. *Canadian Journal of Forest Research*, *38*(8), 2249–2261. https://doi.org/10.1139/X08-070

Hänsch, R., Schulz, K., & Sörgel, U. (2018). Machine learning methods for remote sensing applications: an overview. In U. Michel & K. Schulz (Eds.), *Earth Resources and Environmental Remote Sensing/GIS Applications IX* (p. 1). SPIE. https://doi.org/10.1117/12.2503653

Hansen, Braziunas, K. H., Rammer, W., Seidl, R., & Turner, M. G. (2018). It takes a few to tango: changing climate and fire regimes can cause regeneration failure of two subalpine conifers. *Ecology*, *99*(4), 966–977. https://doi.org/10.1002/ecy.2181

Hansen, Potapov, P. V., Moore, R., Hancher, M., Turubanova, S. A., Tyukavina, A., Thau, D., Stehman, S. V., Goetz, S. J., Loveland, T. R., Kommareddy, A., Egorov, A., Chini, L., Justice, C. O., & Townshend, J. R. G. (2013a). High-Resolution Global Maps of 21st-Century Forest Cover Change. *Science*, *342*(6160), 850–853. https://doi.org/10.1126/science.1244693

Hansen, Potapov, P. V., Moore, R., Hancher, M., Turubanova, S. A., Tyukavina, A., Thau, D., Stehman, S. V., Goetz, S. J., Loveland, T. R., Kommareddy, A., Egorov, A., Chini, L., Justice, C. O., & Townshend, J. R. G. (2013b). High-Resolution Global Maps of 21st-Century Forest Cover Change. *Science*, *342*(6160), 850–853. https://doi.org/10.1126/science.1244693

Hartmann, H., Bastos, A., Das, A. J., Esquivel-Muelbert, A., Hammond, W. M., Martínez-Vilalta, J., McDowell, N. G., Powers, J. S., Pugh, T. A. M. M., Ruthrof, K. X., & Allen, C. D. (2022). *Climate Change Risks to Global Forest Health: Emergence of Unexpected Events of Elevated Tree Mortality Worldwide*. *73*(1), 673–702. https://doi.org/10.1146/annurev-arplant-102820-

Havašová, M., Bucha, T., FerenÄ□Ãk, J., & JakuÅ¡, R. (2015). Applicability of a vegetation indices-based method to map bark beetle outbreaks in the High Tatra Mountains. *Annals of Forest Research*, *58*(2), 295–310. https://doi.org/10.15287/afr.2015.388

Hirschmugl, M., Deutscher, J., Sobe, C., Bouvet, A., Mermoz, S., & Schardt, M. (2020). Use of SAR and Optical Time Series for Tropical Forest Disturbance Mapping. *Remote Sensing*, *12*(4), 727. https://doi.org/10.3390/rs12040727

Hirschmugl, M., Gallaun, H., Dees, M., Datta, P., Deutscher, J., Koutsias, N., & Schardt, M. (2017). Methods for Mapping Forest Disturbance and Degradation from Optical Earth Observation Data: a Review. *Current Forestry Reports*, *3*(1), 32–45. https://doi.org/10.1007/s40725-017-0047-2

Hlásny, T., Augustynczik, A. L. D., & Dobor, L. (2021). Time matters: Resilience of a post-disturbance forest landscape. *Science of the Total Environment*, *799*. https://doi.org/10.1016/j.scitotenv.2021.149377

Hlásny, T., König, L., Krokene, P., Lindner, M., Montagné-Huck, C., Müller, J., Qin, H., Raffa, K. F., Schelhaas, M.-J., Svoboda, M., Viiri, H., & Seidl, R. (2021). Bark Beetle Outbreaks in Europe: State of Knowledge and Ways Forward for Management. *Current Forestry Reports*, *7*(3), 138–165. https://doi.org/10.1007/s40725-021-00142-x

Hlásny, T., Modlinger, R., Gohli, J., Seidl, R., Krokene, P., Bernardinelli, I., Blaser, S., Brazaitis, G., Brazaitytė, G., Brockerhoff, E. G., Csóka, G., Dobor, L., de Groot, M., Duduman, M., Faccoli, M., Georgieva, M., Georgiev, G., Grodzki, W., Hartmann, H., … Liebhold, A. M. (2025). Divergent Trends in Insect Disturbance Across Europe's Temperate and Boreal Forests. *Global Change Biology*, *31*(11). https://doi.org/10.1111/gcb.70580

Hlásny, T., & Turčáni, M. (2013). Persisting bark beetle outbreak indicates the unsustainability of secondary Norway spruce forests: case study from Central Europe. *Annals of Forest Science*, *70*(5), 481–491. https://doi.org/10.1007/s13595-013-0279-7

Hlásny, T., Zimová, S., Merganičová, K., Štěpánek, P., Modlinger, R., & Turčáni, M. (2021). Devastating outbreak of bark beetles in the Czech Republic: Drivers, impacts, and

management implications. *Forest Ecology and Management*, *490*, 119075. https://doi.org/10.1016/j.foreco.2021.119075

Hong, D., Li, C., Zhang, B., Yokoya, N., Benediktsson, J. A., & Chanussot, J. (2024). Multimodal artificial intelligence foundation models: Unleashing the power of remote sensing big data in earth observation. *The Innovation Geoscience*, *2*(1), 100055. https://doi.org/10.59717/j.xinn-geo.2024.100055

Honkaniemi, J., Rammer, W., & Seidl, R. (2021). From mycelia to mastodons – A general approach for simulating biotic disturbances in forest ecosystems. *Environmental Modelling and Software*, *138*. https://doi.org/10.1016/j.envsoft.2021.104977

Huang, Kautz, M., Trowbridge, A. M., Hammerbacher, A., Raffa, K. F., Adams, H. D., Goodsman, D. W., Xu, C., Meddens, A. J. H., Kandasamy, D., Gershenzon, J., Seidl, R., & Hartmann, H. (2020). Tree defence and bark beetles in a drying world: carbon partitioning, functioning and modelling. *New Phytologist*, *225*(1), 26–36. https://doi.org/10.1111/nph.16173

Huang, X., Zhang, Q., Hu, L., Zhu, T., Zhou, X., Zhang, Y., Xu, Z., & Ju, W. (2022). Monitoring Damage Caused by Pantana phyllostachysae Chao to Moso Bamboo Forests Using Sentinel-1 and Sentinel-2 Images. *Remote Sensing*, *14*(19). https://doi.org/10.3390/rs14195012

Huete, A., Didan, K., Miura, T., Rodriguez, E. P., Gao, X., & Ferreira, L. G. (2002). Overview of the radiometric and biophysical performance of the MODIS vegetation indices. *Remote Sensing of Environment*, *83*(1–2), 195–213. https://doi.org/10.1016/S0034-4257(02)00096-2

Hussain, M., Chen, D., Cheng, A., Wei, H., & Stanley, D. (2013). Change detection from remotely sensed images: From pixel-based to object-based approaches. *ISPRS Journal of Photogrammetry and Remote Sensing*, *80*, 91–106. https://doi.org/10.1016/j.isprsjprs.2013.03.006

Jiang, L., Wang, W., Yang, X., Xie, N., & Cheng, Y. (2011). *Classification Methods of Remote Sensing Image Based on Decision Tree Technologies* (pp. 353–358). https://doi.org/10.1007/978-3-642-18333-1_41

Kärvemo, S., Huo, L., Öhrn, P., Lindberg, E., & Persson, H. J. (2023). Different triggers, different stories: Bark-beetle infestation patterns after storm and drought-induced outbreaks. *Forest Ecology and Management*, *545*, 121255. https://doi.org/10.1016/j.foreco.2023.121255

Kautz, M., Dworschak, K., Gruppe, A., & Schopf, R. (2011). Quantifying spatio-temporal dispersion of bark beetle infestations in epidemic and non-epidemic conditions. *Forest Ecology and Management*, *262*(4), 598–608. https://doi.org/10.1016/j.foreco.2011.04.023

Kautz, M., Meddens, A. J. H., Hall, R. J., & Arneth, A. (2017). Biotic disturbances in Northern Hemisphere forests – a synthesis of recent data, uncertainties and implications for forest monitoring and modelling. *Global Ecology and Biogeography*, *26*(5), 533–552. https://doi.org/10.1111/geb.12558

Kennedy, R. E., Yang, Z., & Cohen, W. B. (2010). Detecting trends in forest disturbance and recovery using yearly Landsat time series: 1. LandTrendr — Temporal segmentation

algorithms. *Remote Sensing of Environment*, *114*(12), 2897–2910. https://doi.org/10.1016/j.rse.2010.07.008

Klemmer, K., Rolf, E., Robinson, C., Mackey, L., & Rußwurm, M. (2025). SatCLIP: Global, General-Purpose Location Embeddings with Satellite Imagery. *Proceedings of the AAAI Conference on Artificial Intelligence*, *39*(4), 4347–4355. https://doi.org/10.1609/aaai.v39i4.32457

Kobayashi, T., Nadai, A., Umehara, T., Satake, M., Matsuoka, T., Uratsuka, S., Sawada, H., Mitsuzuka, N., Wakabayashi, H., & Hiuri, T. (2000). Forest monitoring in northern Japan with an airborne high-resolution SAR. *IGARSS 2000. IEEE 2000 International Geoscience and Remote Sensing Symposium. Taking the Pulse of the Planet: The Role of Remote Sensing in Managing the Environment. Proceedings (Cat. No.00CH37120)*, *1*, 408–410. https://doi.org/10.1109/IGARSS.2000.860547

König, S., Thonfeld, F., Förster, M., Dubovyk, O., & Heurich, M. (2023). Assessing Combinations of Landsat, Sentinel-2 and Sentinel-1 Time series for Detecting Bark Beetle Infestations. *GIScience & Remote Sensing*, *60*(1). https://doi.org/10.1080/15481603.2023.2226515

Kunca, A., Zúbrik, M., Galko, J., Vakula, J., Leontovyč, R., Konôpka, B., Nikolov, C., Gubka, A., Longauerová, V., Maľová, M., Rell, S., & Lalík, M. (2019). Salvage felling in the Slovak Republic's forests during the last twenty years (1998–2017). *Central European Forestry Journal*, *65*(1), 3–11. https://doi.org/10.2478/forj-2019-0007

LeCun, Y., Bengio, Y., & Hinton, G. (2015). Deep learning. *Nature*, *521*(7553), 436–444. https://doi.org/10.1038/nature14539

Lehmann, E. A., Caccetta, P., Lowell, K., Mitchell, A., Zhou, Z.-S., Held, A., Milne, T., & Tapley, I. (2015). SAR and optical remote sensing: Assessment of complementarity and interoperability in the context of a large-scale operational forest monitoring system. *Remote Sensing of Environment*, *156*, 335–348. https://doi.org/10.1016/j.rse.2014.09.034

Lei, Y., Wang, Y., Wang, G., Song, C., Cao, H., & Xiao, W. (2024). Estimating Forest Canopy Height based on GEDI Lidar Data and Multi-source Remote Sensing Images. *The International Archives of the Photogrammetry, Remote Sensing and Spatial Information Sciences*, *XLVIII-1–2024*, 297–303. https://doi.org/10.5194/isprs-archives-XLVIII-1-2024-297-2024

Li, W., Niu, Z., Shang, R., Qin, Y., Wang, L., & Chen, H. (2020). High-resolution mapping of forest canopy height using machine learning by coupling ICESat-2 LiDAR with Sentinel-1, Sentinel-2 and Landsat-8 data. *International Journal of Applied Earth Observation and Geoinformation*, *92*, 102163. https://doi.org/10.1016/j.jag.2020.102163

Liu, Chen, Y., & Cheng, X. (2024). Evaluating ICESat-2 and GEDI with Integrated Landsat-8 and PALSAR-2 for Mapping Tropical Forest Canopy Height. *Remote Sensing*, *16*(20), 3798. https://doi.org/10.3390/rs16203798

Liu, Gong, W., Xing, Y., Hu, X., & Gong, J. (2019). Estimation of the forest stand mean height and aboveground biomass in Northeast China using SAR Sentinel-1B, multispectral Sentinel-2A, and DEM imagery. *ISPRS Journal of Photogrammetry and Remote Sensing*, *151*, 277–289. https://doi.org/10.1016/j.isprsjprs.2019.03.016

Löw, M., & Koukal, T. (2020). Phenology Modelling and Forest Disturbance Mapping with Sentinel-2 Time Series in Austria. *Remote Sensing*, *12*(24), 4191. https://doi.org/10.3390/rs12244191

Lukeš, P. (2021). Monitoring of Bark Beetle Forest Damages. In *Big Data in Bioeconomy* (pp. 351–361). Springer International Publishing. https://doi.org/10.1007/978-3-030-71069-9_26

Macek, M., Wild, J., Kopecký, M., Červenka, J., Svoboda, M., Zenáhlíková, J., Brůna, J., Mosandl, R., & Fischer, A. (2017). Life and death of P icea abies after bark-beetle outbreak: ecological processes driving seedling recruitment. *Ecological Applications*, *27*(1), 156–167. https://doi.org/10.1002/eap.1429

Malmström, C. M., & Raffa, K. F. (2000). Biotic disturbance agents in the boreal forest: considerations for vegetation change models. *Global Change Biology*, *6*(S1), 35–48. https://doi.org/10.1046/j.1365-2486.2000.06012.x

Margono, B. A., Turubanova, S., Zhuravleva, I., Potapov, P., Tyukavina, A., Baccini, A., Goetz, S., & Hansen, M. C. (2012). Mapping and monitoring deforestation and forest degradation in Sumatra (Indonesia) using Landsat time series data sets from 1990 to 2010. *Environmental Research Letters*, *7*(3), 034010. https://doi.org/10.1088/1748-9326/7/3/034010

Masiliūnas, D., Tsendbazar, N.-E., Herold, M., & Verbesselt, J. (2021). BFAST Lite: A Lightweight Break Detection Method for Time Series Analysis. *Remote Sensing*, *13*(16), 3308. https://doi.org/10.3390/rs13163308

Matricardi, E. A. T., Skole, D. L., Pedlowski, M. A., Chomentowski, W., & Fernandes, L. C. (2010). Assessment of tropical forest degradation by selective logging and fire using Landsat imagery. *Remote Sensing of Environment*, *114*(5), 1117–1129. https://doi.org/10.1016/j.rse.2010.01.001

McDowell, N. G., & Allen, C. D. (2015). Darcy's law predicts widespread forest mortality under climate warming. *Nature Climate Change*, *5*(7), 669–672. https://doi.org/10.1038/nclimate2641

Mcfeeters, S. K. (1996). The use of the Normalized Difference Water Index (NDWI) in the delineation of open water features. *International Journal of Remote Sensing*, *17*(7), 1425–1432. https://doi.org/10.1080/01431169608948714

Moreira, A., Prats-iraola, P., Younis, M., Krieger, G., Hajnsek, I., & Papathanassiou, K. P. (2013). SAR-Tutorial-March-2013. *IEEE Geoscience and Remote Sensing Magazine*, *1*(1), 6–43.

Nakamura, K., Wakabayashi, H., Shinsho, H., Maeno, H., Uratsuka, S., Nadai, A., Umehara, T., & Moriyama, T. (2004). *<title>A study of the forest observation in Kushiro Wetland by using SAR data</title>* (G. S. Jackson & S. Uratsuka, Eds.; pp. 222–231). https://doi.org/10.1117/12.578580

Netherer, S., & Hammerbacher, A. (2022). The Eurasian spruce bark beetle in a warming climate: Phenology, behavior, and biotic interactions. In *Bark Beetle Management, Ecology, and Climate Change* (pp. 89–131). Elsevier. https://doi.org/10.1016/B978-0-12-822145-7.00011-8

Nordlander, G., Hellqvist, C., Johansson, K., & Nordenhem, H. (2011). Regeneration of European boreal forests: Effectiveness of measures against seedling mortality caused by the pine weevil Hylobius abietis. *Forest Ecology and Management*, *262*(12), 2354–2363. https://doi.org/10.1016/j.foreco.2011.08.033

Norman, S. P., Hargrove, W. W., Spruce, J. P., Christie, W. M., & Schroeder, S. W. (2013). *Highlights of satellite-based forest change recognition and tracking using the ForWarn System*. https://doi.org/10.2737/SRS-GTR-180

Økland, B., & Bjørnstad, O. N. (2006). A RESOURCE-DEPLETION MODEL OF FOREST INSECT OUTBREAKS. *Ecology*, *87*(2), 283–290. https://doi.org/10.1890/05-0135

Ouchi, K. (2013). Recent Trend and Advance of Synthetic Aperture Radar with Selected Topics. *Remote Sensing*, *5*(2), 716–807. https://doi.org/10.3390/rs5020716

Pal, M. (n.d.). Random forests for land cover classification. *IGARSS 2003. 2003 IEEE International Geoscience and Remote Sensing Symposium. Proceedings (IEEE Cat. No.03CH37477)*, *6*, 3510–3512. https://doi.org/10.1109/IGARSS.2003.1294837

Patacca, M., Lindner, M., Lucas-Borja, M. E., Cordonnier, T., Fidej, G., Gardiner, B., Hauf, Y., Jasinevičius, G., Labonne, S., Linkevičius, E., Mahnken, M., Milanovic, S., Nabuurs, G., Nagel, T. A., Nikinmaa, L., Panyatov, M., Bercak, R., Seidl, R., Ostrogović Sever, M. Z., … Schelhaas, M. (2023). Significant increase in natural disturbance impacts on European forests since 1950. *Global Change Biology*, *29*(5), 1359–1376. https://doi.org/10.1111/gcb.16531

Paulino, E., Schlerf, M., Röder, A., Stoffels, J., & Udelhoven, T. (2024). Forest disturbance characterization in the era of earth observation big data: A mapping review. *International Journal of Applied Earth Observation and Geoinformation*, *128*, 103755. https://doi.org/10.1016/j.jag.2024.103755

Pechony, O., & Shindell, D. T. (2010). Driving forces of global wildfires over the past millennium and the forthcoming century. *Proceedings of the National Academy of Sciences*, *107*(45), 19167–19170. https://doi.org/10.1073/pnas.1003669107

Petrovska, R., Bugmann, H., Hobi, M. L., & Brang, P. (2023). Replace me if you can: Abundance of advance regeneration under canopy trees in a primeval beech forest. *Forest Ecology and Management*, *537*, 120939. https://doi.org/10.1016/j.foreco.2023.120939

Pflugmacher, D., Cohen, W. B., & E. Kennedy, R. (2012). Using Landsat-derived disturbance history (1972–2010) to predict current forest structure. *Remote Sensing of Environment*, *122*, 146–165. https://doi.org/10.1016/j.rse.2011.09.025

Piazza, N., Bebi, P., Vacchiano, G., Rigling, A., Wohlgemuth, T., & Bottero, A. (2024). Post-windthrow forest development in spruce-dominated mountain forests in Central Europe. *Forest Ecology and Management*, *561*, 121884. https://doi.org/10.1016/j.foreco.2024.121884

Pirtskhalava-Karpova, N., Trubin, A., Karpov, A., & Jakuš, R. (2024). Drought initialised bark beetle outbreak in Central Europe: Meteorological factors and infestation dynamic. *Forest Ecology and Management*, *554*, 121666. https://doi.org/10.1016/j.foreco.2023.121666

Pohl, C., & Van Genderen, J. L. (1998). Review article Multisensor image fusion in remote sensing: Concepts, methods and applications. *International Journal of Remote Sensing*, *19*(5), 823–854. https://doi.org/10.1080/014311698215748

Potapov, P., Li, X., Hernandez-Serna, A., Tyukavina, A., Hansen, M. C., Kommareddy, A., Pickens, A., Turubanova, S., Tang, H., Silva, C. E., Armston, J., Dubayah, R., Blair, J. B., & Hofton, M. (2021). Mapping global forest canopy height through integration of GEDI and Landsat data. *Remote Sensing of Environment*, *253*, 112165. https://doi.org/10.1016/j.rse.2020.112165

Praks, J., Kugler, F., Papathanassiou, K. P., Hajnsek, I., & Hallikainen, M. (2007). Height Estimation of Boreal Forest: Interferometric Model-Based Inversion at L- and X-Band Versus HUTSCAT Profiling Scatterometer. *IEEE Geoscience and Remote Sensing Letters*, *4*(3), 466–470. https://doi.org/10.1109/LGRS.2007.898083

Raffa, K. F., Aukema, B. H., Bentz, B. J., Carroll, A. L., Hicke, J. A., Turner, M. G., & Romme, W. H. (2008). Cross-scale Drivers of Natural Disturbances Prone to Anthropogenic Amplification: The Dynamics of Bark Beetle Eruptions. *BioScience*, *58*(6), 501–517. https://doi.org/10.1641/B580607

Rakovec, O., Samaniego, L., Hari, V., Markonis, Y., Moravec, V., Thober, S., Hanel, M., & Kumar, R. (2022). The 2018–2020 Multi-Year Drought Sets a New Benchmark in Europe. *Earth's Future*, *10*(3). https://doi.org/10.1029/2021EF002394

Rammer, W., & Seidl, R. (2019). Harnessing Deep Learning in Ecology: An Example Predicting Bark Beetle Outbreaks. *Frontiers in Plant Science*, *10*. https://doi.org/10.3389/fpls.2019.01327

Razi, P., Sumantyo, J. T. S., Izumi, Y., Tadono, T., Mizukami, Y., Ohki, M., & Motohka, T. (2023). Estimation of Potential Earthquake Epicenter Based on Level of Land Deformation Along Coastal Line of South Java. *IGARSS 2023 - 2023 IEEE International Geoscience and Remote Sensing Symposium*, 8194–8197. https://doi.org/10.1109/IGARSS52108.2023.10282176

Rouse, J. W. (1973). *Monitoring vegetation systems in the great plains with ERTS.*

Schüle, M., Domes, G., Schwanitz, C., & Heinken, T. (2023). Early natural tree regeneration after wildfire in a Central European Scots pine forest: Forest management, fire severity and distance matters. *Forest Ecology and Management*, *539*, 120999. https://doi.org/10.1016/j.foreco.2023.120999

Seidl, R. (2014). The Shape of Ecosystem Management to Come: Anticipating Risks and Fostering Resilience. *BioScience*, *64*(12), 1159–1169. https://doi.org/10.1093/biosci/biu172

Seidl, R., Potterf, M., Müller, J., Turner, M. G., & Rammer, W. (2024). Patterns of early post-disturbance reorganization in Central European forests. *Proceedings of the Royal Society B: Biological Sciences*, *291*(2031). https://doi.org/10.1098/rspb.2024.0625

Seidl, R., & Senf, C. (2024). Changes in planned and unplanned canopy openings are linked in Europe's forests. *Nature Communications*, *15*(1), 4741. https://doi.org/10.1038/s41467-024-49116-0

Seidl, R., Thom, D., Kautz, M., Martin-Benito, D., Peltoniemi, M., Vacchiano, G., Wild, J., Ascoli, D., Petr, M., Honkaniemi, J., Lexer, M. J., Trotsiuk, V., Mairota, P., Svoboda, M., Fabrika, M., Nagel, T. A., & Reyer, C. P. O. (2017). Forest disturbances under climate change. In *Nature Climate Change* (Vol. 7, Issue 6, pp. 395–402). Nature Publishing Group. https://doi.org/10.1038/nclimate3303

Seidl, R., & Turner, M. G. (2022). Post-disturbance reorganization of forest ecosystems in a changing world. *Proceedings of the National Academy of Sciences*, *119*(28). https://doi.org/10.1073/pnas.2202190119

Seidl, R., Vigl, F., Rössler, G., Neumann, M., & Rammer, W. (2017). Assessing the resilience of Norway spruce forests through a model-based reanalysis of thinning trials. *Forest Ecology and Management*, *388*, 3–12. https://doi.org/10.1016/j.foreco.2016.11.030

Senf, C., Müller, J., & Seidl, R. (2019). Post-disturbance recovery of forest cover and tree height differ with management in Central Europe. *Landscape Ecology*, *34*(12), 2837–2850. https://doi.org/10.1007/s10980-019-00921-9

Senf, C., & Seidl, R. (2020). Mapping the forest disturbance regimes of Europe. *Nature Sustainability*, *4*(1), 63–70. https://doi.org/10.1038/s41893-020-00609-y

Senf, C., & Seidl, R. (2021a). Mapping the forest disturbance regimes of Europe. *Nature Sustainability*, *4*(1), 63–70. https://doi.org/10.1038/s41893-020-00609-y

Senf, C., & Seidl, R. (2021b). Persistent impacts of the 2018 drought on forest disturbance regimes in Europe. *Biogeosciences*, *18*(18), 5223–5230. https://doi.org/10.5194/bg-18-5223-2021

Senf, C., Seidl, R., & Hostert, P. (2017). Remote sensing of forest insect disturbances: Current state and future directions. *International Journal of Applied Earth Observation and Geoinformation*, *60*, 49–60. https://doi.org/10.1016/j.jag.2017.04.004

Senf, C., Seidl, R., & Poulter, B. (2022). Post-disturbance canopy recovery and the resilience of Europe's forests. *Global Ecology and Biogeography*, *31*(1), 25–36. https://doi.org/10.1111/geb.13406

Sommerfeld, A., Senf, C., Buma, B., D'Amato, A. W., Després, T., Díaz-Hormazábal, I., Fraver, S., Frelich, L. E., Gutiérrez, Á. G., Hart, S. J., Harvey, B. J., He, H. S., Hlásny, T., Holz, A., Kitzberger, T., Kulakowski, D., Lindenmayer, D., Mori, A. S., Müller, J., … Seidl, R. (2018). Patterns and drivers of recent disturbances across the temperate forest biome. *Nature Communications*, *9*(1). https://doi.org/10.1038/s41467-018-06788-9

Sothe, C., Gonsamo, A., Lourenço, R. B., Kurz, W. A., & Snider, J. (2022). Spatially Continuous Mapping of Forest Canopy Height in Canada by Combining GEDI and ICESat-2 with PALSAR and Sentinel. *Remote Sensing*, *14*(20), 5158. https://doi.org/10.3390/rs14205158

Spiecker, H. (2000). Spruce Monocultures in Central Europe – Problems and Prospects. In *Spruce Monocultures in Central Europe-Problems and Prospects* (Issue 33).

Stevens-Rumann, C. S., Prichard, S. J., Whitman, E., Parisien, M.-A., & Meddens, A. J. H. (2022). Considering regeneration failure in the context of changing climate and disturbance regimes in western North America. *Canadian Journal of Forest Research*, *52*(10), 1281–1302. https://doi.org/10.1139/cjfr-2022-0054

Szwarcman, D., Roy, S., Fraccaro, P., Gíslason, Þ. E., Blumenstiel, B., Ghosal, R., Oliveira, P. H. De, Lucas, J., Almeida, D. S., Sedona, R., Kang, Y., Li, W., Alemohammad, H., Olofsson, P., Hain, C. R., Maskey, M., Ramachandran, R., & Moreno, J. B. (2025). *Prithvi-EO-2 . 0 : A Versatile Multi-Temporal Foundation Model for Earth Observation Applications 1 Introduction*.

Tariq, A., Shu, H., Gagnon, A. S., Li, Q., Mumtaz, F., Hysa, A., Siddique, M. A., & Munir, I. (2021). Assessing Burned Areas in Wildfires and Prescribed Fires with Spectral Indices and SAR Images in the Margalla Hills of Pakistan. *Forests*, *12*(10), 1371. https://doi.org/10.3390/f12101371

Thom, D., & Seidl, R. (2016). Natural disturbance impacts on ecosystem services and biodiversity in temperate and boreal forests. *Biological Reviews of the Cambridge Philosophical Society*, *91*(3), 760–781. https://doi.org/10.1111/brv.12193

Torres de Almeida, C., Gerente, J., Rodrigo dos Prazeres Campos, J., Caruso Gomes Junior, F., Providelo, L. A., Marchiori, G., & Chen, X. (2022). Canopy Height Mapping by Sentinel 1 and 2 Satellite Images, Airborne LiDAR Data, and Machine Learning. *Remote Sensing*, *14*(16), 4112. https://doi.org/10.3390/rs14164112

Trisasongko, B. H. (2010). The Use of Polarimetric SAR Data for Forest Disturbance Monitoring. *Sensing and Imaging: An International Journal*, *11*(1), 1–13. https://doi.org/10.1007/s11220-010-0048-8

Tucker, C. J. (1979). Red and photographic infrared linear combinations for monitoring vegetation. *Remote Sensing of Environment*, *8*(2), 127–150. https://doi.org/10.1016/0034-4257(79)90013-0

Turner, M. G., Calder, W. J., Cumming, G. S., Hughes, T. P., Jentsch, A., LaDeau, S. L., Lenton, T. M., Shuman, B. N., Turetsky, M. R., Ratajczak, Z., Williams, J. W., Williams, A. P., & Carpenter, S. R. (2020). Climate change, ecosystems and abrupt change: Science priorities. In *Philosophical Transactions of the Royal Society B: Biological Sciences* (Vol. 375, Issue 1794). Royal Society Publishing. https://doi.org/10.1098/rstb.2019.0105

Turner, M. G., & Seidl, R. (2023). Novel Disturbance Regimes and Ecological Responses. *Annual Review of Ecology, Evolution, and Systematics*, *54*(1), 63–83. https://doi.org/10.1146/annurev-ecolsys-110421-101120

Van Tiel, N., Fopp, F., Brun, P., van den Hoogen, J., Karger, D. N., Casadei, C. M., Lyu, L., Tuia, D., Zimmermann, N. E., Crowther, T. W., & Pellissier, L. (2024). Regional uniqueness of tree species composition and response to forest loss and climate change. *Nature Communications*, *15*(1), 4375. https://doi.org/10.1038/s41467-024-48276-3

Verbesselt, J., Hyndman, R., Newnham, G., & Culvenor, D. (2010). Detecting trend and seasonal changes in satellite image time series. *Remote Sensing of Environment*, *114*(1), 106–115. https://doi.org/10.1016/j.rse.2009.08.014

Wang, J., Xiao, X., Bajgain, R., Starks, P., Steiner, J., Doughty, R. B., & Chang, Q. (2019). Estimating leaf area index and aboveground biomass of grazing pastures using Sentinel-1, Sentinel-2 and Landsat images. *ISPRS Journal of Photogrammetry and Remote Sensing*, *154*, 189–201. https://doi.org/10.1016/j.isprsjprs.2019.06.007

Washaya, P., Modlinger, R., Tyšer, D., & Hlásny, T. (2024). Patterns and impacts of an unprecedented outbreak of bark beetles in Central Europe: A glimpse into the future? *Forest Ecosystems*, *11*, 100243. https://doi.org/10.1016/j.fecs.2024.100243

Wermelinger, B. (2004). Ecology and management of the spruce bark beetle Ips typographus—a review of recent research. *Forest Ecology and Management*, *202*(1–3), 67–82. https://doi.org/10.1016/j.foreco.2004.07.018

Wild, J., Kopecký, M., Svoboda, M., Zenáhlíková, J., Edwards-Jonášová, M., & Herben, T. (2014). Spatial patterns with memory: tree regeneration after stand-replacing disturbance in P icea abies mountain forests. *Journal of Vegetation Science*, *25*(6), 1327–1340. https://doi.org/10.1111/jvs.12189

Winter, M.-B., Baier, R., & Ammer, C. (2015). Regeneration dynamics and resilience of unmanaged mountain forests in the Northern Limestone Alps following bark beetle-induced spruce dieback. *European Journal of Forest Research*, *134*(6), 949–968. https://doi.org/10.1007/s10342-015-0901-3

Wulder, M. A., Masek, J. G., Cohen, W. B., Loveland, T. R., & Woodcock, C. E. (2012). Opening the archive: How free data has enabled the science and monitoring promise of Landsat. *Remote Sensing of Environment*, *122*, 2–10. https://doi.org/10.1016/j.rse.2012.01.010

Wulder, M. A., White, J. C., Goward, S. N., Masek, J. G., Irons, J. R., Herold, M., Cohen, W. B., Loveland, T. R., & Woodcock, C. E. (2008). Landsat continuity: Issues and opportunities for land cover monitoring. *Remote Sensing of Environment*, *112*(3), 955–969. https://doi.org/10.1016/j.rse.2007.07.004

Xi, Z., Xu, H., Xing, Y., Gong, W., Chen, G., & Yang, S. (2022). Forest Canopy Height Mapping by Synergizing ICESat-2, Sentinel-1, Sentinel-2 and Topographic Information Based on Machine Learning Methods. *Remote Sensing*, *14*(2), 364. https://doi.org/10.3390/rs14020364

Xu, X., Li, W., Ran, Q., Du, Q., Gao, L., & Zhang, B. (2018). Multisource Remote Sensing Data Classification Based on Convolutional Neural Network. *IEEE Transactions on Geoscience and Remote Sensing*, *56*(2), 937–949. https://doi.org/10.1109/TGRS.2017.2756851

Ye, F., Li, X., & Zhang, X. (2019). FusionCNN: a remote sensing image fusion algorithm based on deep convolutional neural networks. *Multimedia Tools and Applications*, *78*(11), 14683–14703. https://doi.org/10.1007/s11042-018-6850-3

Zeng, Garcia-Gonzalo, J., Peltola, H., & Kellomäki, S. (2010). The effects of forest structure on the risk of wind damage at a landscape level in a boreal forest ecosystem. *Annals of Forest Science*, *67*(1), 111–111. https://doi.org/10.1051/forest/2009090

Zeng, Hao, D., Huete, A., Dechant, B., Berry, J., Chen, J. M., Joiner, J., Frankenberg, C., Bond-Lamberty, B., Ryu, Y., Xiao, J., Asrar, G. R., & Chen, M. (2022). Optical vegetation indices for monitoring terrestrial ecosystems globally. *Nature Reviews Earth & Environment*, *3*(7), 477–493. https://doi.org/10.1038/s43017-022-00298-5

Zhang. (2010). Multi-source remote sensing data fusion: status and trends. *International Journal of Image and Data Fusion*, *1*(1), 5–24. https://doi.org/10.1080/19479830903561035

Zhang, X., Zhou, Y., & Luo, J. (2022). Deep learning for processing and analysis of remote sensing big data: a technical review. *Big Earth Data*, *6*(4), 527–560. https://doi.org/10.1080/20964471.2021.1964879

Zhu, X. X., Tuia, D., Mou, L., Xia, G.-S., Zhang, L., Xu, F., & Fraundorfer, F. (2017). Deep Learning in Remote Sensing: A Comprehensive Review and List of Resources. *IEEE Geoscience and Remote Sensing Magazine*, *5*(4), 8–36. https://doi.org/10.1109/MGRS.2017.2762307

Zhu, Yang, F., Qiu, Z., He, N., Zhu, X., Li, Y., Xu, Y., & Lu, Z. (2023). Enhancing Forest Canopy Height Retrieval: Insights from Integrated GEDI and Landsat Data Analysis. *Sustainability*, *15*(13), 10434. https://doi.org/10.3390/su151310434

Żywiec, M., & Ledwoń, M. (2008). Spatial and temporal patterns of rowan (Sorbus aucuparia L.) regeneration in West Carpathian subalpine spruce forest. *Plant Ecology*, *194*(2), 283–291. https://doi.org/10.1007/s11258-007-9291-z